



TRC0302

**AASHTO 2002 Pavement Design Guide
Design Input Evaluation Study**

Kevin D. Hall, Steven Beam, Meng Lee

Final Report

2006

FINAL REPORT

TRC-0302

**AASHTO 2002 PAVEMENT DESIGN GUIDE
DESIGN INPUT EVALUATION STUDY**

by

Kevin D. Hall, Steven Beam, and Meng Lee

Conducted by

Department of Civil Engineering
University of Arkansas

In cooperation with

Arkansas State Highway and Transportation Department

U.S. Department of Transportation
Federal Highway Administration

University of Arkansas
Fayetteville, Arkansas 72701

June 2006

Technical Report Documentation Page

| | | | | | |
|---|--|---|--|--|-----------|
| 1. Report No. FHWA/AR-xx-xxx | | 2. Government Accession No. | | 3. Recipient's Catalog No. | |
| 4. Title and Subtitle TRC-03020 AASHTO 2002 Pavement Design Guide - Design Input Evaluation Study Final Report | | | | 5. Report Date June 2006 | |
| | | | | 6. Performing Organization Code | |
| 7. Author(s) Kevin D. Hall Steven Beam Meng Lee | | | | 8. Performing Organization Report No. | |
| 9. Performing Organization Name and Address University of Arkansas, Department of Civil Engineering 4190 Bell Engineering Center Fayetteville, AR 72701 | | | | 10. Work Unit No. (TRAIS) | |
| | | | | 11. Contract or Grant No. TRC-0302 | |
| 12. Sponsoring Agency Name and Address Arkansas State Highway and Transportation Department P.O. Box 2261 Little Rock, AR 72203-2261 | | | | 13. Type of Report and Period covered Final Report 1 Jul 03 thru 30 Jun 05 | |
| | | | | 14. Sponsoring Agency Code | |
| 15. Supplementary Notes Conducted in cooperation with U.S. Department of Transportation, Federal Highway Administration | | | | | |
| 16. Abstract <p>Many highway agencies use AASHTO methods for the design of pavement structures. Current AASHTO methods are based on empirical relationships between traffic loading, materials, and pavement performance developed from the AASHO Road Test (1958-1961). The applicability of these methods to modern-day conditions has been questioned; in addition, the lack of realistic inputs regarding environmental and other factors in pavement design has caused concern. Research sponsored by the National Cooperative Highway Research Program has resulted in the development of a mechanistic-empirical design guide (<i>M-E Design Guide</i>) for pavement structural analysis. The new <i>M-E Design Guide</i> requires over 100 inputs to model traffic, environmental, materials, and pavement performance to provide estimates of pavement distress over the design life of the pavement. Many designers may lack specific knowledge of the data required. A study was performed to assess the relative sensitivity of the models used in the <i>M-E Design Guide</i> to inputs relating to Portland cement concrete (PCC) materials in the analysis of jointed plain concrete pavements (JPCP) and to inputs relating to Hot-Mix Asphalt (HMA) materials in the analysis of flexible pavements. For PCC, a total of 29 inputs were evaluated; the three pavement distress models (cracking, faulting, and roughness) were not sensitive to 17 of the 29 inputs. All three models were sensitive to 6 of 29 inputs. Combinations of only one or two of the distress models were sensitive to 6 of 29 inputs. For HMA, a total of 8 inputs were evaluated for each of two HMA mixtures; the three primary distress models (rutting, fatigue cracking, and roughness) were not sensitive to 6 of the 8 inputs. Distress models exhibited sensitivity to only design air voids and effective binder content. This data may aid designers in focusing on those inputs having the most effect on desired pavement performance.</p> | | | | | |
| 17. Key Words Pavement, Flexible Pavement Design, Rigid Pavement Design, Mechanistic-Empirical Design | | | 18. Distribution Statement No Restrictions | | |
| 19. Security Classif. (Of this report) (none) | | 20. Security Classif. (Of this page) (none) | | 21. No. of Pages 246 | 22. Price |

TRC-0302
AASHTO 2002 Pavement Design Guide
Design Input Evaluation Study

EXECUTIVE SUMMARY

Many highway agencies use AASHTO methods for the design of pavement structures. Current AASHTO methods are based on empirical relationships between traffic loading, materials, and pavement performance developed from the AASHO Road Test (1958-1961). The applicability of these methods to modern-day conditions has been questioned; in addition, the lack of realistic inputs regarding environmental and other factors in pavement design has caused concern. Research sponsored by the National Cooperative Highway Research Program has resulted in the development of a mechanistic-empirical design guide (*M-E Design Guide*) for pavement structural analysis. The new *M-E Design Guide* requires over 100 inputs to model traffic, environmental, materials, and pavement performance to provide estimates of pavement distress over the design life of the pavement. Many designers may lack specific knowledge of the data required. A study was performed to assess the relative sensitivity of the models used in the *M-E Design Guide* to inputs relating to Portland cement concrete (PCC) materials in the analysis of jointed plain concrete pavements (JPCP) and to inputs relating to Hot-Mix Asphalt (HMA) materials in the analysis of flexible pavements. For PCC, a total of 29 inputs were evaluated; the three pavement distress models (cracking, faulting, and roughness) were not sensitive to 17 of the 29 inputs. All three models were sensitive to 6 of 29 inputs. Combinations of only one or two of the distress models were sensitive to 6 of 29 inputs. For HMA, a total of 8 inputs were evaluated for each of two HMA mixtures; the three primary distress models (rutting, fatigue cracking, and roughness) were not sensitive to 6 of the 8 inputs. Distress models exhibited sensitivity to only design air voids and effective binder content. This data may aid designers in focusing on those inputs having the most effect on desired pavement performance.

TABLE OF CONTENTS

| | |
|---|-----|
| CHAPTER ONE: Background | 1 |
| CHAPTER TWO: Rigid Pavement Design | 8 |
| CHAPTER THREE: Flexible Pavement Design | 46 |
| CHAPTER FOUR: Summary and Conclusions | 92 |
| APPENDIX A: Record of Inputs for <i>MEPDG</i> JPCP Analysis | A-1 |
| APPENDIX B: Rigid Pavement Sensitivity Graphs..... | B-1 |
| APPENDIX C: Record of Inputs for <i>MEPDG</i> Flexible Pavement Analysis..... | C-1 |
| APPENDIX D: Flexible Pavement Sensitivity Graphs | D-1 |
| APPENDIX E: Hot-Mix Asphalt Mixture Data | E-1 |

CHAPTER ONE

BACKGROUND

Introduction

The Arkansas State Highway and Transportation Department (AHTD) currently performs structural pavement design in accordance with policies and procedures contained in the 1993 *AASHTO Guide for the Design of Pavement Structures* (hereinafter the *1993 Guide*). The procedures specified in the *1993 Guide* (and the previous versions released in 1972 and 1986) were developed from empirical relationships determined during the AASHTO Road Test conducted from 1958 to 1961 outside Ottawa, Illinois.

AASHTO Road Test

“The principal objective of the AASHTO Road Test was to determine the significant relationship between the number of repetitions of specific axle loads of different magnitude and arrangement, and the performance of different thicknesses of uniformly designed and constructed asphaltic concrete and reinforced Portland cement surfacings on different thicknesses of base and subbase when laid on a basement soil of known characteristics.” [1]

The AASHTO test roads were located just northwest of Ottawa, Illinois, about 80 miles southwest of Chicago, whereby the climate and the soil topography of the area were typical of those in the northern United States region. The test roads were constructed entirely on embankment to meet requirements. The test roads consisted of 6 loops (1 to 6) by which loops 2 to 6 were trafficked while loop 1 was used for climatic and other observations. Each loop had two 12 ft wide traffic lanes which were independently trafficked. The test roads were subjected to truck loads moving at a constant speed of 35 mph, for about 19 hours a day over a period of about 2 years. The total number of axle loads over each experimental section in the test roads was over 1.1 million. The axles loads used ranged from 2 kips in single axles to 48 kips in

tandem axles. The subbase used on the test sections was a local plant modified sandy gravel mix. The road base used was a wet-mix crushed limestone.

The Present Serviceability Concept

The concept of serviceability was used to quantify the condition of each experimental pavement section along with the more commonly used observations of major pavement distresses such as permanent deformation and cracking. Serviceability is based on the assumption that road users are more interested in the ride quality of a pavement rather than the extent of the structural deterioration of a pavement. A subjective assessment panel of drivers of both private and commercial vehicles was formed to assess the concept of “ride quality” on 99 selected lengths of roads, equally divided between flexible and concrete pavements, in the states of Illinois, Minnesota, and Indiana. Each member of the panel was asked to rate the serviceability of each road using a scale of 0 to 5 as defined in a rating form. Furthermore, each member was asked to give an overall evaluation of the acceptability of each pavement section and whether or not the pavement should be allowed for continued service. The purpose of the acceptability evaluation was to establish a level of acceptability in the rating scale. The mean rating and the mean acceptability of the panel were used to define the present serviceability rating (PSR) of each pavement. The results of the assessment showed that a PSR value of 2.5 reflected the critical condition likely to require future attention while a PSR of 1.5 indicated that the road was unfit for service [1].

With the results of the PSR ratings from 99 sites, engineers and statisticians involved in the AASHO road test produced equations relating the ride quality and major distresses to give a present serviceability index (PSI) which matched the PSR values produced from the assessment panel.

NCHRP 1-37a

The AASHO Road Test, which at the time represented the most comprehensive pavement design study ever undertaken, has weaknesses which make it obsolete compared to current pavement performance information. These weaknesses are purported to be addressed with the release of new pavement design guidelines prepared under National Cooperative Highway Research Program (NCHRP) Project 1-37a, which was completed in 2004.

The primary product of NCHRP 1-37a is the *Mechanistic-Empirical Pavement Design Guide* (hereinafter the *MEPDG*). The *MEPDG* utilizes a mechanistic-empirical (M-E) design approach as opposed to the current purely empirical approach. Similar to former methods, the M-E approach will characterize the materials, traffic, and environment using relationships developed from field experience, thus the term "empirical". The difference between the older "empirical" methods and this new M-E approach lies in that the pavement performance will be modeled using a rational process where the mechanics of the pavement structure are analyzed. Due to the "empirical" nature of the predictive performance models, it is imperative that the models be calibrated by each agency that uses the software. This will involve modeling existing pavements that have detailed information about the initial design as well as monitoring data over the life of the pavement. Figure 1 shows a flow chart describing the design process.

Another feature new to pavement design is the option of the design to use hierarchical input levels. This allows the designer to input project specific information for some aspects of the pavement design (Level 1) where that information is available or to accept nationally averaged default values for inputs where no information is available (Level 3). There is also a middle level of input, Level 2, where the designer might be able to input a different parameter than what is required and the software will make the correlation, or a more specific regional

value can be used. This hierarchal input system allows for greater flexibility for application of the software. Not all pavements would warrant the level of information required for Level 1 inputs because theoretically, a design with Level 1 inputs is more accurate than a design with Level 3 inputs. Once again, though, the accuracy of any model depends on the level of calibration that the system has undergone.

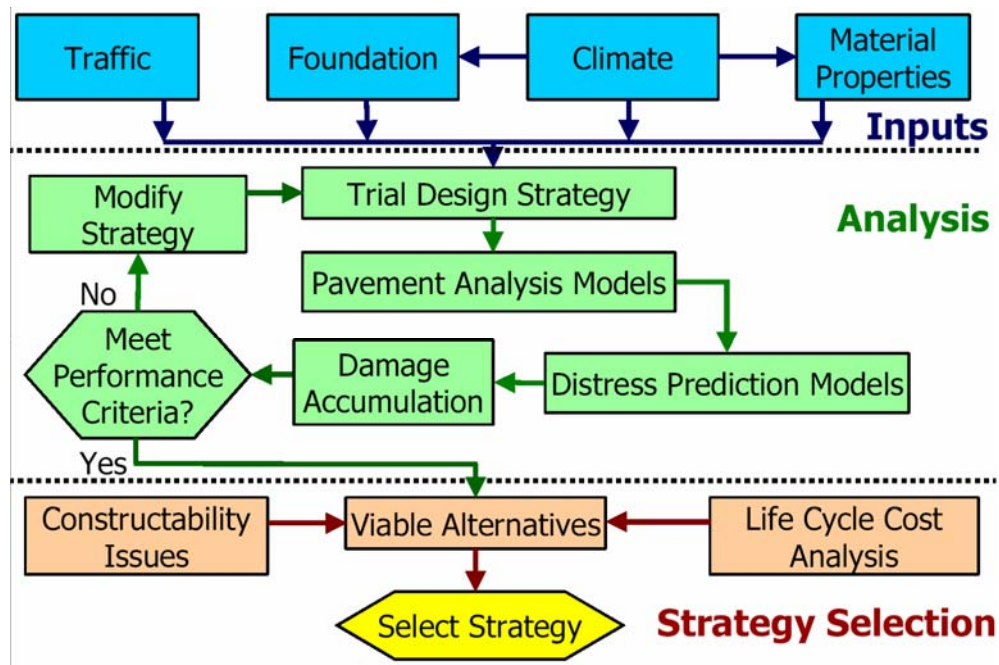


Figure 1: Flow Chart for Mechanistic Design of Pavements (from Draft Design Guide) [4]

Due to the computationally intensive procedure utilizing mechanistic principles, software was developed for the *MEPDG* to aid pavement designers. The primary purpose of TRC-0302 is to evaluate, by means of a quasi-sensitivity analysis, the inputs for the design of jointed plain concrete pavements (JPCP) and hot-mix asphalt (HMA) pavements to provide designers with guidance regarding the relative sensitivity of the performance prediction models contained in the

MEPDG and regarding appropriate values for those inputs. Such information will make pavement design more efficient and aid the adoption and implementation of the *MEPDG* by AHTD.

MEPDG Background

Although the previous versions of the AASHTO *Guide* have been very useful for the last several decades, there are significant limitations to its continued effectiveness. The limitations have been summarized as follows: [2]

- Pavement rehabilitation design procedures were not considered at the Road Test.
- Since the Road Test was conducted at one specific geographic location, it is difficult to address the effects of differences in climatic conditions on pavement performance.
- Only one type of subgrade was used for all of the test sections at the Road Test.
- Only unstabilized, dense granular bases were included in the main pavement sections (limited use of treated bases was included for flexible pavements).
- Vehicle suspension, axle configurations, and tire types were representative of the types used in the late 1950s, and many of these are outmoded in the 1990s.
- Pavement designs, materials, and construction were representative of those used at the time of the Road Test. No subdrainage was included in the Road Test sections.
- Axle configurations and tire pressures used for the Road Test do not reflect those of today.
- Previous procedures relate structural integrity to pavement thickness, however, this is not always the case. Rutting is an example of this. Mechanistic design can model the stresses within the pavement to design a cross section that will resist rutting.
- The Road Test only lasted approximately 2 years, and has been used for the design of pavements that are supposed to last 20 years, for example. This requires significant extrapolation.
- The Road Test only involved a total of approximately two million ESALs as a result of the limited time period. Therefore, the effects of the loading were also extrapolated.

These limitations have long been recognized by the pavement design community, and beginning in 1987 with the NCHRP Project 1-26, formal steps were taken to include mechanistic principles in the AASHTO design procedures. The report published in 1990 as a result of this project included the first recommendations of mechanistic procedures to be included in the AASHTO guide. This research proposed two programs -- ILLI-PAVE and ILLI-SLAB -- for flexible and rigid pavement design, respectively, to be the basis of the AASHTO mechanistic design procedure. In turn, mechanistic design procedures for rigid pavement were included as a supplement to the *1993 Guide*. [3]

Realizing the shortfalls of the mechanistic procedures included in the *1993 Guide*, the AASHTO Joint Task Force on Pavements (JTTF – now the Joint Technical Committee on Pavements) began an effort to develop an improved guide in 1997. NCHRP Project 1-37 was the initial step toward developing this new *Guide*. Under Project 1-37, all the necessary parties were brought together to facilitate the development of the *MEPDG* coupled with the development of rudimentary software for M-E pavement design. One very important aspect of the NCHRP 1-37a work is the restriction that the *MEPDG* developed would be based on existing M-E technology to model the pavement performance over its life. The completed NCHRP 1-37a was to deliver a fully developed *MEPDG*, rudimentary software, calibration/ validation procedures for adaptation to local conditions, plans for implementation and training on the software, and strategies to promote national interest and acceptance of the new design procedures. [4]

Purported benefits of the mechanistic-empirical basis of the *MEPDG* include [2]:

"The consequences of non-traditional loading conditions can be evaluated. For example, the damaging effects of increased loads, high tire pressures, and multiple axles can be modeled."

"Better use of available materials can be made. For example, the use of stabilized materials in both rigid and flexible pavements can be simulated to predict future performance."

“Improved procedures to evaluate premature distress can be developed to analyze why some pavements exceed their design expectations. In effect, better diagnostic techniques can be developed. Aging effects can be included in estimates of performance. For example, asphalt hardens with time, which, in turn, affects both fatigue cracking and rutting.”

“Seasonal effects such as thaw weakening can be included in estimates of performance.”

“Consequences of subbase erosion under rigid pavements can be evaluated.”

“Methods can be developed to better evaluate the long-term benefits of providing improved drainage in the roadway section.”

Recently, a follow-up project to NCHRP 1-37a – NCHRP Project 1-40 – was initiated to provide a critical third-party review of the work performed and the products produced. The final report of the NCHRP 1-40 project is expected in 2006. In addition, other NCHRP and State Highway Agency (SHA) projects have been initiated to “fill in” the perceived gaps in material models, distress mechanisms, and processes contained in the 1-37a *MEPDG*.

Project Objectives

The primary global objective for TRC-0302 was to provide Arkansas pavement designers guidance concerning design inputs for the *MEPDG*, both in terms of suggested initial (or default) values and in terms of the sensitivity of pavement performance predictions to specific input variables. Specific project objectives included:

- *Completely document design inputs.*
- *Develop recommendations regarding input sensitivity.*
- *Develop recommendations regarding initial design inputs.*
- *Suggest methods for refining input values for Arkansas.*

The bulk of this report is divided into two main sections – Rigid Pavement Design (Chapter 2) and Flexible Pavement Design (Chapter 3). Summaries of the project findings and conclusions are contained in Chapter 4.

CHAPTER TWO

RIGID PAVEMENT DESIGN

Overview of the *MEPDG*

As mentioned, the *MEPDG* Software uses a mechanistic-empirical approach to model the pavement structure supplied by the designer. This is important to understand because the performance model can only be as good as the characterization of the environmental conditions, traffic loadings, and material parameters. A fundamental objective of this study is to relate the accuracy of the input parameters to the accuracy of the performance prediction for a given pavement.

The analysis that is performed to produce the performance model is based on the ISLAB2000 finite element program. [5] However, the ISLAB2000 program does not run behind the design guide software. Instead, because of the time it would require to perform the finite element analysis, neural networks were trained using thousand of results from the ISLAB2000 program. Once the pavement responses are determined with the analysis, transfer functions relate the pavement responses to pavement damage. Using the pavement responses and pavement damage at many increments, typically monthly, over the design life, the damage is accumulated to produce the pavement performance model for each type of damage. For JPCP pavements, these models predict the percent slabs cracked, the inches of faulting, and the smoothness expressed as the International Roughness Index (IRI).

With the pavement performance model, the designer can look at the predicted damage at any point during the design life and make changes to the design to bring the pavement performance into compliance with performance criteria.

***MEPDG* Performance Models**

As mentioned previously, three performance models are included in the *MEPDG* JPCP design software to aid the designer in choosing a pavement structure that will serve the needs of the traffic facility. Those models are a cracking model (Top-down and Bottom-up cracking), a faulting model, and an IRI model. While this study focuses on JPCP, the rigid pavement design software also includes CRCP design which includes a punchout model to the list of models previously mentioned. Each of these performance models are based on responses that are the result of the mechanistic analysis of the input pavement structure using the neural networks based on the ISLAB2000 program. The general categories of inputs for the responses to be calculated are the following:

- Traffic loading
- Pavement cross section
- Poisson's Ratio for each layer
- Elastic Modulus for each layer
- Layer to layer friction
- Thermal properties of each layer
- Temperature and moisture gradients

From these inputs, stresses and resulting strains are calculated at various locations within the pavement structure. The three strains are calculated using the following three equations based on the Poisson Ratio and Elastic Modulus of the layer.

$$\text{Major Strain:} \quad \varepsilon_z = \frac{1}{E} [\sigma_z - \mu(\sigma_r + \sigma_t)] \quad \text{Eq. 1}$$

$$\text{Intermediate Strain:} \quad \varepsilon_r = \frac{1}{E} [\sigma_r - \mu(\sigma_r + \sigma_t)] \quad \text{Eq. 2}$$

$$\text{Minor Strain:} \quad \varepsilon_t = \frac{1}{E} [\sigma_t - \mu(\sigma_r + \sigma_z)] \quad \text{Eq. 3}$$

where: E = Elastic Modulus
 μ = Poisson Ratio

$$\begin{aligned}\sigma_z &= \text{Major Stress} \\ \sigma_r &= \text{Intermediate Stress} \\ \sigma_t &= \text{Minor Stress}\end{aligned}$$

The question, then, is how to determine the Elastic Modulus and Poisson's Ratio of the PCC layer to determine the strains that will be used in the performance models. These two material characteristics are determined by different means depending on the level of analysis desired (i.e. Level 1, 2, or 3). Poisson's Ratio has to be specifically input by the designer. This means that they can either test a specific mix for Poisson's Ratio (Level 1) or they can use typical values (Level 3). Level 2 is not applicable because there are no correlations developed between other material properties and the Poisson Ratio. Table 1, adapted from the Draft *MEPDG*, shows the procedure used to determine the PCC Elastic Modulus depending on the level of analysis the designer selects in the program.

As Table 1 shows, Level 1 requires that E_c be input directly for the 7, 14, 28, and 90 day curing times as well as a ratio of the 20-year to 28-day E_c . However, of these values only the 28-day compressive strength is routinely tested. For this circumstance, Level 2 could be used because the program will use the compressive strength at the aforementioned times to calculate the E_c at those times using the following relationship:

$$E_c = 33\rho^{1.5}f'_c{}^{0.5} \quad \text{Eq. 4}$$

where:

$$\begin{aligned}\rho &= \text{Unit Weight (pcf)} \\ f'_c &= \text{Compressive Strength (psi)}\end{aligned}$$

For both Levels 1 and 2, once E_c is determined, the mix specific regression constants for the Modulus Gain Curve will be determined and used to predict the modulus at each time increment that strain is computed. The basic form of the modulus gain curve is below.

$$STRRATIO = \alpha_1 + \alpha_2 \log_{10}(AGE) + \alpha_3 [\log_{10}(AGE)]^2 \quad \text{Eq. 5}$$

where: $STRRATIO$ = ratio of E_c at AGE to 28-day E_c
 AGE = age of specimen in years
 α_i = regression constants

| Material Category | Type Design | Input Level | Description |
|-------------------|-------------|-------------|--|
| PCC (Slabs) | New | 1 | <p>E_c, determined directly by laboratory testing. Chord modulus (ASTM C-469) at various ages (7, 14, 28, 90-days).</p> <p>Estimate the 20-year to 28-day (long-term) elastic modulus ratio.</p> <p>Develop modulus gain curve using the test data and long term modulus ratio to predict E_c over the design life.</p> <p>E_c, determined indirectly from compressive strength testing at various ages (7, 14, 28, 90-days) from AASHTO T-22.</p> <p>Estimate the 20-year to 28-day compressive strength ratio.</p> |
| | | 2 | <p>Convert f'_c to E_c using the following relationship: $E_c = 33\rho^{3/2}(f'_c)^{1/2}$ psi where ρ = concrete unit weight (pcf)</p> <p>Develop modulus gain curve using the test data and long term modulus ratio to predict E_c at any time over the design life.</p> <p>E_c, determined indirectly from 28-day estimates of flexural strength (MR) or f'_c. MR determined from testing (AASHTO T97) or historical records. Likewise f'_c estimated from testing (AASHTO T22) or from historical records.</p> |
| | | 3 | <p>If 28-day MR is estimated, its value at any given time, t, is determined using: $MR(t) = (1 + \log_{10}(t/0.0767) - 0.01566 * \log_{10}(t/0.0767)^2) * MR_{28\text{-day}}$</p> <p>Estimate $E_c(t)$ by first estimating $f'_c(t)$ from MR(t) and then converting $f'_c(t)$ to $E_c(t)$ using the following relationships: $MR = 9.5 (f'_c)^{1/2}$ psi $E_c = 33\rho^{3/2}(f'_c)^{1/2}$ psi</p> <p>If 28-day f'_c is estimated, first convert it to an MR value using equation above and then project MR(t) as noted above and from it $E_c(t)$ over time.</p> |

Table 1: Determination of PCC Modulus of Elasticity [5]

When using Level 3 to determine E_c , the designer has two options: 1) to enter the 28-day flexural strength; or 2) enter the 28-day compressive strength. If the flexural strength is entered, it is estimated at any given time by an equation similar to the Modulus Gain Curve listed below:

$$MR(t) = 1 + 0.12 \log_{10} \left(\frac{t}{0.0767} \right) - 0.01566 \left[\log_{10} \left(\frac{t}{0.0767} \right) \right]^2 \quad \text{Eq. 6}$$

Then, using $MR(t)$, the compressive strength at time (t) is estimated using the next relationship:

$$MR = 9.5 f'_c{}^{0.5} \quad \text{Eq. 7}$$

Finally, using Eq. 4, $E_c(t)$ can be computed. If the designer chooses to input the 28-day compressive strength, it is converted to the 28-day flexural strength using Eq.7, and the same procedure is followed to reach $E_c(t)$.

Equations 1-7 and the accompanying discussions show how the software uses different levels of input to determine the parameters used in the actual performance models. It is important to note that the neural networks and performance models always use the exact same information to create the output regardless of the level of input used by the designers. The information is essentially the information entered at Level 1, and if Level 3 information is input into the program, then it is translated through mathematical relationships to yield the information that must be input at Level 1. The performance models then use the input or calculated data to report measures of distresses (cracking, faulting, and IRI) based on the conditions set by the pavement designer

Those performance models used to predict the distresses were developed from creating regression equations using data from the LTPP pavement sections. The specifics of each of the models will be discussed later, but because the models are based on regression equations, they yield an answer representing what would be expected to occur on average. This correlates to a

reliability of 50%, or in other words, half of the observations would be less than and half would be greater than the reported result. In any design, being adequate only half of the time is not good enough, so to be confident that the actual performance of the pavement is not worse than the model, software allows the designer to choose a higher level of reliability, 90% for instance. If the designer chooses a 90% reliability, the distress at 90% reliability is calculated using a normal distribution curve where the distress at 90% reliability is shifted by the product of the standard deviation of the model and the standard normal deviate (Z) for the specified reliability. This will yield a resulting distress measurement that should be conservative in 90% of the observations. Another way to explain this is that the distress measurement of the pavement would only be exceeded 10% of observations. This allows the designer to be assured that it is unlikely that the pavement is underdesigned.

Cracking Model

The cracking model was based on 522 observations at 196 field sections from 24 states and yielded a standard error of estimate (SEE) of 5.4 percent and a R^2 value of 0.86, which is quite good considering the fact that there are many variables that can affect the cracking of a pavement section. The sections were part of the Long Term Pavement Performance (LTPP) study as well as from the Federal Highway Administration's study *Performance of Concrete Pavements*. [4] The model used for both top-down and bottom-up cracking by the *MEPDG* Software is shown in Equation 8.

$$CRK = \frac{1}{1 + FD^{-1.68}} \quad \text{Eq. 8}$$

where: CRK = predicted amount of cracking
 FD = Fatigue damage

For top-down versus bottom-up cracking, the fatigue damage is different based on the stress and strains within the pavement. Then using both the top-down and bottom-up cracking, the total cracking reported for a roadway, in percent slabs cracked, is calculated using Equation 9.

$$TCRACK = (CRK_{Bottom-up} + CRK_{Top-down} - (CRK_{Bottom-up} \bullet CRK_{Top-down})) \bullet 100\% \quad \text{Eq. 9}$$

where: $TCRACK$ = Total cracking in percent
 $CRK_{Bottom-up}$ = Predicted bottom-up cracking
 $CRK_{Top-down}$ = Predicted top-down cracking

While this seems fairly simple, the problem lies in calculating the fatigue damage because of the high number of variables that could affect the cracking of the pavement. The fatigue damage can be described as the sum of the number of loads applied divided by the number of loads allowed under a set of specified conditions as shown in Equation 10.

$$FD = \sum \frac{n_{i,j,k,l,m,n}}{N_{i,j,k,l,m,n}} \quad \text{Eq. 10}$$

where: FD = total fatigue damage
 $n_{i,j,k,l,m,n}$ = applied number of loads
 $N_{i,j,k,l,m,n}$ = allowable number of loads
 i = age (accounts for change in Modulus of rupture, interface bonding, and should LTE)
 j = month (accounts form change in base and effective modulus of subgrade reaction because of temperature and moisture changes)
 k = axle type
 l = load level – i.e. weight on the axle
 m = temperature difference
 n = traffic path – i.e. location of load on pavement

For all of these combinations of wheel loads, positions, pavement age, temperature differences, etc., the *MEPDG* states that there are approximately 1 million cases that must be analyzed each year over the design life of the pavement. [4] A finite element analysis program must be used in

the determination of fatigue damage. Due to the complexity of the analysis, neural networks were created for this design software.

Faulting Model

Similar to the cracking model, the faulting model was developed using both LTPP and FHWA study sections for a total of 248 sections in 22 states for a total of 560 observations, yielding a model with an R² value of 74.4 percent and a SEE of 0.0267 inches. [4] The faulting model is based on an incremental approach where the faulting a specific time is calculated based on the conditions at that time and added to the previous faulting measures. In other words, it is incrementally calculated and accumulated over time for the current value reported as can be seen by the following equations.

$$Fault_m = \sum_{i=1}^m \Delta Fault_i \quad \text{Eq. 11}$$

$$\Delta Fault_i = C_{34} * (FAULTMAX_{i-1} - Fault_{i-1})^2 * DE_i \quad \text{Eq. 12}$$

$$FAULTMAX_i = FAULTMAX_0 + C_7 * \sum_{j=1}^m DE_j * \log(1 + C_5 * 5.0^{EROD})^{C_6} \quad \text{Eq. 13}$$

$$FAULTMAX_0 = C_{12} * \delta_{curling} * \left[\log(1 + C_5 * 5.0^{EROD}) * \log\left(\frac{P_{200} * WetDays}{p_s}\right) \right] \quad \text{Eq. 14}$$

where:

- $Fault_m$ = mean joint faulting at the end of month m , in
- $\Delta Fault_i$ = incremental change in faulting during month i
- $FAULTMAX_i$ = maximum mean transverse joint faulting for month i , in
- $FAULTMAX_0$ = initial maximum mean joint faulting, in
- $EROD$ = base/ subbase erodibility factor
- DE_i = differential deformation energy accumulated during month i
- $\delta_{curling}$ = maximum mean monthly slab corner upward deflection due to curling and warping
- P_{200} = percent subgrade material passing #200 sieve
- p_s = overburden on subgrade, lb

WetDays = average annual number days with greater than 0.1 in of rainfall

$$C_{12} = C_1 + C_2 * FR^{0.25} \quad \text{Eq. 15}$$

$$C_{34} = C_3 + C_4 * FR^{0.25} \quad \text{Eq. 16}$$

where: $C_1 = 1.29$ $C_5 = 250$

$C_2 = 1.1$ $C_6 = 0.4$

$C_3 = 0.001725$ $C_7 = 1.2$

$C_4 = 0.0008$

FR = base freezing index = percentage of time the temperature at the top of the base is below freezing

Smoothness Model

The model used for calculating the International Roughness Index (IRI) is used in determining the smoothness of the pavement at any particular time through the life of the pavement. The smoothness model is much simpler than either the cracking or faulting models. However, the smoothness model is dependent upon what the cracking and faulting models yield. The model for smoothness given in equation 17 was based on 183 observations and produced an R^2 value of 0.70 and SEE of 22.2 in/mi. [4]

$$IRI = IRI_1 + C_1 CRK + C_2 SPALL + C_3 TFAULT + C_4 SF \quad \text{Eq. 17}$$

where: *IRI* = predicted smoothness measured as IRI, in/mile

IRI₁ = initial smoothness measures as IRI, in/mile

CRK = percent slabs with transverse cracks

SPALL = percentage of joints with spalling (medium to high severities only)

SF = Site factor

$C_1 = 0.0823$ $C_3 = 1.4929$

$C_2 = 0.4417$ $C_4 = 25.24$

$$SF = AGE(1 + 0.5556FI)(1 + P_{200}) / 1,000,000 \quad \text{Eq. 18}$$

where: *AGE* = pavement age, yr

FI = freezing index, °F-days

P_{200} = percent subgrade material passing #200 sieve

Notice that the smoothness model also includes a factor for spalling, but no model for spalling has been discussed. The spalling model is contained within the smoothness model since this is the only place that the information is used. The spalling model is given in equation 19 was based on 170 observations yielding an R^2 value of 0.78 and an SEE of 0.068. [4]

$$SPALL = \left[\frac{AGE}{AGE + 0.01} \right] \left[\frac{100}{1 + 1.005^{(-12 * AGE * SCF)}} \right] \quad \text{Eq. 19}$$

$$SCF = -1400 + 350 * AIR\% * (0.5 + PREFORM) + 3.4 f'_c * 0.4 - 0.2(FTCYC * AGE) + 43 h_{PCC} - 536 WC_Ratio \quad \text{Eq. 20}$$

where:

- SCF = spalling prediction scaling factor
- $AIR\%$ = PCC air content, percent
- AGE = time since construction, years
- $PREFORM$ = 1 if preformed sealant
0 if not preformed
- f'_c = PCC compressive strength, psi
- $FTCYC$ = average annual number of freeze-thaw cycles
- h_{PCC} = PCC slab thickness, in
- WC_Ratio = PCC water/cement ratio

Research Approach

To successfully realize the objectives of this research, the action plan was divided into three phases:

Phase I: Perform analysis of theoretical pavements varying one input per trial to show the sensitivity of the program to that particular input.

Phase II: Determine which inputs have a significant impact on the overall performance of the pavement and rationalize conclusions with the performance model equations.

Phase III: Delineate what inputs to alter to yield better performance with respect to a specific model (e.g. pavement cracking).

Phase I

Phase I represented the bulk of the work which produced the data that was used in Phases II and III to draw conclusions about how the inputs affect the pavement performance prediction. The inputs that were analyzed are checked in the list of inputs in Appendix A, and the baseline data for the study is shown to the right of the input descriptions. Using that baseline data, each one of the tested inputs was varied over some typical range of values to determine how each affects each of the three performance models for JPCP.

Phase II

Once Phase I was completed, the data were analyzed to estimate which inputs have a significant impact on the performance models. This was not done using a statistical analysis – but rather by comparing the graphs representing the performance models of the pavement and assessing the impact of varying the input over its typical range relative to ranges the performance prediction.

Phase III

The data generated in Phase I, in conjunction with the conclusions drawn from Phase II, were used to define the relationship(s) between specific distress models and design inputs.

Analysis and Results

The results from the *MEPDG* Software is reported in an Microsoft Excel spreadsheet file that includes an Input Summary, tabular output of the performance models, and graphical output of the performance models. To compare the output when varying a single input over a typical range of values allowed in the program, the tabular output of the models were compiled and graphs generated so that all of the models for varying one input could be compared on the same graph. The comparison graphs for each varied input are included in Appendix B and discussed in the subsections that follow.

Curl/Warp Effective Temperature Difference

The curling and warping effective temperature difference is a new parameter introduced to rigid pavement design. The curling and warping effective temperature difference is defined in the software as the “equivalent temperature gradient that will produce the same slab curling or warping that locks into the slab at the time of concrete set.” The curling and warping effective temperature difference was tested at values of -5, -10, and -20 degrees Fahrenheit, with the program default value being -10 degrees.

The curling and warping effective temperature difference, as the name implies, will influence the degree of curling or warping that the slab experiences when curing. As the gradient increases, so does the degree of curling or warping. Likewise, as curling or warping increases, this results in more faulting as is reflected in Figure B1. Similarly, as the temperature gradient increases, so does the stress developed because of that temperature gradient. This stress results in the curling or warping of the pavement which will cause tensile forces one side of the pavement. Since concrete is weak in tension, the pavement cracking will increase as curling or warping increases. This trend is reflected in Figure B2, but is not as significant if the Curl/Warp Effective Temperature Difference is less in magnitude than -10 °F since the difference between the -5 °F and -10 °F curves are hardly noticeable.

As is shown in Equation 17 (the smoothness model) the IRI is a regression equation developed based on field observations of faulting, cracking, and spalling with the regression coefficients for each distress being indicative of the relative strength of each correlation. One can notice that the coefficient applied to the faulting value is much higher than that applied to the cracking. Thus one would expect that faulting would have more influence on the smoothness than the cracking. This is logical since a simple crack does not affect the smoothness of the

pavement until movement occurs. This observation is difficult to see in Figure 4 since both the cracking and the faulting models are both sensitive to the curling and warping temperature differential. However, in the other inputs discussed, this trend will be more easily observed. Additionally, since the sensitivity of the smoothness model is dependent on the faulting and cracking model sensitivities, not every figure showing that sensitivity will be discussed. Instead, only those that emphasize what has been discussed or have particularly interesting trends will be discussed.

Joint Spacing

Joint spacing is a common aspect of JPCP design; however, the performance of those joints has never been modeled as it is in this program. As the name implies, it is simply the distance between transverse joints in the rigid pavement. The joint spacing in this study was varied from 10 to 20 feet as a continuous spacing for the length of the project.

As can be seen in Figures B4-B6, the pavement joint spacing is an important parameter in modeling pavement performance, especially in terms of designing to resist faulting. You can see that over the typical range of spacing that a smaller spacing will yield less faulting, as expected. One thing to keep in mind is that these joints are dowelled and therefore, it is reasonable to expect that closer joints would increase the likelihood that the cracking in the slab would take place at the dowelled joints. This would allow the dowels to resist the faulting at the cracks.

The results for cracking are also reasonable based on the rationale that the concrete will tend to crack at some fairly consistent interval, with that interval being dependent on the characteristics of the pavement section and the concrete mix. Based on this, one could infer that if the joints are placed at an interval smaller than the cracking interval, there would be little effect by decreasing the joint spacing. However, if the joints were placed at spacing larger than

that cracking interval, then there would be increased cracking in the pavement slab. This is reflected in Figure 6 in that for the smaller spacing, there is little difference in the performance models, but once the spacing is increased, a great increase in cracking occurs. It may appear that the data is in error since the percent slabs cracked is shown to be greater than 100%, but this occurs because of the normal distribution approach that the software uses in determining the 90% reliability model as discussed in the section titled “*MEPDG Performance Models.*”

As was discussed previously, since the faulting and cracking models are sensitive to the joint spacing, it is expected that the smoothness model is sensitive as well. This is evident in Figure B6. The sensitivity shown in the smoothness model is because of the high sensitivity of the cracking model when the spacing is larger than the cracking interval of the concrete along with the sensitivity of the faulting model.

Joint Sealant Type

As with joint spacing, the type of sealant used to seal the joints has long been considered in the design of the pavement, but the type selected was based only on what worked by experience and the project budget. The design software allows selection of three different types of sealant or no sealant at all. The sealants that the program allows the user to choose from are no sealant, liquid sealant, silicone sealant, or preformed sealant. One aspect with joint sealants that is difficult to quantify in a performance model is the maintenance that must take place to keep any joint sealant performing as intended. Nonetheless, the performance models’ sensitivity to the sealant type is shown below in Figures B7-B9.

The faulting sensitivity to joint sealant type shown in Figure B7 proves to be null. At first thought, one may want to think that the joint sealant type would have at least some effect on the faulting of the pavement. However, in reality, it is more likely a function of the maintenance

of the joint sealant, which would be very difficult to quantify in the model. A liquid sealant should have the same potential of protecting from infiltration of water through the joint as a preformed sealant if it is maintained to keep it performing properly. The difference lies in that a preformed sealant requires less maintenance than the liquid sealant, and maintenance is often the victim of budget cuts leading to poorly performing sealants.

Similar to the trend in the faulting model, the cracking model yields little sensitivity to the joint sealant selected. This is likely due to the fact that the maintenance issues between the sealant types is really what separates their performance and, again, that is difficult to quantify in a mathematical model.

The smoothness model shows slightly more sensitivity than might be expected due to the lack of sensitivity of the faulting and cracking model. However, the difference in the smoothness model lies between the preformed sealant and the other two sealants. This is because of what is shown in Equations 19 and 20 for accounting for spalling in the smoothness model. Equation 20 will be affected by whether or not the joint sealant is preformed. It is this effect that is being shown in Figure B9.

Joint Dowel Diameter

The joint dowel diameter allowed in the program ranges from 1.0 inches to 1.5 inches because this is the range over which the field sections that the models were built from varied, and is in fact a reasonable range for commonly used dowels.

The sensitivity of the faulting to the joint dowel diameter shown in Figure B10 shows that the faulting is highly influenced by the joint dowel diameter. This makes sense in that at the same spacing, the load that each dowel has to carry will not change, but a smaller dowel bar will

have less bearing surface thus less resistance to faulting. Based on this, the trend shown in Figure B10 makes sense. The larger bars yield less faulting than the smaller bars.

Figure B11 shows that the cracking model is not affected by the joint dowel diameter. This makes logical sense because as mentioned in the joint spacing discussion, cracking is a function of the pavement section and mix properties and results in some relatively consistent interval and does not consider the joint dowels. Where dowels do impact the slab cracking is when they become “locked” or where they do not allow the pavement to expand and contract with changes in temperature and moisture, but the size of the dowel doesn’t impact the likelihood of a dowel becoming locked.

Figure B12 shows well the trend already discussed that the smoothness model is affected by the faulting model much more so than the cracking model. The faulting model is highly sensitive to the dowel diameter but the cracking model shows no sensitivity. The fact that the smoothness model shows sensitivity to the dowel diameter supports the mathematical model showing that the faulting value is given more weight than the cracking model based on the regression coefficients.

Joint Dowel Spacing

The joint dowel spacing parameter is simply what the name states – the spacing between dowels at each transverse joint. The program only allows for a small range of values to be entered and the models were tested over a range of 10 - 14 inches, which is a typical range used for rigid pavement construction. The cracking model, shown in Figure B14, showed absolutely no difference over this range of values, which was expected and reinforced by the fact that the joint dowel diameter had no effect on the cracking. Additionally, while the faulting model was expected to show some sensitivity, over this small range, the faulting showed almost no

difference between spacings. Again, this is likely because of the small range of spacings that could be tested because it is logical that at some point the spacing would be so large that faulting would increase greatly because the stress at the joint could not be adequately transferred across the joint.

Edge Support

The edge support allowed in the model can be handled in two ways. The user can choose to use a widened slab on the edge of the pavement where the concrete slab extends beyond the traveled way, or the user can input a specific load transfer efficiency between the traveled way and the shoulder. The purpose of this edge support is so that the software can properly model the load distribution at the edge of the pavement. The comparison of each of these types of edge support are shown in Figures B16-B18 and discussed in the paragraphs that follow.

The faulting model shows some sensitivity to the type of edge support selected as can be seen in Figure B16. This is fairly reasonable to expect based on the fact that corner loading is one of the load locations that has shown to be important in the design of rigid pavements. If this loading at the corner can be distributed across the edge of the pavement, then the corner cracking will be reduced, as will be seen in Figure B17. In turn, if the corner cracking is reduced, the faulting associated with it will also be reduced. When Figure B16 is examined, one will notice that a 12-ft slab width yields the same result as no edge support, which would be expected if the lane width is 12 feet. However, if the slab is widened one foot to a width of 13 feet, the faulting decreases substantially. This is because the stresses at the corner of the slab are spread across the edge of the pavement as discussed earlier. However, additional widening to 14 feet has hardly any improvement over the 13 feet wide slab. The other option allowed under edge support is to specify load transfer efficiency for the edge support, whatever the type to be constructed will be.

These values would have to be determined by testing unless an estimate is made based on engineering judgment and experience. As was expected, as the load transfer efficiency increases, the faulting decreases.

As was discussed under Figure B16, the edge support is very important in predicting the corner cracking of a slab. This is very evident in Figure B17 showing the sensitivity of the cracking model to the chosen edge support. The same trend discussed concerning the faulting is followed by the cracking model, only at a more sensitive degree. The 12-ft wide slab and no edge support yield the same results, but at the 13-ft wide slab, substantial improvements in the pavements resistance to cracking were seen. No more improvements were made when the slab increased to 14-ft wide. The cracking model does show more sensitivity to the values of load transfer efficiency chosen, however, and as expected, higher load transfer efficiencies will lead to less cracking.

Once again, since both the cracking and faulting models show sensitivity to the edge support, the smoothness model should be sensitive as well. This is reflected in Figure B18.

PCC-Base Interface

The PCC-Base Interface is modeled as bonded or unbonded. If the interface is unbonded, meaning that the slab is not fixed to the base, then the slab will move independently of the base layer. For example, due to temperature changes, when the concrete slab expands or contracts, the base layer will not create any additional resistance to the movement. If the interface is bonded, then the concrete slab and base are fully connected and act as one unit. If the interface is selected to be bonded, an additional input is required stating at what age will be pavement loose the bonded quality and begin acting as unbonded. The sensitivity of the models to several interface options is represented in Figures B19-B21.

The PCC-base interface shows that it does not affect the faulting of a concrete pavement as shown in Figure B19. This makes sense because of the definition of the interface and the mechanism of faulting. The interface is defined to be bonded or unbonded based on how the pavement and subgrade interact during horizontal and/or lateral movement. Contrarily, faulting is the result of vertical movement. While there may be a slight amount of horizontal or lateral movement when vertical movement takes place, it would be negligible, thus faulting never would invoke the interface relationship between the concrete and the base.

Where faulting is a vertical movement, cracking can be the result of horizontal tensile strains resulting from expansion and contraction of the concrete slab. When this horizontal movement takes place, the interface properties of the slab become important in calculating the stresses and strains within the pavement, which in turn affects the damage produced in the slab. Figure B20 illustrates this phenomenon by showing the relative sensitivity of predicted cracking to the bonding condition of the base/slab interface. A trend that is noticed in the graph is that the 36 month bonded period is farther away from the unbonded condition than the 60 and 84 month bonded periods. This does not seem logical since a 36 month bonded period would become unbonded after that 36 month period and would then act as an unbonded pavement. It would then be logical for the 36 month curve to be closer to the unbonded curve rather than farther away. This is an area that the software and/or performance models might require further refinement.

Figure B21 shows that predicted pavement smoothness, as represented by IRI, is not sensitive to the base/slab interface. This seems reasonable due to the fact that the IRI model is more dependent on faulting (not sensitive) than cracking.

Base Erodibility Index

The base erodibility index in the terms of the program is described as “a numerical expression of the potential for a soil to erode considering the physical and chemical properties of the soil and the climatic conditions where it is located.” The index ranges from 1-Erosion Resistant to 5-Very Erodable, so by the naming convention, an index of 1 would be a better base material than one with an index of 5. Figures B22-B24 show the relationship between the performance models and the erodibility index.

The faulting model shows little sensitivity to the base erodibility index for this particular pavement section when one looks at the y-axis of the sensitivity graph. This is good because the base erodibility index is not a well defined input. It is a measure of the likelihood of the pavement losing its base support, but the baseline of the measurement is never established by the documentation of the program or design guide. This could be improved in future releases of the design guide, but until then, engineering judgment will have to be used in selecting the proper index value. It may be best to perform the specific analysis with different indices to test the specific sensitivity and use that information to select a reasonable value. The sensitivity of the faulting model to the erodibility index does seem logical, though, since pumping is one of the main mechanisms allowing faulting to occur. Pumping occurs when moisture infiltrates the joint, and when a load passes over the joint, the compression forces the moisture out of the joint, taking with it soil particles. This is essentially a form of erosion.

On the other hand, the cracking model shows little sensitivity to the erodibility index as can be seen in Figure B23. There is a slight difference, however, between indices 1-3 and 4-5, although this difference is very minor.

Since the faulting model showed little sensitive to the base erodibility index, the IRI model would be expected to reflect the same trend, and this is the case shown in Figure B24.

Surface Shortwave Absorptivity

The surface shortwave absorptivity is one of the many inputs of the new design software with which most pavement designers will not be familiar. It is defined by the design guide as “a property of the body surface and is dependent on the temperature of the body and the wavelength of the incident radiation. It is a dimensionless value and measured as a fraction of incident radiation that is absorbed by the body.” (4) In simpler terms, it is a measure of how much solar energy can be absorbed by the pavement surface and is dependent on the composition, color, and texture of the pavement surface. As for values, the Draft Design Guide recommends that for Level 1, the value be determined by laboratory testing although there is no AASHTO standard test for pavements. For Level 3, it recommends using a value between 0.70 and 0.90 correlating to aged PCC surface. Figures B25-B27 show how the performance models relate to the surface shortwave absorptivity.

While the surface shortwave absorptivity is a new parameter, several inferences can be made based on the definition of the parameter, and these are shown to be supported by the output of the design software. Since the surface shortwave absorptivity is a measure the solar energy that is absorbed by the pavement, this solar energy could cause a higher temperature at the surface of the pavement. This pavement temperature change would not appear to affect the faulting to a high degree. This is what is reflected in Figure B25. When the value of surface shortwave absorptivity is increased over the range of values recommended by the *MEPDG*, the faulting model only increases slightly.

On the other hand, Figure B26 shows that the cracking model is quite sensitive to the surface shortwave absorptivity. The cracking increases as the surface shortwave absorptivity increases. This trend follows the logical expectation based on the definition of the surface

shortwave absorptivity. It is realized by pavement designers that concrete will crack under high temperature because the material tries to expand creating thermal stresses in the concrete, leading to cracking. Well, this same phenomenon would occur when the solar energy absorbed by the pavement creates higher temperatures at the surface, and the thermal stresses created will result in cracks at the surface. These cracks will then propagate through the slab because of the concentration of stresses that occur at the tip of the crack.

The IRI model seems to be only slightly sensitive to the surface shortwave absorptivity. This is because the faulting model shows little sensitivity to the parameter.

Infiltration of Surface Water

The infiltration is measure of the amount of precipitation that will penetrate the pavement to contact the first layer of base material. This could be through pores, cracks, or joints in the pavements. It is measured as a percentage with the designer choosing 0%, 10%, 50%, or 100% of the precipitation infiltrating the pavement surface. The *MEPDG* recommends that the 10% option be chosen when a proactive maintenance program will be followed or when tied shoulders or widened slabs are used; otherwise, the 50% option should be taken. It states that the 100% will rarely be used for new or reconstructed pavements. The sensitivity of the performance models to the selected infiltration is shown in Figures B28-B30.

As can be seen in Figure B28, the faulting model is not very sensitive to the infiltration selected. Since there is a slight difference between no infiltration and the other selections, it appears that the model is only sensitive as to whether or not there is any infiltration. This trend really is not what was expected since one would think that a higher degree of infiltration would yield more faulting since the base and subgrade would loose strength due to the additional moisture.

The cracking model follows the same trend as the faulting model as can be seen in Figure B29. That trend is that the only real difference is noted when varying the infiltration is between no infiltration and a selection that allows any degree of infiltration.

The effect that the infiltration has on the smoothness model is negligible as shown in Figure B30. This is because the sensitivity of the faulting and cracking models where only slight and the smoothness model is a function of those two models.

Length of Drainage Path

The length of the drainage path is measured from the highest point on the cross section to the point where drainage occurs. For example, if pavement edge drains are used, the distance could be from the crown of the road to the drain pipe. If edge drains are not used, the distance could be from the crown to the centerline of a drainage ditch alongside the road. This parameter is used for calculation of the time it takes to drain the pavement. The drain time, in turn, will affect the subgrade and base strengths because of the exposure to moisture. The values were tested over a range of 12 feet to represent a single lane of traffic with edge drains to 24 feet to represent two lanes of traffic. The program will allow values that range from 5 feet to 25 feet. Figures B31-B33 show the relationship between the drainage path length and the performance models. While this parameter was included in the design software to calculate the time required to drain the pavement, the performance models show no sensitivity to variations in the drainage path for typical pavement sections.

Pavement Cross Slope

The pavement cross slope has long been an important parameter in roadway design, but was considered more from a geometric design standpoint rather than a pavement design view. It has always been realized that adequate cross slope was needed to drain surface runoff, but rarely

has it been included in affecting the pavement performance from a structural viewpoint. The software allows for a range of 0 to 5 percent for the cross slope, and the parameter was tested from 1 to 4 percent with the results being shown in Figures B34-B36. Similar to the pavement drainage path, the performance models show no sensitivity to the pavement cross slope. However, in design of the typical section, a cross slope should always be selected to provide positive drainage across the pavement so as to minimize standing water on the pavement, as well as for the safety of the users of the roadway.

Concrete Thickness

The thickness of concrete is obviously an important parameter the design of the pavement section. The program allows for a range from 1-inch to 20-inches for the thickness of the PCC layer. The parameter was tested over a more typical range of 6-inches to 18-inches and the results are discussed below Figures B37-B39.

Something very unusual was observed when looking at the sensitivity of the faulting model to the concrete thickness. As can be seen in Figure B37, the 10” thick pavement appears to have much more faulting than the 6” and 18” pavements. After comparing the input files for each of the pavements, there are not any differences between the files except for the thickness input for the pavement. Furthermore, the cracking model shown in Figure B38 appears to be reasonable in that the 10” pavement shows less cracking between the 6” and 18” pavement. Considering these things, it appears that there could be a error in the performance model or software code for faulting.

While the faulting model appears to have an error, the cracking model shows a logical trend that as the pavement thickness increases, the cracking decreases. Also, as Figure B38 shows, as the pavement increases in thickness, the gain in resistance to cracking decreases, and

the opposite is true as well. Notice that the 6” pavement exhibits much more cracking than the 10” pavement. This is logical in that as the pavement thickness decreases, the cracking increases.

Since the faulting model appears to have an error, and the smoothness model is dependent on that faulting model, the smoothness model, too, is in error.

Concrete Unit Weight

The concrete unit weight is another parameter that is familiar to concrete pavement designers even though it was not considered in the current and past editions of the AASHTO pavement design procedures. It was, however, measured for quality control purposes. Traditionally, concrete was assumed to have a unit weight of 150 pounds per cubic foot (pcf), but the program allows for a range from 140 to 160 pcf. This is the range over which the sensitivity of the program was tested and the data shown in Figures B40-B42.

The faulting model is quite sensitive to the concrete unit weight. Figure B40 shows that when the unit weight of the concrete decreases, then the faulting of the pavement will increase. This is expected based on the discussion summarized in Table 1, specifically Equation 4. The concrete unit weight is used to estimate the Modulus of Elasticity if that is not directly input into the program. Since this study focused on Level 3 inputs, the Modulus of Elasticity was indeed estimated from the concrete unit weight. Therefore, the sensitivity shown for the concrete unit weight will coincide with the sensitivity to the Modulus of Elasticity.

Traditionally, the unit weight of concrete is assumed to be 150 pounds per cubic foot, however, there are many aspects of the concrete mix that can affect the unit weight. The aggregate types and amounts, the amount of cement, and the amount of water, all will impact the unit weight of the resultant concrete mix. Since the unit weight of the mix does impact the

model, the actual unit weight of the mix to be used should be input into the software to ensure the model is as accurate as possible. While some agencies may not directly test this parameter for quality control, many contractors do test this parameter to verify the yield of the concrete delivered to the site. Because of this, the test is not uncommon or difficult to perform, and actually, it is a test that must be performed to achieve certification by the American Concrete Institute (ACI) as a concrete testing technician.

Similar to the faulting model, the cracking model shown in Figure B41 is also sensitive to the concrete unit weight. However, while the lighter concrete mix showed more faulting, it shows less cracking than a heavier mix. For the same reason as the faulting model, once again, the actual unit weight of the mix should be entered to ensure the integrity of the model.

Since the faulting and the cracking models are both sensitive to the unit weight, the smoothness model should be sensitive to the unit weight, as well. This is not reflected in Figure B42 as evidently as was expected. However, since the relationship between faulting and unit weight is the opposite of the relationship between cracking and unit weight, the changes in the two models tend to offset one another when reflected in the smoothness model.

Poisson's Ratio

Poisson's Ratio is commonly used by material scientists and engineers; however, it has never been explicitly considered in pavement design until now. Poisson's Ratio is defined as the ratio of lateral to longitudinal strain when a material is loaded in the longitudinal direction. (4) The *MEPDG* states that the Poisson's Ratio has little effect on the response models but is required for computation of the stresses and strains within the pavement. A typical range of values for PCC slabs is 0.15 to 0.25 (4) and this is the range of values shown in Figures B43-B45.

The Poisson's Ratio is a very important parameter in calculating the stresses and strains in the pavement, as has already been stated. This is further emphasized in the performance models response to variations in the Poisson's Ratio of the concrete. Specifically, in the faulting model, the sensitivity is not too great, but the Poisson's Ratio does have some effect. This is likely due to the mechanism of joint faulting being a vertical strain in the subgrade and has little to do with the concrete parameters aside from being able to support the bearing stress caused by the dowel bars. This is where the Poisson's Ratio likely comes into play, and the effect is shown in Figure B43.

The real effect of the Poisson's Ratio on the predicted performance of a concrete pavement is reflected in Figure B44, showing the sensitivity of the cracking model to the parameter. Since cracking is the result of lateral strain created under vertical loading, the Poisson's Ratio, by definition, would be extremely important in predicting a pavements tendency to crack. This is reflected in the cracking model's sensitivity to the Poisson's Ratio as shown in the Figure B44. As the Poisson's Ratio increases, meaning that the lateral strain in the pavement is higher relative to the longitudinal strain, the cracking model shows more cracking.

Figure B45 shows that the IRI model is only slightly sensitive to the Poisson's Ratio, despite the fact that the cracking model is so sensitive to the Poisson's Ratio. This is because, as has already been stated, the smoothness model is much more sensitive to the faulting than the cracking in the pavement, as it should be. Since the faulting is not very sensitive to variations in the Poisson's Ratio, in turn, the smoothness model is not as well.

Coefficient of Thermal Expansion

The coefficient of thermal expansion is the change in unit length per degree of temperature change. In the case of the design software, it is reported per °F x 10⁻⁶. This is an

important parameter because the curling stress is very sensitive to the coefficient of thermal expansion. (4) The coefficient of thermal expansion of the concrete is really a composite value of that of the components of the mix. It can be tested directly as the concrete mix or it can be calculated as a weighted average of the materials comprising the mix. The *MEPDG* gives a range of values to use for the coefficient of thermal expansion for different aggregate types and cement pastes for use in the weighted average method. A range of values for concrete in general is also given. The sensitivity of the performance models to the concrete coefficient of thermal expansion is shown in Figures B46-B48.

As can be seen in Figure B46, the sensitivity of the performance models were tested over a range of 3 to 9 ($\times 10^{-6} \text{ } ^\circ\text{F}^{-1}$), while the typical values for a concrete pavement are between 4 and 7 according to the *MEPDG*. (4) Within this range, the faulting model is very sensitive to coefficient of thermal expansion. This is in line with the fact that this parameter greatly influences the curling stresses. These curling stresses can directly lead to faulting at the joints in addition to contributing to corner cracking.

The coefficient of thermal expansion is also important to the cracking model; however, the influence is smaller within the range of typical values that the *MEPDG* suggests. Figure B47 shows that within the range of 4 – 7, the cracking model is only slightly sensitive, however if the value of the thermal expansion is larger than this range, the cracking will greatly increase. This shows that the designer should be assured that the mix used for the concrete pavement be within the range of typical values.

Since the faulting and cracking models showed sensitivity to the coefficient of thermal expansion, the smoothness model is also expected to be sensitive to the parameter. This is shown in Figure B48.

Thermal Conductivity

The program defines the thermal conductivity as the “ratio of heat flux to temperature gradient.” It is “a measure of the uniform flow of heat through a unit thickness, when two faces of unit area are subjected to a unit temperature difference.” This is an important parameter because it defines how much heat can penetrate the pavement increasing the temperature to create differentials and stresses within the pavement. (5) The *MEPDG* does not give much guidance as to selection of values except that for Level 1, it should be tested directly (ASTM E1952) and for Level 3, it typically ranges from 1.0 to 1.5 BTU/ft-hr-°F with a typical value being 1.25 BTU/ft-hr-°F. (4) However, similar to the coefficient of thermal expansion, it will be a composite value of the materials that enter the concrete mix. It is also dependent on the density of the material because the air contained in the pores of the concrete will not transfer heat efficiently. (5) The results from the performance models when the thermal conductivity was varied over the typical range are shown in Figures B49-B51.

As can be seen in Figure B49, the faulting model shows some sensitivity to the thermal conductivity; however, this effect is not great. In a practical sense, concrete pavement could expand due to increased temperatures. If there is not adequate room for the pavement to expand, likely because the joints were not properly designed or maintained, then the concrete could crack under compression at the joint. In extreme cases, a blow-up could occur. However, such considerations would be difficult to quantify for design purposes.

Unlike the faulting, the cracking model is quite sensitive to the thermal conductivity of the concrete. This is shown in the high degree of change in the cracking prediction for various values of thermal conductivity. This is expected because of what was stated in the introduction of the parameter. The thermal conductivity is a measure of how much heat can pass through the

pavement, thus creating temperature differentials and thermal stresses that would lead to thermal cracks. The trend shown in Figure B50 is that the cracking model is much more sensitive to values below the typical value of 1.25 suggested by the *MEPDG* than it is to values higher. In both cases, however, a lower value for thermal conductivity yields more cracking.

Since the cracking model is so sensitive to the thermal conductivity, and the faulting shows some sensitivity, a similar trend is expected for the smoothness mode. This trend is, indeed, reflected in Figure B51.

Heat Capacity

Selection of values for the heat capacity of concrete is similar to thermal conductivity in that for Level 1, the *MEPDG* recommends laboratory testing of the mix (AASHTO D2766) and for Level 3, a value within the typical range be chosen. The typical range is from 0.20 to 0.28 BTU/lb-°F with a recommended value of 0.28 BTU/lb-°F. (4) Unlike thermal conductivity and coefficient of thermal expansion, this value has little to do with the cement type or aggregates placed into the mix. However, the heat capacity has been found to be effected by the water-cement ratio, porosity, water content, and temperature of the concrete. (5)

Figures B52-B54 show the response of the performance models to varying the heat capacity of the recommended range. Figure B52 shows that the faulting model is not very sensitive to the heat capacity within the typical range of values and acts similarly to the thermal conductivity. Contrarily, the cracking model of Figure B53 does show sensitivity to the heat capacity. This is likely because of the temperature gradients within the pavement will cause tensile stresses resulting in cracking. However, since neither one of the faulting or cracking models have high sensitivity to the heat capacity, the smoothness model is relatively unaffected by changes in the input for heat capacity.

Cement Type

The cement type is another input that has been considered in concrete pavement design but not from a standpoint of performance of the pavement over its life. Instead, the cement type was selected based on whether or not a fast setting mix was needed, for example. The program allows for selection of Type I, Type II, and Type III cements. Type I cement is the most common cement type and does not have any particularly special properties. Type III cement, on the other hand, will reach high strengths earlier than Type I, and is often used when it is necessary to allow traffic onto the pavement soon after the concrete is placed. Type II cement is often used when a low heat of hydration and standard set time is desired.

Figures B55-B57 show how the performance models respond to the different cement types. The sensitivity of the models to the cement type is very minimal, but the same trend is followed throughout all of the models. That trend is that Type III cement will yield more faulting and cracking, most likely because of the relationship between its strength gain and heat of hydration. Since the strength gain occurs quickly, this means that more cement is being hydrated. This cement hydration is an exothermic reaction meaning that it releases heat as the reaction occurs. This fast set time and excess heat can contribute to thermal and shrinkage cracking if proper curing precautions are not taken. The cracking can then allow for faulting since the cracks will likely occur where there are no dowels to transfer loads across the crack.

Cement Content

The cement content is simply the measure of the weight of cement used in the concrete mix. It has not been directly considered in previous concrete pavement design methods; however, the compressive strength and modulus of rupture (which are functions of cement content, but more so the w/c) have been considered. The cement content will also affect other

overall properties of the concrete because as more cement is introduced, the effect of the water and aggregates to the mix will change. Using a range of 500 to 700 lb, Figures B58-B60 show the response of the performance models to the range of cement content.

The sensitivity of the faulting model to the cement content shown in Figure B58 shows that faulting is minimally effected by the cement content. This does stand to reason in one respect. That is that, often, faulting is the result of a loss of support at the edge of the joint and not the strength of the concrete. However, a stronger concrete would be able to support greater loads without support, but such strength is not common in pavements.

The cracking model show almost no response in variations of the cement content as can be seen in Figure B59. This was somewhat unexpected, because of the additional heat generated during hydration with more cement would increase the likelihood of thermal cracking.

Since the cracking and faulting models did not show much sensitivity to the cement content, the IRI model should not show much sensitivity either. This was the case reflected in Figure B60.

Water-Cement Ratio

The water-cement ratio (w/c) is another parameter considered in mix design, similar to the cement content, but not traditionally considered in structural pavement design. The w/c also has similar effects as the cement content to the concrete properties. The w/c was tested over a broad range of values from 0.30 to 0.55 with the results being presented in Figures B61-B63. The w/c followed nearly the same trend as the cement content, which was expected since the two influence the same characteristics of a concrete mix. Neither the cracking nor faulting modes show much sensitivity to changes in the w/c, and, therefore, neither did the smoothness model.

Aggregate Type

The aggregate type is a completely new parameter to structural concrete pavement design. In the past, the aggregate type was just accepted as what was available and no consideration made about the effect on the performance of the pavement aside from desiring a high strength aggregate and compensating for D-cracking, alkali reactive aggregates, or other aggregate related distresses. As was already discussed about the coefficient of thermal expansion, the aggregate type influences this value which has a high influence on pavement stresses. The aggregate types that the program allows the user to choose from a list which includes Basalt, Chert, Dolomite, Gabbro, Granite, Limestone, Quartz, Ryolite, and Syenite. Figures B64-B66 show the performance responses to the aggregate type.

As can be seen in Figures B64-B66, none of the performance models are affected by the aggregate type chosen except for the cracking model which shows less cracking only when Limestone is selected as the aggregate. While this is the case, the aggregate material properties would definitely impact the material properties of the concrete mix. For example, it has already been discussed that the coefficient of thermal expansion is often determined by the aggregate type chosen in the mix. Since this information can be more specifically entered into the program at that point, it is not reflected in the model based on the aggregate type selection. Other considerations with aggregates are their size and angularity which also impacts the faulting and cracking of a concrete pavement because of the bond strength between the cement paste and aggregate, as well as, aggregate interlock at the joints. This type of information is not inherent to any particular mineral type of aggregate; instead, it has more to do with the source and processing of the aggregate.

PCC Set Temperature

The PCC set temperature is called the zero stress temperature within the program; however, the PCC set temperature is more descriptive of the input. It is simply the temperature of the concrete at the time of set. The program allows for a range from 50°F to 125°F, however, the values were tested over a more typical range of 110 – 125°F. The values over the higher range are due to the fact that the concrete will generate heat through the hydration process, and while there will be heat loss in colder conditions, the heat generated by the concrete remains fairly constant. Figures B67-B69 show that the performance models are not sensitive to the set temperature within the tested range of values.

The *MEPDG* does not give much information on the impact of the set temperature to the calculation of the pavement stresses; however, based on the sensitivity of the models to varying the set temperature, there does not seem to be much of an impact. In fact, the cracking model shows no sensitivity whatsoever. Figures B67-B69 show how the models changed if the PCC set temperature was varied.

Ultimate Shrinkage at 40% R.H. (microstrain)

The ultimate shrinkage is the shrinkage strain when exposed to extended drying conditions at 40% relative humidity. The 40% relative humidity was chosen as a standard for this design guide. (4) The *MEPDG* gives guidance as to the selection of the ultimate shrinkage by recommending that for Level 1, laboratory testing should be used, but for Levels 2 & 3, there are equations to estimate the input. The program allows a range from 300 to 1000 microstrain, but the input was tested over a range of 600 to 800 microstrain and shown in Figures B70-B72.

The figures do not show much sensitivity to the ultimate shrinkage aside from the slight sensitivity of the faulting model. The faulting model shows that when the shrinkage is higher, then slightly more faulting will occur than if the shrinkage were lower. This makes sense

because as each slab shrinks between joints, then the aggregate interlock at the joint is reduced because of the additional space between the joints. Furthermore, this creates a greater distance for the dowels to transfer load, thus reducing the efficiency of the load transfer causing one side of the joint to carry a larger percentage of the total load.

Reversible Shrinkage

The reversible shrinkage is defined as the amount of shrinkage that can be recovered when the drying concrete slab is rewetted. The *MEPDG* does not give a great deal of guidance on values for the input except for stating that unless more reliable information is available, a value of 50 percent of the ultimate shrinkage be recommended. The input was tested over a range of 40 to 65 percent. Figures B73-B75 show the sensitivity of the performance models to changes in the reversible shrinkage.

Even at the range tested, the models have little to no response at variations in the value for reversible shrinkage. For this reason, the 50% default value seems to be reasonable for all pavements.

Time to Develop 50% Ultimate Shrinkage

The time to develop 50% ultimate shrinkage is defined by its name. Once again, little guidance is given in the Draft Design Guide as to selection of values to input for this parameter. Essentially, it can be tested to determine a specific value of the mix, or the ACI suggested value of 35 days can be used. (4) Figures B76-B78 show the performance models' response to variations of the time to develop 50% ultimate shrinkage. Similar to the reversible shrinkage, the time to develop 50% ultimate shrinkage has practically no effect on the performance models. Once again, the default suggested value of 35 days should suffice for nearly all mixes.

Curing Method

The curing method is another parameter that has never been considered directly in rigid pavement design. However, it has been considered to be important and often included in construction specifications. Now the effect of the curing method to the pavement performance has been considered and is shown in Figures B79-B81. The program allows for the selection of either wet curing or the use of a curing compound, but not a selection for natural curing. The curing method does show that the performance models respond differently to the different curing methods, but the difference is not at all profound.

28-day Modulus of Rupture

The modulus of rupture, which the software uses as a measure of flexural strength, measured at 28 days of curing has always been recognized as a very important parameter in concrete pavement design. It has been included in the rigid pavement design procedures published by AASHTO ever since the AASHTO Road Test. As was discussed about the performance models, the software uses the modulus of rupture to calculate the modulus of elasticity, which along with Poisson's Ratio, is used directly in calculating the pavement stresses and strains to transfer to pavement response models. Those performance models' responses to variations in the flexural strength are shown in Figures B82-B84.

The faulting model does not show any sensitivity to the Modulus of Rupture of the concrete as can be seen in Figure B82. This stands to reason since the mechanism for faulting is often associated with a loss of support at the joint or lack of load transfer across the joint. Neither of these mechanisms is affected a great deal by the concrete strength. The trend does show that a higher flexural strength will yield less faulting, however. This difference is likely due in part to the increased resistance to corner cracking often found in conjunction with faulting.

While the faulting model shows little sensitivity to the flexural strength of the concrete, the cracking model, as shown in Figure B83, proves to be much more sensitive. This, too, stands to reason, since traffic loads tend to “flex” a concrete slab – producing tensile strains in the bottom of the slab which lead to crack development and propagation. The trend of the cracking model is that a higher flexural strength will yield less cracking, but that as the flexural strength increases, the gain in resistance to cracking becomes less. This also seems logical, because once the concrete reaches a strength that is adequate to carry the loads, then there is no need for additional strength. This is one of the benefits of this program – that the pavement can be tailored to the specific conditions to yield the most economical design, potentially eliminating over-design.

While the smoothness model is impacted most by the faulting of a pavement, in this case, the cracking model’s significant sensitivity to the flexural strength is why the IRI shows the sensitivity shown in Figure B84. Additionally, Equation 19 shows that the strength of the concrete is factored directly into the spalling of the pavement, and the spalling value has a large impact on the smoothness based on the coefficient that is applied in the smoothness model.

28-day Compressive Strength

While it has been recognized that the compressive strength of concrete is not the best parameter to model the performance characteristics of a concrete pavement since pavements fail due to tension more often than compression, the compressive strength of a mix is probably the material property with which pavement designers and contractors are most familiar. Similar to the flexural strength, the compressive strength is used to determine the PCC modulus of elasticity which is used in determining the pavement stresses and strains, and ultimately the

performance responses. The sensitivity of the performance responses to the 28-day compressive strength is shown in Figures B85-B87.

The trends observed in Figures B85-B87 are nearly identical to those discussed about the modulus of rupture or flexural strength. This is because in the program, the two can be selected to be used individually or together. Since this research only focuses on the sensitivity of the models to one specific input and not interactions between inputs, they were tested individually. When only one of the properties is input into the program, the software uses Equation 7 to convert between modulus of rupture and compressive strength of the concrete for use in the performance models.

CHAPTER THREE

FLEXIBLE PAVEMENT DESIGN

Overview of Flexible Pavement Design

The *MEPDG* software utilizes the M-E approach in analyzing a theoretical pavement section provided by a designer. Ultimately, it is important to recognize that the resulting predicted performance of the theoretical pavement is significantly influenced by the characterization of the traffic loadings, environmental conditions, and material properties. The primary thrust of this research is to assess the relationship between each input and the predicted response model for a given pavement section.

Out of the many techniques available to determine the stresses, strains, and deformations in a flexible pavement, two flexible pavement analysis methods have been incorporated into the *MEPDG* software. The JULEA multilayer elastic theory program is used to determine the pavement response for pavements that are treated as linearly elastic while the 2-D finite element system code (2SD2D) developed by Dr. C. Desai is used to determine the pavement response where unbound material nonlinearity is also considered [6].

Once the pavement response is determined, transfer functions relate the pavement responses to pavement damage. Transfer functions relate the theoretical computation of “damage” at some critical point in a pavement with measured distress to complete the M-E loop of the pavement design. The *MEPDG* accumulates damage in increments, usually on a monthly basis, over an entire design period. Within each increment, critical stresses and/or strain values are calculated and converted to incremental distresses, which include percent damage for top down and bottom up fatigue cracking, total depth for rutting, and IRI for pavement smoothness. Incremental damage for all distresses are summed and output at the end of each analysis period

by the *MEPDG* software [6]. Therefore, a designer can check the extent of each distress at a particular time period (for instance at the 10 year/120 month point), and make changes to the pavement design in order to meet required compliance levels.

MEPDG Material Inputs

The primary inputs required for flexible pavement analysis in the *MEPDG* include the following:

- Traffic loading
- Pavement cross-section
- Poisson’s ratio for each layer
- Elastic modulus for each layer
- Thickness of each layer
- Coefficient of thermal expansion (*I*)

From the inputs provided, the stresses, strains, and displacements, at “critical” locations within the pavement structure, are calculated. Three critical strains are determined using equations 21-23 using two material properties for each layer, the Poisson’s ratio, μ , and the elastic modulus, E .

$$\text{Major strain:} \quad \varepsilon_z = (1/E)[\sigma_z - \mu(\sigma_r + \sigma_t)] \quad \text{Eq. 21}$$

$$\text{Intermediate strain:} \quad \varepsilon_r = (1/E)[\sigma_r - \mu(\sigma_t + \sigma_z)] \quad \text{Eq. 22}$$

$$\text{Minor strain:} \quad \varepsilon_t = (1/E)[\sigma_t - \mu(\sigma_r + \sigma_z)] \quad \text{Eq. 23}$$

where E = Elastic modulus
 μ = Poisson’s ratio
 σ_z = Major stress
 σ_r = Intermediate stress
 σ_t = Minor stress

Based on equations 21-23, it is evident that the user is required to provide the Elastic modulus, E , and the Poisson’s ratio, μ , of each HMA layer in order to calculate the strains that will be used in

the performance models. The *MEPDG* software allows three hierarchical “levels” of inputs for the material properties, E and μ ; this hierarchical approach was discussed previously.

Poisson’s Ratio

In the *MEPDG* software, the Poisson’s ratio is a user-supplied input. However, a Level 1 approach to determine the Poisson’s ratio of a mix is not necessary until pavement response models are implemented that utilize non-linear moduli to model dilation effects on the pavement response on a regular basis in the *MEPDG* software. Therefore, it is recommended that a designer use the typical Level 2 or Level 3 Poisson’s ratio values provided in the software. Under level 2, there are three sublevels to estimate the Poisson’s ratio as explained below: [7]

- Level 2A: Use equation 24 with user defined parameters a and b estimated for specific mixtures.

$$\mu_{ac} = 0.15 + \frac{0.35}{1 + e^{(a+bE_{ac})}} \quad \text{Eq. 24}$$

where μ_{ac} = Poisson’s ratio of an asphalt mixture at a specific temperature.
 E_{ac} = Modulus of an asphalt mixture at a specific temperature, psi.

The a and b parameters can be developed from a regression analysis of laboratory estimated modulus mixture values and Poisson’s ratios.

- Level 2B: Use equation 25 with typical a and b values to estimate Poisson’s ratio.

$$\mu_{ac} = 0.15 + \frac{0.35}{1 + e^{(-1.63+3.84 \times 10^{-6} E_{ac})}} \quad \text{Eq. 25}$$

where μ_{ac} = Poisson’s ratio of an asphalt mixture at a specific temperature.
 E_{ac} = Modulus of an asphalt mixture at a specific temperature, psi.

- Level 2C: Select from typical range of Poisson’s ratio shown in the Table 2.

| Temperature, °F | Level 2C, μ range |
|-----------------|-----------------------|
| < 0 °F | < 0.15 |
| 0 – 40 °F | 0.15 – 0.20 |
| 40 –70 °F | 0.20 – 0.30 |
| 70 – 100 °F | 0.30 – 0.40 |
| 100 – 130 °F | 0.40 – 0.48 |
| >130 °F | 0.45 – 0.48 |

Table 2: Typical Poisson’s ratio ranges for input Level 2C for dense-graded HMA

Typical values for Level 3 Poisson’s ratio are shown in Table 3:

| Temperature, °F | Level 3, μ |
|-----------------|----------------|
| < 0 °F | 0.15 |
| 0 – 40 °F | 0.20 |
| 40 –70 °F | 0.25 |
| 70 – 100 °F | 0.35 |
| 100 – 130 °F | 0.45 |
| >130 °F | 0.48 |

Table 3: Typical Poisson’s ratio ranges for input Level 3 for dense-graded HMA

Dynamic Modulus

The *MEPDG* uses the dynamic modulus (E^*), rather than elastic modulus, to characterize the stiffness of hot mix asphalt (HMA). There are several procedures to determine the Dynamic modulus of the HMA based on the input level chosen in the *MEPDG* software. Table 4 shows different procedures for deriving the dynamic modulus at various hierarchical levels [7].

The dynamic modulus, E^* , of hot-mix asphalt concrete (HMA) is a function of several properties including temperature, rate of loading, age, and mixture characteristics (e.g. air voids, binder content, and mix gradation). In order to account for the effects of rate of loading and temperature, the E^* is determined by constructing a Master Curve at the reference temperature of 70°F. Master Curves are constructed based on the principles of time-temperature superposition –

that is, once a reference temperature is determined, the data at various temperatures are shifted with respect to time (rate of loading) until the curves converge to form a single smooth function.

| Material Group Category | Input Level | Description |
|-------------------------|-------------|--|
| Asphalt materials | 1 | <ul style="list-style-type: none"> Conduct E* dynamic modulus laboratory (NCHRP 1-28A) at loading frequencies and temperatures of interest for the given mixture. Conduct binder complex shear modulus (G*) and phased angle (δ) testing on the proposed asphalt binder (AASHTO T315) at $\omega = 1.59$ Hz (10 rads/s) over a range of temperatures. From binder test estimate Ai-VTSi for mix compaction temperature. Develop master curve for the asphalt mixture that accurately defines the time-temperature dependency including aging. |
| | 2 | <ul style="list-style-type: none"> No E* laboratory test required. Use E* predictive equation. Conduct binder complex shear modulus (G*) and phased angle (δ) testing on the proposed asphalt binder (AASHTO T315) at $\omega = 1.59$ Hz (10 rads/s) over a range of temperatures. The binder viscosity or stiffness can also be estimated using conventional asphalt test data such as Ring and Ball Softening Point, absolute and kinematic viscosities, or using Brookfield viscometer. Develop Ai-VTSi for mix-compaction temperature. Develop master curve for the asphalt mixture that accurately defines the time-temperature dependency including aging. |
| | 3 | <ul style="list-style-type: none"> No E* laboratory test required. Use E* predictive equation. Use typical Ai-VTSi values provided in the Design Guide software based on PG, viscosity, or penetration grade of the binder. Develop master curve for the asphalt mixture that accurately defines the time-temperature dependency including aging. |

Table 4: Asphalt dynamic modulus (E*) estimation at various hierarchical input levels for new or reconstructed design

The master curve of modulus formed as a function of load rate relays the time dependency of the material, and the shifting of data at various temperatures to form the master curve relays the temperature dependency of the material. Hence, it is imperative that both the master curve and the shift factors are known to completely describe the effects of the rate of loading and time on a particular mix. Figure 3 shows an example of a Master Curve constructed in this manner and the resulting shift factor [7].

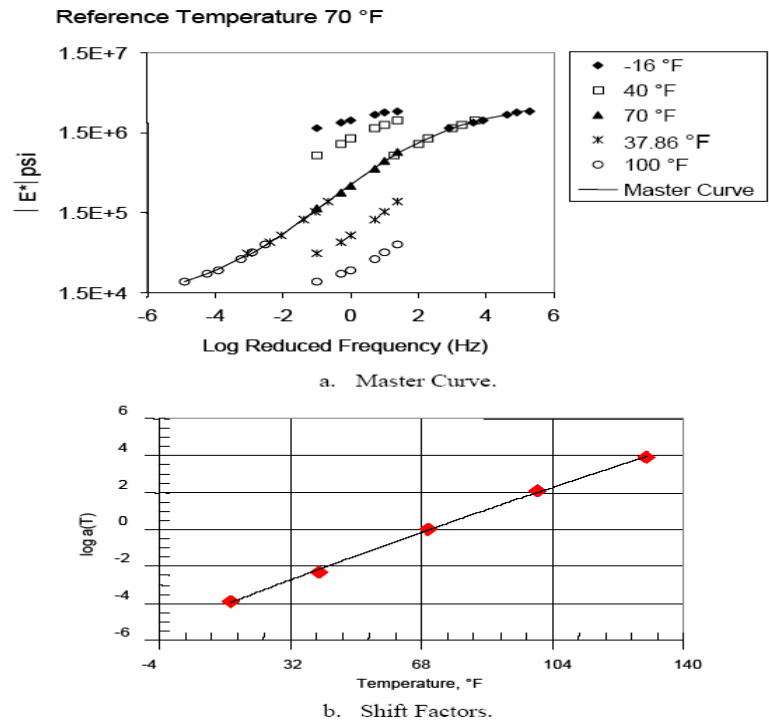


Figure 2: Schematic of Master Curve and Shift Factor

Equation 26 describes the sigmoidal function that represents the dynamic modulus master curve:

[7]

$$\log(E^*) = \delta + \frac{\alpha}{1 + e^{\beta + \gamma \log(t_r)}} \quad \text{Eq. 26}$$

- where E^* = dynamic modulus, psi.
 t_r = time of loading at the reference temperature.
 δ, α = fitting parameters, for a given set of data, δ represents the minimum value of E^* and $\delta + \alpha$ represents the maximum value of E^* .
 β, γ = parameters describing the shape of the sigmoidal function.

The fitting parameters, δ and α , depend on the aggregate gradation, binder content, and air void content while the fitting parameters, β and γ , depend on the characteristics of the asphalt binder and the magnitude of δ and α ". The shift factors for the master curve can be best described by the following equations 27a and 27b. [7]

$$t_r = \frac{t}{a(T)} \quad \text{Eq. 27a}$$

$$\log(t_r) = \log(t) - \log[a(T)] \quad \text{Eq. 27b}$$

where t_r = time of loading at the reference temperature.
 t = time of loading at the given temperature of interest.
 $a(T)$ = shift factor as a function of temperature.
 T = temperature of interest.

Therefore with Equation 27a, the time of loading at the reference temperature can be calculated for any time of loading at any temperature and used in Equation 26 to calculate the corresponding E^* value.

The viscosity of the asphalt binder at the temperature of interest is an important parameter in the development of the master curve and shift factors discussed earlier. The viscosity of the asphalt binder at the temperature of interest can be determined from the ASTM viscosity-temperature relationship equation shown by Equation 28, which only works for unaged conditions. [7]

$$\log \log \eta = A + VTS \log T_R \quad \text{Eq. 28}$$

where η = viscosity, cP.
 T_R = temperature, Rankine.
 A = regression intercept.
 VTS = regression slope of viscosity temperature susceptibility.

The procedures to determine the A and VTS values for the three different levels in the *MEPDG* software are shown in Table 4 earlier. Alternately, there will be further subsequent discussion concerning these parameters for input Level 2 and 3.

Level 1 E^* values can be calculated by developing master curves and corresponding shift factors using the procedures described in Table 4. However, due to technical complications with the *MEPDG* software, only Level 3 runs could be completed for this research. Therefore, a

designer can only determine the Level 3 Dynamic modulus, E^* using the E^* predictive equation shown as Equation 29 (also applicable to Level 2 E^*). The Level 3 E^* predictive equation incorporated in the *MEPDG* software is based on the recalibrated Witczak-Fonseca Dynamic Modulus Predictive Equation developed by Witczak and colleagues at the University of Maryland. This equation was chosen because it was considered to be able to accurately predict the E^* of asphalt mixtures over a range of temperatures, rates of loading, and aging conditions, regardless of the range of aggregate gradations, and does not lose accuracy at extreme temperatures/frequency conditions. (2)

$$\begin{aligned} \log E^* = & 3.750063 + 0.02932\rho_{200} - 0.001767(\rho_{200})^2 \\ & - 0.002841\rho_4 - 0.058709V_a - 0.802208\left(\frac{V_{beff}}{V_{beff} + V_a}\right) \\ & + \frac{3.871977 - 0.0021\rho_4 + 0.003958\rho_{38} - 0.000017(\rho_{38})^2 + 0.005470\rho_{34}}{1 + e^{(-0.603313 - 0.313351\log(f) - 0.393532\log(\eta))}} \end{aligned} \quad \text{Eq. 29}$$

where E^* = dynamic modulus, psi.
 η = bitumen viscosity, 10^6 Poise.
 f = loading frequency, Hz.
 V_a = air void content, % by volume.
 V_{beff} = effective bitumen content, % by volume.
 ρ_{34} = cumulative % retained by the $\frac{3}{4}$ in sieve.
 ρ_{38} = cumulative % retained by the $\frac{3}{8}$ in sieve.
 ρ_4 = cumulative % retained on the No. 4 sieve.
 ρ_{200} = cumulative % retained by the No. 200 in sieve.

Equation 29 can also be represented by the sigmoidal function (Equation 26) repeated below:

$$\log(E^*) = \delta + \frac{\alpha}{1 + e^{\beta + \gamma \log(t_r)}}$$

where E^* = dynamic modulus, psi.
 t_r = time of loading at the reference temperature.
 δ = Minimum value of E^* .
 $\delta + \alpha$ = Maximum value of E^* .
 β, γ = parameters describing the shape of the sigmoidal function.

and:

$$\delta = 3.750063 + 0.02932\rho_{200} - 0.001767(\rho_{200})^2 - 0.002841\rho_4 - 0.058097V_a - 0.802208\left[\frac{V_{beff}}{V_{beff} + V_a}\right]$$

$$\alpha = 3.871977 - 0.0021\rho_4 + 0.003958\rho_{38} - 0.000017\rho_{38}^2 + 0.005470\rho_{34}$$

$$\beta = -.603313 - .393593 \log(\eta T_r)$$

$$\log(t_r) = \log(t) - c(\log(\eta) - \log(\eta T_r))$$

$$\gamma = 0.313351$$

$$c = 1.255882$$

It is evident from the earlier discussion on Equation 26 that the parameter δ is a function of aggregate gradation, effective binder content, and air void content while the parameter α is a function of aggregate gradation. Thus, the minimum and maximum values of E^* are in fact independent of the binder stiffness. Therefore, in order to account for binder effects, the relationship between binder viscosity and temperature must first be established. This can be done by converting the binder stiffness data at each temperature to viscosity using equation 30. The parameters of the ASTM VTS equation are then found by the linear regression of Equation 31 after log-log transformation of the viscosity data and log transformation of the temperature data.

$$\eta = \frac{G^*}{10} \left(\frac{1}{\sin \delta} \right)^{4.8628} \quad \text{Eq. 30}$$

$$\log \log \eta = A + VTS \log T_r \quad \text{Eq. 31}$$

where G^* = binder complex shear modulus, Pa.
 δ = binder phase angle, °.
 η = viscosity, cP.
 T_r = temperature in Rankine at which the viscosity is estimated.
 A, VTS = regression parameters.

For a Level 2 E*, the viscosity-temperature relationship can be established using various methods described in Table 4 earlier. After the viscosity-temperature relationship is established, the master curve for Level 2 can be developed using Equation 26.

Level 2 shift factors for the master curve are derived from Equation 32.

$$\log(t_r) = \log(t) - 1.25588(\log(\eta) - \log(\eta T_r)) \quad \text{Eq. 32}$$

where t_r = reduced time, sec.
 t = loading time, sec.
 η = Viscosity at the age and temperature of interest, CPoise.
 ηT_r = Viscosity at reference temperature and RTFO aging, CPoise.

Based on equation 26, it is obvious that the shift factors are only dependent on the binder viscosity for the age and temperature of interest and the RTFOT aged viscosity at the reference temperature. The viscosity at the age and temperature of interest are calculated using the global aging model.

The method to develop the master curve at input Level 3 is similar to that described in Level 2 earlier. The only difference is the usage of default A and VTS values available in the *MEPDG*, in place of those derived from laboratory testing. Since there is no laboratory testing required, the A and VTS values can be estimated if the following is known:

- Binder Performance Grade (PG) based on AASHTO M320.
- Binder Viscosity Grade based on AASHTO M226.
- Binder Penetration Grade based on AASHTO M20.

Tables 5, 6, and 7 represent the recommended A and VTS values based on the criteria listed above [7].

| High Temp Grade | Low Temperature Grade | | | | | | | | | | | | | | |
|-----------------|-----------------------|--------|--------|--------|--------|--------|--------|--------|--------|--------|--------|--------|--------|--------|-------|
| | -10 | | -16 | | -22 | | -28 | | -34 | | -40 | | -46 | | |
| | VTS | A | VTS | A | VTS | A | VTS | A | VTS | A | VTS | A | VTS | A | |
| 46 | | | | | | | | | | -3.901 | 11.504 | -3.393 | 10.101 | -2.905 | 8.755 |
| 52 | -4.570 | 13.386 | -4.541 | 13.305 | -4.342 | 12.755 | -4.012 | 11.840 | -3.602 | 10.707 | -3.164 | 9.496 | -2.736 | 8.310 | |
| 58 | -4.172 | 12.316 | -4.147 | 12.248 | -3.981 | 11.787 | -3.701 | 11.010 | -3.350 | 10.035 | -2.968 | 8.976 | | | |
| 64 | -3.842 | 11.432 | -3.822 | 11.375 | -3.680 | 10.980 | -3.440 | 10.312 | -3.134 | 9.461 | -2.798 | 8.524 | | | |
| 70 | -3.566 | 10.690 | -3.548 | 10.641 | -3.426 | 10.299 | -3.217 | 9.715 | -2.948 | 8.965 | -2.648 | 8.129 | | | |
| 76 | -3.331 | 10.059 | -3.315 | 10.015 | -3.208 | 9.715 | -3.024 | 9.200 | -2.785 | 8.532 | | | | | |
| 82 | -3.128 | 9.514 | -3.114 | 9.475 | -3.019 | 9.209 | -2.856 | 8.750 | -2.642 | 8.151 | | | | | |

Table 5: Recommended RTFO A and VTS parameters based on asphalt PG grade

| Grade | A | VTS |
|--------|---------|---------|
| AC-2.5 | 11.5167 | -3.8900 |
| AC-5 | 11.2614 | -3.7914 |
| AC-10 | 11.0134 | -3.6954 |
| AC-20 | 10.7709 | -3.6017 |
| AC-30 | 10.6316 | -3.5480 |
| AC-40 | 10.5338 | -3.5104 |

Table 6: Recommended RTFO A and VTS parameters based on asphalt viscosity grade

| Grade | A | VTS |
|---------|---------|---------|
| 40-50 | 10.5254 | -3.5047 |
| 60-70 | 10.6508 | -3.5537 |
| 85-100 | 11.8232 | -3.6210 |
| 120-150 | 11.0897 | -3.7252 |
| 200-300 | 11.8107 | -4.0068 |

Table 7: Recommended RTFO A and VTS parameters based on asphalt penetration grade

Level 3 shift factors are also derived following the methods discussed for Level 2 shift factors. However, the shift factors depend only on binder viscosity for the temperature of interest

and the RTFOT aged viscosity at the reference temperature. Again, the viscosity at the temperature of interest can be obtained using Equation 30.

The discussions associated with Equations 24 to 32 shows the flexibility of the *MEPDG* software in dealing and using multilevel inputs for various material characteristics to determine the necessary parameters used in the pavement performance models. It is important to note that no matter what level input designs are used, the computational damage algorithm remains the same. This means that the same model and procedures are used to predict distress and smoothness regardless of the input levels used. Therefore, if a Level 1 input, i.e. a Level 1 E^* value, is used along with a different Level 3 input, i.e. a Level 3 Poisson's ratio value, the software will mathematically change the Level 3 Poisson's ratio into an equivalent Level 1 Poisson's ratio, and then compute the damage with both inputs using a similar performance model, i.e. the Rutting Model.

Flexible Pavement Performance Models

There are three performance models that are incorporated in the *MEPDG* software to aid a designer in creating the best pavement structure that can handle the needs of the traffic facility over a given time period. The three models are:

- Fatigue cracking model (top-down and bottom-up)
- Rutting model
- Pavement Smoothness (IRI) model

There is also a thermal cracking model included in the software; however, results of this research showed that for all the types of inputs varied over the chosen ranges, none of the results obtained indicated any significant change in pavement performance for thermal cracking. These results were to be expected since all of the runs only used one specific climate. Furthermore, all of the

runs were made using the low temperature binder grades (PG 64-22, 70-22, 76-22), which were proven to be reliable throughout the state of Arkansas.

All three pavement performance models (fatigue cracking, rutting, and smoothness) are developed from regression equations created using the data from Long Term Pavement Performance (LTPP) pavement sections and the data from several research projects tied to the NCHRP 1-37A project. Since the models are based on regression equations, solutions produced by the models represent an “average”, coinciding with a 50 percent reliability solution – that is, about half of the observations would be less than the reported solution while another half of the observations would be greater. Obviously, using a 50 percent reliability pavement design is insufficient for real life applications and is not cost effective.

To counter this problem, the *MEPDG* software allows a designer to analyze a theoretical pavement using a higher reliability. Hence, if a designer chooses to work with a 90 percent reliability analysis, the software will proceed by using a normal distribution curve where the distress calculated at 90 percent reliability will be shifted by the product of the standard deviation of the model and the standard normal deviate (Z) for the specified reliability. The inclusion of this reliability analysis in the software helps reduce the chances that a designer would produce an underdesigned pavement.

Fatigue Cracking Model (Top-down and Bottom-up)

The *MEPDG* uses an approach that models both the top-down and bottom-up cracking in a HMA pavement based on calculating the fatigue damage at the surface for the top-down cracking and at the bottom of the asphalt layer for the bottom-up cracking. The fatigue damage, estimated through the Miner’s Law equation shown in Equation 33, is then interrelated to the fatigue cracking using calibrated data [8].

$$D = \sum_{i=1}^T \frac{n_i}{N_i} \quad \text{Eq. 33}$$

where D = damage.
T = total number of periods.
n_i = actual traffic for period i.
N_i = traffic allowed under conditions prevailing in i.

The fatigue cracking model used in the *MEPDG* software has been calibrated based on 82 LTPP sections located in 24 states. The final model used in the software, based on the recalibrated Asphalt Institute MS-1 fatigue model, is shown in Equations 34a to 34c. [8]

$$N_f = 0.00432 * k'_1 * C \left(\frac{1}{\varepsilon_t} \right)^{3.9492} \left(\frac{1}{E} \right)^{1.281} \quad \text{Eq. 34a}$$

$$C = 10^M \quad \text{Eq. 34b}$$

$$M = 4.84 \left(\frac{V_b}{V_a + V_b} - 0.69 \right) \quad \text{Eq. 34c}$$

where N_f = number of repetitions to fatigue cracking.
ε_t = tensile strain at critical location.
E = stiffness of the material
V_a = air voids, %.
V_b = effective binder content, %

The parameter “k’₁” serves to provide a correction for different asphalt layer thickness (h_{ac}) effects and can be defined by equations 35a and 35b. [8]

i. For bottom-up cracking

$$k'_1 = \frac{1}{0.000398 + \frac{0.003602}{1 + e^{(11.02 - 3.49 * h_{ac})}}} \quad \text{Eq. 35a}$$

ii. For top-down cracking

$$k'_1 = \frac{1}{0.01 + \frac{12}{1 + e^{(15.676 - 2.8186 * hac)}}}$$
Eq. 35b

where hac = total thickness of the asphalt layers, in.

The final transfer function to calculate the fatigue cracking from the fatigue damage is expressed in equations 36a and 36b.

i. Bottom-up cracking (% of total lane area)

$$FC_{bottom} = \left(\frac{6000}{1 + e^{(C_1 * C'_1 + C_2 * C'_2 * \log_{10}(D * 100))}} \right) * \left(\frac{1}{60} \right)$$
Eq. 36a

where FC_{bottom} = bottom-up fatigue cracking, percent lane area.
 D = bottom-up fatigue damage.
 C_1 = 1.0
 C'_1 = $-2 * C'_2$
 C_2 = 1.0
 C'_2 = $-2.40874 - 39.748 * (1 + hac)^{-2.856}$

N = 461 observations.
 S_e = 6.2 percent.
 S_e/S_y = 0.947

ii. For top-down cracking (feet/mile)

$$FC_{top} = \left(\frac{1000}{1 + e^{(7.0 - 3.5 * \log_{10}(D * 100))}} \right) * (10.56)$$
Eq. 36b

where FC_{top} = top-down fatigue cracking, ft/mile.
 D = top-down fatigue damage.

N = 414 observations.
 S_e = 1242.25 ft/mile.
 S_e/S_y = 0.977

Rutting Model

The *MEPDG* uses an approach that models both the primary and secondary stages of rutting, where the primary stage is modeled using the extrapolated secondary stage trend. The

tertiary stage of rutting is not considered in the *MEPDG* due to difficulty in testing and a lack of prediction methodology for implementation. The three stages of rutting can be briefly described as the following: [8]

- Primary stage: high initial level of rutting, with a decreasing rate of plastic deformations, predominantly associated with volumetric change.
- Secondary stage: small rate of rutting exhibiting a constant rate of change of rutting that is also associated with volumetric changes; however, shear deformations increase at increasing rate.
- Tertiary stage: high level of rutting predominantly associated with plastic (shear) deformations under no volume change conditions.

The *MEPDG* Rutting model also assumes that there is no permanent deformation that occur for chemically stabilized layers, bedrock, and PCC fractured slab materials. Therefore, a predictive rutting system was developed to account for permanent deformation in all rut-susceptible layers (asphaltic materials and all unbound material layers) within a specified analysis period where individual layer rut depths are predicted for each layer as a function of traffic repetition and time. This system also allows for the prediction of total rut depth. [8]

As with the fatigue cracking model mentioned before, the rutting model in the *MEPDG* software was also calibrated based on 88 LTPP new sections located in 28 states. The final model used in the software, is shown in Equations 37a and 37b. [8]

$$\frac{\varepsilon_p}{\varepsilon_r} = k_1 * 10^{-3.4488} T^{1.5606} N^{0.479244} \quad \text{Eq. 37a}$$

and

$$\varepsilon_r = \frac{1}{|E^*|} (\sigma_z - \mu\sigma_x - \mu\sigma_y) \quad \text{Eq. 37b}$$

where ϵ_p = Accumulated plastic strains at N repetition of loads, in/in.
 ϵ_r = Resilient strain of the asphalt material as a function of mix properties, temperature, and time rate of loading, in/in.
N = Number of load repetitions.
T = Temperature, °F.

The parameter “ k_1 ”, based on trench studies from the MnRoad test site, serves to provide as accurate a rut depth prediction model as possible and can be defined by equations 38a to 38c. [8]

$$k_1 = (C_1 + C_2 * depth) * 0.328196^{depth} \quad \text{Eq. 38a}$$

$$C_1 = -0.1039 * h_{ac}^2 + 2.4868 * h_{ac} - 17.342 \quad \text{Eq. 38b}$$

$$C_2 = 0.0172 * h_{ac}^2 - 1.7331h_{ac} + 27.428 \quad \text{Eq. 38c}$$

where k_1 = function of total asphalt layers (h_{ac} , in), and depth ($depth$, in) to computational point, to correct for confining pressure at different depths.

R^2 = 0.648
N = 387 observations.
 S_e = 0.063 in.
 S_e/S_y = 0.574

Smoothness Model

The *MEPDG* uses the International Roughness Index (IRI) model to calculate pavement smoothness at any particular time over the design life of the pavement. The IRI model was developed under a separate NHCRP project that correlates IRI over time to the site and structural features of flexible pavements. The IRI model allows a designer to directly enter potential occurrences of distresses while modeling smoothness. In addition, the IRI model also accounts for climatic and geographic factors through the use of the “site factor” term (Equation 39b). The model used to calculate IRI for conventional flexible pavements with thick granular base is shown in Equation 39a. [8]

$$IRI = IRI_o + 0.0463 \left(SF \left[e^{\frac{age}{20}} - 1 \right] \right) + 0.00119(TCL)_T + 0.1834(COV_{RD})$$

Eq. 39a

$$+ 0.00384(FC)_T + 0.00736(BC)_T + 0.00155(LC_{SNWP})_{MH}$$

where IRI_o = IRI measured within six months after construction, m/km.
 $(TCL)_T$ = Total length of transverse cracks (low, medium, and high severity levels), m/km.
 (COV_{RD}) = Rut depth coefficient of variation, percent.
 $(FC)_T$ = Total area of fatigue cracking (low, medium, and high severity levels), percent of wheel path area, %.
 $(BC)_T$ = Total area of block cracking (low, medium, and high severity levels), percent of total lane area, %.
 $(LC_{SNWP})_{MH}$ = Medium and high severity sealed longitudinal cracks outside the wheel path, m/km.
Age = Age after construction, years.

$$SF = \left[\frac{(R_{SD})(P_{0.075} + 1)(PI)}{2 \times 10^4} \right] + \left[\frac{\ln(FI + 1)(P_{0.02} + 1)(\ln(R_m + 1))}{10} \right]$$

Eq. 39b

RSD = Standard deviation in the monthly rainfall, mm.
 R_m = Average annual rainfall, mm.
 $P_{0.075}$ = Percent passing the 0.075 mm sieve.
 $P_{0.02}$ = Percent passing the 0.02 mm sieve.
 PI = Plasticity index.
 FI = Annual average freezing index.

There are two inputs, block cracking, and longitudinal cracking outside the wheel path, which are included in the smoothness equation, but not covered in the *MEPDG*. The equations to calculate these inputs are only included in the smoothness model since it is not discussed elsewhere. Equations 40 and 41 are used to calculate these inputs. [8]

$$(BC)_T = \frac{100}{1 + \exp^{(DP - 1.008age)}}$$

Eq. 40

where DP = potential level of block cracking and is defined in Table 8.

| Level “DP” | Value | Standard Error (Se) |
|------------|-------|---------------------|
| High | 10 | 13.6 |
| Medium | 20 | 6.0 |
| Low | 30 | 2.9 |
| None | 40 | 0.0 |

Table 8: DP values for block cracking

Equation 40 has an asymptotic value of 100, representing 100 percent cracking. Furthermore, Table 8 shows the standard error calculated for each distress potential equation.

$$(LC_{SNWP})_{MH} = 2000 \exp[DP - 0.15age] \quad \text{Eq. 41}$$

where DP = potential level of longitudinal cracks outside the wheel path and is defined in Table 9.

| Level “DP” | Value | Standard Error (Se) |
|------------|-------|---------------------|
| High | 1.9 | 176.6 |
| Medium | 3.4 | 32.5 |
| Low | 5.0 | 44.2 |
| None | 8.5 | 0.0 |

Table 9: DP values for longitudinal cracking outside the wheel path

Equation 41 has an asymptotic value of 2000 which means that the model will have a maximum value of 2000 meters in one-kilometer length.

Research Approach

A four phase action plan was devised to complete the objectives of the study.

Phase I: Perform multiple runs of a standard pavement section while varying one input at a time.

Phase II: Determine the degree to which each input affected the pavement distress prediction and check the results of the runs for rationality when compared to the models used.

Phase III: Identify limitations of the runs of Phase I and make improved runs that are more realistic to predicted pavement performance response.

Phase IV: Determine specific inputs to alter to affect and improve overall pavement performance with respect to certain models (i.e. Rutting Model).

Phase I

Phase I represents the bulk of the work required to proceed to Phases II, III, and IV. The first task in Phase 1 was determining the specific inputs that would be varied within the scope of the research (HMA material inputs). A list of the inputs that were considered and analyzed can be found in Appendix C. The second task of Phase 1 was to determine the appropriate base values that would be used for each run, which is also documented in Appendix C. The final task of Phase 1 was to make multiple runs using the determined base values and varying only one input at a time using the values shown.

Phase II

Upon completion of Phase I, the data was analyzed to determine those inputs having significant impact on the predicted performance of the HMA pavement with respect the three distress models discussed earlier. In this phase, a one-way ANOVA analysis will be required to confirm the analysis made by making reference from the plots of results obtained by the variance of each input. This is probably the most important phase of the research since the results of this phase will allow a designer to work more efficiently with the software as well as allow him or her to make recommendations on the types of inputs that would require more quality control attention and vice versa. For instance, if the result of varying the parameter of surface shortwave absorptivity (SSA) shows no significant changes in the three distress plots, a designer may then choose to ignore that parameter and use the default values provided in the *MEPDG*. However, if

the results show significant change in the distress plots, then he or she may have to perform further research to determine the general and influential range of values of that parameter.

Phase III

This phase encompassed additional runs needed after the analysis of the initial runs in Phase II. Since the *MEPDG* software is not completely working yet, all initial flaws and failed runs were analyzed, and a new set of runs were performed that accounted for incorrect assumptions that were discovered from Phase I and Phase II. For instance, it was discovered that the Air Void and Percent Binder Effective parameter was in terms of percent by volume instead of percent by weight as initially assumed. In addition, it was discovered that Air Voids required as-constructed values rather than design values. Therefore, a new set of runs that used a larger range of Air Voids values along with the original and recalculated Percent Binder Effective values were conducted to cover initial mistakes.

Phase IV

In this phase, the results of the three previous phases were used to determine the relationship between each input and each distress. This phase is also very important since it allows a designer to determine which input to alter in order to obtain better results in certain distresses. For instance, if a pavement section was found to meet the fatigue cracking and the IRI model but not the rutting model, a designer would only need to alter specific inputs that are influential to the rutting model based on the results determined by this phase. This would save a designer time and effort since he or she would not have to adjust each input in order to meet design specifications.

RESULTS AND ANALYSIS

As stated previously, due to technical complications of the software no Level 1 or Level 2 type runs could be completed. Therefore, all the runs that will be discussed in the following sections are Level 3 runs. After the completion of each run, the *MEPDG* software displays the following results:

1. Input summary.
2. Output summary.
3. Flexible summary, including tabular and graphical output of the performance models.

To determine the sensitivity of each input with respect to the performance models, a number of runs were performed in which one input was varied at a time. Then, a tabular summary of the results of the variation of each input were compiled and graphs generated in order to produce performance plots that showed the effects of the variation of each input for comparison purposes.

The following sections will discuss the results of the Phase I and Phase III runs.

One feature of the analysis of project data involves a statistical comparison of predicted pavement distress when varying a particular design input. Strictly speaking, a statistical analysis may not be entirely warranted for these comparisons; the data being compared are not randomly drawn from defined populations. Rather, the data was output (“answers”) from mathematical models. As such, the data do not comprise a population. Further, the prediction error associated with the distress models is not known – suggesting that a given predicted distress value is not truly a discreet quantity.

The preceding discussion notwithstanding, it is useful to assess relative changes in predicted distress using statistical tools. Such analyses help the designer evaluate the relative sensitivity of distress prediction models to given inputs. In other words, the statistical results may provide a qualitative assessment of sensitivity in lieu of a strict quantitative determination.

Combined with the other evaluative methods used in this project, the statistical analyses provide a more comprehensive picture of the distress prediction models contained in the M-E Design Guide.

Phase II Analysis of Phase I Results

It is important to note that the Phase 1 runs were made based on the predetermined base input values shown in Table C1 of Appendix C. It was later discovered that two of the base input values, the Air Voids (AV), and the Percent Binder Effective (P_{be}), which was calculated based on “design” and percent by weight respectively, were actually too low since further reading of the *MEPDG* software manual indicated that AV should be reported “as constructed” while P_{be} should be reported in terms of percent by volume. Table 10 shows the inputs that were varied in the Phase I runs as well as the range of values chosen.

| Input | Range of values |
|--------------------------------------|-------------------------|
| Poisson’s ratio | 0.30/ 0.35 /0.40 |
| Surface Shortwave Absorptivity (SSA) | 0.80/ 0.85 /0.90 |
| Heat Capacity (HC) | 0.10/ 0.23 /0.50 |
| Thermal Conductivity (TC) | 0.50/ 0.67 /1.00 |

* Values in bold indicate the default values used in the software.

Table 10: Phase I inputs that were varied and the corresponding range values

The comparison graphs for each input in the Phase I runs can be found in Appendix D. For each input, a one-way ANOVA was performed using the reported damage for each performance model with respect to pavement age at a time interval of 5 years, 10 years, 15 years, and 20 years. The results of the one-way ANOVA analysis will be used to further consolidate any uncertainties of the conclusions drawn from the graphical analysis of the comparison graphs for each input. Table 11 shows the results of the one-way ANOVA analysis performed on each input in Phase I.

| Input | Performance model | F crit. | F | Significance |
|-----------------|---|---------|------------|--------------|
| Poisson's ratio | Surface down cracking (surface) (SDC 1) | 4.2565 | 1.3041 | I |
| | Surface down cracking (0.5") (SDC 2) | 4.2565 | 1.5106 | I |
| | Bottom up Cracking (BUD) | 4.2565 | 0.1163 | I |
| | Rutting | 4.2565 | 0.5276 | I |
| | IRI | 4.2565 | 4.2365E-05 | I |
| SSA | Surface down cracking (surface) (SDC 1) | 4.2565 | 0.5469 | I |
| | Surface down cracking (0.5") (SDC 2) | 4.2565 | 0.6063 | I |
| | Bottom up Cracking (BUD) | 4.2565 | 0.1241 | I |
| | Rutting | 4.2565 | 0.1462 | I |
| | IRI | 4.2565 | 4.0167E-05 | I |
| HC | Surface down cracking (surface) (SDC 1) | 4.2565 | 0.1681 | I |
| | Surface down cracking (0.5") (SDC 2) | 4.2565 | 0.2705 | I |
| | Bottom up Cracking (BUD) | 4.2565 | 0.0953 | I |
| | Rutting | 4.2565 | 0.6721 | I |
| | IRI | 4.2565 | 4.2293E-05 | I |
| TC | Surface down cracking (surface) (SDC 1) | 4.2565 | 0.0168 | I |
| | Surface down cracking (0.5") (SDC 2) | 4.2565 | 0.0164 | I |
| | Bottom up Cracking (BUD) | 4.2565 | 0.0014 | I |
| | Rutting | 4.2565 | 0.0084 | I |
| | IRI | 4.2565 | 0 | I |

* I = Insignificant
S = Significant

Table 11: Phase I One-way ANOVA results

The results of the Phase I ANOVA analysis for all four inputs indicated that there is insufficient evidence to conclude that there is a significant difference in the reported damage for all three performance models with respect to pavement age. This means that the variation of values for each of the four inputs listed in Table 11 does not have a significant impact on the results of the performance models. Further inspections of the comparison plots (shown in Appendix D) for each input also support this conclusion. However, due to the fact that all of the Phase I runs were done using a low effective binder percent and a low air void content, the results of these runs may be flawed. Therefore, to check the validity of the conclusions for the Phase I results, a new set of runs were performed. The results of the new set of runs will be further discussed in the following section.

Phase III Results

After realizing the flaws of the initial runs performed in Phase I, a new set of runs was devised to verify the results of the Phase I runs. In the Phase III runs, a new set of gradation data, obtained from concurrent projects related to the *MEPDG*, was used. The gradation data used (shown in Appendix E) includes four 12.5 mm mixes and four 25.0 mm mixes from four different sources, Arkhola (ARK), Granite Mountain Quarry (GMQ), Jet Asphalt (JET), and McClinton-Anchor (MCA), currently available in Arkansas. To verify the results of the four parameters tested in Table 11, a new set of runs using the inputs shown in Table C2 of Appendix C, were conducted. Furthermore, another set of runs to observe the effects of Air Void content, Binder Grade, and Total Unit Weight, were conducted using the inputs shown in Table C3 and C4 of Appendix C. The inputs for the runs performed to analyze the effects of Percent Binder Effective are shown in Table C5 and C6 of Appendix C. The results of each parameter analyzed in the Phase III runs will be discussed in the following sections.

Poisson's Ratio

The Poisson's ratio is defined as the ratio of the lateral strain to the axial strain. The Poisson's ratio was tested at values of 0.30, 0.35, and 0.40, with 0.35 being the default value given by the software. Table 12 shows the summary of results for the one-way ANOVA analysis performed on the output of the Phase III Poisson's ratio runs for each pavement performance model based on different gradation mixes. It is clear that the results of the ANOVA analysis from the Phase III runs coincide with the results from Phase I runs even though new gradations, air void content, and percent binder effective values were used. In fact, further inspections of the comparison plots created from Phase I (Figure 1D to 5D) and the comparison plots from Phase III (Figure 21D to 40D) show the same trends in all three performance model plots, the fatigue cracking plot which is divided into three separate plots (top down cracking plot at surface and

0.5” depth, and bottom up cracking plot), the rutting plot, and the IRI plot. Both fatigue cracking and rutting plots showed similar linear increases in maximum damage with respect to time as the Poisson’s ratio value decreases while the IRI plots showed no changes in IRI values regardless of the value of the Poisson’s ratio used.

| Source | Performance model | F crit. | F | Significance |
|-----------|---|---------|----------|--------------|
| ARK 70-22 | Surface down cracking (surface) (SDC 1) | 4.2565 | 1.1083 | I |
| | Surface down cracking (0.5”) (SDC 2) | 4.2565 | 1.3556 | I |
| | Bottom up Cracking (BUD) | 4.2565 | 0.1081 | I |
| | Rutting | 4.2565 | 0.7209 | I |
| | IRI | 4.2565 | 2.07E-05 | I |
| GMQ 70-22 | Surface down cracking (surface) (SDC 1) | 4.2565 | 0.9196 | I |
| | Surface down cracking (0.5”) (SDC 2) | 4.2565 | 1.1531 | I |
| | Bottom up Cracking (BUD) | 4.2565 | 0.0959 | I |
| | Rutting | 4.2565 | 0.6812 | I |
| | IRI | 4.2565 | 1.42E-05 | I |
| JET 70-22 | Surface down cracking (surface) (SDC 1) | 4.2565 | 1.0186 | I |
| | Surface down cracking (0.5”) (SDC 2) | 4.2565 | 1.2482 | I |
| | Bottom up Cracking (BUD) | 4.2565 | 0.1000 | I |
| | Rutting | 4.2565 | 0.7270 | I |
| | IRI | 4.2565 | 2.07E-05 | I |
| MCA 70-22 | Surface down cracking (surface) (SDC 1) | 4.2565 | 0.9612 | I |
| | Surface down cracking (0.5”) (SDC 2) | 4.2565 | 1.1899 | I |
| | Bottom up Cracking (BUD) | 4.2565 | 0.0991 | I |
| | Rutting | 4.2565 | 0.6867 | I |
| | IRI | 4.2565 | 2.07E-05 | I |

* I = Insignificant
S = Significant

Table 12: Phase III One-way ANOVA results for Poisson’s ratio

Based on the results of both the ANOVA analysis and the comparison plots, it is reasonable to conclude that the Poisson’s ratio does not have a significant impact on pavement performance models. Therefore, as Huang states in his book, “it is customary to assume a reasonable value for use in design, rather than to determine it from actual tests”. [9]

Surface Shortwave Absorptivity (SSA)

The *MEPDG* states that the SSA of a layer is dependent on three factors, the composition, the color, and the texture, of a layer. This parameter correlates with the amount of

solar energy that is absorbed by a layer. The amount of solar energy absorbed will naturally affect the temperature regime within the pavement structure and the associated structural response. In general, darker, less reflective surfaces such as a fresh coat of HMA, have higher SSA than lighter, more reflective surfaces. Since this is a new parameter in the *MEPDG*, there is currently no method, laboratory testing, or correlations, to determine the Level 1 or Level 2 SSA input. The SSA was tested at 0.80, 0.85, and 0.90, with 0.85 being the default value given by the software. Table 13 shows a summary of the one-way ANOVA analysis performed on the results of the SSA Phase III runs.

| Source | Performance model | F crit. | F | Significance |
|-----------|---|---------|----------|--------------|
| ARK 70-22 | Surface down cracking (surface) (SDC 1) | 4.2565 | 0.4180 | I |
| | Surface down cracking (0.5") (SDC 2) | 4.2565 | 0.4586 | I |
| | Bottom up Cracking (BUD) | 4.2565 | 0.0961 | I |
| | Rutting | 4.2565 | 0.1379 | I |
| | IRI | 4.2565 | 1.33E-05 | I |
| GMQ 70-22 | Surface down cracking (surface) (SDC 1) | 4.2565 | 0.3833 | I |
| | Surface down cracking (0.5") (SDC 2) | 4.2565 | 0.4213 | I |
| | Bottom up Cracking (BUD) | 4.2565 | 0.1082 | I |
| | Rutting | 4.2565 | 0.1347 | I |
| | IRI | 4.2565 | 2.07E-05 | I |
| JET 70-22 | Surface down cracking (surface) (SDC 1) | 4.2565 | 0.3821 | I |
| | Surface down cracking (0.5") (SDC 2) | 4.2565 | 0.4128 | I |
| | Bottom up Cracking (BUD) | 4.2565 | 0.1106 | I |
| | Rutting | 4.2565 | 0.1454 | I |
| | IRI | 4.2565 | 3.04E-05 | I |
| MCA 70-22 | Surface down cracking (surface) (SDC 1) | 4.2565 | 0.3900 | I |
| | Surface down cracking (0.5") (SDC 2) | 4.2565 | 0.4307 | I |
| | Bottom up Cracking (BUD) | 4.2565 | 0.1091 | I |
| | Rutting | 4.2565 | 0.1339 | I |
| | IRI | 4.2565 | 3.05E-05 | I |

* I = Insignificant
S = Significant

Table 13: Phase III One-way ANOVA results for SSA

As with the Poisson's ratio Phase III runs discussed before, the ANOVA analysis of the SSA Phase III runs also depict similar results with those obtained from the SSA Phase I runs. General observations of Figure 41D to Figure 60D in comparison to Figure 6D to Figure 10D indicated

that although the gradations, air voids content, and the percent binder effective has been modified, the trends of the graphs still fell along the same manner. The fatigue cracking and rutting comparison plots for all four gradation mixes showed that when SSA increased, the maximum damage in fatigue cracking and rutting depth increased. There was almost no change in the IRI plots for all four gradation mixes for the three SSA values tested.

Based on the results of the ANOVA analysis and the graphical analysis of the comparison plots for each performance model, it can be concluded that there is insufficient evidence to prove that there is a significant difference in the reported damage for all three performance models with respect to pavement age. This conclusion was to be expected since the SSA parameter was not present in all three of the performance model equations. Therefore, it would be advisable to use the default SSA value given in the DG M-E software when performing any HMA pavement analysis.

Heat Capacity (HC)

The *MEPDG* defines the HC parameter as the amount of heat energy, Q , needed to change the temperature of one unit mass by one degree. The Level 1 input for this parameter can be obtained through direct measurement by means of the ASTM D 2766 “Specific Heat of Liquid and Solids” test. As with the SSA, there are no current correlations for a Level 2 HC input while the Level 3 HC can be obtained by using agencies’ historical data or the recommended default values given by the software. Although the recommended Level 3 HC range of values given by the software was between 0.22 – 0.40 Btu/(lb)(°F), the following HC values of 0.10, 0.23, and 0.50, were used to check the sensitivity of the parameter at the maximum ends of the recommended spectrum. Table 14 shows the results of the one way ANOVA analysis performed on the results of the HC Phase III runs.

| Source | Performance model | F crit. | F | Significance |
|-----------|---|---------|----------|--------------|
| ARK 70-22 | Surface down cracking (surface) (SDC 1) | 4.2565 | 0.0367 | I |
| | Surface down cracking (0.5") (SDC 2) | 4.2565 | 0.0468 | I |
| | Bottom up Cracking (BUD) | 4.2565 | 0.1547 | I |
| | Rutting | 4.2565 | 0.6281 | I |
| | IRI | 4.2565 | 3.05E-05 | I |
| GMQ 70-22 | Surface down cracking (surface) (SDC 1) | 4.2565 | 0.0499 | I |
| | Surface down cracking (0.5") (SDC 2) | 4.2565 | 0.0437 | I |
| | Bottom up Cracking (BUD) | 4.2565 | 0.1765 | I |
| | Rutting | 4.2565 | 0.5993 | I |
| | IRI | 4.2565 | 3.05E-05 | I |
| JET 70-22 | Surface down cracking (surface) (SDC 1) | 4.2565 | 0.0539 | I |
| | Surface down cracking (0.5") (SDC 2) | 4.2565 | 0.0450 | I |
| | Bottom up Cracking (BUD) | 4.2565 | 0.1852 | I |
| | Rutting | 4.2565 | 0.6627 | I |
| | IRI | 4.2565 | 5.64E-05 | I |
| MCA 70-22 | Surface down cracking (surface) (SDC 1) | 4.2565 | 0.0429 | I |
| | Surface down cracking (0.5") (SDC 2) | 4.2565 | 0.0402 | I |
| | Bottom up Cracking (BUD) | 4.2565 | 0.1757 | I |
| | Rutting | 4.2565 | 0.5982 | I |
| | IRI | 4.2565 | 3.91E-05 | I |

* I = Insignificant
S = Significant

Table 14: Phase III One-way ANOVA results for Heat Capacity

By comparing the results of the ANOVA analysis from Table 11 before and the results shown in Table 14, it is fairly obvious that the results of the Phase I and Phase III runs have not significantly changed despite the use of new gradations, air void content, and percent binder effective. Further graphical analysis of the comparison plots created from the results of the run supported the results of the ANOVA analysis since there was no significant change in the gradient of the Phase III plots (Figure 61D to Figure 80D), from those obtained through the Phase I runs (Figure 11D to Figure 15D). The only noticeable trend from both phases occurred in both SDC and BUD plots where the maximum damage for HC = 0.50 increased at a steeper gradient than the other two values of HC used. This may be due to the fact that the HC value of 0.50 used was beyond the recommended range value of the *MEPDG* software.

However, based on the results of the ANOVA and graphical analysis of the Phase III HC runs, it is safe to conclude that there was insufficient evidence to prove that there was a significant difference in the reported damage for all three performance models with respect to pavement age. This conclusion was also to be expected since the HC parameter was not used in any of the performance model equations. Therefore, it would be advisable to use the default HC value of 0.23 given by the DG M-E software whenever performing any HMA pavement analysis.

Thermal Conductivity (TC)

The *MEPDG* defines the TC parameter as the quantity of heat that flows normally across the surface of unit area per unit of time and per unit of temperature gradient. The presence and amount of moisture content controls the TC parameter of asphalt concrete. If the moisture content is low, the difference between unfrozen, freezing, and frozen thermal conductivity is small but if the moisture content is high, then the difference between the three conditions is substantial. The Level 1 TC input can be obtained using the direct measurement method of the ASTM E 1952 “Standard Test Method for Thermal Conductivity and Thermal Diffusivity by Modulated Temperature Differential Scanning Calorimetry”. As with the SSA and HC, there are also no correlations for a Level 2 TC input while the recommended range of values for a Level 3 TC input is between 0.44 – 0.81 Btu/(ft)(hr)(°F). The TC values of 0.50, 0.67, and 1.00 Btu/(ft)(hr)(°F), was tested during the Phase III TC runs. Table 15 shows the results of the one way ANOVA analysis performed on the results of the Phase III TC runs.

As with the three parameters discussed earlier, the results of the ANOVA analysis for the Phase III TC runs did not change significantly from the results obtained from Phase I. The graphical analysis of the Phase III TC comparison plots also support the results of the ANOVA analysis in which all of the pavement performance plots (Figure 81D to Figure 100D) depicted

the same trends as the pavement performance plots from Phase I (Figure 16D to Figure 20D). It is particularly noticeable that both rutting and smoothness plots show almost no change in reported damage with all three of the tested TC values. Another noticeable trait occurred in all of the SDC and BUD plots whereby the gradient of the plots for TC = 1.0 was much steeper than that for the other two TC values tested. Again, this is probably due to fact that the TC value of 1.0 used was beyond the *MEPDG* recommended range value of 0.81 Btu/(ft)(hr)(°F).

| Source | Performance model | F crit. | F | Significance |
|-----------|---|---------|----------|--------------|
| ARK 70-22 | Surface down cracking (surface) (SDC 1) | 4.2565 | 0.0074 | I |
| | Surface down cracking (0.5") (SDC 2) | 4.2565 | 0.0075 | I |
| | Bottom up Cracking (BUD) | 4.2565 | 0.0024 | I |
| | Rutting | 4.2565 | 0.0040 | I |
| | IRI | 4.2565 | 0 | I |
| GMQ 70-22 | Surface down cracking (surface) (SDC 1) | 4.2565 | 0.0049 | I |
| | Surface down cracking (0.5") (SDC 2) | 4.2565 | 0.0053 | I |
| | Bottom up Cracking (BUD) | 4.2565 | 0.0030 | I |
| | Rutting | 4.2565 | 0.0046 | I |
| | IRI | 4.2565 | 0 | I |
| JET 70-22 | Surface down cracking (surface) (SDC 1) | 4.2565 | 0.0043 | I |
| | Surface down cracking (0.5") (SDC 2) | 4.2565 | 0.0050 | I |
| | Bottom up Cracking (BUD) | 4.2565 | 0.0031 | I |
| | Rutting | 4.2565 | 0.0026 | I |
| | IRI | 4.2565 | 1.09E-06 | I |
| MCA 70-22 | Surface down cracking (surface) (SDC 1) | 4.2565 | 0.0055 | I |
| | Surface down cracking (0.5") (SDC 2) | 4.2565 | 0.0057 | I |
| | Bottom up Cracking (BUD) | 4.2565 | 0.0029 | I |
| | Rutting | 4.2565 | 0.0045 | I |
| | IRI | 4.2565 | 3.26E-06 | I |

* I = Insignificant
S = Significant

Table 15: Phase III One-way ANOVA results for TC

Based on the results of the ANOVA and graphical analysis of the Phase III TC runs, it can be concluded that there was insufficient evidence to prove that there was a significant difference in the reported damage for all three performance models with respect to pavement age. This conclusion was to be expected since it coincides with the fact that there was no TC parameter included in the all three pavement performance equations used by the software.

Therefore, it is advisable to use the recommended software default value of 0.23 Btu/(ft)(hr)(°F) whenever performing a HMA pavement analysis.

Air Voids (AV)

Air voids (AV), is one of the many volumetric properties of a HMA mix. AV can be defined as the total volume of the small pockets of air between the coated aggregate particles throughout a compacted paving mixture, expressed as a percent of the bulk volume of the mixture. The amount of AV in a mixture is extremely important and closely related to stability and durability of the mix. In-place AV content plays a major role in HMA performance. In addition, there are very few performance prediction models available that directly relate asphalt binder content and in-place air void content to rutting and fatigue performance of in-service pavements. With this in mind, higher priorities were given to the air voids parameter in order to check and verify the validity and reasonability of the performance models used in the software with respect to change to the air voids parameter. The in-place air voids parameter can be obtained by performing field coring and establishing the mix volumetric data.

The air voids (AV) values of 3.0 percent, 4.0 percent, 4.5 percent, 5.0 percent, 6.0 percent, and 8.0 percent, were tested for both the 12.5mm and 25.0mm gradation mixes, during the Phase III AV runs. Tables 16 and 16 show the results of the one-way ANOVA analysis performed on the results of the Phase III AV runs. Although the Phase III AV runs were performed using four different gradations from four different sources as mentioned earlier, only the ARK results for both the 12.5mm and 25.0mm mixes are shown due to the fact that all four gradations mixes yielded similar results and pavement performance plots.

| Source | Performance model | F crit. | F | Significance |
|-----------|---|---------|---------|--------------|
| ARK 64-22 | Surface down cracking (surface) (SDC 1) | 2.7729 | 7.1659 | S |
| | Surface down cracking (0.5") (SDC 2) | 2.7729 | 7.3045 | S |
| | Bottom up Cracking (BUD) | 2.7729 | 7.1907 | S |
| | Rutting | 2.7729 | 0.1309 | I |
| | IRI | 2.7729 | 3.8295 | S |
| ARK 70-22 | Surface down cracking (surface) (SDC 1) | 2.7729 | 11.8338 | S |
| | Surface down cracking (0.5") (SDC 2) | 2.7729 | 7.2224 | S |
| | Bottom up Cracking (BUD) | 2.7729 | 7.1429 | S |
| | Rutting | 2.7729 | 0.1230 | I |
| | IRI | 2.7729 | 3.4080 | S |
| ARK 76-22 | Surface down cracking (surface) (SDC 1) | 2.7729 | 7.0944 | S |
| | Surface down cracking (0.5") (SDC 2) | 2.7729 | 7.1605 | S |
| | Bottom up Cracking (BUD) | 2.7729 | 7.0045 | S |
| | Rutting | 2.7729 | 0.1157 | I |
| | IRI | 2.7729 | 3.0289 | S |

* I = Insignificant
S = Significant

Table 16: Phase III One-way ANOVA results for Air Voids (12.5mm Mixes)

| Source | Performance model | F crit. | F | Significance |
|-----------|---|---------|--------|--------------|
| ARK 64-22 | Surface down cracking (surface) (SDC 1) | 2.7729 | 0.4144 | I |
| | Surface down cracking (0.5") (SDC 2) | 2.7729 | 0.3708 | I |
| | Bottom up Cracking (BUD) | 2.7729 | 6.9994 | S |
| | Rutting | 2.7729 | 0.0011 | I |
| | IRI | 2.7729 | 0.0041 | I |
| ARK 70-22 | Surface down cracking (surface) (SDC 1) | 2.7729 | 0.4754 | I |
| | Surface down cracking (0.5") (SDC 2) | 2.7729 | 0.4386 | I |
| | Bottom up Cracking (BUD) | 2.7729 | 6.8475 | S |
| | Rutting | 2.7729 | 0.0006 | I |
| | IRI | 2.7729 | 0.0028 | I |
| ARK 76-22 | Surface down cracking (surface) (SDC 1) | 2.7729 | 0.5447 | I |
| | Surface down cracking (0.5") (SDC 2) | 2.7729 | 0.5314 | I |
| | Bottom up Cracking (BUD) | 2.7729 | 6.7358 | S |
| | Rutting | 2.7729 | 0.0003 | I |
| | IRI | 2.7729 | 0.0020 | I |

* I = Insignificant
S = Significant

Table 17: Phase III One-way ANOVA results for Air Voids (25.0mm Mixes)

For the 12.5mm mixes, the ANOVA results indicated a significant difference for both the fatigue performance models and the IRI model. However, the results for the rutting model indicated no significant difference. Further visual inspections of the generated pavement

performance plots (Figure 101D to Figure 115D) supported the results indicated by the ANOVA analysis. All of the SDC and BUD plots showed a significant increase in both the maximum damage values as well as the change in the gradient of the plots, when the AV was increased from 6.0% to 8.0%. The results of the Phase III AV runs were to be expected since the fatigue model used by the DG M-E software incorporates the AV value for the calculation of M variable, and the calculation of the stiffness of the mix, E^* . Therefore, it is not surprising to see that as the AV increases, the fatigue damage increases. By conventional wisdom, a pavement engineer would expect to see a significant difference in the rutting results when AV is increased. However, the results of both the pavement performance plots and the ANOVA analysis indicated otherwise. All of the rutting plots generated showed a minimal increase in rutting depth even with a dramatic increase of 2% in the AV values used (6% to 8%). Further scrutiny of the rutting model used in the software actually indicated that the results were reasonable. Based on an analysis of the rutting model form, one can deduct that air voids would not have a significant impact towards the rutting performance of a pavement because the air voids parameter was built deep within the model. The only time that air voids comes into play in the rutting model is during the calculation of E^* , which is just one of the parameters used to determine pavement rutting. The results of the ANOVA analysis for the IRI were to be expected since the IRI model takes into account the extent of pavement damage in both types of fatigue damage and rutting. Since, there was a significant difference in both types of fatigue damage when AV was varied, it came to no surprise that the IRI results showed the same trend.

For the 25.0mm mixes, the ANOVA analysis results only indicated a significant difference in the BUD part of the fatigue cracking performance model. Through visual inspections of the pavement performance plots generated (Figure 116D to Figure 130D), it was

found that although there was an increase in maximum damage for the SDC plots in all three binder grades tested when AV was increased from 6% to 8%, the rate of increase in damage was similar. This was not the case with the BUD plots. The BUD plots showed a more definitive increase in maximum damage in terms of a steeper gradient compared to the SDC plots when AV was increased from 6% to 8%. This would explain the difference in the ANOVA analysis results for both fatigue cracking models. As with the results of the 12.5mm mixes before, the results for both the ANOVA analysis and the pavement performance plots for the 25.0mm mixes indicated that there was no significant change in pavement rutting performance when AV was varied. Again, these results were to be expected as explained before in the previous discussion. Lastly, the IRI ANOVA analysis and pavement performance plots showed no significant difference when AV was varied. This was probably due to the fact that there was no significant difference in both the SDC type fatigue cracking and the rutting results.

Binder Grade (BG)

AHTD uses the Superpave system which ties asphalt binder, aggregate selection, traffic loads, and climate, into the mix design process. The Superpave system uses its own unique asphalt binder selection process based on the Superpave asphalt binder performance grading (PG) system which selects the appropriate PG asphalt binders based on the expected pavement temperature extremes in the area of their intended use. After determining the expected design pavement temperature through the use of a Superpave software, they can be matched to an appropriate PG asphalt binder.

The binder grade values of PG 64-22, PG 70-22, and PG 76-22, were tested for both the 12.5mm and 25.0mm mixes, at both 6% AV and 8% AV, for the Phase III BG runs. It was determined that it would be necessary to check the effects of binder grade at both AV ranges

because it was found in the earlier results that AV had a significant impact on pavement performance when the values were increased from 6% to 8%. Therefore, it was important to ensure whether the effects of binder grade would defer at these particular AV ranges. Tables 18 through 21 show the results of the one way ANOVA analysis performed on the results of those runs.

| Source | Performance model | F crit. | F | Significance |
|--------|---|---------|--------|--------------|
| ARK | Surface down cracking (surface) (SDC 1) | 4.2565 | 0.0209 | I |
| | Surface down cracking (0.5") (SDC 2) | 4.2565 | 0.0050 | I |
| | Bottom up Cracking (BUD) | 4.2565 | 0.3729 | I |
| | Rutting | 4.2565 | 0.5110 | I |
| | IRI | 4.2565 | 0.1416 | I |

* I = Insignificant

S = Significant

Table 18: Phase III One-way ANOVA results for Binder Grade (6% Air Voids, 12.5mm Mixes)

| Source | Performance model | F crit. | F | Significance |
|--------|---|---------|--------|--------------|
| ARK | Surface down cracking (surface) (SDC 1) | 4.2565 | 0.0081 | I |
| | Surface down cracking (0.5") (SDC 2) | 4.2565 | 0.0005 | I |
| | Bottom up Cracking (BUD) | 4.2565 | 0.3356 | I |
| | Rutting | 4.2565 | 0.5474 | I |
| | IRI | 4.2565 | 0.2170 | I |

* I = Insignificant

S = Significant

Table 19: Phase III One-way ANOVA results for Binder Grade (8% Air Voids, 12.5mm Mixes)

| Source | Performance model | F crit. | F | Significance |
|--------|---|---------|--------|--------------|
| ARK | Surface down cracking (surface) (SDC 1) | 4.2565 | 1.9981 | I |
| | Surface down cracking (0.5") (SDC 2) | 4.2565 | 1.9122 | I |
| | Bottom up Cracking (BUD) | 4.2565 | 0.3733 | I |
| | Rutting | 4.2565 | 0.0010 | I |
| | IRI | 4.2565 | 0.0001 | I |

* I = Insignificant

S = Significant

Table 20: Phase III One-way ANOVA results for Binder Grade (6% Air Voids, 25.0mm Mixes)

| Source | Performance model | F crit. | F | Significance |
|--------|---|---------|--------|--------------|
| ARK | Surface down cracking (surface) (SDC 1) | 4.2565 | 1.8444 | I |
| | Surface down cracking (0.5") (SDC 2) | 4.2565 | 1.7276 | I |
| | Bottom up Cracking (BUD) | 4.2565 | 0.3775 | I |
| | Rutting | 4.2565 | 0.0020 | I |
| | IRI | 4.2565 | 0.0007 | I |

* I = Insignificant

S = Significant

Table 21: Phase III One-way ANOVA results for Binder Grade (8% Air Voids, 25.0mm Mixes)

The tables only show the results of the Arkhola source for both the 12.5mm and the 25.0mm mixes because it was found that the additional three sources tested also showed similar results. Based on the results of the ANOVA analysis performed on the results of the Phase III BG runs, it is fairly obvious that the BG parameter does not have a significant impact on all three pavement performance models previously discussed. Further inspections of the pavement performance plots (Figure 131D to Figure 150D) generated by the results of the runs also supported this conclusion since all the plots showed either almost no change in pavement performance (e.g. Figure 137D) or a slight change but similar gradients (e.g. Figure 141D).

Therefore, it can be concluded that there was insufficient evidence to prove that there was a significant difference in the reported damage for all three performance models with respect to pavement age. This result was to be expected since the three PGs selected for testing in the Phase III runs has been found to provide the best reliability values throughout the state of Arkansas. It is also important to note that since the selection of binder grades are determined from climatic information, binder grades are more sensitive to climatic effects. However, it was previously mentioned that only one type of climate (Fayetteville, AR), and low temperature binder grade was used throughout this research. Also, the three binder grades used have been found to be adequate for the climate input used in the runs. Hence, it was to be expected that there should not be any significant difference in the pavement performance models using the three PGs tested.

Total Unit Weight (TUV)

The total unit weight (TUV) parameter describes one of the volumetric HMA properties. The TUV parameter can be best defined as the total weight of a HMA mix divided by the total volume of a HMA mix. The typical range of the TUV for a dense graded HMA typically falls between 134 lb/ft³ to 148 lb/ft³ (pcf). The TUV values of 122, 135, and 148 pcf were tested for

both the 12.5mm and 25.0mm mix using two sources, ARK and GMQ, at a particular binder grade (PG 64-22), during the Phase III TUV runs. Tables 22 and 23 show the results of the one way ANOVA analysis performed on the results of those runs.

| Source | Performance model | F crit. | F | Significance |
|-----------|---|---------|--------|--------------|
| ARK 64-22 | Surface down cracking (surface) (SDC 1) | 4.2565 | 0.0065 | I |
| | Surface down cracking (0.5") (SDC 2) | 4.2565 | 0.0068 | I |
| | Bottom up Cracking (BUD) | 4.2565 | 0.0044 | I |
| | Rutting | 4.2565 | 0.0084 | I |
| | IRI | 4.2565 | 0.0018 | I |
| GMQ 64-22 | Surface down cracking (surface) (SDC 1) | 4.2565 | 0.0062 | I |
| | Surface down cracking (0.5") (SDC 2) | 4.2565 | 0.0068 | I |
| | Bottom up Cracking (BUD) | 4.2565 | 0.0037 | I |
| | Rutting | 4.2565 | 0.0072 | I |
| | IRI | 4.2565 | 0.0015 | I |

* I = Insignificant
S = Significant

Table 22: Phase III One-way ANOVA results for Total Unit Weight (12.5mm Mixes)

| Source | Performance model | F crit. | F | Significance |
|-----------|---|---------|-------------|--------------|
| ARK 64-22 | Surface down cracking (surface) (SDC 1) | 4.2565 | 0.0001 | I |
| | Surface down cracking (0.5") (SDC 2) | 4.2565 | 0.0001 | I |
| | Bottom up Cracking (BUD) | 4.2565 | 0.0014 | I |
| | Rutting | 4.2565 | 0.0005 | I |
| | IRI | 4.2565 | 1.0761E-06 | I |
| GMQ 64-22 | Surface down cracking (surface) (SDC 1) | 4.2565 | 0.0005 | I |
| | Surface down cracking (0.5") (SDC 2) | 4.2565 | 0.0007 | I |
| | Bottom up Cracking (BUD) | 4.2565 | 0.0018 | I |
| | Rutting | 4.2565 | 0.0005 | I |
| | IRI | 4.2565 | -1.8682E-14 | I |

* I = Insignificant
S = Significant

Table 23: Phase III One-way ANOVA results for Total Unit Weight (25.0mm Mixes)

Based on the results of the ANOVA analysis and the pavement performance plots (Figure 151D to Figure 170D), it is obvious that the TUV parameter does not have a significant effect on all three pavement performance models. In fact, all of the pavement performance plots generated showed almost no change in all three pavement distresses for all of the TUV values tested. Therefore, it can be concluded that there was insufficient evidence to prove that there was a

significant difference in the reported damage for all three performance models with respect to pavement age for this particular parameter. Based on this conclusion, it is recommended that a pavement engineer use the software default value of 148 pcf whenever performing a HMA pavement analysis. This is significant; in many cases pavement design is performed months or years prior to construction, so mixture data (e.g. TUW) is unknown to the designer.

Percent Binder Effective (Pbe)

Along with air voids, the percent binder effective (Pbe) also plays a major role in HMA performance. Pbe is also another important volumetric property of a HMA mix and is defined as the total asphalt binder content of the HMA minus that portion of asphalt binder that is absorbed into the aggregate. It was discovered that the initial assumption of Pbe being reported in terms of percent by weight (Phase I) was wrong. After careful investigation of the MEPDG manual, it was determined that Pbe should have been reported in terms of percent by volume. With this discovery, a new set of runs were devised by recalculating the Pbe based on percent by volume. The objective of these new set of runs was to check the sensitivity of the HMA pavement performance with respect to change in Pbe from the initial assumption. The recalculated values of Pbe used in the Phase III Pbe runs can be found in Appendix E (in the gradation data). The pavement performance plots generated from the results of the Phase III Pbe runs can be found in Appendix B (Figure 171D to Figure 210D).

For the 12.5mm mixes (Figure 171D to Figure 190D), all four sources tested (ARK, GMQ, JET, and MCA), showed similar results in all three pavement performance models. There was a significant decrease in fatigue cracking and IRI for the recalculated Pbe value while the rutting plots showed only a slight change in rutting depth as shown in Figures 3 through 7.

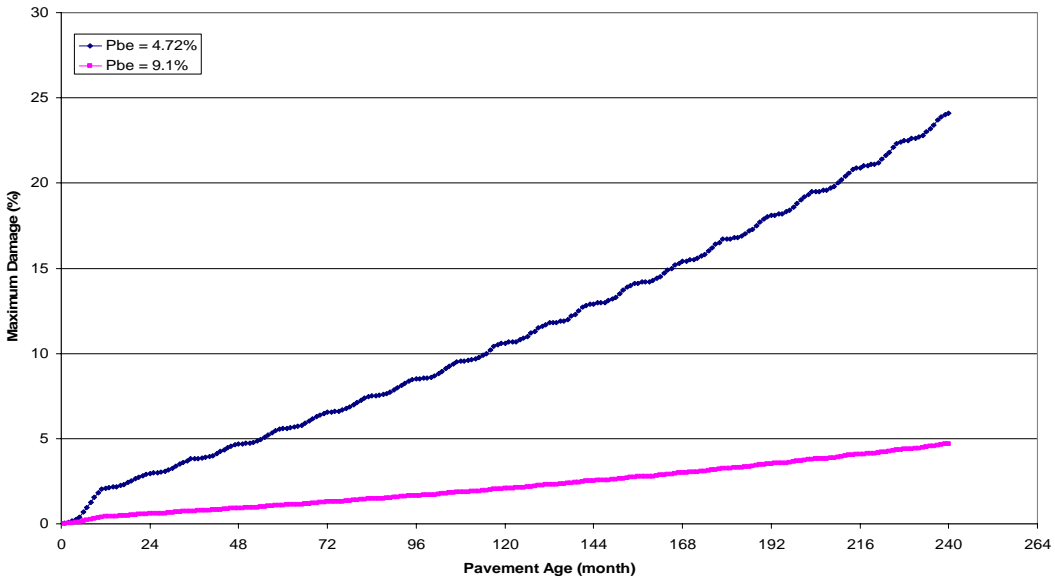


Figure 3: Surface Down Cracking Plot (at surface) for 12.5mm ARK 70-22 mix

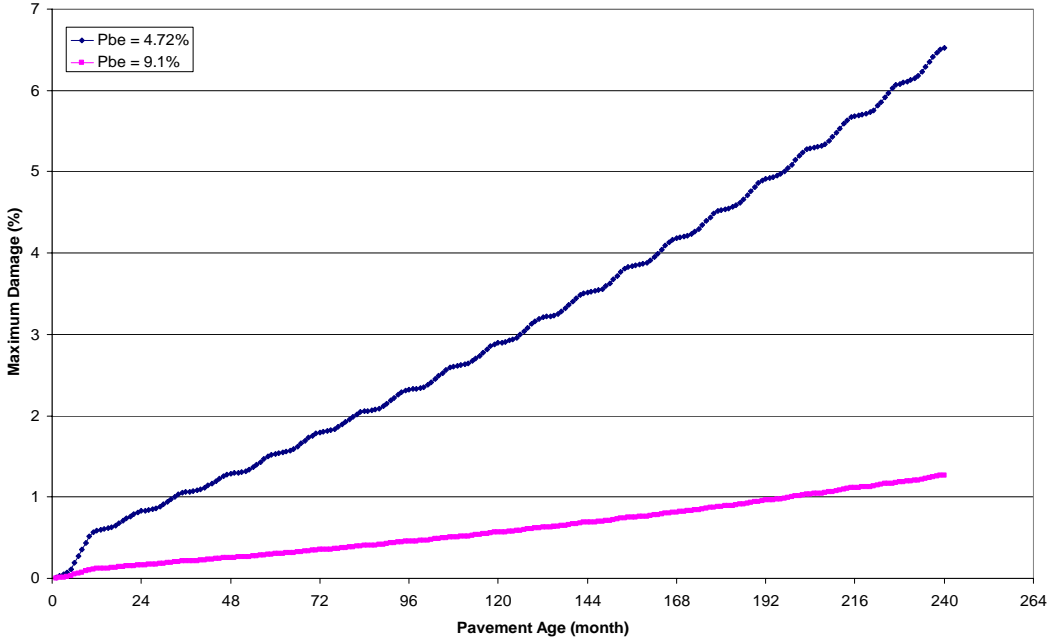


Figure 4: Surface Down Cracking Plot (at 0.5 in. depth) for 12.5mm ARK 70-22 mix

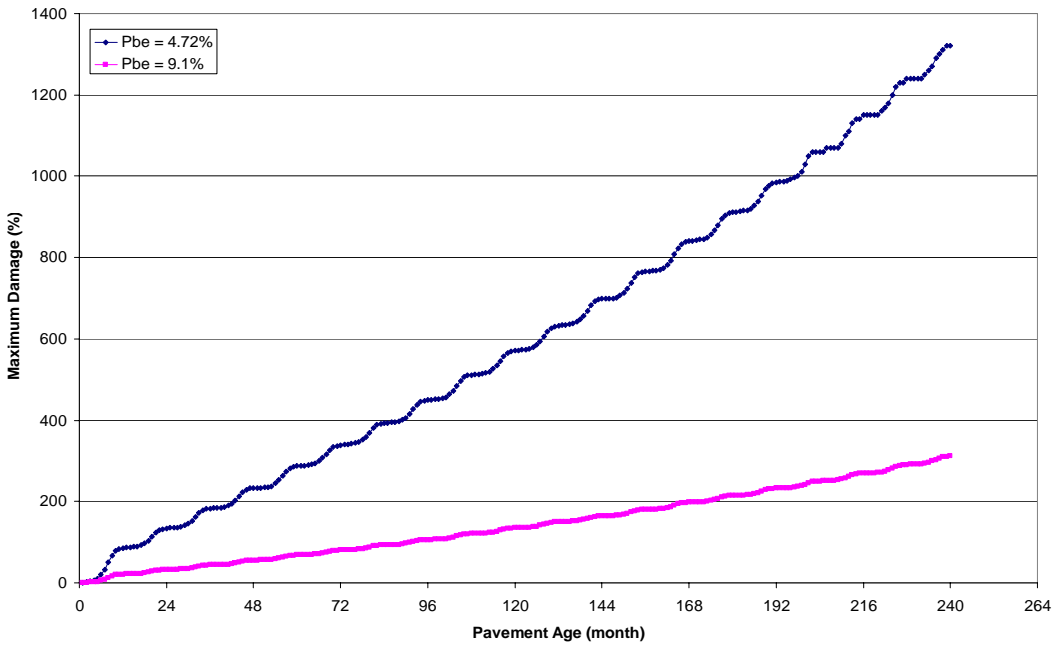


Figure 5: Bottom Up Cracking Plot for 12.5mm ARK 70-22 mix

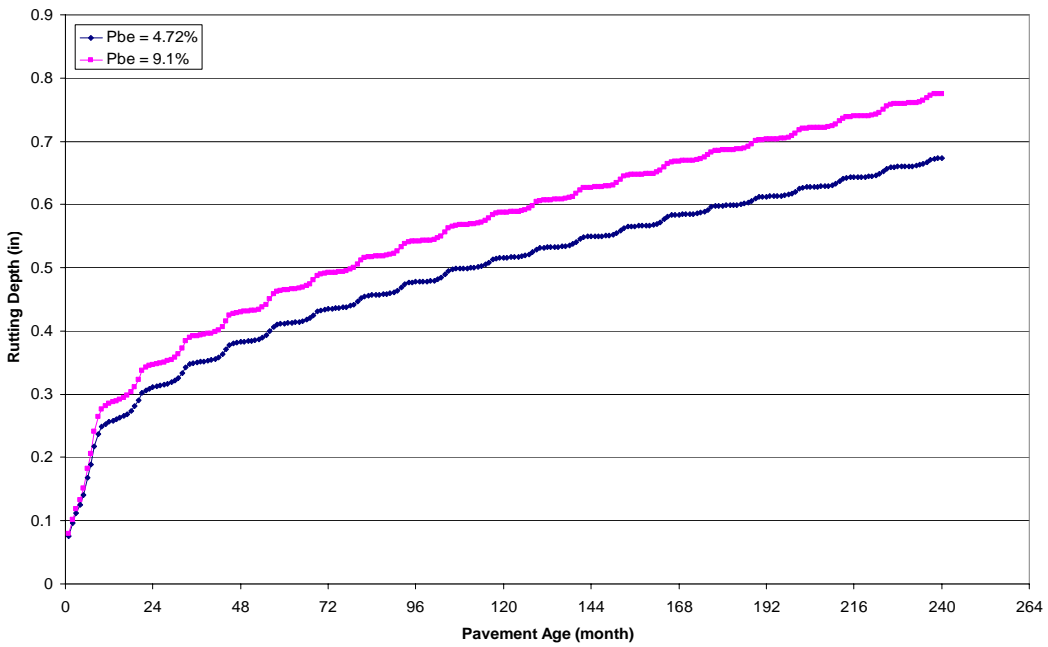


Figure 6: Rutting Plot for 12.5mm ARK 70-22 mix

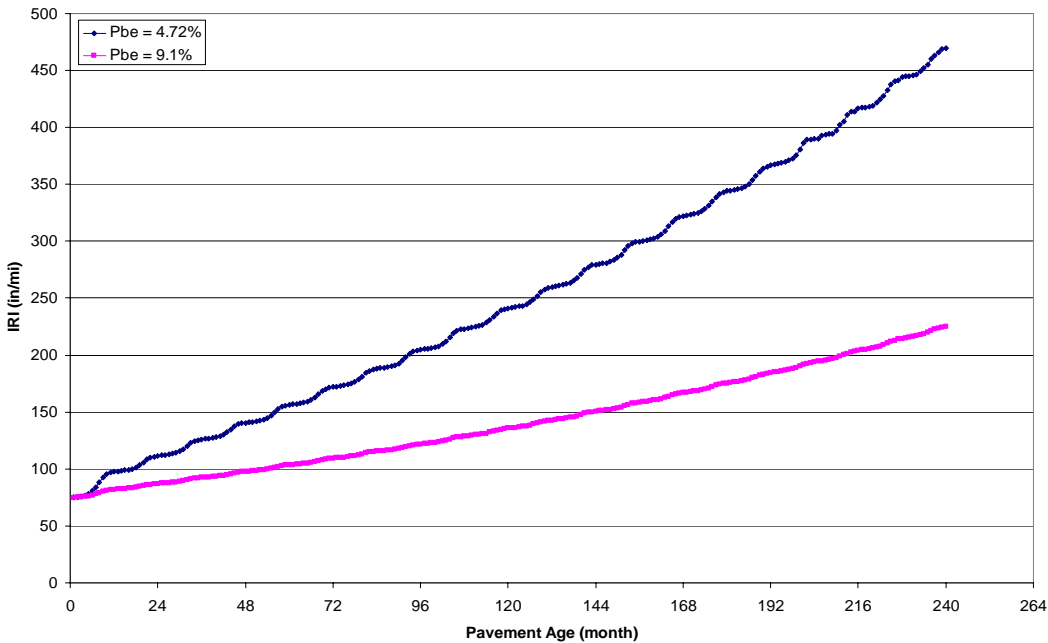


Figure 7: IRI Plot for 12.5mm ARK 70-22 mix

Again, these results were to be expected since it was determined that the Pbe parameter would have an influential role in the fatigue cracking model used in the software since it was used to calculate both the C factor and also the mix stiffness factor (E^*). Furthermore, the results were found to be reasonable with respect to the fatigue model used since the plots showed that as Pbe increased, the fatigue damage decreased. As with the AV results, it was astounding to find that Pbe did not have a significant impact on rutting. However, the results of the runs were justified since it was also determined that as with AV, Pbe only plays a minor role in the rutting model. This is because Pbe is only integrated in the calculation of rutting in the determination of the E^* parameter. At least the results were found to be reasonable with respect to the rutting model used since the plots showed that as Pbe increased, the rut depth reported also increased. As mentioned before, the IRI was found to have significantly decreased as Pbe increased. These

results were reasonable since the IRI model used was a function of the total fatigue damage and total rutting damage in the pavement. Due to the fact that there was a significant decrease in fatigue cracking (especially in the BUD plots) as P_{be} increased, it was natural that the IRI would decrease as well.

For the 25.0mm mixes (Figure 191D to Figure 210D), only the BUD and rutting plots depicted similar trends as the ones produced by the 12.5mm mixes. However, the magnitude of reported damage in the BUD plots differed greatly from those reported by the 12.5mm mixes. For instance, Figure 10 showed similar trends as Figure 5 in which as P_{be} increased, the fatigue damage decreased substantially but the magnitude of difference in damage at the 240 month point for the Figure 5 was much higher than that of Figure 10. This difference in magnitude of reported fatigue damage probably affected the IRI plots for the 25.0mm mixes since the IRI model in the software was a function of the total fatigue cracking damage and total rutting damage. Due to the fact that the fatigue cracking damage for the 25.0mm mixes was significantly less than that of the 12.5mm mixes, it is reasonable that the IRI plots showed no significant change as P_{be} was increased. Figures 8 through 12 show an example of the pavement performance plots generated for one of the 25.0mm mixes.

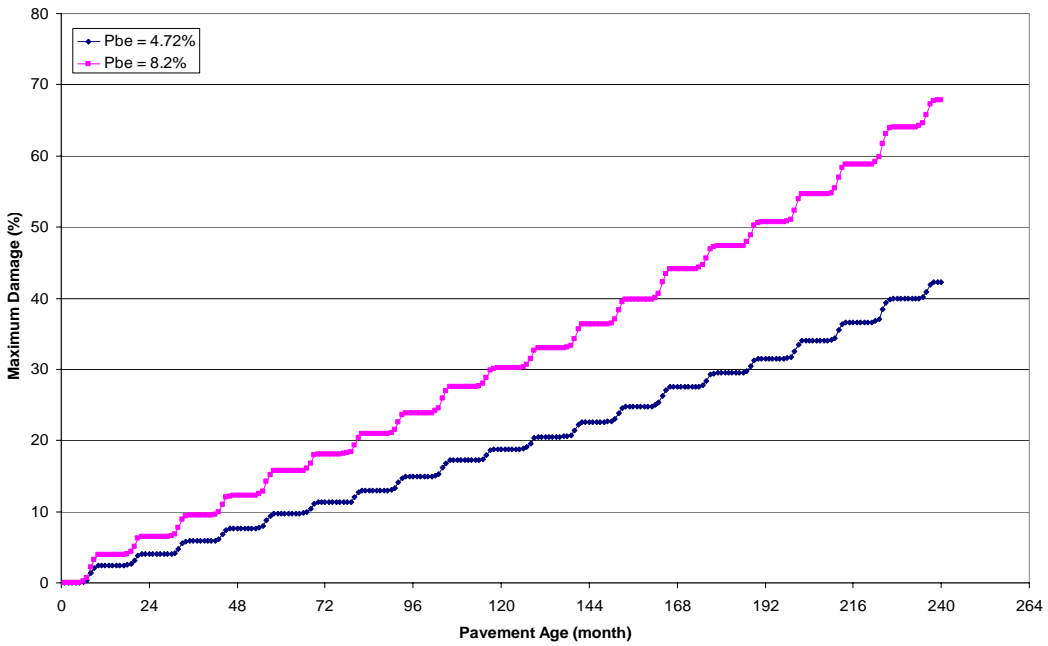


Figure 8: Surface Down Cracking Plot (at surface) for 25.0mm ARK 70-22 mix

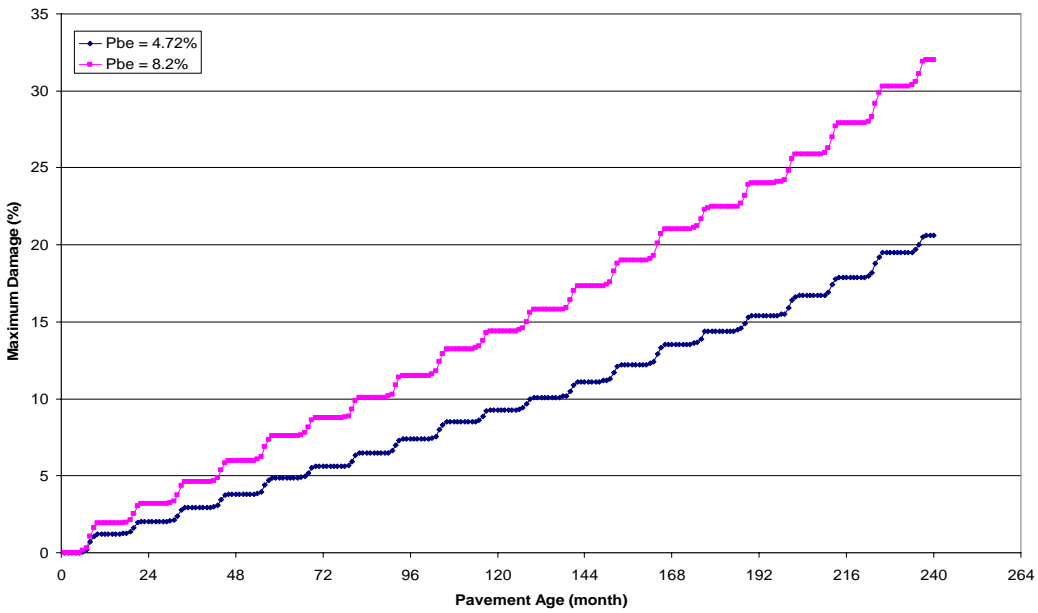


Figure 9: Surface Down Cracking Plot (at 0.5 in. depth) for 25.0mm ARK 70-22 mix

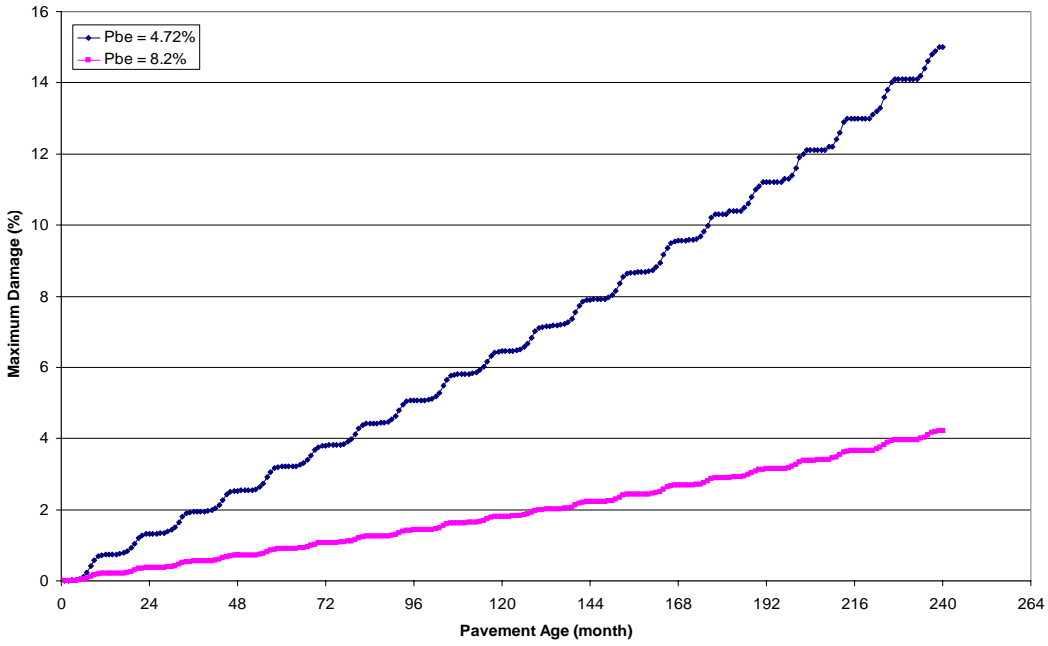


Figure 10: Bottom Up Cracking Plot for 25.0mm ARK 70-22 mix

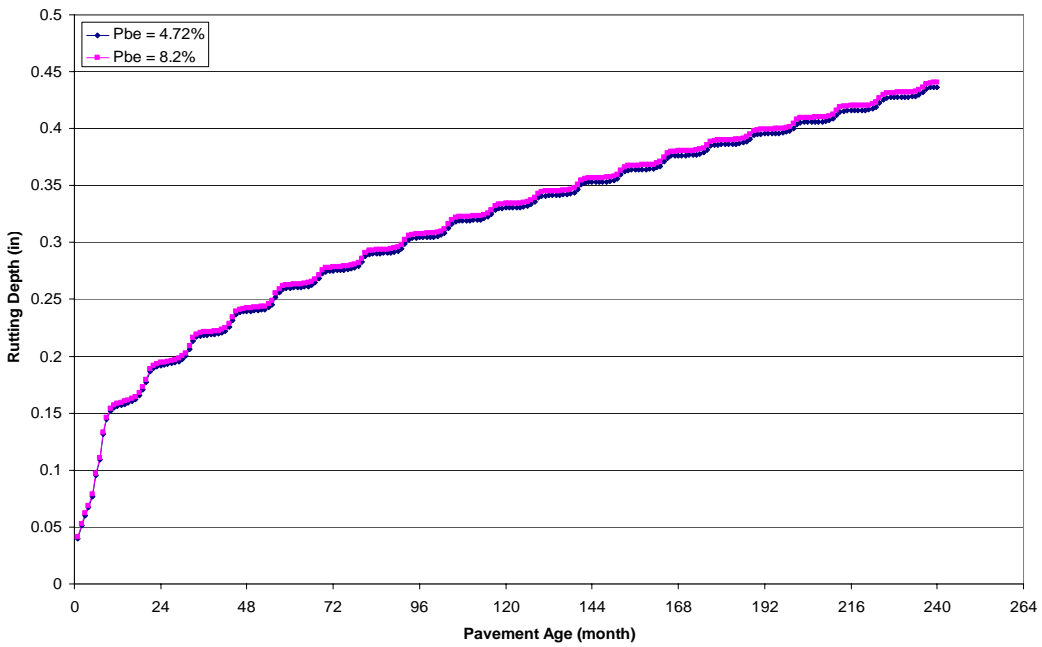


Figure 11: Rutting Plot for 25.0mm ARK 70-22 mix

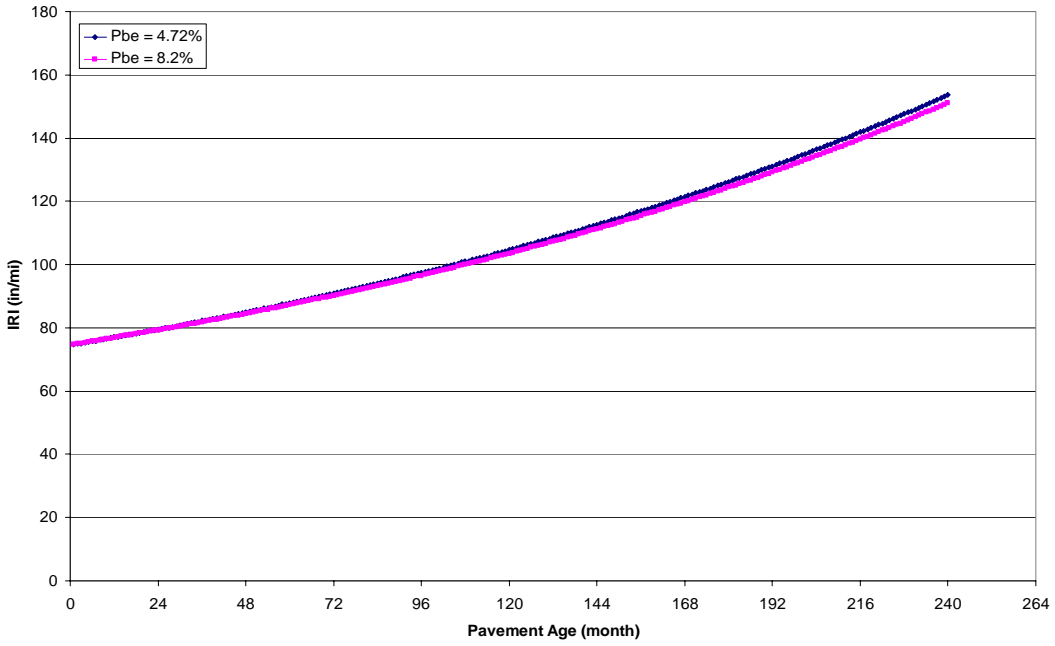


Figure 12: IRI Plot for 25.0mm ARK 70-22 mix

CHAPTER FOUR

SUMMARY AND CONCLUSIONS

Rigid Pavement Design

As can be seen, the *MEPDG* Software is a rather complex system of models that have been developed based on a large database of field pavement sections. Additionally, the results of the models generally follow the industry's "conventional wisdom" concerning concrete pavements, the distress mechanisms, and the distresses that result. Despite this, there are still new parameters required by the program with which pavement designers of today are not familiar because they have not been explicitly considered in the past. Some of these new parameters prove to have a significant impact on the results of the performance models and others do not. Table 24 delineates which of the inputs are significant to the performance models and those that have almost no impact on the models.

The information in Table 24 can be used to streamline the pavement design process because it shows pavement designers which inputs can be ignored, in a sense, by accepting the default values and which inputs they should concentrate on to produce as accurate of a performance model as possible. However, once again, remember that the accuracy of the model, no matter how good the inputs, can only be as good as the calibration that has been put into the models. For this reason, if an agency wants accurate performance models, the agency must undergo a rigorous calibration effort. Another direct use of the data from this research summarized in Table 24 is that pavement designers know which inputs to target when performance models do not meet the performance criteria to determine acceptance of the design. For instance, if a particular design meets the faulting and smoothness criteria, fails to meet the cracking criteria, the

designer can use Table 24 to determine which inputs to the program, or aspects of the pavement design, to alter to improve the pavement's resistance to cracking.

| JPCP Concrete Material Characteristics | Performance Models | | |
|--|--------------------|----------|------------|
| | Faulting | Cracking | Smoothness |
| Curl/warp Effective Temperature Difference | S | S | S |
| Joint Spacing | S | S | S |
| Sealant type | I | I | I |
| Dowell Diameter | S | I | S |
| Dowell Spacing | I | I | I |
| Edge Support | S | S | S |
| PCC-Base Interface | I | | I |
| Erodibility index | I | I | I |
| Surface shortwave absorptivity | I | S | I |
| Infiltration of Surface Water | I | I | I |
| Drainage path length | I | I | I |
| Pavement cross slope | I | I | I |
| Layer Thickness | S | S | S |
| Unit Weight | S | S | S |
| Poisson's ratio | I | S | I |
| Coefficient of thermal expansion | S | S | S |
| Thermal conductivity | I | S | I |
| Heat capacity | I | I | I |
| Cement type | I | I | I |
| Cement content | I | I | I |
| Water/cement ratio | I | I | I |
| Aggregate type | I | I | I |
| PCC set temperature | I | I | I |
| Ultimate shrinkage at 40% R.H. | I | I | I |
| Reversible shrinkage | I | I | I |
| Time to develop 50% of ultimate shrinkage | I | I | I |
| Curing Method | I | I | I |
| 28-day PCC modulus of rupture | I | S | S |
| 28-day PCC compressive strength | I | S | S |

S = Significant to the performance models.

I = Insignificant to the performance models.

Table 24. Summary of the Significance of Concrete Material Inputs

The Need for Additional Research

While there were many questions answered and applicable knowledge gained through this research, this research also unveiled several areas where additional research will be required to achieve the fullest use of the *MEPDG*. There were a few instances where the software or models appeared to have errors, but these issues will surely be repaired with future versions of the software. Aside from the software, many of the inputs shown as significant in Table 24 are not commonly known for specific mix designs. Since the models have proven to be sensitive to these inputs, each of these parameters should be known for agency-approved mix designs that will be used on various projects. This could be accomplished by periodic testing of the mix designs used by different mixing plants. Such testing is imperative if the *MEPDG* is used to the fullest benefit of the users.

One area that was not a part of this study, but is very important to be able to fully understand the inputs to the software, is the interactions between inputs. When one input is changed, what other inputs should also change as a result? And, ultimately, how would these interactions affect the performance models?

While many of these parameters were not tested for in the past because the information was not needed, many of the tests required would be costly to the agencies or designers. Since these tests will become more frequent, additional research should focus on improving these tests, not only to provide more precise results, but also to simplify the testing procedures, thus reducing the cost of these tests. This will then encourage more testing and therefore increasing once again the accuracy of the performance models generated by the software.

And finally, as has been stressed throughout, the final and possibly the most important research that is needed in the future for the implementation of the *MEPDG* is the calibration of the performance models by the various agencies that will use the guidelines. Without the calibration effort, it would be naïve to expect the performance models to follow the actual performance of field sections. The calibration process would require two important areas of information on a pavement section. Detailed data about the pavement section and material used in the section would be required so that the section could be input into the software to model the performance of the section, and data from monitoring the distresses of the pavement section must be collected to compare to the performance models generated by the software. Once this information has been gathered on sufficient pavement sections, then the calibration constants in the software can be adjusted so the software will generate performance models that closely reflect the observed field performance. The calibrated performance models will allow for pavements to be designed to serve a more exact purpose and avoid wasting time, money, and energy on constructing oversized pavements. In addition, the calibrated performance models will aid in the maintenance of the miles of pavement that an agency oversees. By having the calibrated performance models, the agency will be able to see when the faulting, for example, reaches a point that may require minor diamond grinding at the joints. Ultimately, by undertaking such a calibration effort, the agencies will be able to make better use of their resources reducing overdesign and improved long-term planning and budgeting for maintenance.

Flexible Pavement Design

The *MEPDG* software can be hailed as a much needed breakthrough in the pavement industry. The software presents state of the art pavement performance modeling techniques developed by researchers through the use of extensive database of field pavement databases from all over the United States. Furthermore, the complex models used in the software were developed based on both sound theory and conventional wisdom in the industry in relation to asphalt pavements, the distress mechanisms, and the distresses that follow. However, there are many new parameters introduced in this software that have not been considered by pavement engineers. Some of the parameters were proven to be influential while others were not, with respect to pavement performance. The main objective of this study was to determine the sensitivity as well as the degree of impact of these parameters with respect to pavement performance. Table 25 shows the results of this study summarizing the significance or non-significance of each parameter considered. Using the information provided by Table 25, pavement designers can work more efficiently with the knowledge of which parameter (or parameters) may be emphasized in terms of the accuracy of input values. Table 25 can also help provide insight into which parameters can be adjusted to affect the desired pavement performance. For instance, if the designer knows that the pavement section designed was meeting BUD damage specifications but not IRI specifications, he or she may then choose to adjust only the parameters that are significantly affect IRI to obtain better pavement performance.

Need for Further Research

Although there were many questions asked and answered through the course of this research, many more came to mind after this research was completed. Firstly, due to the narrow time frame of this research, difficulties experienced with the software, and sheer number of

parameters involved, several parameters were not explored and tested in this research. Due to the inability of the software to complete Level 1 or Level 2 runs, important parameters such as E* and the GAS model used in the software could not be tested. In time, the future versions of the software should be able to resolve these simulation problems and future researchers may then conduct sensitivity analyses on the parameters not covered by this research.

| HMA Material Characteristics | Performance Models | | | |
|---|--------------------|--------------|---------|-----|
| | SDC Cracking | BUD Cracking | Rutting | IRI |
| Poisson's Ratio | I | I | I | I |
| Surface Shortwave Absorptivity | I | I | I | I |
| Heat Capacity | I | I | I | I |
| Thermal Conductivity | I | I | I | I |
| Air Voids (12.5mm mixes) | S | S | I | S |
| Air Voids (25.0mm mixes) | I | S | I | I |
| Binder Grade (12.5mm mixes) | I | I | I | I |
| Binder Grade (25.0mm mixes) | I | I | I | I |
| Total Unit Weight (12.5mm mixes) | I | I | I | I |
| Total Unit Weight (25.0mm mixes) | I | I | I | I |
| Percent Binder Effective (12.5mm mixes) | S | S | I | S |
| Percent Binder Effective (25.0mm mixes) | I | S | I | I |

S = Significant to the performance models.
 I = Insignificant to the performance models.

Table 25: Summary of the Significance of HMA Material Inputs

Secondly, the most important assumption during the course of this research was that there was no interaction between each input. By common knowledge, this assumption was incorrect, but was necessary as it was the only viable and cost effective way to conduct this research. Some of the inputs tested in this research such as AV and Pbe are clearly interrelated; the unanswered question relates to what degree and how much does this interaction affect pavement performance.

The last but most important research needed in ensuring a successful implementation of the DG M-E is the calibration of performance models by the state agencies that would be using the guide. Without the proper calibration process, one cannot expect and hope that the performance models will follow the actual performance in the field. Although there were extensive research projects conducted in various regions of the United States in the process of developing the pavement performance models used in the *MEPDG* software, one cannot claim that the pavement sections used in the calibration process would match the actual pavement sections used in real life since there could be climatic, geographic, and loading differences. Basically, there are two important inputs needed to run a successful calibration process. Firstly, the state agency will need to collect specific data on the pavement sections as well as the material used to construct the actual pavement sections so that the exact inputs can be used in the DG M-E software. Secondly, the state agency will need to monitor and collect pavement performance data of the actual pavement sections on a timely basis, in order to compare with the pavement performance models generated by the software. When there is enough information collected on a sufficient number of pavement sections throughout the state, then the calibration constants used in the software can be adjusted such that the pavement performance models generated by the software will closely follow the actual field performance of the pavement sections.

REFERENCES

- [1] *Special Report 61G: The AASHO Road Test, Report 7: Summary Report*. HRB, National Academy of Sciences, National Research Council, *Publication 1061*, Washington D.C., 1962.
- [2] “Development of the 2002 Pavement Design Guide.” *Milestones 2002 - Moving Towards the 2002 Pavement Design Guide*, NCHRP Project 1-37A, 2000.
- [3] “Calibrated Mechanistic Structural Analysis Procedures for Pavements - Final Report.” *NCHRP Project 1-26*. University of Illinois Construction Technology Laboratories. March 1990.
- [4] NCHRP Project 1-37A, “Development of the *MEPDG* for the Design of New and Rehabilitated Pavement Structures: Phase II,” TRB, <http://www.4.trb.org/>. Accessed August 2002.
- [5] “*MEPDG*: Design of New and Rehabilitated Pavement Structures, Draft Final Report” ERES Division of ARA, Inc., Champaign, Illinois, December 2002.
- [6] “Development of the 2002 Guide for the Design of New and Rehabilitated Pavement Structures, Draft Part 1-Introduction” ERES Division of ARA, Inc., Champaign, Illinois, October 2001.
- [7] “Development of the 2002 Guide for the Design of New and Rehabilitated Pavement Structures, Draft Part 2-Design Inputs” ERES Division of ARA, Inc., Champaign, Illinois, October 2001.
- [8] “Development of the 2002 Guide for the Design of New and Rehabilitated Pavement Structures, Draft Part 3-Design Analysis” ERES Division of ARA, Inc., Champaign, Illinois, August 2001.
- [9] Yang H. Huang. “Pavement Analysis and Design.” Prentice-Hall, Inc., Upper Saddle River, N. J. 1993.

APPENDIX A

Record of Inputs for *MEPDG* JPCP Analysis

| Project Information | Value |
|--|--------------|
| ◆ General Information | |
| ◆ Design Life | 20 |
| ◆ Base/Subgrade Construction Month | Sept. |
| ◆ Pavement Construction Month | Sept. |
| ◆ Traffic Open Month | Sept. |
| ◆ Type of Design (New Pavements: Flexible Pavement, JPCP, CRCP; Restoration: JPCP; Overlay: Asphalt or PCC) | JPCP |
| ◆ Site/Project Identification | |
| ◆ Location | Fay. |
| ◆ Project ID | |
| ◆ Section ID | |
| ◆ Functional class | |
| ◆ Date | |
| ◆ Station/milepost format | |
| ◆ Station/milepost begin | |
| ◆ Traffic direction | |
| ◆ Analysis Parameters | |
| ◆ Terminal IRI (International Roughness Index) (in/mi) | 252 |
| ◆ Transverse Cracking (% slab cracked) | 15 |
| ◆ Mean Joint Faulting (in) | 0.15 |
| Inputs | |
| ◆ Traffic | |
| ◆ General | |
| ◆ Two-way average annual daily truck traffic (or Two-way annual average daily traffic and Percent of heavy vehicles) | Need Value |
| ◆ Number of lanes in design direction | 2 |
| ◆ Percent of trucks in design direction | 55.0 |
| ◆ Percent of trucks in design lane | 95.0 |
| ◆ Operational speed | 60 |
| ◆ Traffic Volume Adjustment Factors | |
| ◆ Monthly Adjustment – Table of Monthly Adjustment Factors (MAF) for each month for Classes 4-13; Level 1 is Site Specific, Level 3 is Default | 1.0 for all |
| ◆ Vehicle Class Distribution | Default |

| | |
|---|----------------|
| ◆ Hourly Truck Distribution | Default |
| ◆ Traffic Growth Factor (%) | 4-Comp. |
| ◆ Axle Load Distribution Factors | Default |
| ◆ General Traffic Inputs | |
| ◆ Mean wheel location (in from lane marking) | 18 |
| ◆ Traffic wander standard deviation (in) | 9 |
| ◆ Design lane width (ft) | 12 |
| ◆ Number Axles/Truck – Table showing values for Single through Quad-axle trucks from Class 4 – Class 13 | Default |
| ◆ Axle Configuration | |
| ◆ Average axle width (ft) | 8.5 |
| ◆ Dual tire spacing (in) | 12 |
| ◆ Tire Pressure – Single and Dual Tire (psi) | 120/120 |
| ◆ Axle Spacing – Tandem, Tridem, and Quad axle (in) | 51.6/49.2/49.2 |
| ◆ Wheelbase – Information for Short, Medium, and Long wheelbases | |
| ◆ Average Axle Spacing (ft) | 12/15/18 |
| ◆ Percent of trucks | 2/20/78 |
| ◆ Climate | |
| ◆ Climate Data File from included weather station data (may require depth of water table) | Need Location |
| ◆ Structure | |
| ◆ Design Features | |
| ◆ Permanent curl/warp effective temperature difference (°F) | -10 ✓ |
| ◆ Joint Design | |
| ◆ Joint Spacing (ft) | 15 ✓ |
| ◆ Sealant type (None, Liquid, Silicone, Preformed) | Liquid ✓ |
| ◆ Doweled Transverse Joints(None, diameter / spacing) | 1.25”/12” ✓ |
| ◆ Optional – Random joint spacing (Enter four different spacings) | |
| ◆ Edge Support (Nothing or Tied PCC shoulder and/or Widened slab) | |
| ◆ Tied PCC shoulder – Long-term LTE (%) | 40 ✓ |
| ◆ Widened slab – Slab width (ft) | 12 ✓ |
| ◆ Base Properties | |
| ◆ Base Type – edited under “Layers” | |
| ◆ PCC-Base Interface (Bonded or Unbonded) | ✓ |
| ◆ Erodibility index (“Extremely Resistant” to | Very Erosion |

| | |
|---|-----------------------------|
| “Very Erodable”) | Resistant (2) ✓ |
| ◆ For “Bonded” only – Loss of bond age (mo) | 60 ✓ |
| ◆ Drainage and Surface Properties | |
| ◆ Surface shortwave absorptivity | 0.85 ✓ |
| ◆ Infiltration (0, 10, 50, or 100%) | 10 ✓ |
| ◆ Drainage path length (ft) | 12 ✓ |
| ◆ Pavement cross slope (%) | 2 ✓ |
| ◆ Layers | |
| ◆ Layer 1 – PCC | |
| ◆ PCC Material Properties | |
| ◆ Thermal | |
| ◆ General Properties | |
| ◆ Layer Thickness (in) | ✓ |
| ◆ Unit Weight (pcf) | 150 ✓ |
| ◆ Poisson’s ratio | 0.20 ✓ |
| ◆ Thermal Properties | |
| ◆ Coefficient of thermal expansion (per °F $\times 10^{-6}$) | 6 ✓ |
| ◆ Thermal conductivity (BTU/hr-ft- °F) | 1.25 ✓ |
| ◆ Heat capacity (BTU/lb-°F) | 0.28 ✓ |
| ◆ Mix | |
| ◆ Cement type (Type I –III) | Type I ✓ |
| ◆ Cement content (lb/yd ³) | 600 ✓ |
| ◆ Water/cement ratio | 0.42 ✓ |
| ◆ Aggregate type (Quartzite, Limestone, Dolomite, Granite, Rhyolite, Basalt, Synetite, Gabbro, Chert) | Limestone ✓ |
| ◆ Optional – PCC set temperature (°F) | 120 ✓ |
| ◆ Optional – Ultimate shrinkage at 40% R.H. (microstrain) | 700 ✓ |
| ◆ Reversible shrinkage (% of ultimate shrinkage) | 50 ✓ |
| ◆ Time to develop 50% of ultimate shrinkage (days) | 35 ✓ |
| ◆ Curing Method (Curing compound, Wet curing) | Curing comp. ✓ |
| ◆ Strength | |
| ◆ Level 1 – the following parameters at 7, 14, 28, and 90 days, as well as the ratio of each at 20 years to 28 days | |
| ◆ Compressive Strength (psi) | 1500/2000/3000/3 500/1.2 |

| | |
|---|---|
| ◆ E (psi) | 2/2.5/3/3.5 x10 ⁶ /1.2 |
| ◆ Modulus of Rupture (psi) | 300/400/600/600/ 1.2 |
| ◆ S.T. (psi) | 300/400/600/600/ 1.2 |
| ◆ Level 2 – the following parameters at 7, 14, 28, and 90 days, as well as the ratio of each at 20 years to 28 days | |
| ◆ Compressive Strength (psi) | 1500/2000/3000/3 500/1.2 |
| ◆ Level 3 – choose one of the following | |
| ◆ 28-day PCC modulus of rupture (psi) (or) | 650 ✓ |
| ◆ 28-day PCC compressive strength (psi) | 4000 ✓ |
| ◆ Layer 2 – Unbound Material | |
| ◆ Strength Properties | |
| ◆ Level 2 | |
| ◆ Analysis Type – Using ICM or Not, if Not, Seasonal inputs or representative value | Values Dependent on the Material Selected. |
| ◆ Poisson’s ratio | |
| ◆ Coefficient of lateral pressure | |
| ◆ Material Property | You can choose from Crushed Stone or Gravel, River run gravel, and many more descriptive classifications, as well as the AASHTO and Unified Soil Classification Names. |
| ◆ Modulus – Directly or estimated by either CBR, R-value, Layer Coefficient (ai), or based on PI and Gradation | |
| ◆ Level 3 – Same as Level 2, but do not have the option of using Seasonal inputs if not using the ICM | |
| ◆ ICM | |
| ◆ Plasticity Index | |
| ◆ Passing #200 sieve (%) | |
| ◆ Passing #4 sieve (%) | |
| ◆ D60 (mm) | |
| ◆ Optional - Maximum dry unit weight (pcf) | |
| ◆ Optional - Specific gravity of solids | |
| ◆ Optional - Saturated hydraulic conductivity (ft/hr) | |
| ◆ Optional - Optimum gravimetric water content (%) | |
| (Note: The above optional values aid in the | |

estimation of the Degree of Saturation.)

- ◆ Layer 3 – Bedrock
 - ◆ Material Type (Massive and Continuous Bedrock or Highly Fractured and Weathered Bedrock)
 - ◆ Unit Weight (pcf) 140
 - ◆ Poisson's ratio 0.35
 - ◆ Resilient modulus (psi) 1000000

APPENDIX B

RIGID PAVEMENT SENSITIVITY GRAPHS

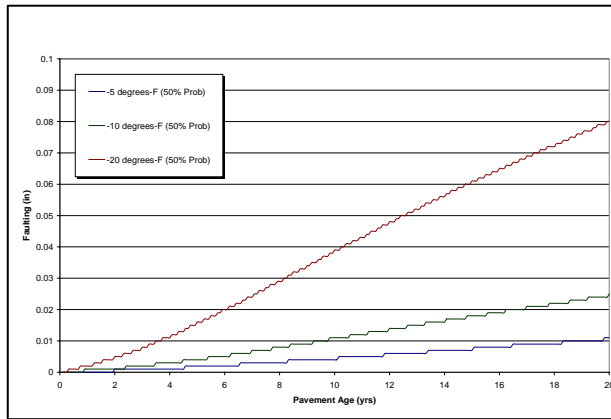


Figure B1. Sensitivity of Faulting to the Curl/Warp Effective Temperature Difference

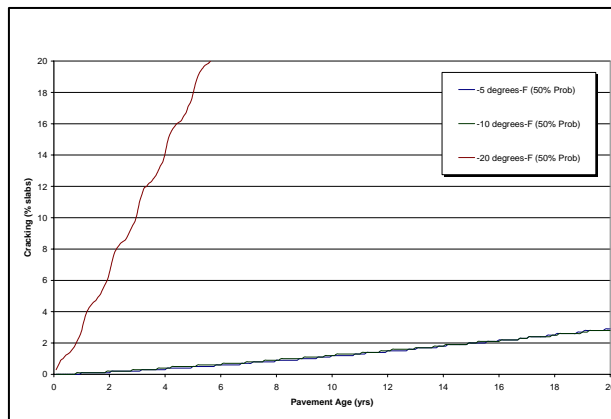


Figure B2. Sensitivity of Cracking to the Curl/Warp Effective Temperature Difference

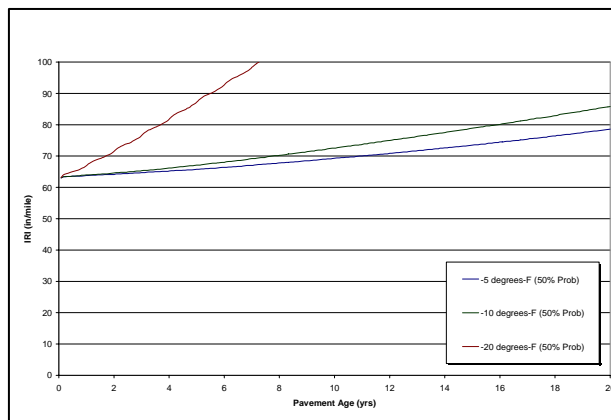


Figure B3. Sensitivity of IRI to the Curl/Warp Effective Temperature Difference

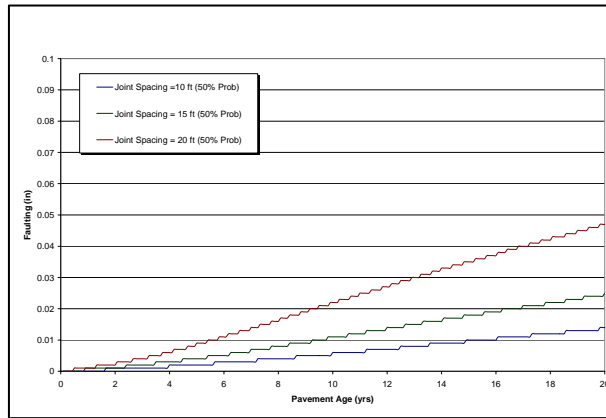


Figure B4. Sensitivity of Faulting to the Pavement Joint Spacing

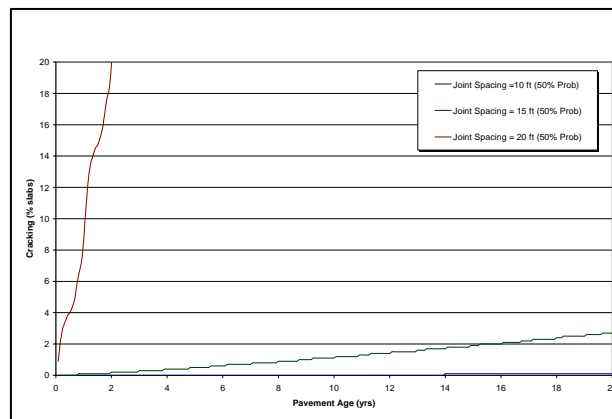


Figure B5. Sensitivity of Cracking to the Pavement Joint Spacing

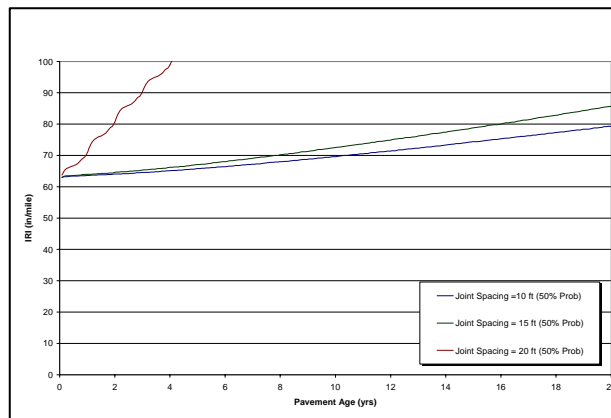


Figure B6: Sensitivity of IRI to the Pavement Joint Spacing

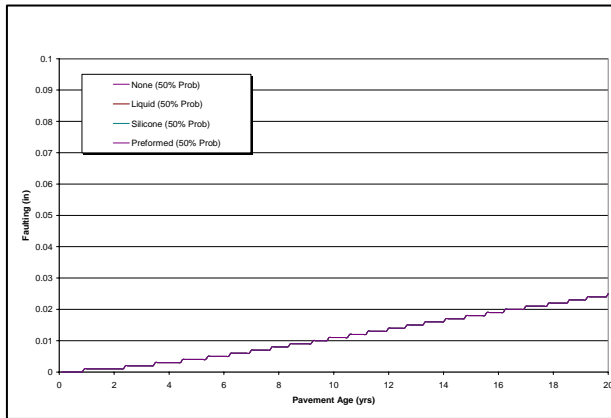


Figure B7. Sensitivity of Faulting to Joint Sealant Type

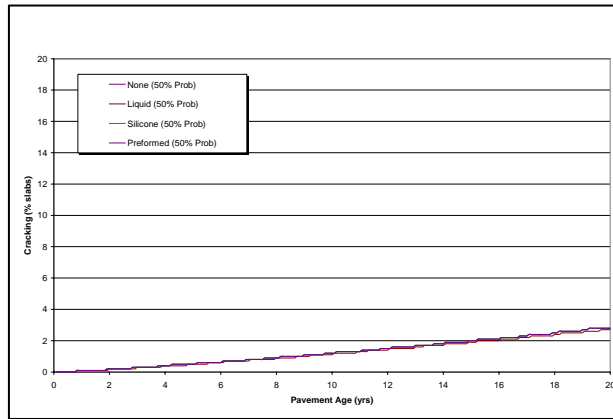


Figure B8. Sensitivity of Cracking to Joint Sealant Type

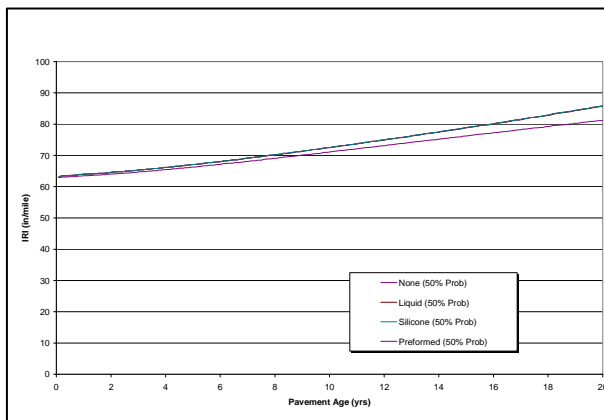


Figure B9. Sensitivity of IRI to Joint Sealant Type

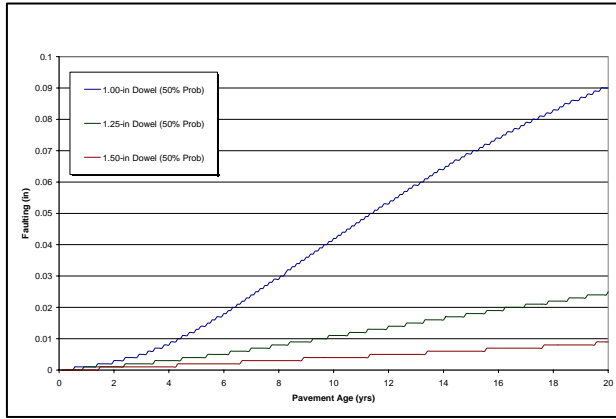


Figure B10. Sensitivity of Faulting to Joint Dowel Diameter

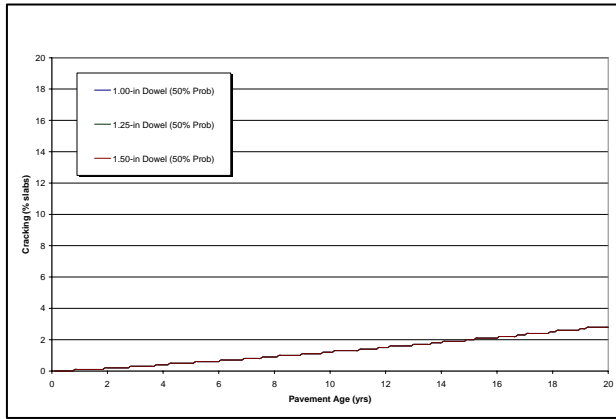


Figure B11. Sensitivity of Cracking to Joint Dowel Diameter

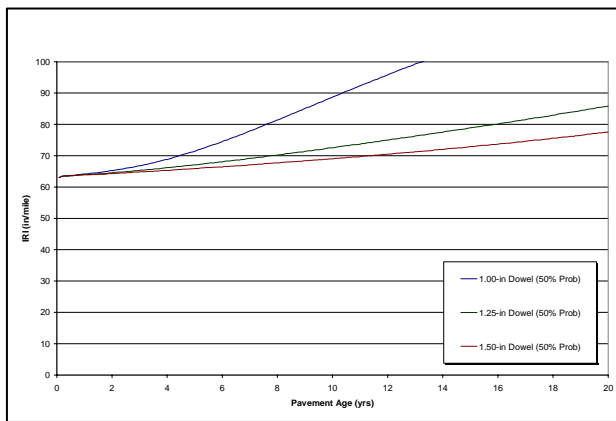


Figure B12. Sensitivity of IRI to Joint Dowel Diameter

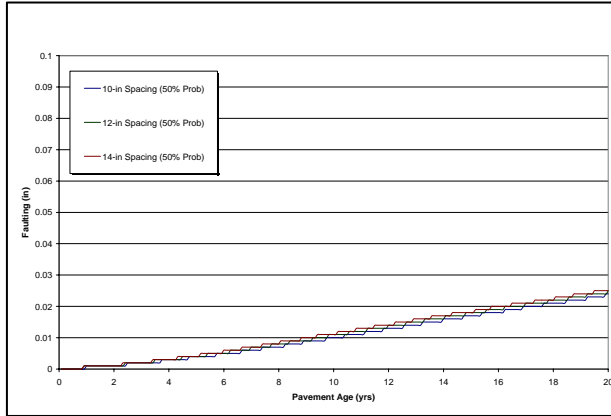


Figure B13. Sensitivity of Faulting to Joint Dowel Spacing

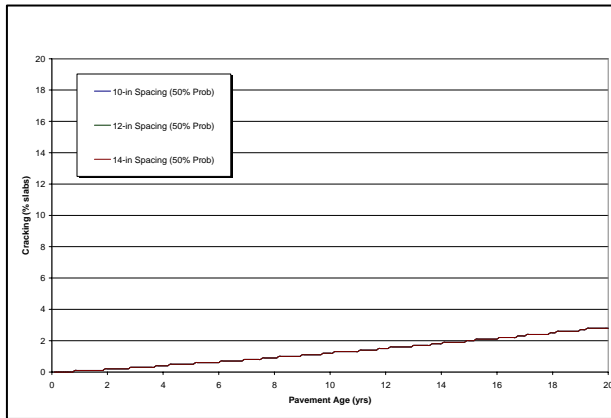


Figure B14. Sensitivity of Cracking to Joint Dowel Spacing

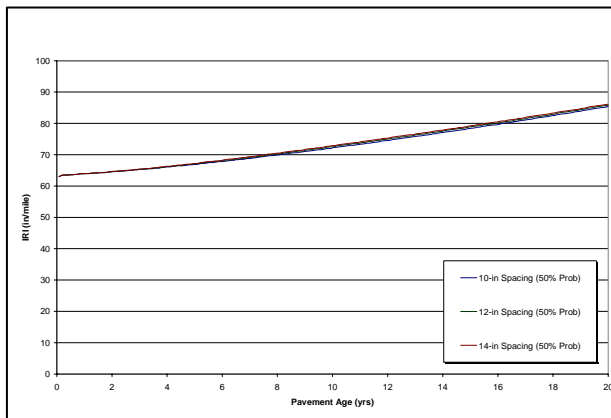


Figure B15. Sensitivity of IRI to Joint Dowel Spacing

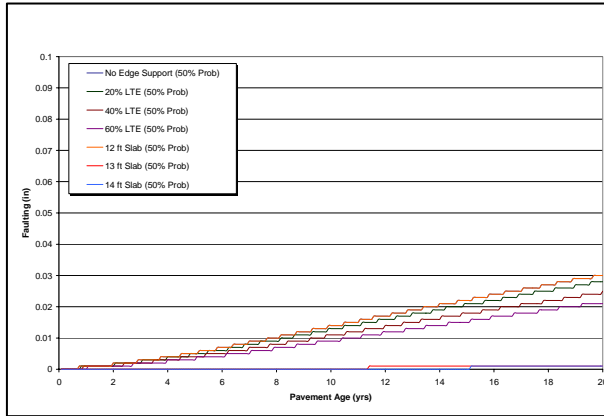


Figure B16. Sensitivity of Faulting to Edge Support

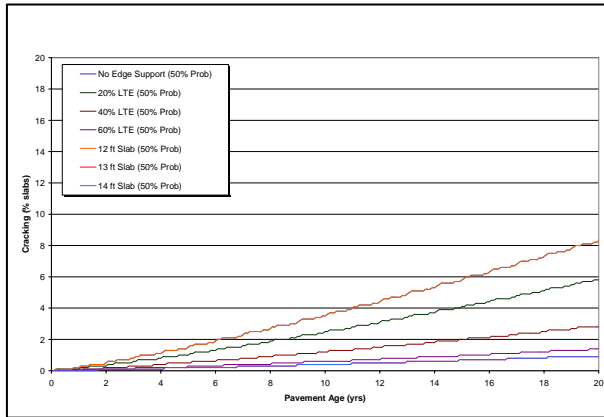


Figure B17. Sensitivity of Cracking to Edge Support

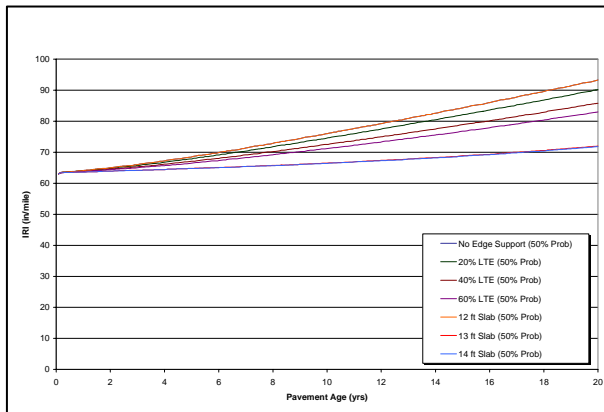


Figure B18. Sensitivity of IRI to Edge Support

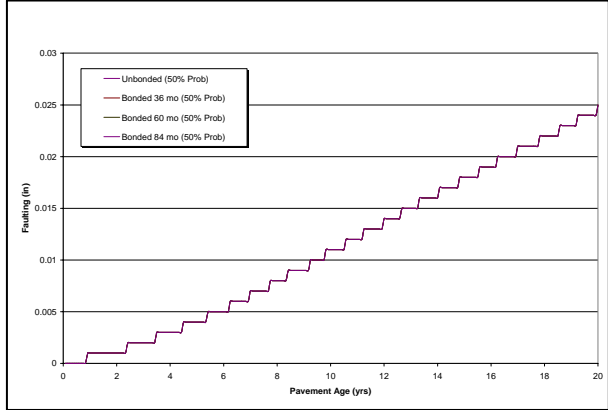


Figure B19. Sensitivity of Faulting to PCC/Base Interface

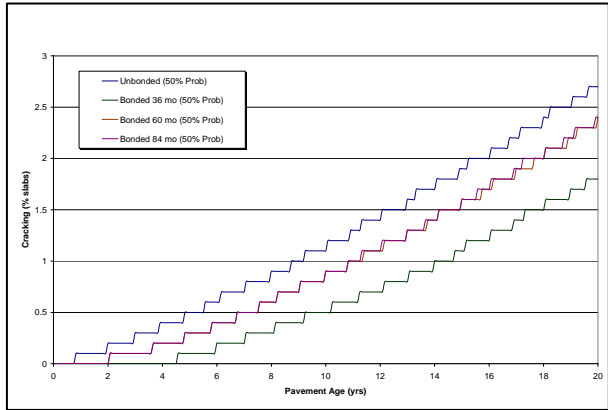


Figure B20. Sensitivity of Cracking to PCC/Base Interface

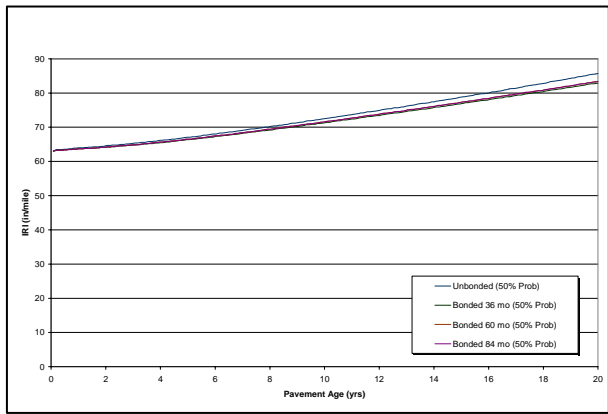


Figure B21. Sensitivity of IRI to PCC/Base Interface

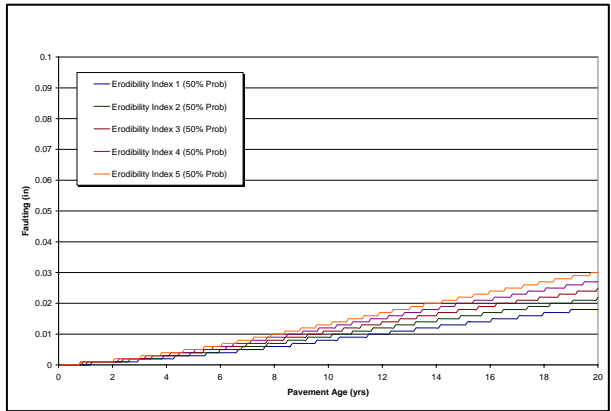


Figure B22. Sensitivity of Faulting to the Base Erodibility Index

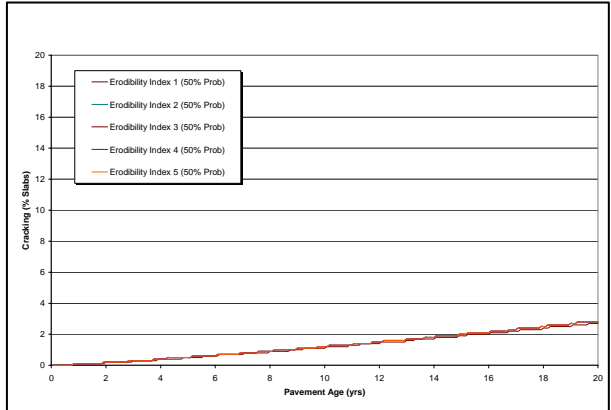


Figure B23. Sensitivity of Cracking to the Base Erodibility Index

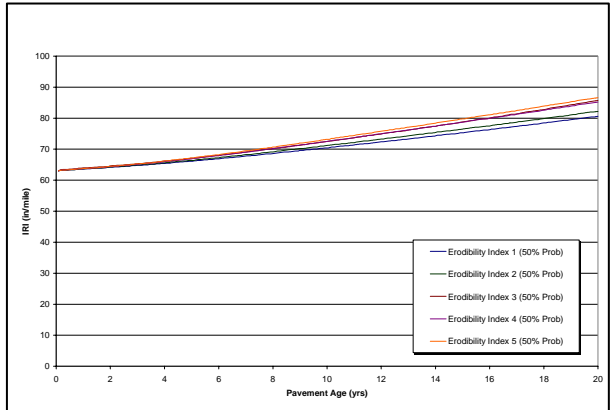


Figure B24. Sensitivity of IRI to the Base Erodibility Index

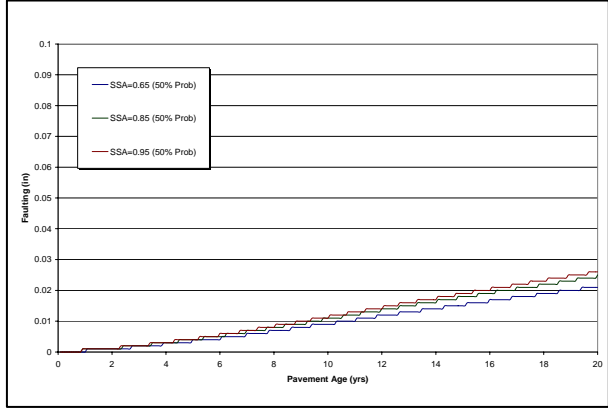


Figure B25. Sensitivity of Faulting to the Surface Shortwave Absorptivity

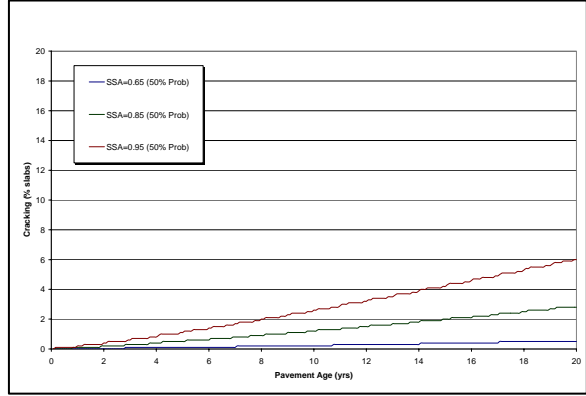


Figure B26. Sensitivity of Cracking to the Surface Shortwave Absorptivity.

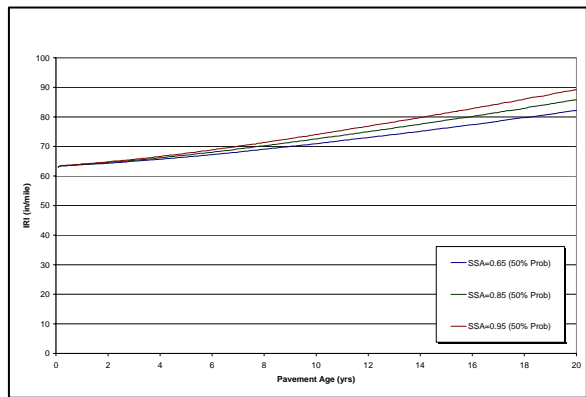


Figure B27. Sensitivity of IRI to the Surface Shortwave Absorptivity

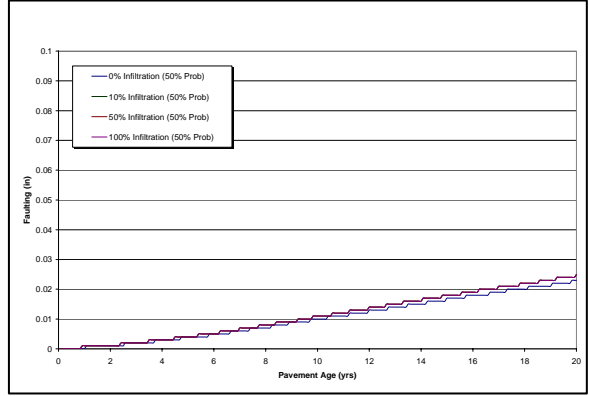


Figure B28. Sensitivity of Faulting to the Infiltration of Surface Water

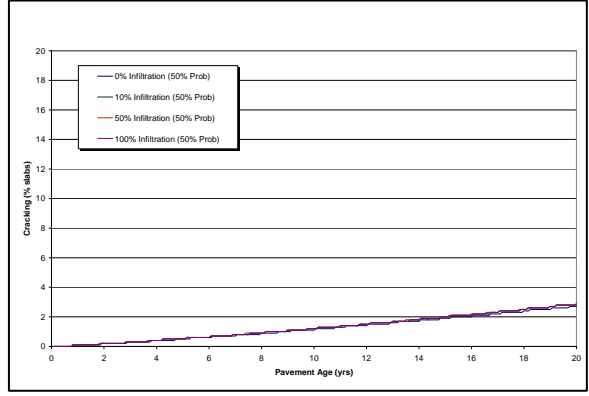


Figure B29. Sensitivity of Cracking to the Infiltration of Surface Water

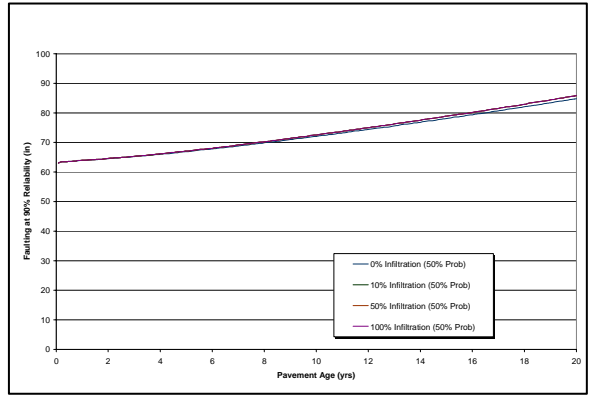


Figure B30. Sensitivity of IRI to the Infiltration of Surface Water

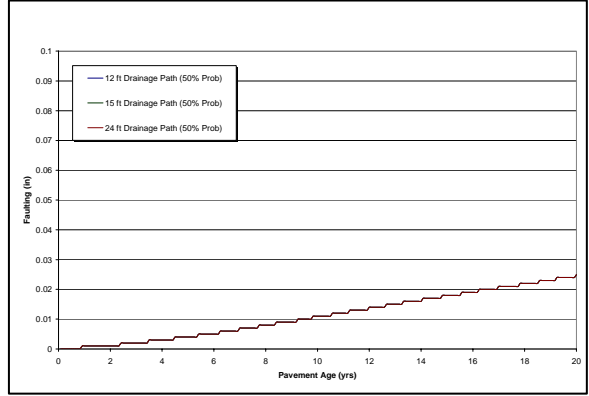


Figure B31. Sensitivity of Faulting to the Length of Drainage Path

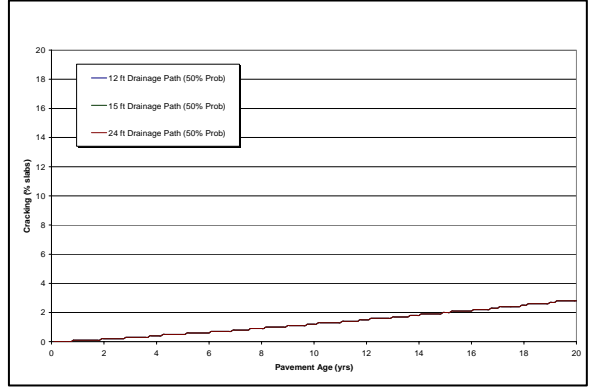


Figure B32. Sensitivity of Cracking to the Length of Drainage Path

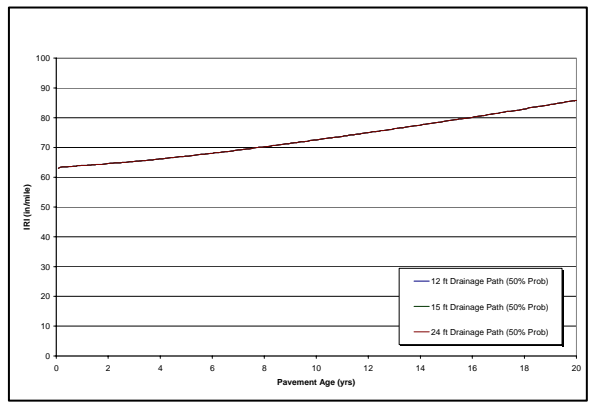


Figure B33. Sensitivity of IRI to the Length of Drainage Path

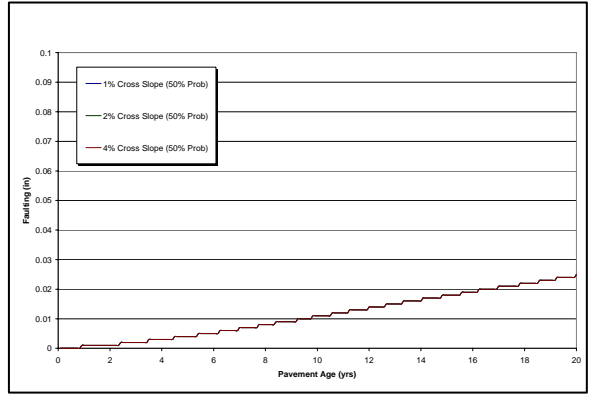


Figure B34. Sensitivity of Faulting to the Pavement Cross Slope

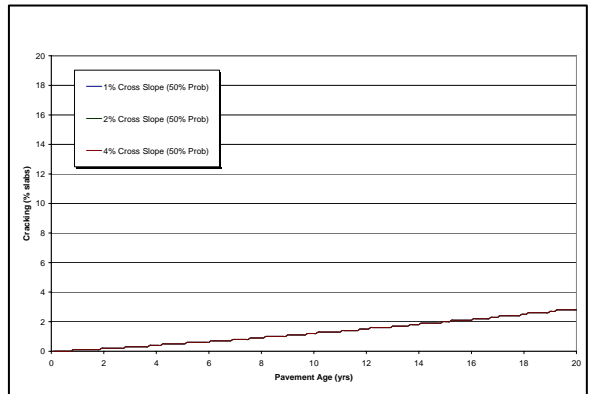


Figure B35. Sensitivity of Cracking to the Pavement Cross Slope

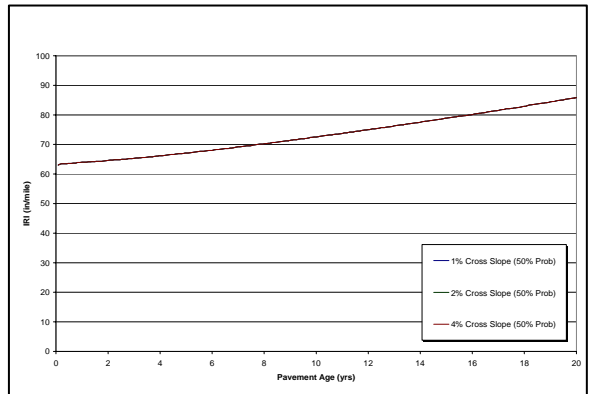


Figure B36. Sensitivity of IRI to the Pavement Cross Slope

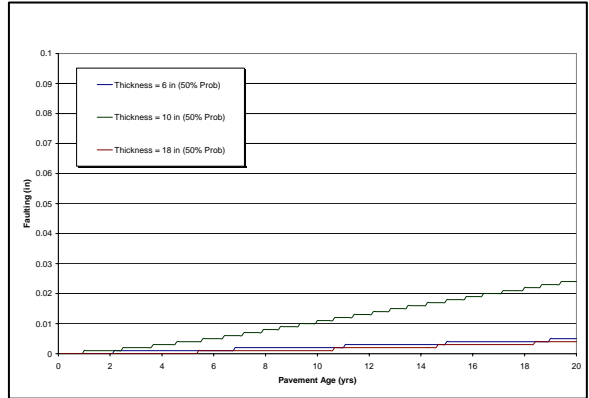


Figure B37. Sensitivity of Faulting to Concrete Thickness

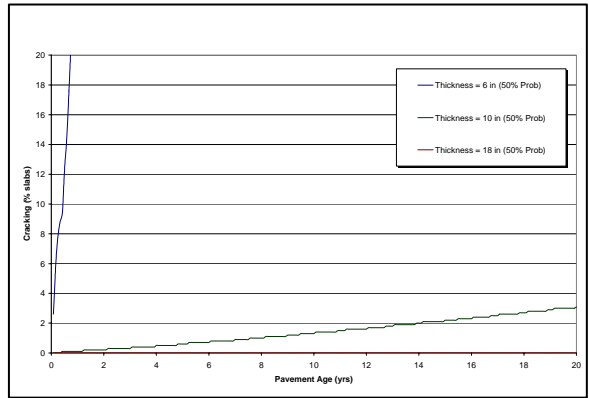


Figure B38. Sensitivity of Cracking to Concrete Thickness

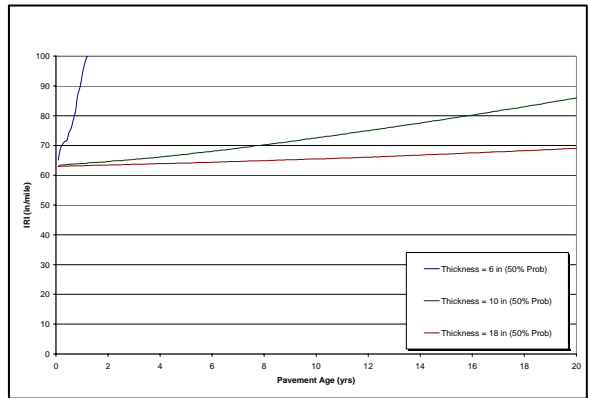


Figure 39. Sensitivity of IRI to Concrete Thickness

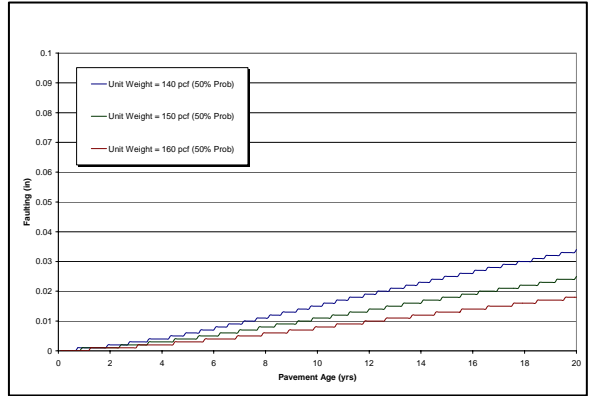


Figure B40. Sensitivity of Faulting to Concrete Unit Weight

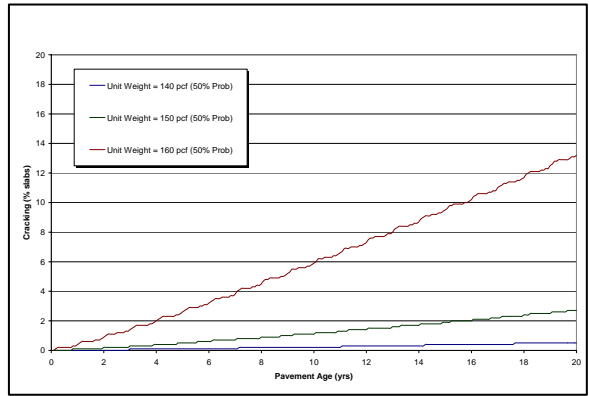


Figure B41. Sensitivity of Cracking to Concrete Unit Weight

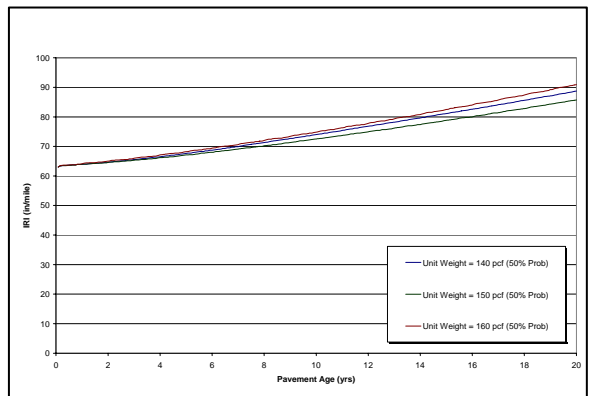


Figure B42. Sensitivity of IRI to Concrete Unit Weight

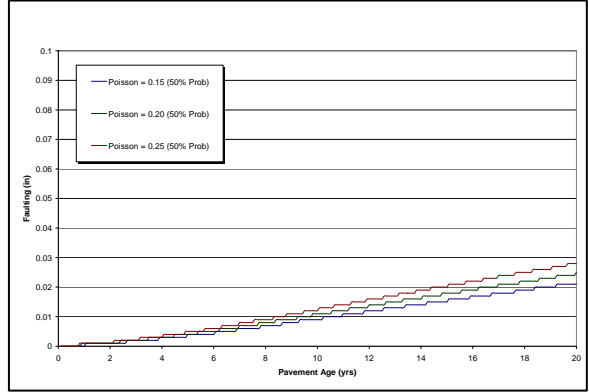


Figure B43. Sensitivity of Faulting to Poisson's Ratio

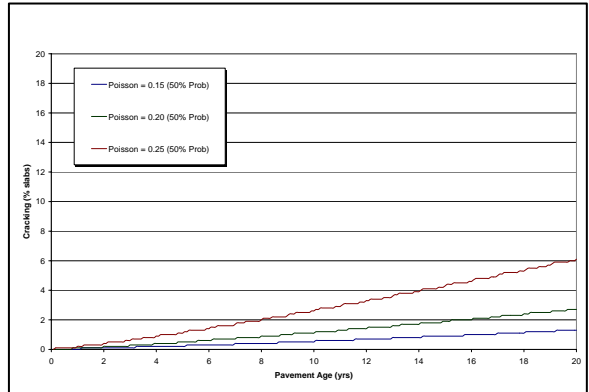


Figure B44. Sensitivity of Cracking to Poisson's Ratio

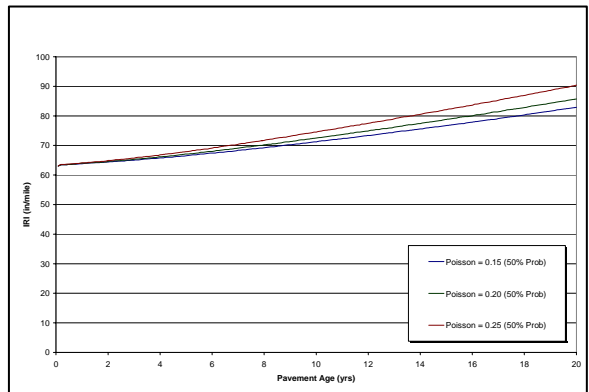


Figure B45. Sensitivity of IRI to Poisson's Ratio

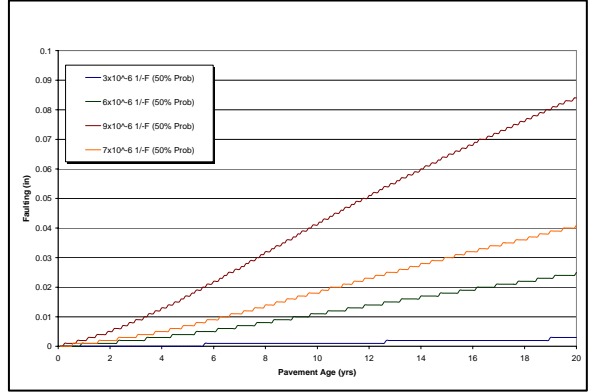


Figure B46. Sensitivity of Faulting to Coefficient of Thermal Expansion

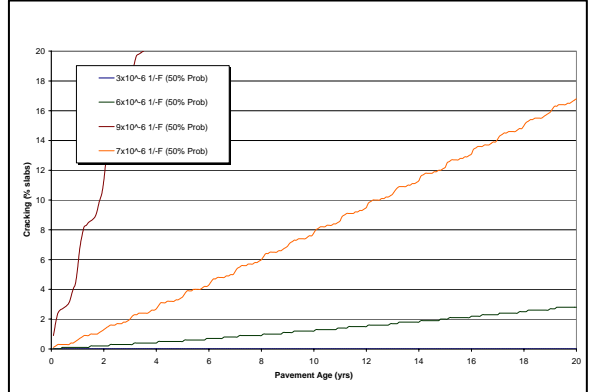


Figure B47. Sensitivity of Cracking to Coefficient of Thermal Expansion

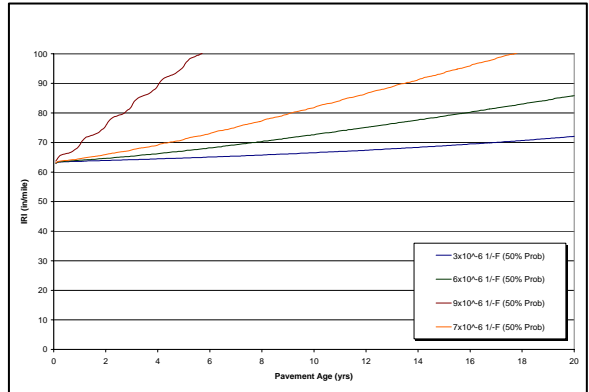


Figure B48. Sensitivity of IRI to Coefficient of Thermal Expansion

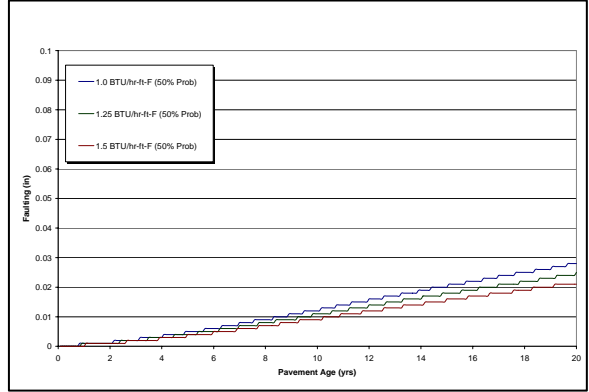


Figure B49. Sensitivity of Faulting to Thermal Conductivity

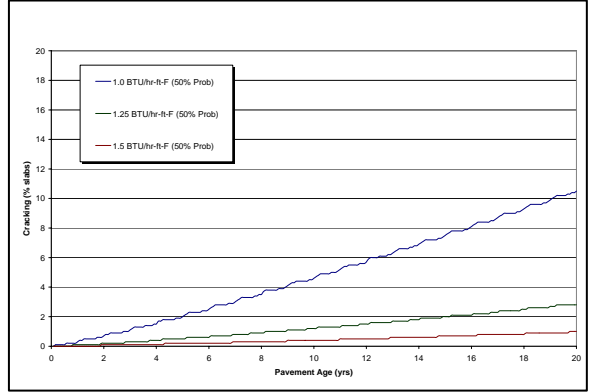


Figure B50. Sensitivity of Cracking to Thermal Conductivity

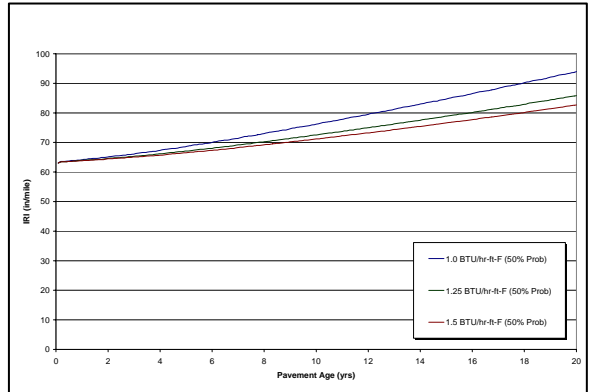


Figure B51. Sensitivity of IRI to Thermal Conductivity

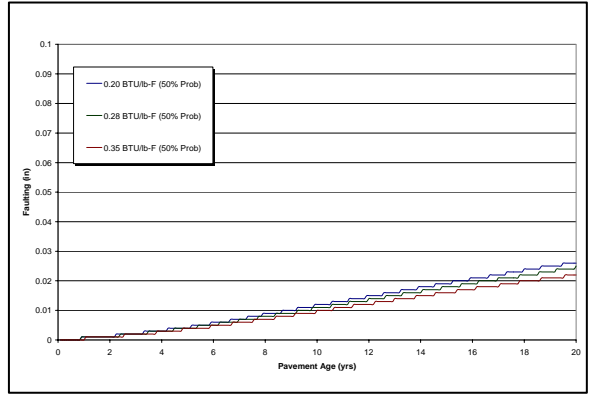


Figure B52. Sensitivity of Faulting to Heat Capacity

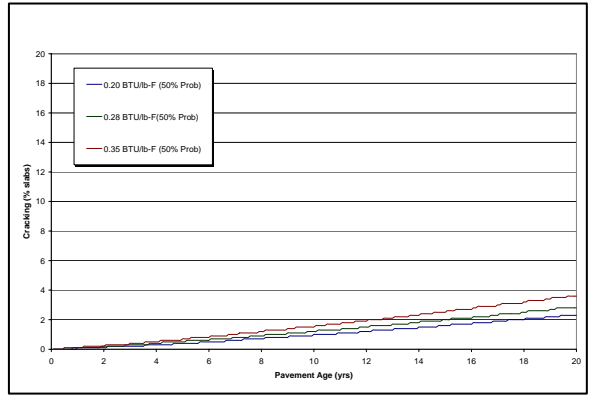


Figure B53. Sensitivity of Cracking to Heat Capacity

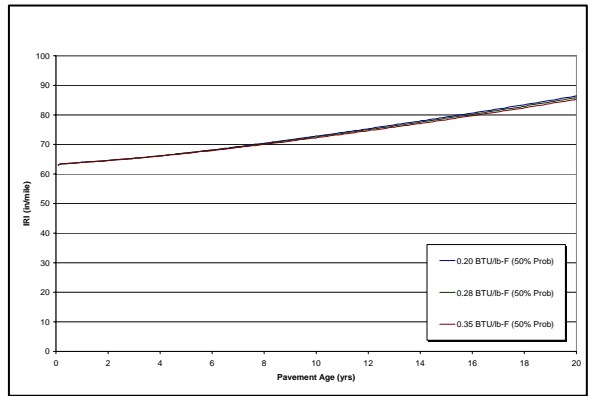


Figure B54. Sensitivity of IRI to Heat Capacity

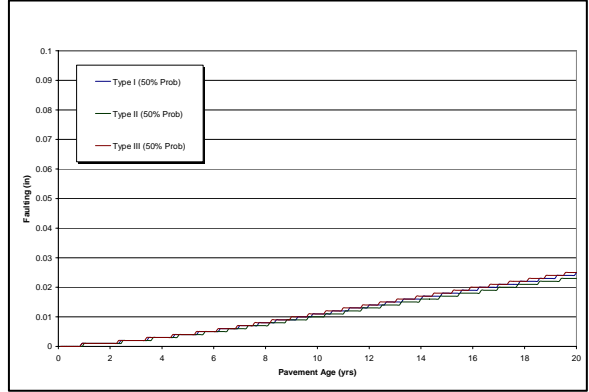


Figure B55. Sensitivity of Faulting to Cement Type

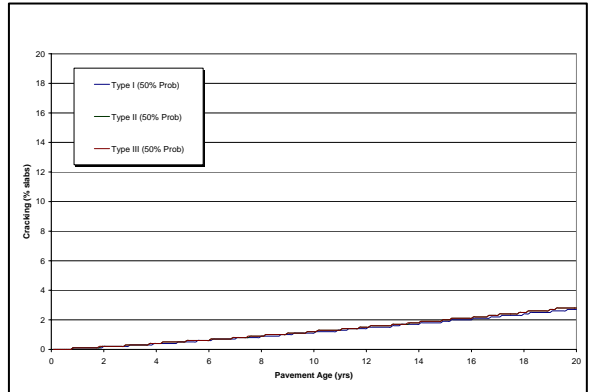


Figure B56. Sensitivity of Cracking to Cement Type

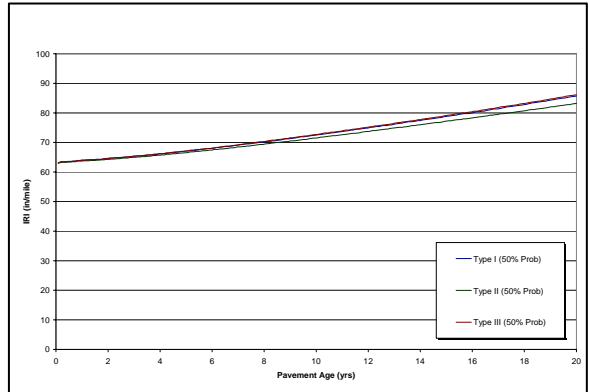


Figure B57. Sensitivity of IRI to Cement Type

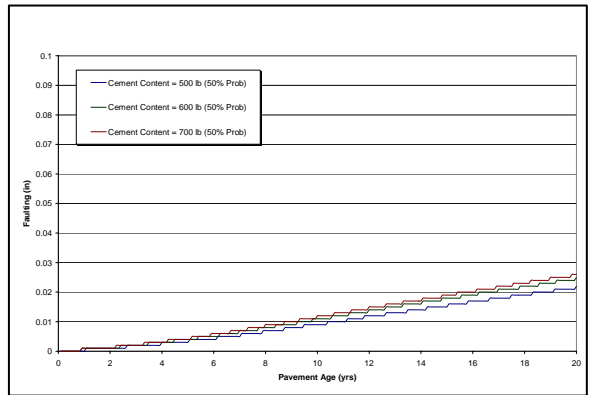


Figure B58. Sensitivity of Faulting to Cement Content

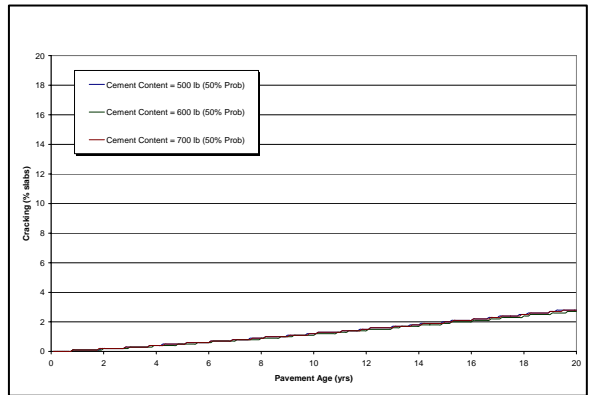


Figure B59. Sensitivity of Cracking to Cement Content

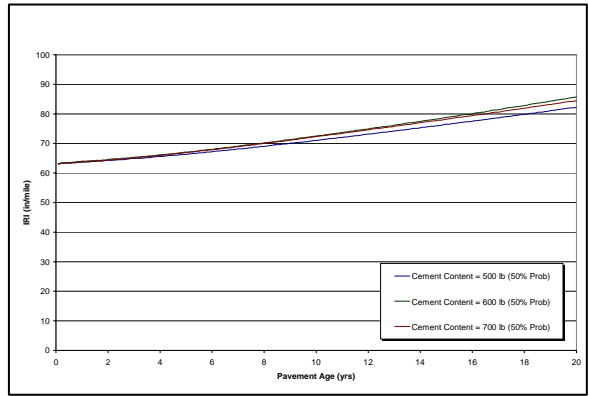


Figure B60. Sensitivity of IRI to Cement Content

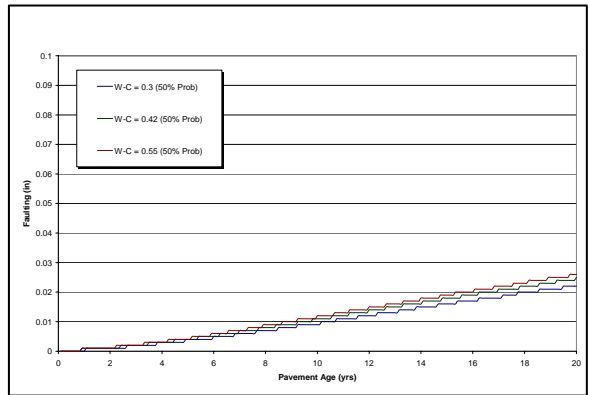


Figure B61. Sensitivity of Faulting to Water-Cement Ratio

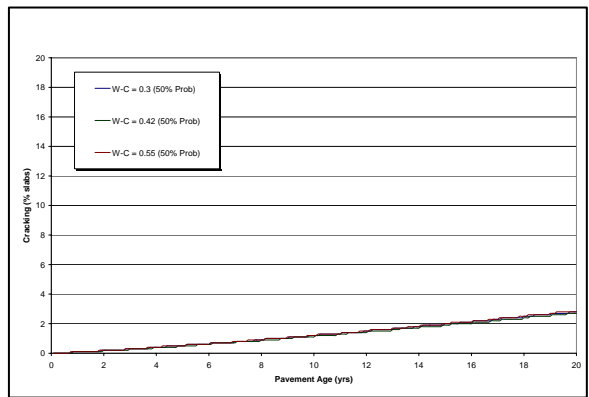


Figure B62. Sensitivity of Cracking to Water-Cement Ratio

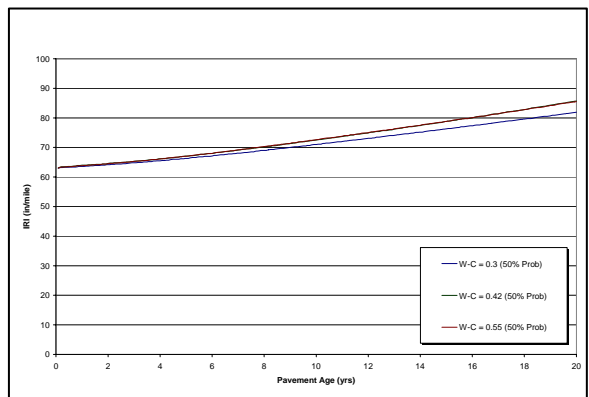


Figure B63. Sensitivity of IRI to Water-Cement Ratio

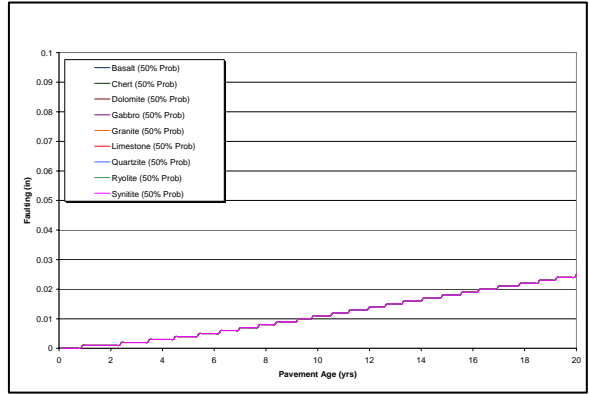


Figure B64. Sensitivity of Faulting to Aggregate Type

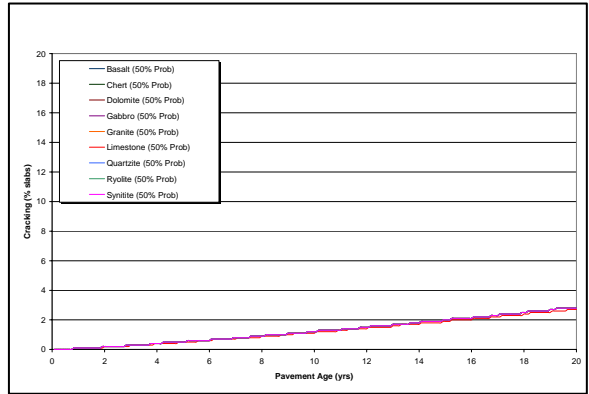


Figure B65. Sensitivity of Cracking to Aggregate Type

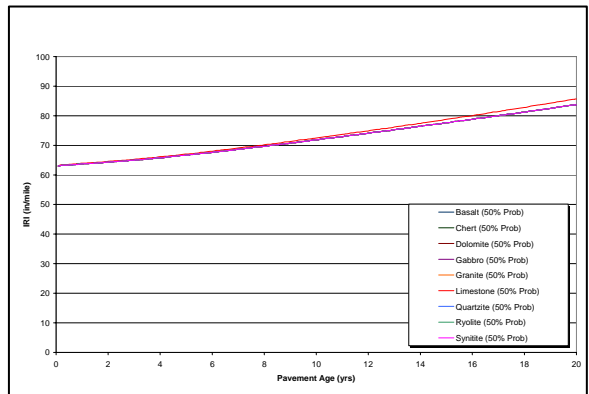


Figure B66. Sensitivity of IRI to Aggregate Type

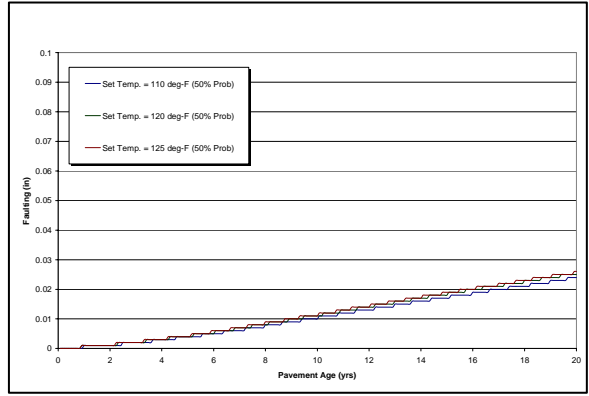


Figure B67. Sensitivity of Faulting to PCC Set Temperature

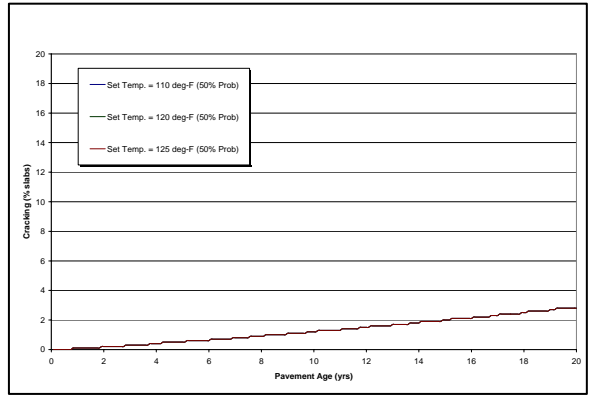


Figure B68. Sensitivity of Cracking to PCC Set Temperature

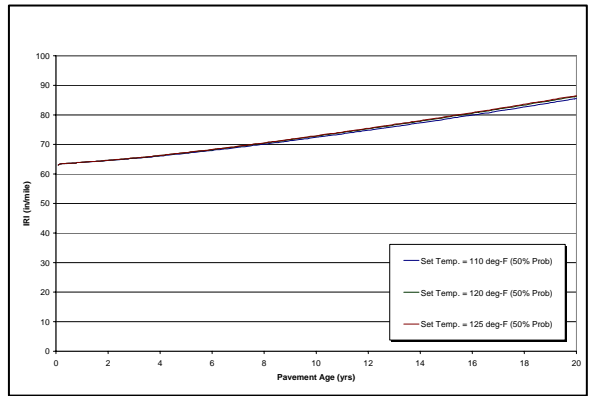


Figure B69. Sensitivity of IRI to PCC Set Temperature

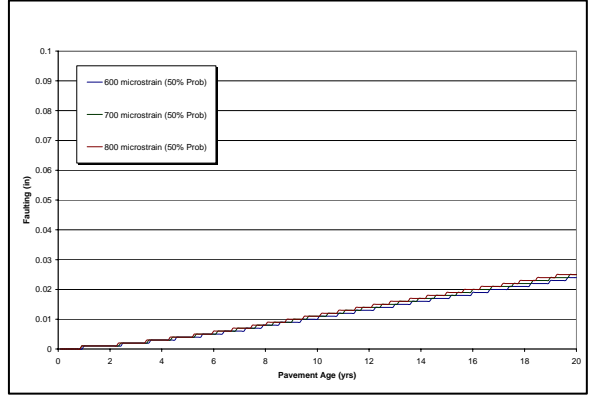


Figure B70. Sensitivity of Faulting to Ultimate Shrinkage at 40% R.H.

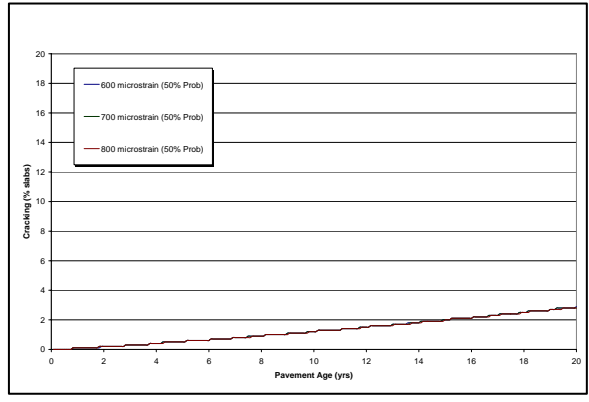


Figure B71. Sensitivity of Cracking to Ultimate Shrinkage at 40% R.H.

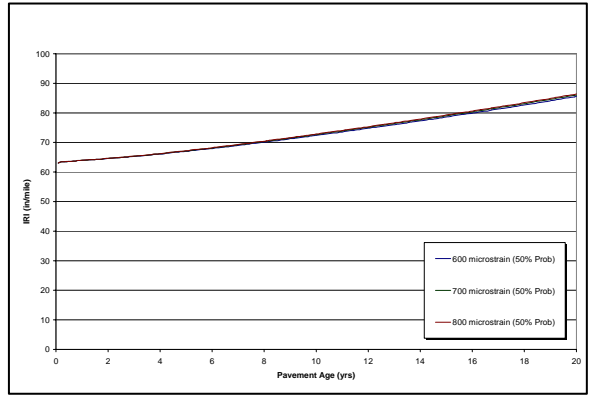


Figure B72. Sensitivity of IRI to Ultimate Shrinkage at 40% R.H.

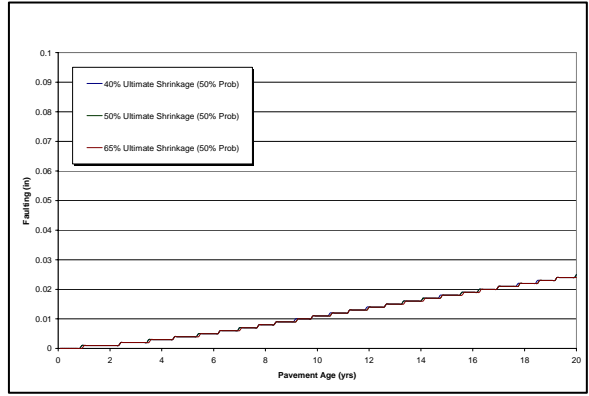


Figure B73. Sensitivity of Faulting to Reversible Shrinkage

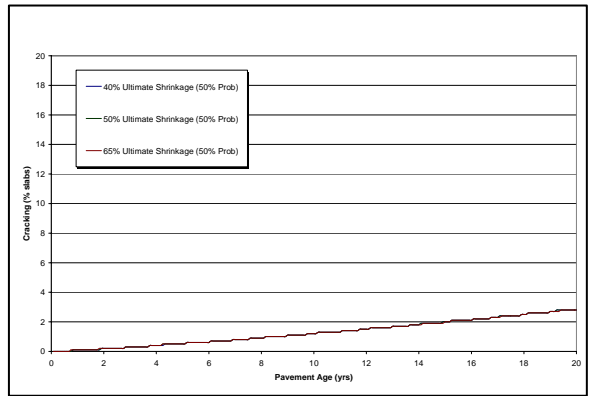


Figure B74. Sensitivity of Cracking to Reversible Shrinkage

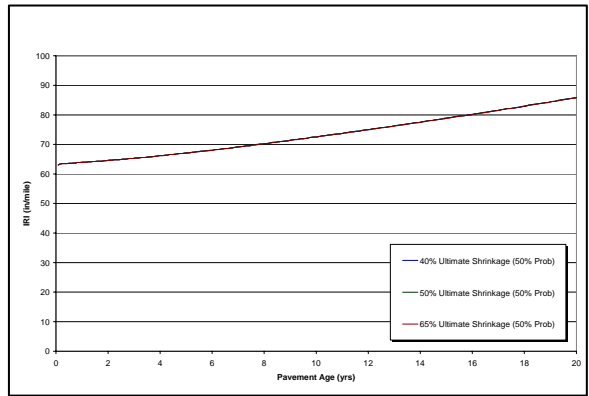


Figure B75. Sensitivity of IRI to Reversible Shrinkage

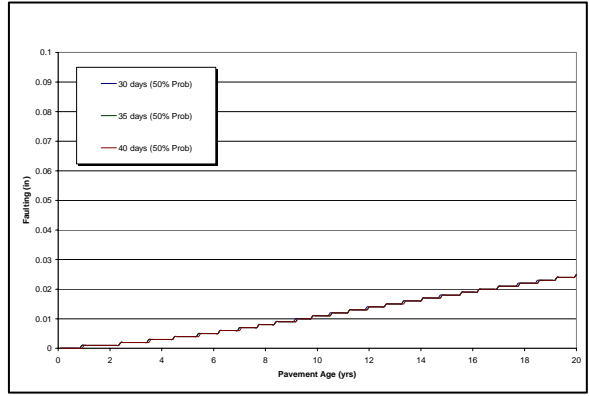


Figure B76. Sensitivity of Faulting to Time to Develop 50% Ultimate Shrinkage

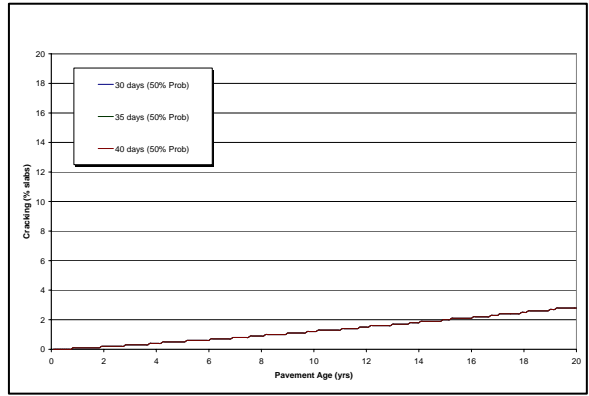


Figure B77. Sensitivity of Cracking to Time to Develop 50% Ultimate Shrinkage

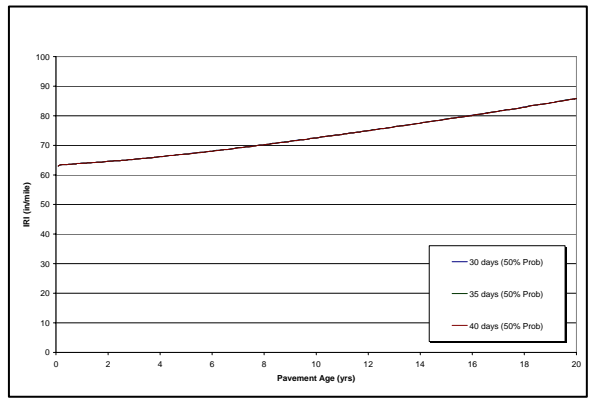


Figure B78. Sensitivity of IRI to Time to Develop 50% Ultimate Shrinkage

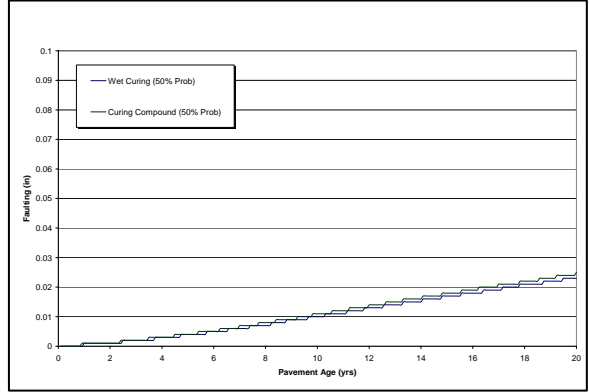


Figure B79. Sensitivity of Faulting to Curing Method

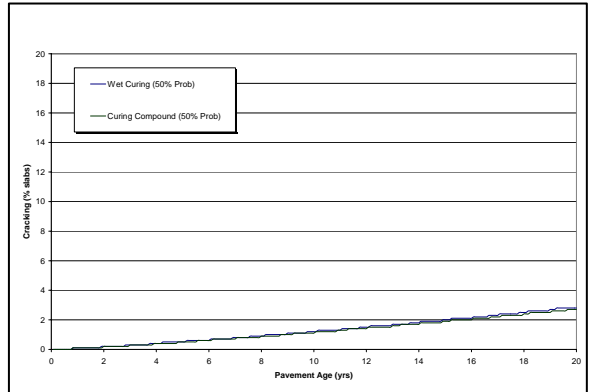


Figure B80. Sensitivity of Cracking to Curing Method

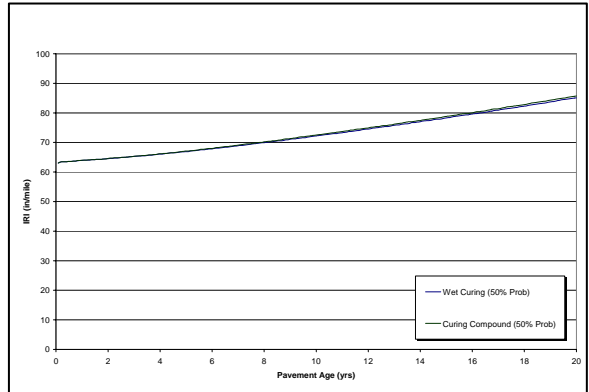


Figure B81. Sensitivity of IRI to Curing Method

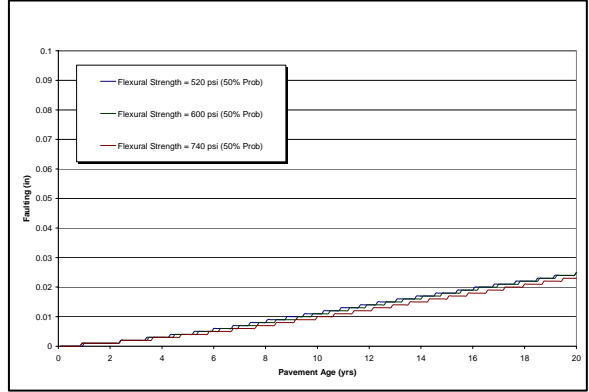


Figure B82. Sensitivity of Faulting to 28-day Modulus of Rupture

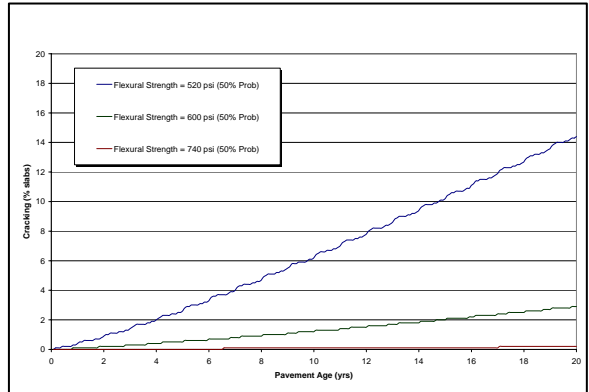


Figure B83. Sensitivity of Cracking to 28-day Modulus of Rupture

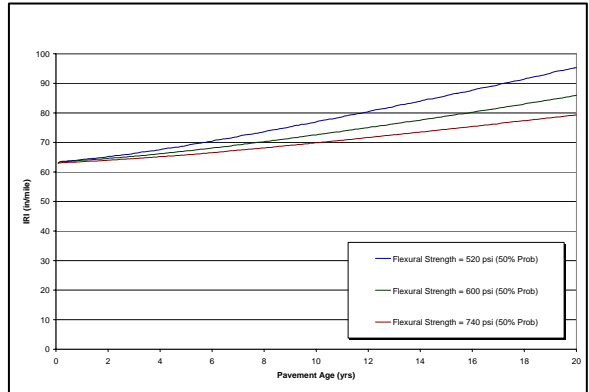


Figure B84. Sensitivity of IRI to 28-day Modulus of Rupture

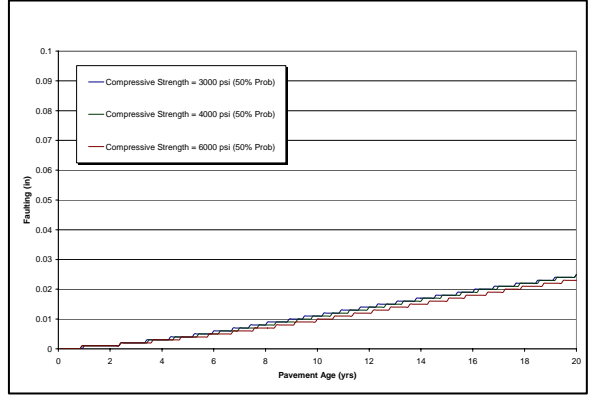


Figure B85. Sensitivity of Faulting to 28-day Compressive Strength

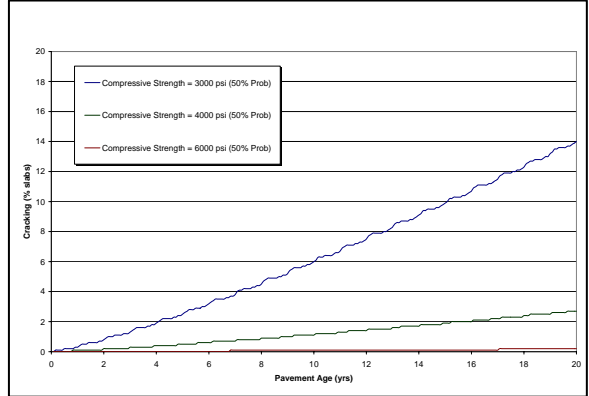


Figure B86. Sensitivity of Cracking to 28-day Compressive Strength

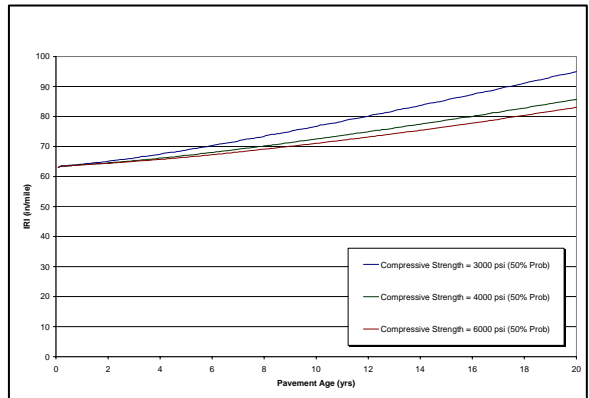


Figure B87. Sensitivity of IRI to 28-day Compressive Strength

APPENDIX C

Record of Inputs for *MEPDG* Flexible Pavement Analysis

Table C1: Record of inputs for Phase I DG 2002 HMA runs

| Project Information | Value |
|--|---------------------------|
| ◆ General Information | |
| ◆ Design Life | 20 |
| ◆ Base/Subgrade Construction Month | Sept. |
| ◆ Pavement Construction Month | Sept. |
| ◆ Traffic Open Month | Sept. |
| ◆ Type of Design (New Pavements: Flexible Pavement, JPCP, CRCP; Restoration: JPCP; Overlay: Asphalt/PCC) | New Flexible Pavement |
| ◆ Site/Project Identification | |
| ◆ Location | Fay. |
| ◆ Project ID | |
| ◆ Section ID | |
| ◆ Functional class | |
| ◆ Date | |
| ◆ Station/milepost format | |
| ◆ Station/milepost begin | |
| ◆ Traffic direction | |
| ◆ Analysis Parameters | |
| ◆ Terminal IRI (International Roughness Index) (in/mi) | 172 |
| ◆ AC Surface Down Cracking Long. Cracking (ft/mi) | 1000 |
| ◆ AC Bottom Up Cracking Alligator Cracking (ft/mi) | 25 |
| ◆ AC Thermal Fracture (ft/mi) | 1000 |
| ◆ Chemically Stabilized Layer Fatigue fracture (%) | 25 |
| ◆ Permanent Deformation – Total Pavement (in) | 0.75 |
| Inputs | |
| ◆ Traffic | |
| ◆ General | |
| ◆ Two-way average annual daily truck traffic (or Two-way annual average daily traffic and Percent of heavy vehicles) | Need Value (Used 1000) |
| ◆ Number of lanes in design direction | 2 |
| ◆ Percent of trucks in design direction | 50.0 |
| ◆ Percent of trucks in design lane | 95.0 |
| ◆ Operational speed | 60 |
| ◆ Traffic Volume Adjustment Factors | |
| ◆ Monthly Adjustment – Table of Monthly | 1.0 for all |

| | |
|---|---|
| Adjustment Factors (MAF) for each month for Classes 4-13; Level 1 is Site Specific, Level 3 is Default | |
| ◆ Vehicle Class Distribution | Default |
| ◆ Hourly Distribution | Default |
| ◆ Traffic Growth Factor (%) | 4-Comp. |
| ◆ Axle Load Distribution Factors | Default |
| ◆ General Traffic Inputs | |
| ◆ Mean wheel location (in from lane marking) | 18 |
| ◆ Traffic wander standard deviation (in) | 10 |
| ◆ Design lane width (ft) | 12 |
| ◆ Number Axles/Truck – Table showing values for Single through Quad-axle trucks from Class 4 – Class 13 | Default |
| ◆ Axle Configuration | Default |
| ◆ Wheelbase – Information for Short, Medium, and Long wheelbases | Default |
| ◆ Climate | |
| ◆ Climate Data File from included weather station data (may require depth of water table) | Need Location (Used Fayetteville with depth of water table = 20 ft) |
| ◆ Structure | |
| ◆ Thermal Cracking | |
| ◆ Average Tensile Strength at 14°F (psi) | Default |
| ◆ Creep Test Duration (sec) | Default |
| ◆ Loading Time vs. Creep Compliance Table | Default |
| ◆ Compute Mix Coefficient of Thermal Contraction | ✓ |
| ◆ Mixture VMA (%) | Default value |
| ◆ Aggregate Coefficient of Thermal Contraction | Default value |
| ◆ Drainage and Surface Properties | |
| ◆ Surface shortwave absorptivity | 0.80/0.85/0.90 |
| ◆ Layers | |
| ◆ Layer 1 – Asphalt | |
| ◆ Asphalt Material Type | Asphalt Concrete |
| ◆ Layer Thickness | 4 in |
| ◆ Asphalt Mix | |
| ◆ Cumulative % Retained ¾ inch Sieve | 0 |
| ◆ Cumulative % Retained 3/8 inch | 24 |

| | |
|--|--------------------------|
| Sieve | |
| ◆ Cumulative % Retained #4 Sieve | 58 |
| ◆ % Passing #200 Sieve | 3.6 |
| ◆ Asphalt Binder | |
| ◆ Options (Superpave Binder Grading, Conventional Viscosity Grade, Conventional Penetration Grade) | Superpave Binder Grading |
| ◆ Binder Grade | 64-22 |
| ◆ A | Defaults |
| ◆ VTS | Defaults |
| ◆ Asphalt General | |
| ◆ General | |
| ◆ Reference Temperature (°F) | 70 |
| ◆ Volumetric Properties | |
| ◆ Effective Binder Content (%) | 4.72 |
| ◆ Air Voids (%) | 4.5 |
| ◆ Total Unit Weight (pcf) | 148 |
| ◆ Poisson's ratio | 0.30/0.35/0.40 |
| ◆ Thermal Properties | |
| ◆ Thermal Conductivity Asphalt (BTU/hr-ft-F°) | 0.50/0.67/1.00 |
| ◆ Heat Capacity (BTU/lb-F°) | 0.10/0.23/0.50 |
| ◆ Layer 2 – Asphalt | |
| ◆ Asphalt Material Type | Asphalt Concrete |
| ◆ Layer Thickness | 6 in |
| ◆ Asphalt Mix | |
| ◆ Cumulative % Retained ¾ inch Sieve | 15 |
| ◆ Cumulative % Retained 3/8 inch Sieve | 36 |
| ◆ Cumulative % Retained #4 Sieve | 66 |
| ◆ % Passing #200 Sieve | 3.6 |
| ◆ Asphalt Binder | |
| ◆ Options (Superpave Binder Grading, Conventional Viscosity Grade, Conventional Penetration Grade) | Superpave Binder Grading |
| ◆ Binder Grade | 70-22 |
| ◆ A | Defaults |
| ◆ VTS | Defaults |

| | |
|---|--------------------------|
| ◆ Asphalt General | |
| ◆ General | |
| ◆ Reference Temperature (°F) | 70 |
| ◆ Volumetric Properties | |
| ◆ Effective Binder Content (%) | 3.81 |
| ◆ Air Voids (%) | 4.5 |
| ◆ Total Unit Weight (pcf) | 148 |
| ◆ Poisson's ratio | 0.30/0.35/0.40 |
| ◆ Thermal Properties | |
| ◆ Thermal Conductivity Asphalt (BTU/hr-ft-F°) | 0.50/0.67/1.00 |
| ◆ Heat Capacity (BTU/lb-F°) | 0.10/0.23/0.50 |
| ◆ Layer 3 – Granular Base | |
| ◆ Unbound Material | Crushed Stone |
| ◆ Thickness (in) | 12 |
| ◆ Strength Properties | |
| ◆ Input Level (Level 1, 2, 3) | 3 |
| ◆ Poisson's Ratio | 0.35 |
| ◆ Coefficient of Lateral Pressure, Ko | 0.5 |
| ◆ Material Property | Modulus (psi) ✓ |
| ◆ Modulus (input)(psi) | 10000 |
| ◆ Analysis Type | ICM Calculated Modulus ✓ |
| ◆ ICM | |
| ◆ Gradation and Plasticity Index | |
| ◆ Plasticity Index, PI | 1 |
| ◆ Passing #200 Sieve (%) | 7 |
| ◆ Passing #4 Sieve (%) | 40 |
| ◆ D60 (mm) | 15 |
| ◆ Compacted Unbound Material | ✓ |
| ◆ Calculated/Derived Parameters | Use Defaults |
| ◆ Layer 4 – Subgrade | |
| ◆ Unbound Material | A-6 |
| ◆ Thickness (in) | Semi-infinite |
| ◆ Strength Properties | |
| ◆ Input Level (Level 1, 2, 3) | 3 |
| ◆ Poisson's Ratio | 0.35 |
| ◆ Coefficient of Lateral Pressure, Ko | 0.5 |
| ◆ Material Property | Modulus (psi) ✓ |
| ◆ Modulus (input)(psi) | 17000 |

| | |
|----------------------------------|--------------------------|
| ◆ Analysis Type | ICM Calculated Modulus ✓ |
| ◆ ICM | |
| ◆ Gradation and Plasticity Index | |
| ◆ Plasticity Index, PI | 25 |
| ◆ Passing #200 Sieve (%) | 80 |
| ◆ Passing #4 Sieve (%) | 95 |
| ◆ D60 (mm) | 0.01 |
| ◆ Compacted Unbound Material | ✓ |
| ◆ Calculated/Derived Parameters | Use Defaults |

* Shaded row indicates the parameter that will be analyzed.

Table C2: Record of inputs for Phase III DG 2002 HMA runs where Poisson's ratio, SSA, HC, and TC values are varied

| Project Information | Value |
|--|---------------------------|
| ◆ General Information | |
| ◆ Design Life | 20 |
| ◆ Base/Subgrade Construction Month | Sept. |
| ◆ Pavement Construction Month | Sept. |
| ◆ Traffic Open Month | Sept. |
| ◆ Type of Design (New Pavements: Flexible Pavement, JPCP, CRCP; Restoration: JPCP; Overlay: Asphalt or PCC) | New Flexible Pavement |
| ◆ Site/Project Identification | |
| ◆ Location | Fay. |
| ◆ Project ID | |
| ◆ Section ID | |
| ◆ Functional class | |
| ◆ Date | |
| ◆ Station/milepost format | |
| ◆ Station/milepost begin | |
| ◆ Traffic direction | |
| ◆ Analysis Parameters | |
| ◆ Terminal IRI (International Roughness Index) (in/mi) | 172 |
| ◆ AC Surface Down Cracking Long. Cracking (ft/mi) | 1000 |
| ◆ AC Bottom Up Cracking Alligator Cracking (ft/mi) | 25 |
| ◆ AC Thermal Fracture (ft/mi) | 1000 |
| ◆ Chemically Stabilized Layer Fatigue fracture (%) | 25 |
| ◆ Permanent Deformation – Total Pavement (in) | 0.75 |
| Inputs | |
| ◆ Traffic | |
| ◆ General | |
| ◆ Two-way average annual daily truck traffic (or Two-way annual average daily traffic and Percent of heavy vehicles) | Need Value (Used 1000) |
| ◆ Number of lanes in design direction | 2 |
| ◆ Percent of trucks in design direction | 50.0 |
| ◆ Percent of trucks in design lane | 95.0 |
| ◆ Operational speed | 60 |
| ◆ Traffic Volume Adjustment Factors | |

| | |
|--|---|
| ◆ Monthly Adjustment – Table of Monthly Adjustment Factors (MAF) for each month for Classes 4-13; Level 1 is Site Specific, Level 3 is Default | 1.0 for all |
| ◆ Vehicle Class Distribution | Default |
| ◆ Hourly Distribution | Default |
| ◆ Traffic Growth Factor (%) | 4-Comp. |
| ◆ Axle Load Distribution Factors | Default |
| ◆ General Traffic Inputs | |
| ◆ Mean wheel location (in from lane marking) | 18 |
| ◆ Traffic wander standard deviation (in) | 10 |
| ◆ Design lane width (ft) | 12 |
| ◆ Number Axles/Truck – Table showing values for Single through Quad-axle trucks from Class 4 – Class 13 | Default |
| ◆ Axle Configuration | Default |
| ◆ Wheelbase – Information for Short, Medium, and Long wheelbases | Default |
| ◆ Climate | |
| ◆ Climate Data File from included weather station data (may require depth of water table) | Need Location (Used Fayetteville with depth of water table = 20 ft) |
| ◆ Structure | |
| ◆ Thermal Cracking | |
| ◆ Average Tensile Strength at 14°F (psi) | Default |
| ◆ Creep Test Duration (sec) | Default |
| ◆ Loading Time vs. Creep Compliance Table | Default |
| ◆ Compute Mix Coefficient of Thermal Contraction | ✓ |
| ◆ Mixture VMA (%) | Default value |
| ◆ Aggregate Coefficient of Thermal Contraction | Default value |
| ◆ Drainage and Surface Properties | |
| ◆ Surface shortwave absorptivity | 0.80/0.85/0.90 |
| ◆ Layers | |
| ◆ Layer 1 – Asphalt | |
| ◆ Asphalt Material Type | Asphalt Concrete |
| ◆ Layer Thickness | 4 in |
| ◆ Asphalt Mix | |
| ◆ Cumulative % Retained ¾ inch Sieve | Based on gradation data |

| | |
|--|--|
| ◆ Cumulative % Retained 3/8 inch Sieve | Based on gradation data |
| ◆ Cumulative % Retained #4 Sieve | Based on gradation data |
| ◆ % Passing #200 Sieve | Based on gradation data |
| ◆ Asphalt Binder | |
| ◆ Options (Superpave Binder Grading, Conventional Viscosity Grade, Conventional Penetration Grade) | Superpave Binder Grading |
| ◆ Binder Grade | 64-22 |
| ◆ A | Defaults |
| ◆ VTS | Defaults |
| ◆ Asphalt General | |
| ◆ General | |
| ◆ Reference Temperature (°F) | 70 |
| ◆ Volumetric Properties | |
| ◆ Effective Binder Content (%) | Based on recalculated value shown in Appendix C for each mix |
| ◆ Air Voids (%) | 8.0 |
| ◆ Total Unit Weight (pcf) | 148 |
| ◆ Poisson's ratio | 0.30/0.35/0.40 |
| ◆ Thermal Properties | |
| ◆ Thermal Conductivity Asphalt (BTU/hr-ft-F°) | 0.50/0.67/1.00 |
| ◆ Heat Capacity (BTU/lb-F°) | 0.10/0.23/0.50 |
| ◆ Layer 2 – Asphalt | |
| ◆ Asphalt Material Type | Asphalt Concrete |
| ◆ Layer Thickness | 6 in |
| ◆ Asphalt Mix | |
| ◆ Cumulative % Retained 3/4 inch Sieve | Based on gradation data |
| ◆ Cumulative % Retained 3/8 inch Sieve | Based on gradation data |
| ◆ Cumulative % Retained #4 Sieve | Based on gradation data |
| ◆ % Passing #200 Sieve | Based on gradation data |

| | |
|--|--|
| ◆ Asphalt Binder | |
| ◆ Options (Superpave Binder Grading, Conventional Viscosity Grade, Conventional Penetration Grade) | Superpave Binder Grading |
| ◆ Binder Grade | 70-22 |
| ◆ A | Defaults |
| ◆ VTS | Defaults |
| ◆ Asphalt General | |
| ◆ General | |
| ◆ Reference Temperature (°F) | 70 |
| ◆ Volumetric Properties | |
| ◆ Effective Binder Content (%) | Based on recalculated value shown in Appendix C for each mix |
| ◆ Air Voids (%) | 8.0 |
| ◆ Total Unit Weight (pcf) | 148 |
| ◆ Poisson's ratio | 0.30/0.35/0.40 |
| ◆ Thermal Properties | |
| ◆ Thermal Conductivity Asphalt (BTU/hr-ft-F°) | 0.50/0.67/1.00 |
| ◆ Heat Capacity (BTU/lb-F°) | 0.10/0.23/0.50 |
| ◆ Layer 3 – Granular Base | |
| ◆ Unbound Material | Crushed Stone |
| ◆ Thickness (in) | 12 |
| ◆ Strength Properties | |
| ◆ Input Level (Level 1, 2, 3) | 3 |
| ◆ Poisson's Ratio | 0.35 |
| ◆ Coefficient of Lateral Pressure, Ko | 0.5 |
| ◆ Material Property | Modulus (psi) ✓ |
| ◆ Modulus (input)(psi) | 10000 |
| ◆ Analysis Type | ICM Calculated Modulus ✓ |
| ◆ ICM | |
| ◆ Gradation and Plasticity Index | |
| ◆ Plasticity Index, PI | 1 |
| ◆ Passing #200 Sieve (%) | 7 |
| ◆ Passing #4 Sieve (%) | 40 |
| ◆ D60 (mm) | 15 |

| | |
|---------------------------------------|--------------------------|
| ◆ Compacted Unbound Material | ✓ |
| ◆ Calculated/Derived Parameters | Use Defaults |
| ◆ Layer 4 – Subgrade | |
| ◆ Unbound Material | A-6 |
| ◆ Thickness (in) | Semi-infinite |
| ◆ Strength Properties | |
| ◆ Input Level (Level 1, 2, 3) | 3 |
| ◆ Poisson's Ratio | 0.35 |
| ◆ Coefficient of Lateral Pressure, Ko | 0.5 |
| ◆ Material Property | Modulus (psi) ✓ |
| ◆ Modulus (input)(psi) | 17000 |
| ◆ Analysis Type | ICM Calculated Modulus ✓ |
| ◆ ICM | |
| ◆ Gradation and Plasticity Index | |
| ◆ Plasticity Index, PI | 25 |
| ◆ Passing #200 Sieve (%) | 80 |
| ◆ Passing #4 Sieve (%) | 95 |
| ◆ D60 (mm) | 0.01 |
| ◆ Compacted Unbound Material | ✓ |
| ◆ Calculated/Derived Parameters | Use Defaults |

* Shaded row indicates the parameter that will be analyzed.

Table C3: Record of inputs for Phase III DG 2002 HMA runs where Air Voids, Binder Grade, and Total Unit Weight values are varied (12.5mm Mix)

| Project Information | Value |
|--|---------------------------|
| ◆ General Information | |
| ◆ Design Life | 20 |
| ◆ Base/Subgrade Construction Month | Sept. |
| ◆ Pavement Construction Month | Sept. |
| ◆ Traffic Open Month | Sept. |
| ◆ Type of Design (New Pavements: Flexible Pavement, JPCP, CRCP; Restoration: JPCP; Overlay: Asphalt or PCC) | New Flexible Pavement |
| ◆ Site/Project Identification | |
| ◆ Location | Fay. |
| ◆ Project ID | |
| ◆ Section ID | |
| ◆ Functional class | |
| ◆ Date | |
| ◆ Station/milepost format | |
| ◆ Station/milepost begin | |
| ◆ Traffic direction | |
| ◆ Analysis Parameters | |
| ◆ Terminal IRI (International Roughness Index) (in/mi) | 172 |
| ◆ AC Surface Down Cracking Long. Cracking (ft/mi) | 1000 |
| ◆ AC Bottom Up Cracking Alligator Cracking (ft/mi) | 25 |
| ◆ AC Thermal Fracture (ft/mi) | 1000 |
| ◆ Chemically Stabilized Layer Fatigue fracture (%) | 25 |
| ◆ Permanent Deformation – Total Pavement (in) | 0.75 |
| Inputs | |
| ◆ Traffic | |
| ◆ General | |
| ◆ Two-way average annual daily truck traffic (or Two-way annual average daily traffic and Percent of heavy vehicles) | Need Value (Used 1000) |
| ◆ Number of lanes in design direction | 2 |
| ◆ Percent of trucks in design direction | 50.0 |
| ◆ Percent of trucks in design lane | 95.0 |
| ◆ Operational speed | 60 |
| ◆ Traffic Volume Adjustment Factors | |

| | |
|--|---|
| ◆ Monthly Adjustment – Table of Monthly Adjustment Factors (MAF) for each month for Classes 4-13; Level 1 is Site Specific, Level 3 is Default | 1.0 for all |
| ◆ Vehicle Class Distribution | Default |
| ◆ Hourly Distribution | Default |
| ◆ Traffic Growth Factor (%) | 4-Comp. |
| ◆ Axle Load Distribution Factors | Default |
| ◆ General Traffic Inputs | |
| ◆ Mean wheel location (in from lane marking) | 18 |
| ◆ Traffic wander standard deviation (in) | 10 |
| ◆ Design lane width (ft) | 12 |
| ◆ Number Axles/Truck – Table showing values for Single through Quad-axle trucks from Class 4 – Class 13 | Default |
| ◆ Axle Configuration | Default |
| ◆ Wheelbase – Information for Short, Medium, and Long wheelbases | Default |
| ◆ Climate | |
| ◆ Climate Data File from included weather station data (may require depth of water table) | Need Location (Used Fayetteville with depth of water table = 20 ft) |
| ◆ Structure | |
| ◆ Thermal Cracking | |
| ◆ Average Tensile Strength at 14°F (psi) | Default |
| ◆ Creep Test Duration (sec) | Default |
| ◆ Loading Time vs. Creep Compliance Table | Default |
| ◆ Compute Mix Coefficient of Thermal Contraction | ✓ |
| ◆ Mixture VMA (%) | Default value |
| ◆ Aggregate Coefficient of Thermal Contraction | Default value |
| ◆ Drainage and Surface Properties | |
| ◆ Surface shortwave absorptivity | 0.85 |
| ◆ Layers | |
| ◆ Layer 1 – Asphalt | |
| ◆ Asphalt Material Type | Asphalt Concrete |
| ◆ Layer Thickness | 4 in |
| ◆ Asphalt Mix | |
| ◆ Cumulative % Retained $\frac{3}{4}$ inch Sieve | Based on gradation data |

| | |
|--|--------------------------|
| ◆ Cumulative % Retained 3/8 inch Sieve | Based on gradation data |
| ◆ Cumulative % Retained #4 Sieve | Based on gradation data |
| ◆ % Passing #200 Sieve | Based on gradation data |
| ◆ Asphalt Binder | |
| ◆ Options (Superpave Binder Grading, Conventional Viscosity Grade, Conventional Penetration Grade) | Superpave Binder Grading |
| ◆ Binder Grade | 64/70/76-22 |
| ◆ A | Defaults |
| ◆ VTS | Defaults |
| ◆ Asphalt General | |
| ◆ General | |
| ◆ Reference Temperature (°F) | 70 |
| ◆ Volumetric Properties | |
| ◆ Effective Binder Content (%) | 4.72 |
| ◆ Air Voids (%) | 3.0/4.0/4.5/5.0/6.0/8.0 |
| ◆ Total Unit Weight (pcf) | 122/135/148 |
| ◆ Poisson's ratio | 0.35 |
| ◆ Thermal Properties | |
| ◆ Thermal Conductivity Asphalt (BTU/hr-ft-F°) | 0.67 |
| ◆ Heat Capacity (BTU/lb-F°) | 0.23 |
| ◆ Layer 2 – Granular Base | |
| ◆ Unbound Material | Crushed Stone |
| ◆ Thickness (in) | 12 |
| ◆ Strength Properties | |
| ◆ Input Level (Level 1, 2, 3) | 3 |
| ◆ Poisson's Ratio | 0.35 |
| ◆ Coefficient of Lateral Pressure, Ko | 0.5 |
| ◆ Material Property | Modulus (psi) ✓ |
| ◆ Modulus (input)(psi) | 10000 |
| ◆ Analysis Type | ICM Calculated Modulus ✓ |
| ◆ ICM | |
| ◆ Gradation and Plasticity Index | |
| ◆ Plasticity Index, PI | 1 |

| | |
|---------------------------------------|--------------------------|
| ◆ Passing #200 Sieve (%) | 7 |
| ◆ Passing #4 Sieve (%) | 40 |
| ◆ D60 (mm) | 15 |
| ◆ Compacted Unbound Material | ✓ |
| ◆ Calculated/Derived Parameters | Use Defaults |
| ◆ Layer 3 – Subgrade | |
| ◆ Unbound Material | A-6 |
| ◆ Thickness (in) | Semi-infinite |
| ◆ Strength Properties | |
| ◆ Input Level (Level 1, 2, 3) | 3 |
| ◆ Poisson's Ratio | 0.35 |
| ◆ Coefficient of Lateral Pressure, Ko | 0.5 |
| ◆ Material Property | Modulus (psi) ✓ |
| ◆ Modulus (input)(psi) | 17000 |
| ◆ Analysis Type | ICM Calculated Modulus ✓ |
| ◆ ICM | |
| ◆ Gradation and Plasticity Index | |
| ◆ Plasticity Index, PI | 25 |
| ◆ Passing #200 Sieve (%) | 80 |
| ◆ Passing #4 Sieve (%) | 95 |
| ◆ D60 (mm) | 0.01 |
| ◆ Compacted Unbound Material | ✓ |
| ◆ Calculated/Derived Parameters | Use Defaults |

* Shaded row indicates the parameter that will be analyzed.

Table C4: Record of inputs for Phase III DG 2002 HMA runs where Air Voids, Binder Grade, and Total Unit Weight values are varied (25.0 mm Mix)

| Project Information | Value |
|--|---------------------------|
| ◆ General Information | |
| ◆ Design Life | 20 |
| ◆ Base/Subgrade Construction Month | Sept. |
| ◆ Pavement Construction Month | Sept. |
| ◆ Traffic Open Month | Sept. |
| ◆ Type of Design (New Pavements: Flexible Pavement, JPCP, CRCP; Restoration: JPCP; Overlay: Asphalt or PCC) | New Flexible Pavement |
| ◆ Site/Project Identification | |
| ◆ Location | Fay. |
| ◆ Project ID | |
| ◆ Section ID | |
| ◆ Functional class | |
| ◆ Date | |
| ◆ Station/milepost format | |
| ◆ Station/milepost begin | |
| ◆ Traffic direction | |
| ◆ Analysis Parameters | |
| ◆ Terminal IRI (International Roughness Index) (in/mi) | 172 |
| ◆ AC Surface Down Cracking Long. Cracking (ft/mi) | 1000 |
| ◆ AC Bottom Up Cracking Alligator Cracking (ft/mi) | 25 |
| ◆ AC Thermal Fracture (ft/mi) | 1000 |
| ◆ Chemically Stabilized Layer Fatigue fracture (%) | 25 |
| ◆ Permanent Deformation – Total Pavement (in) | 0.75 |
| Inputs | |
| ◆ Traffic | |
| ◆ General | |
| ◆ Two-way average annual daily truck traffic (or Two-way annual average daily traffic and Percent of heavy vehicles) | Need Value (Used 1000) |
| ◆ Number of lanes in design direction | 2 |
| ◆ Percent of trucks in design direction | 50.0 |
| ◆ Percent of trucks in design lane | 95.0 |
| ◆ Operational speed | 60 |
| ◆ Traffic Volume Adjustment Factors | |

| | |
|--|---|
| ◆ Monthly Adjustment – Table of Monthly Adjustment Factors (MAF) for each month for Classes 4-13; Level 1 is Site Specific, Level 3 is Default | 1.0 for all |
| ◆ Vehicle Class Distribution | Default |
| ◆ Hourly Distribution | Default |
| ◆ Traffic Growth Factor (%) | 4-Comp. |
| ◆ Axle Load Distribution Factors | Default |
| ◆ General Traffic Inputs | |
| ◆ Mean wheel location (in from lane marking) | 18 |
| ◆ Traffic wander standard deviation (in) | 10 |
| ◆ Design lane width (ft) | 12 |
| ◆ Number Axles/Truck – Table showing values for Single through Quad-axle trucks from Class 4 – Class 13 | Default |
| ◆ Axle Configuration | Default |
| ◆ Wheelbase – Information for Short, Medium, and Long wheelbases | Default |
| ◆ Climate | |
| ◆ Climate Data File from included weather station data (may require depth of water table) | Need Location (Used Fayetteville with depth of water table = 20 ft) |
| ◆ Structure | |
| ◆ Thermal Cracking | |
| ◆ Average Tensile Strength at 14°F (psi) | Default |
| ◆ Creep Test Duration (sec) | Default |
| ◆ Loading Time vs. Creep Compliance Table | Default |
| ◆ Compute Mix Coefficient of Thermal Contraction | ✓ |
| ◆ Mixture VMA (%) | Default value |
| ◆ Aggregate Coefficient of Thermal Contraction | Default value |
| ◆ Drainage and Surface Properties | |
| ◆ Surface shortwave absorptivity | 0.85 |
| ◆ Layers | |
| ◆ Layer 1 – Asphalt | |
| ◆ Asphalt Material Type | Asphalt Concrete |
| ◆ Layer Thickness | 4 in |
| ◆ Asphalt Mix | |
| ◆ Cumulative % Retained ¾ inch Sieve | Based on gradation data |

| | |
|--|--------------------------|
| ◆ Cumulative % Retained 3/8 inch Sieve | Based on gradation data |
| ◆ Cumulative % Retained #4 Sieve | Based on gradation data |
| ◆ % Passing #200 Sieve | Based on gradation data |
| ◆ Asphalt Binder | |
| ◆ Options (Superpave Binder Grading, Conventional Viscosity Grade, Conventional Penetration Grade) | Superpave Binder Grading |
| ◆ Binder Grade | 64/70/76-22 |
| ◆ A | Defaults |
| ◆ VTS | Defaults |
| ◆ Asphalt General | |
| ◆ General | |
| ◆ Reference Temperature (°F) | 70 |
| ◆ Volumetric Properties | |
| ◆ Effective Binder Content (%) | 4.72 |
| ◆ Air Voids (%) | 3.0/4.0/4/5/5.0/6.0/8.0 |
| ◆ Total Unit Weight (pcf) | 122/135/148 |
| ◆ Poisson's ratio | 0.35 |
| ◆ Thermal Properties | |
| ◆ Thermal Conductivity Asphalt (BTU/hr-ft-F°) | 0.67 |
| ◆ Heat Capacity (BTU/lb-F°) | 0.23 |
| ◆ Layer 2 – Asphalt | |
| ◆ Asphalt Material Type | Asphalt Concrete |
| ◆ Layer Thickness | 6 in |
| ◆ Asphalt Mix | |
| ◆ Cumulative % Retained 3/4 inch Sieve | Based on gradation data |
| ◆ Cumulative % Retained 3/8 inch Sieve | Based on gradation data |
| ◆ Cumulative % Retained #4 Sieve | Based on gradation data |
| ◆ % Passing #200 Sieve | Based on gradation data |
| ◆ Asphalt Binder | |
| ◆ Options (Superpave Binder Grading, Conventional Viscosity | Superpave Binder Grading |

| | |
|---|--------------------------|
| Grade, Conventional Penetration Grade) | |
| ◆ Binder Grade | 64/70/76-22 |
| ◆ A | Defaults |
| ◆ VTS | Defaults |
| ◆ Asphalt General | |
| ◆ General | |
| ◆ Reference Temperature (°F) | 70 |
| ◆ Volumetric Properties | |
| ◆ Effective Binder Content (%) | 4.72 |
| ◆ Air Voids (%) | 3.0/4.0/4.5/5.0/6.0/8.0 |
| ◆ Total Unit Weight (pcf) | 122/135/148 |
| ◆ Poisson's ratio | 0.35 |
| ◆ Thermal Properties | |
| ◆ Thermal Conductivity Asphalt (BTU/hr-ft-F°) | 0.67 |
| ◆ Heat Capacity (BTU/lb-F°) | 0.23 |
| ◆ Layer 3 – Granular Base | |
| ◆ Unbound Material | Crushed Stone |
| ◆ Thickness (in) | 12 |
| ◆ Strength Properties | |
| ◆ Input Level (Level 1, 2, 3) | 3 |
| ◆ Poisson's Ratio | 0.35 |
| ◆ Coefficient of Lateral Pressure, Ko | 0.5 |
| ◆ Material Property | Modulus (psi) ✓ |
| ◆ Modulus (input)(psi) | 10000 |
| ◆ Analysis Type | ICM Calculated Modulus ✓ |
| ◆ ICM | |
| ◆ Gradation and Plasticity Index | |
| ◆ Plasticity Index, PI | 1 |
| ◆ Passing #200 Sieve (%) | 7 |
| ◆ Passing #4 Sieve (%) | 40 |
| ◆ D60 (mm) | 15 |
| ◆ Compacted Unbound Material | ✓ |
| ◆ Calculated/Derived Parameters | Use Defaults |
| ◆ Layer 4 – Subgrade | |
| ◆ Unbound Material | A-6 |
| ◆ Thickness (in) | Semi-infinite |
| ◆ Strength Properties | |

| | |
|---------------------------------------|--------------------------|
| ◆ Input Level (Level 1, 2, 3) | 3 |
| ◆ Poisson's Ratio | 0.35 |
| ◆ Coefficient of Lateral Pressure, Ko | 0.5 |
| ◆ Material Property | Modulus (psi) ✓ |
| ◆ Modulus (input)(psi) | 17000 |
| ◆ Analysis Type | ICM Calculated Modulus ✓ |
| ◆ ICM | |
| ◆ Gradation and Plasticity Index | |
| ◆ Plasticity Index, PI | 25 |
| ◆ Passing #200 Sieve (%) | 80 |
| ◆ Passing #4 Sieve (%) | 95 |
| ◆ D60 (mm) | 0.01 |
| ◆ Compacted Unbound Material | ✓ |
| ◆ Calculated/Derived Parameters | Use Defaults |

* Shaded row indicates the parameter that will be analyzed.

Table C5: Record of inputs for Phase III DG 2002 runs where the Percent Binder Effective value is varied (12.5mm Mix)

| Project Information | Value |
|--|---------------------------|
| ◆ General Information | |
| ◆ Design Life | 20 |
| ◆ Base/Subgrade Construction Month | Sept. |
| ◆ Pavement Construction Month | Sept. |
| ◆ Traffic Open Month | Sept. |
| ◆ Type of Design (New Pavements: Flexible Pavement, JPCP, CRCP; Restoration: JPCP; Overlay: Asphalt or PCC) | New Flexible Pavement |
| ◆ Site/Project Identification | |
| ◆ Location | Fay. |
| ◆ Project ID | |
| ◆ Section ID | |
| ◆ Functional class | |
| ◆ Date | |
| ◆ Station/milepost format | |
| ◆ Station/milepost begin | |
| ◆ Traffic direction | |
| ◆ Analysis Parameters | |
| ◆ Terminal IRI (International Roughness Index) (in/mi) | 172 |
| ◆ AC Surface Down Cracking Long. Cracking (ft/mi) | 1000 |
| ◆ AC Bottom Up Cracking Alligator Cracking (ft/mi) | 25 |
| ◆ AC Thermal Fracture (ft/mi) | 1000 |
| ◆ Chemically Stabilized Layer Fatigue fracture (%) | 25 |
| ◆ Permanent Deformation – Total Pavement (in) | 0.75 |
| Inputs | |
| ◆ Traffic | |
| ◆ General | |
| ◆ Two-way average annual daily truck traffic (or Two-way annual average daily traffic and Percent of heavy vehicles) | Need Value (Used 1000) |
| ◆ Number of lanes in design direction | 2 |
| ◆ Percent of trucks in design direction | 50.0 |
| ◆ Percent of trucks in design lane | 95.0 |
| ◆ Operational speed | 60 |
| ◆ Traffic Volume Adjustment Factors | |

| | |
|--|---|
| ◆ Monthly Adjustment – Table of Monthly Adjustment Factors (MAF) for each month for Classes 4-13; Level 1 is Site Specific, Level 3 is Default | 1.0 for all |
| ◆ Vehicle Class Distribution | Default |
| ◆ Hourly Distribution | Default |
| ◆ Traffic Growth Factor (%) | 4-Comp. |
| ◆ Axle Load Distribution Factors | Default |
| ◆ General Traffic Inputs | |
| ◆ Mean wheel location (in from lane marking) | 18 |
| ◆ Traffic wander standard deviation (in) | 10 |
| ◆ Design lane width (ft) | 12 |
| ◆ Number Axles/Truck – Table showing values for Single through Quad-axle trucks from Class 4 – Class 13 | Default |
| ◆ Axle Configuration | Default |
| ◆ Wheelbase – Information for Short, Medium, and Long wheelbases | Default |
| ◆ Climate | |
| ◆ Climate Data File from included weather station data (may require depth of water table) | Need Location (Used Fayetteville with depth of water table = 20 ft) |
| ◆ Structure | |
| ◆ Thermal Cracking | |
| ◆ Average Tensile Strength at 14°F (psi) | Default |
| ◆ Creep Test Duration (sec) | Default |
| ◆ Loading Time vs. Creep Compliance Table | Default |
| ◆ Compute Mix Coefficient of Thermal Contraction | ✓ |
| ◆ Mixture VMA (%) | Default value |
| ◆ Aggregate Coefficient of Thermal Contraction | Default value |
| ◆ Drainage and Surface Properties | |
| ◆ Surface shortwave absorptivity | 0.85 |
| ◆ Layers | |
| ◆ Layer 1 – Asphalt | |
| ◆ Asphalt Material Type | Asphalt Concrete |
| ◆ Layer Thickness | 4 in |
| ◆ Asphalt Mix | |
| ◆ Cumulative % Retained ¾ inch Sieve | Based on gradation data |

| | |
|--|---|
| ◆ Cumulative % Retained 3/8 inch Sieve | Based on gradation data |
| ◆ Cumulative % Retained #4 Sieve | Based on gradation data |
| ◆ % Passing #200 Sieve | Based on gradation data |
| ◆ Asphalt Binder | |
| ◆ Options (Superpave Binder Grading, Conventional Viscosity Grade, Conventional Penetration Grade) | Superpave Binder Grading |
| ◆ Binder Grade | 70-22 |
| ◆ A | Defaults |
| ◆ VTS | Defaults |
| ◆ Asphalt General | |
| ◆ General | |
| ◆ Reference Temperature (°F) | 70 |
| ◆ Volumetric Properties | |
| ◆ Effective Binder Content (%) | 4.72/Based on recalculated value shown in Appendix C for each mix |
| ◆ Air Voids (%) | 8.0 |
| ◆ Total Unit Weight (pcf) | 148 |
| ◆ Poisson's ratio | 0.35 |
| ◆ Thermal Properties | |
| ◆ Thermal Conductivity Asphalt (BTU/hr-ft-F°) | 0.67 |
| ◆ Heat Capacity (BTU/lb-F°) | 0.23 |
| ◆ Layer 2 – Granular Base | |
| ◆ Unbound Material | Crushed Stone |
| ◆ Thickness (in) | 12 |
| ◆ Strength Properties | |
| ◆ Input Level (Level 1, 2, 3) | 3 |
| ◆ Poisson's Ratio | 0.35 |
| ◆ Coefficient of Lateral Pressure, Ko | 0.5 |
| ◆ Material Property | Modulus (psi) ✓ |
| ◆ Modulus (input)(psi) | 10000 |
| ◆ Analysis Type | ICM Calculated Modulus ✓ |

| | |
|---------------------------------------|--------------------------|
| ◆ ICM | |
| ◆ Gradation and Plasticity Index | |
| ◆ Plasticity Index, PI | 1 |
| ◆ Passing #200 Sieve (%) | 7 |
| ◆ Passing #4 Sieve (%) | 40 |
| ◆ D60 (mm) | 15 |
| ◆ Compacted Unbound Material | ✓ |
| ◆ Calculated/Derived Parameters | Use Defaults |
| ◆ Layer 3 – Subgrade | |
| ◆ Unbound Material | A-6 |
| ◆ Thickness (in) | Semi-infinite |
| ◆ Strength Properties | |
| ◆ Input Level (Level 1, 2, 3) | 3 |
| ◆ Poisson's Ratio | 0.35 |
| ◆ Coefficient of Lateral Pressure, Ko | 0.5 |
| ◆ Material Property | Modulus (psi) ✓ |
| ◆ Modulus (input)(psi) | 17000 |
| ◆ Analysis Type | ICM Calculated Modulus ✓ |
| ◆ ICM | |
| ◆ Gradation and Plasticity Index | |
| ◆ Plasticity Index, PI | 25 |
| ◆ Passing #200 Sieve (%) | 80 |
| ◆ Passing #4 Sieve (%) | 95 |
| ◆ D60 (mm) | 0.01 |
| ◆ Compacted Unbound Material | ✓ |
| ◆ Calculated/Derived Parameters | Use Defaults |

* Shaded row indicates the parameter that will be analyzed.

Table C6: Record of inputs for Phase III DG 2002 runs where the Percent Binder Effective value is varied (25.0mm Mix)

| Project Information | Value |
|--|---------------------------|
| ◆ General Information | |
| ◆ Design Life | 20 |
| ◆ Base/Subgrade Construction Month | Sept. |
| ◆ Pavement Construction Month | Sept. |
| ◆ Traffic Open Month | Sept. |
| ◆ Type of Design (New Pavements: Flexible Pavement, JPCP, CRCP; Restoration: JPCP; Overlay: Asphalt or PCC) | New Flexible Pavement |
| ◆ Site/Project Identification | |
| ◆ Location | Fay. |
| ◆ Project ID | |
| ◆ Section ID | |
| ◆ Functional class | |
| ◆ Date | |
| ◆ Station/milepost format | |
| ◆ Station/milepost begin | |
| ◆ Traffic direction | |
| ◆ Analysis Parameters | |
| ◆ Terminal IRI (International Roughness Index) (in/mi) | 172 |
| ◆ AC Surface Down Cracking Long. Cracking (ft/mi) | 1000 |
| ◆ AC Bottom Up Cracking Alligator Cracking (ft/mi) | 25 |
| ◆ AC Thermal Fracture (ft/mi) | 1000 |
| ◆ Chemically Stabilized Layer Fatigue fracture (%) | 25 |
| ◆ Permanent Deformation – Total Pavement (in) | 0.75 |
| Inputs | |
| ◆ Traffic | |
| ◆ General | |
| ◆ Two-way average annual daily truck traffic (or Two-way annual average daily traffic and Percent of heavy vehicles) | Need Value (Used 1000) |
| ◆ Number of lanes in design direction | 2 |
| ◆ Percent of trucks in design direction | 50.0 |
| ◆ Percent of trucks in design lane | 95.0 |
| ◆ Operational speed | 60 |
| ◆ Traffic Volume Adjustment Factors | |

| | |
|--|---|
| ◆ Monthly Adjustment – Table of Monthly Adjustment Factors (MAF) for each month for Classes 4-13; Level 1 is Site Specific, Level 3 is Default | 1.0 for all |
| ◆ Vehicle Class Distribution | Default |
| ◆ Hourly Distribution | Default |
| ◆ Traffic Growth Factor (%) | 4-Comp. |
| ◆ Axle Load Distribution Factors | Default |
| ◆ General Traffic Inputs | |
| ◆ Mean wheel location (in from lane marking) | 18 |
| ◆ Traffic wander standard deviation (in) | 10 |
| ◆ Design lane width (ft) | 12 |
| ◆ Number Axles/Truck – Table showing values for Single through Quad-axle trucks from Class 4 – Class 13 | Default |
| ◆ Axle Configuration | Default |
| ◆ Wheelbase – Information for Short, Medium, and Long wheelbases | Default |
| ◆ Climate | |
| ◆ Climate Data File from included weather station data (may require depth of water table) | Need Location (Used Fayetteville with depth of water table = 20 ft) |
| ◆ Structure | |
| ◆ Thermal Cracking | |
| ◆ Average Tensile Strength at 14°F (psi) | Default |
| ◆ Creep Test Duration (sec) | Default |
| ◆ Loading Time vs. Creep Compliance Table | Default |
| ◆ Compute Mix Coefficient of Thermal Contraction | ✓ |
| ◆ Mixture VMA (%) | Default value |
| ◆ Aggregate Coefficient of Thermal Contraction | Default value |
| ◆ Drainage and Surface Properties | |
| ◆ Surface shortwave absorptivity | 0.85 |
| ◆ Layers | |
| ◆ Layer 1 – Asphalt | |
| ◆ Asphalt Material Type | Asphalt Concrete |
| ◆ Layer Thickness | 4 in |
| ◆ Asphalt Mix | |
| ◆ Cumulative % Retained $\frac{3}{4}$ inch Sieve | 0 |

| | |
|--|--------------------------|
| ◆ Cumulative % Retained 3/8 inch Sieve | 24 |
| ◆ Cumulative % Retained #4 Sieve | 58 |
| ◆ % Passing #200 Sieve | 3.6 |
| ◆ Asphalt Binder | |
| ◆ Options (Superpave Binder Grading, Conventional Viscosity Grade, Conventional Penetration Grade) | Superpave Binder Grading |
| ◆ Binder Grade | 64-22 |
| ◆ A | Defaults |
| ◆ VTS | Defaults |
| ◆ Asphalt General | |
| ◆ General | |
| ◆ Reference Temperature (°F) | 70 |
| ◆ Volumetric Properties | |
| ◆ Effective Binder Content (%) | 4.72 |
| ◆ Air Voids (%) | 4.5 |
| ◆ Total Unit Weight (pcf) | 148 |
| ◆ Poisson's ratio | 0.35 |
| ◆ Thermal Properties | |
| ◆ Thermal Conductivity Asphalt (BTU/hr-ft-F°) | 0.67 |
| ◆ Heat Capacity (BTU/lb-F°) | 0.23 |
| ◆ Layer 2 – Asphalt | |
| ◆ Asphalt Material Type | Asphalt Concrete |
| ◆ Layer Thickness | 6 in |
| ◆ Asphalt Mix | |
| ◆ Cumulative % Retained ¾ inch Sieve | Based on gradation data |
| ◆ Cumulative % Retained 3/8 inch Sieve | Based on gradation data |
| ◆ Cumulative % Retained #4 Sieve | Based on gradation data |
| ◆ % Passing #200 Sieve | Based on gradation data |
| ◆ Asphalt Binder | |
| ◆ Options (Superpave Binder Grading, Conventional Viscosity Grade, Conventional Penetration Grade) | Superpave Binder Grading |

| | |
|---|---|
| ◆ Binder Grade | 70-22 |
| ◆ A | Defaults |
| ◆ VTS | Defaults |
| ◆ Asphalt General | |
| ◆ General | |
| ◆ Reference Temperature (°F) | 70 |
| ◆ Volumetric Properties | |
| ◆ Effective Binder Content (%) | 4.72/Based on recalculated value shown in Appendix C for each mix |
| ◆ Air Voids (%) | 8.0 |
| ◆ Total Unit Weight (pcf) | 148 |
| ◆ Poisson's ratio | 0.35 |
| ◆ Thermal Properties | |
| ◆ Thermal Conductivity Asphalt (BTU/hr-ft-F°) | 0.67 |
| ◆ Heat Capacity (BTU/lb-F°) | 0.23 |
| ◆ Layer 3 – Granular Base | |
| ◆ Unbound Material | Crushed Stone |
| ◆ Thickness (in) | 12 |
| ◆ Strength Properties | |
| ◆ Input Level (Level 1, 2, 3) | 3 |
| ◆ Poisson's Ratio | 0.35 |
| ◆ Coefficient of Lateral Pressure, Ko | 0.5 |
| ◆ Material Property | Modulus (psi) ✓ |
| ◆ Modulus (input)(psi) | 10000 |
| ◆ Analysis Type | ICM Calculated Modulus ✓ |
| ◆ ICM | |
| ◆ Gradation and Plasticity Index | |
| ◆ Plasticity Index, PI | 1 |
| ◆ Passing #200 Sieve (%) | 7 |
| ◆ Passing #4 Sieve (%) | 40 |
| ◆ D60 (mm) | 15 |
| ◆ Compacted Unbound Material | ✓ |
| ◆ Calculated/Derived Parameters | Use Defaults |
| ◆ Layer 4 – Subgrade | |
| ◆ Unbound Material | A-6 |
| ◆ Thickness (in) | Semi-infinite |

| | |
|---------------------------------------|--------------------------|
| ◆ Strength Properties | |
| ◆ Input Level (Level 1, 2, 3) | 3 |
| ◆ Poisson's Ratio | 0.35 |
| ◆ Coefficient of Lateral Pressure, Ko | 0.5 |
| ◆ Material Property | Modulus (psi) ✓ |
| ◆ Modulus (input)(psi) | 17000 |
| ◆ Analysis Type | ICM Calculated Modulus ✓ |
| ◆ ICM | |
| ◆ Gradation and Plasticity Index | |
| ◆ Plasticity Index, PI | 25 |
| ◆ Passing #200 Sieve (%) | 80 |
| ◆ Passing #4 Sieve (%) | 95 |
| ◆ D60 (mm) | 0.01 |
| ◆ Compacted Unbound Material | ✓ |
| ◆ Calculated/Derived Parameters | Use Defaults |

* Shaded row indicates the parameter that will be analyzed.

APPENDIX D
FLEXIBLE PAVEMENT SENSITIVITY GRAPHS

Figure 1B: Sensitivity of Poisson's ratio to SDC 1 for Phase I

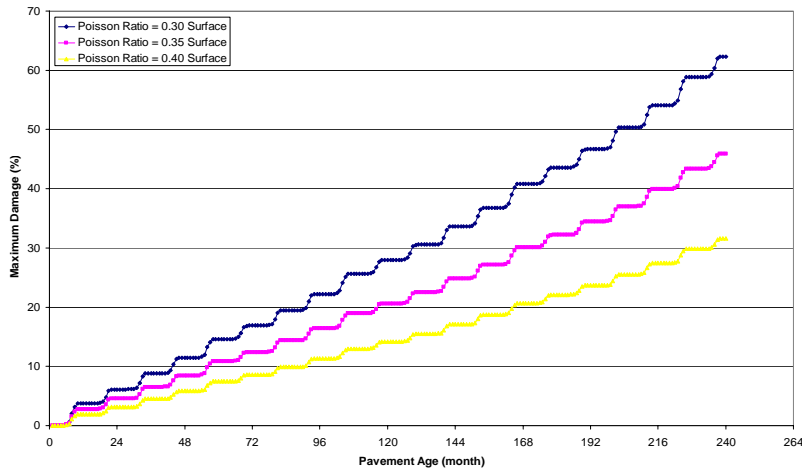


Figure 2B: Sensitivity of Poisson's ratio to SDC 2 for Phase I

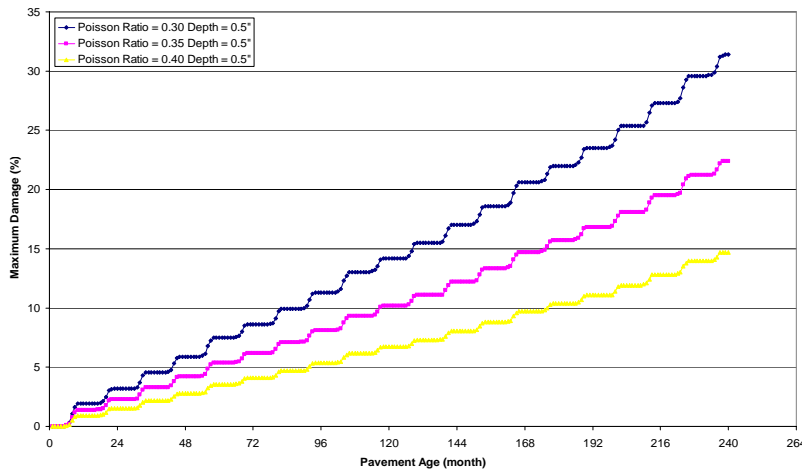


Figure 3B: Sensitivity of Poisson's ratio to BUD for Phase I

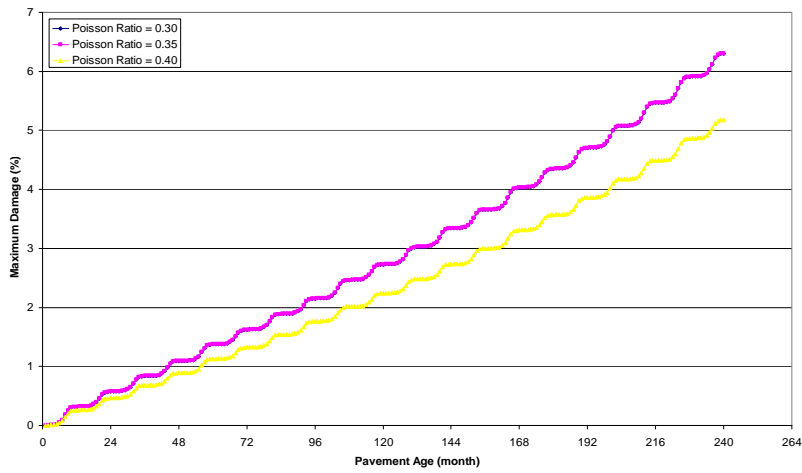


Figure 4B: Sensitivity of Poisson's ratio to Rutting for Phase I

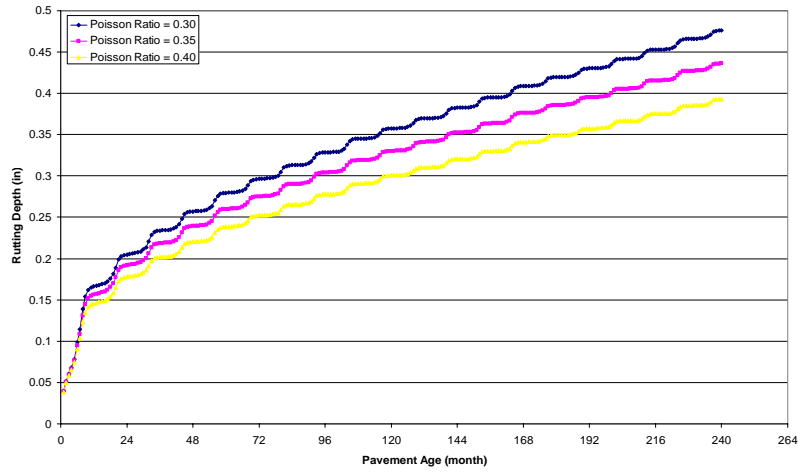


Figure 5B: Sensitivity of Poisson's ratio to IRI for Phase I

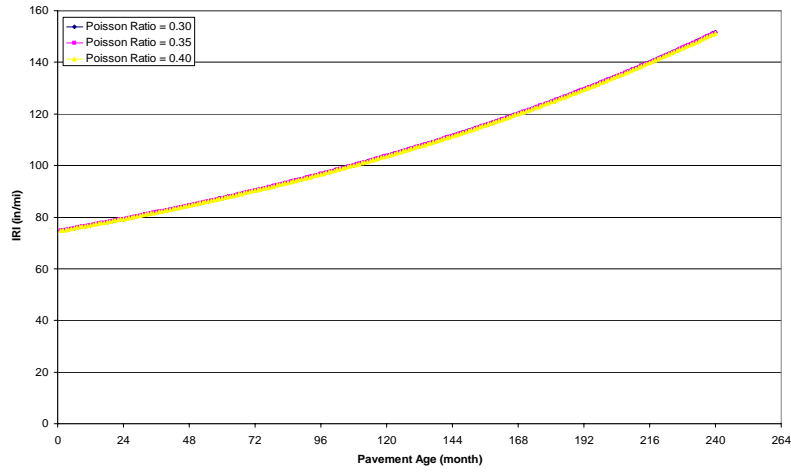


Figure 6B: Sensitivity of SSA to SDC 1 for Phase I

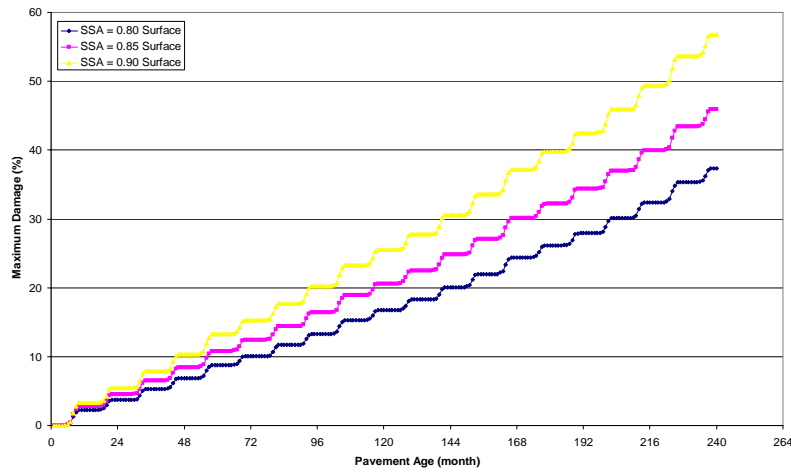


Figure 7B: Sensitivity of SSA to SDC 2 for Phase I

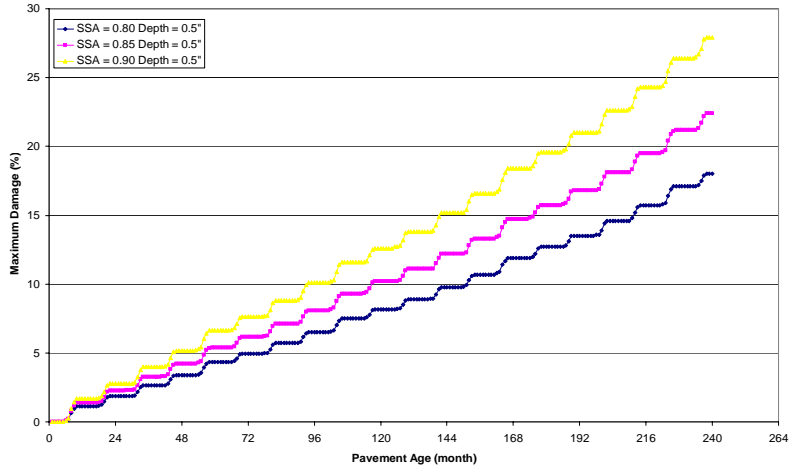


Figure 8B: Sensitivity of SSA to BUD for Phase I

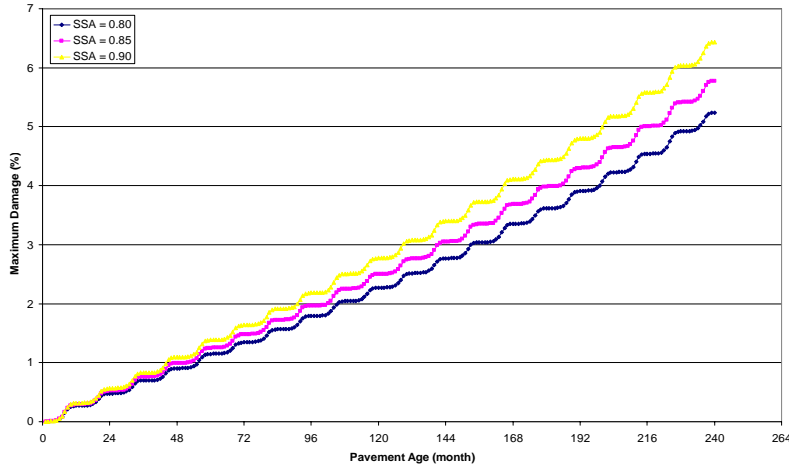


Figure 9B: Sensitivity of SSA to Rutting for Phase I

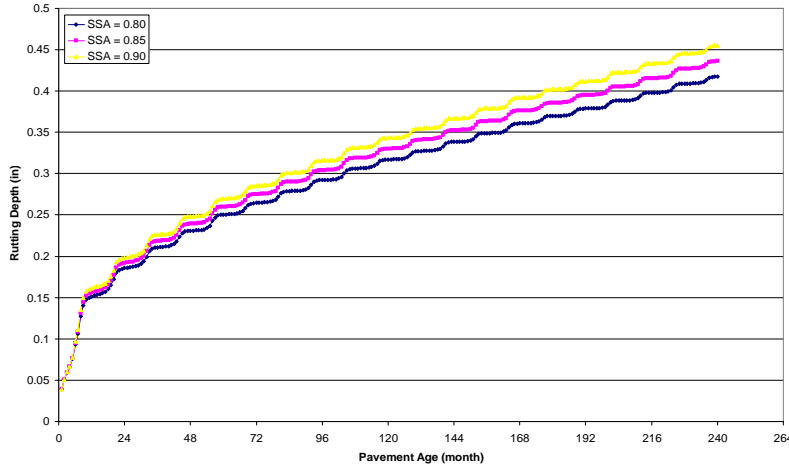


Figure 10B: Sensitivity of SSA to IRI for Phase I

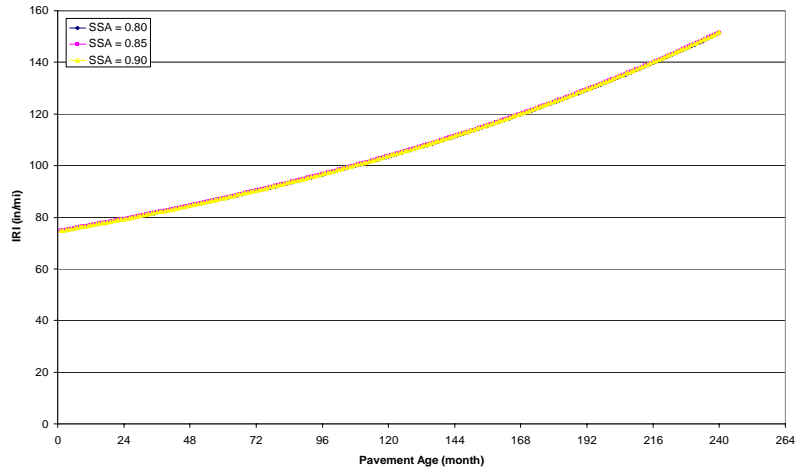


Figure 11B: Sensitivity of HC to SDC 1 for Phase I

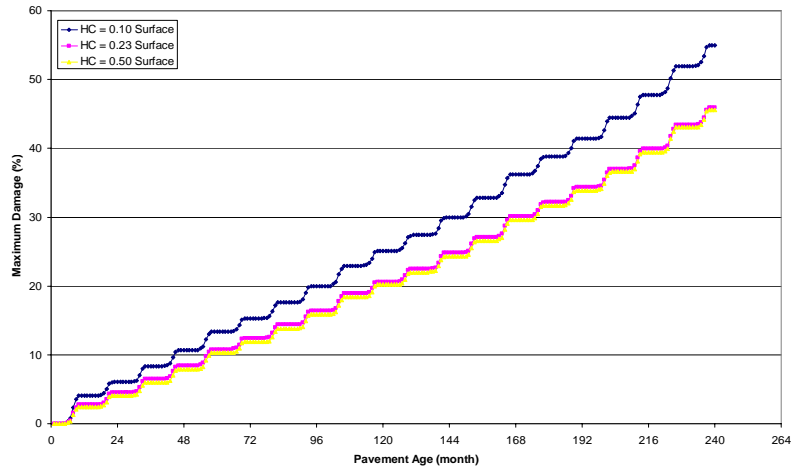


Figure 12B: Sensitivity of HC to SDC 2 for Phase I

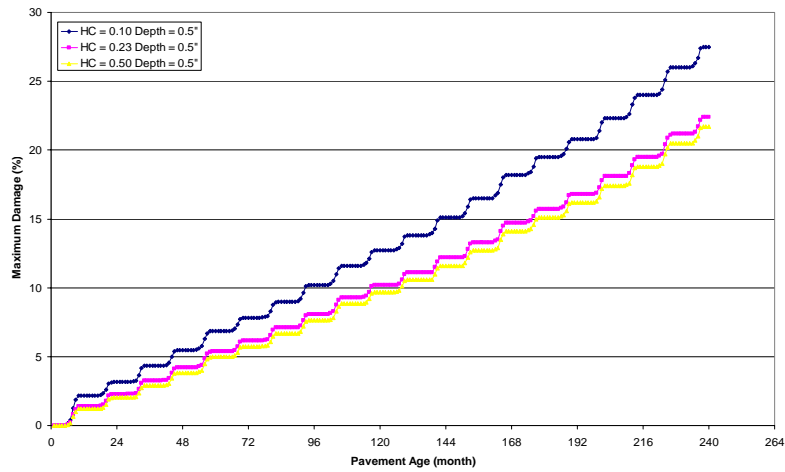


Figure 13B: Sensitivity of HC to BUD for Phase I

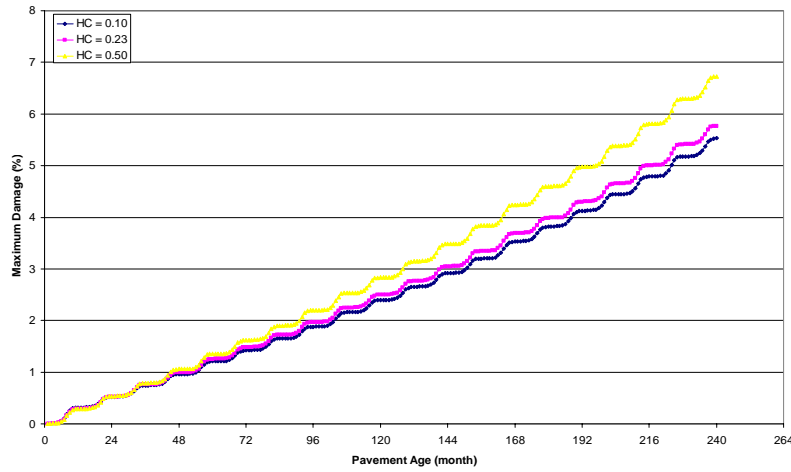


Figure 14B: Sensitivity of HC to Rutting for Phase I

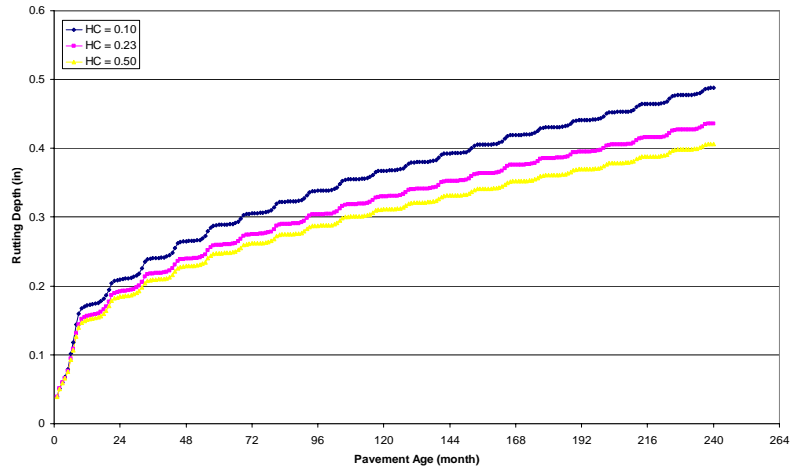


Figure 15B: Sensitivity of HC to IRI for Phase I

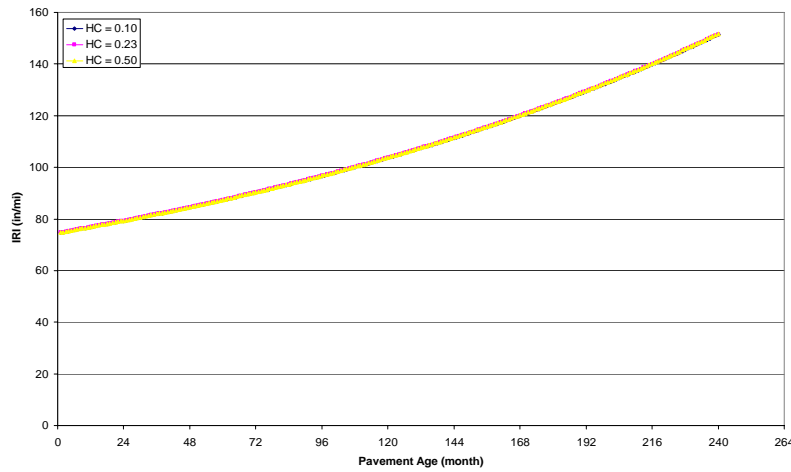


Figure 16B: Sensitivity of TC to SDC 1 for Phase I

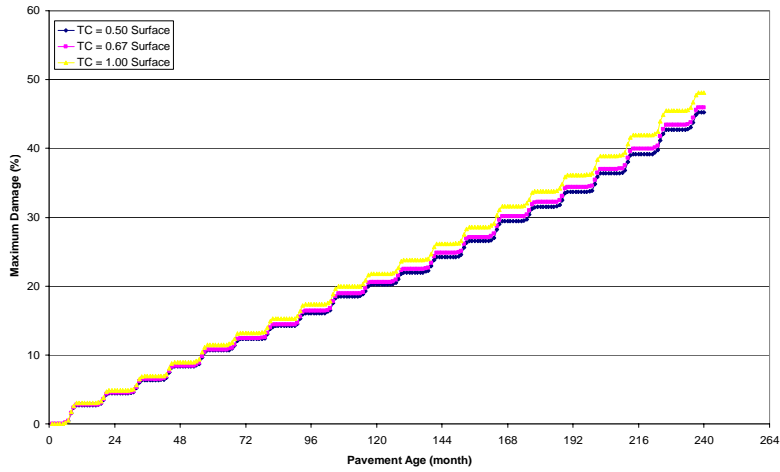


Figure 17B: Sensitivity of TC to SDC 2 for Phase I

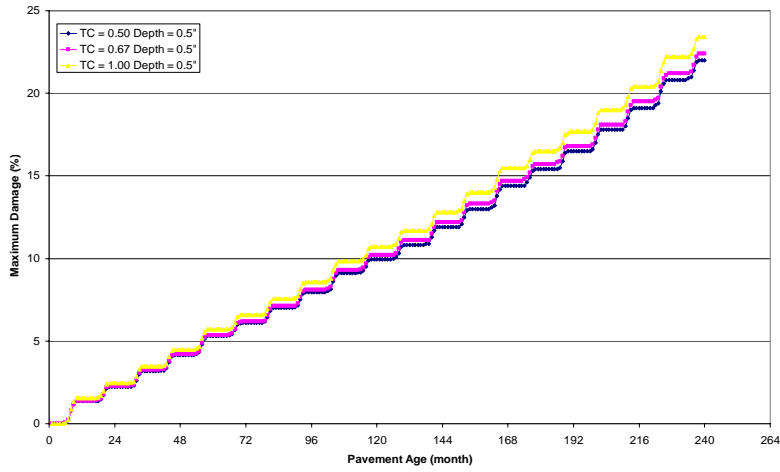


Figure 18B: Sensitivity of TC to BUD for Phase I

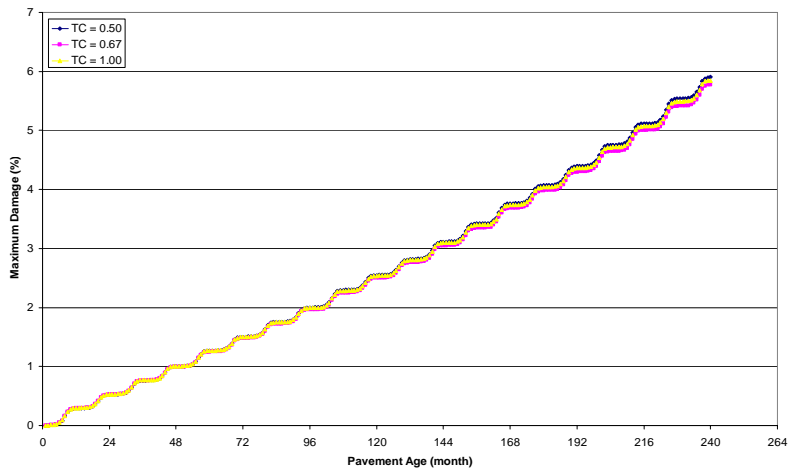


Figure 19B: Sensitivity of TC to Rutting for Phase I

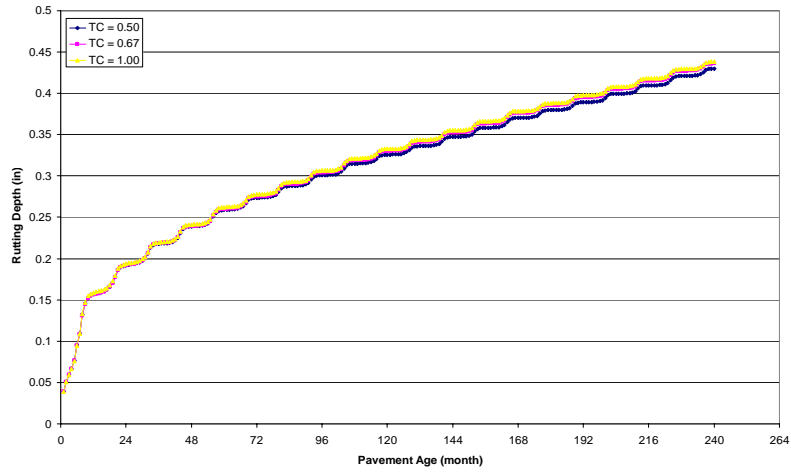


Figure 20B: Sensitivity of TC to IRI for Phase I

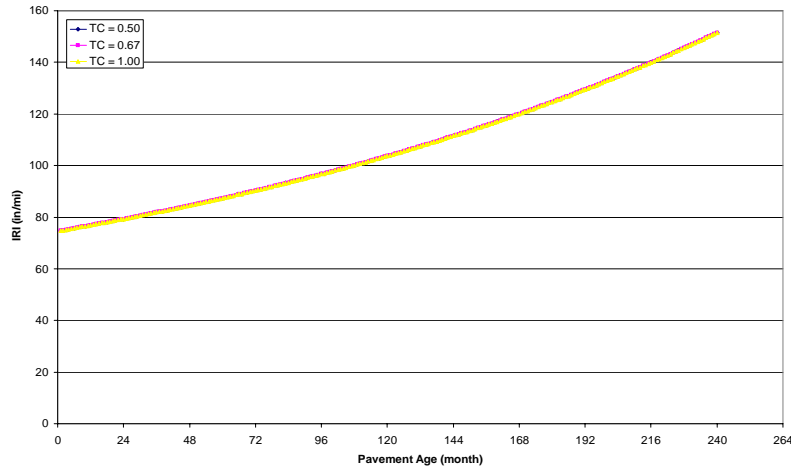


Figure 21B: Sensitivity of Poisson's ratio to SDC 1 for Phase III (ARK 70-22)

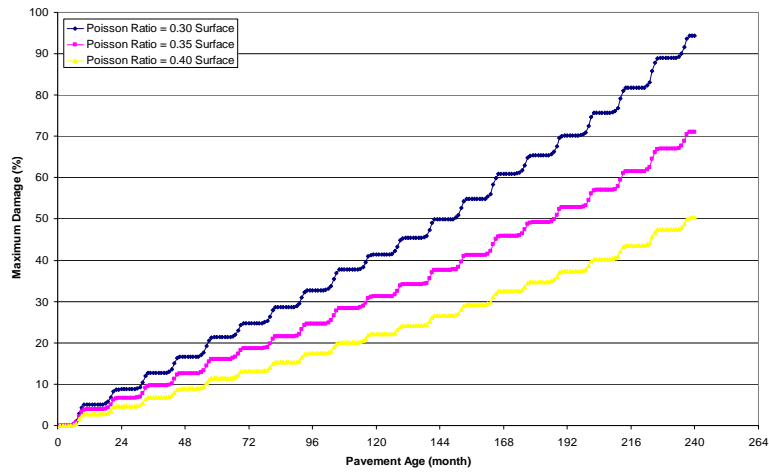


Figure 22B: Sensitivity of Poisson's ratio to SDC 2 for Phase III (ARK 70-22)

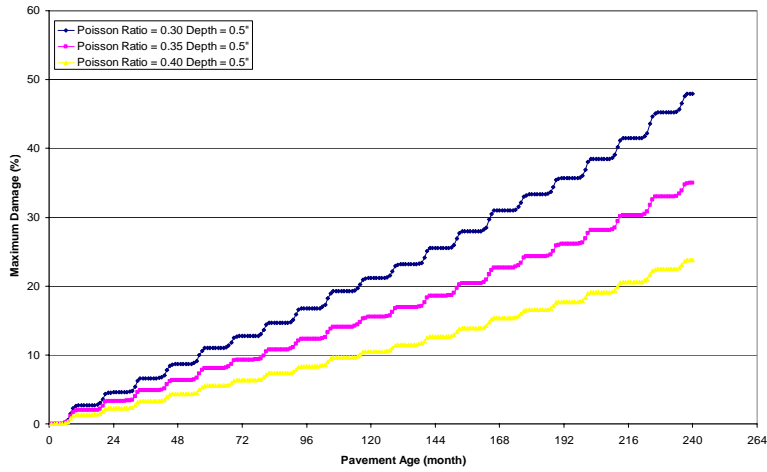


Figure 23B: Sensitivity of Poisson's ratio to BUD for Phase III (ARK 70-22)

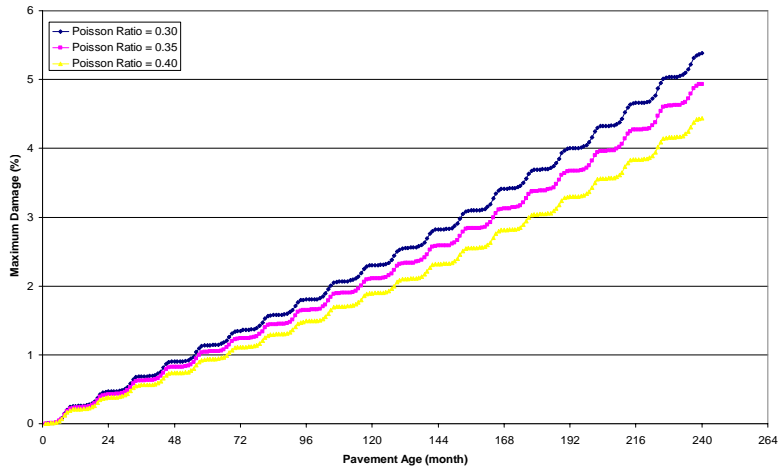


Figure 24B: Sensitivity of Poisson's ratio to Rutting for Phase III (ARK 70-22)

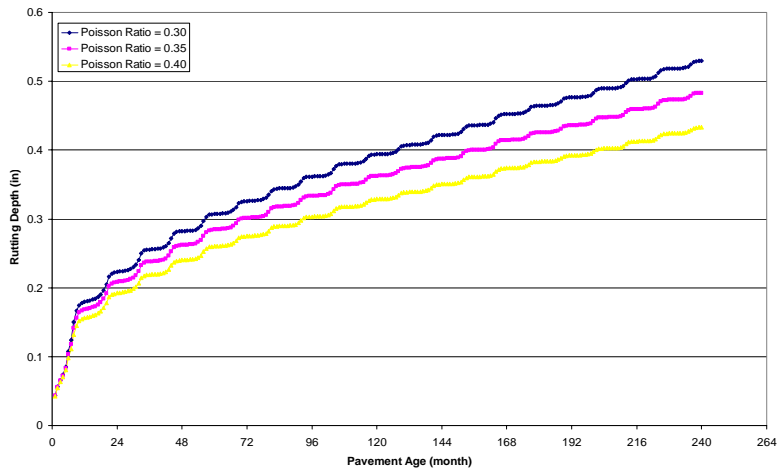


Figure 25B: Sensitivity of Poisson's ratio to IRI for Phase III (ARK 70-22)

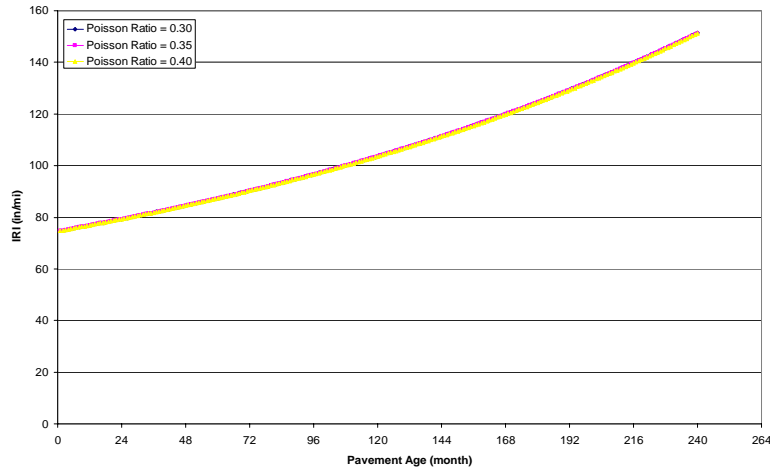


Figure 26B: Sensitivity of Poisson's ratio to SDC 1 for Phase III (GMQ 70-22)

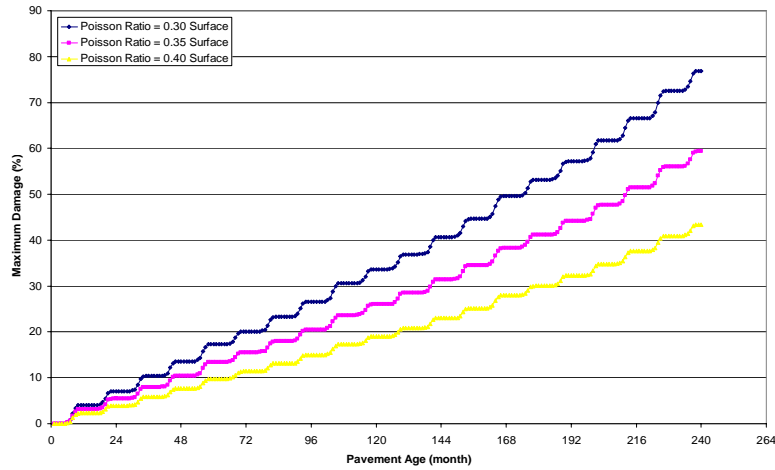


Figure 27B: Sensitivity of Poisson's ratio to SDC 2 for Phase III (GMQ 70-22)

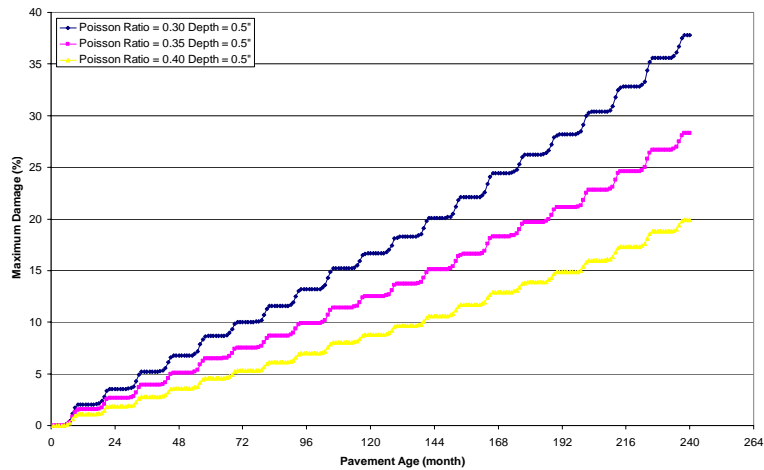


Figure 28B: Sensitivity of Poisson's ratio to BUD for Phase III (GMQ 70-22)

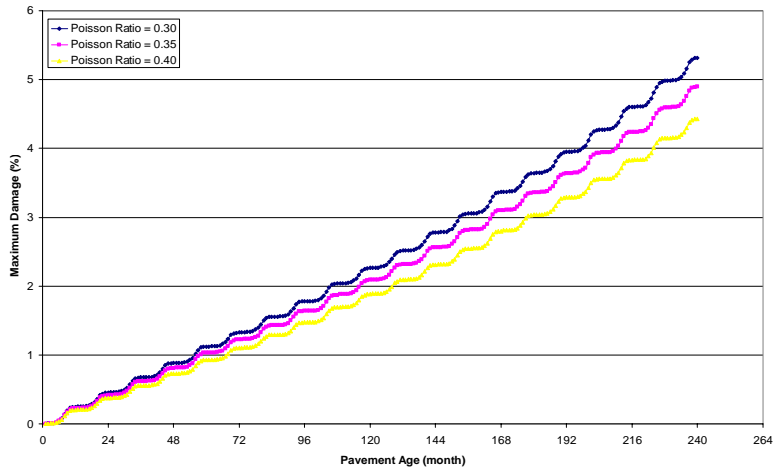


Figure 29B: Sensitivity of Poisson's ratio to Rutting for Phase III (GMQ 70-22)

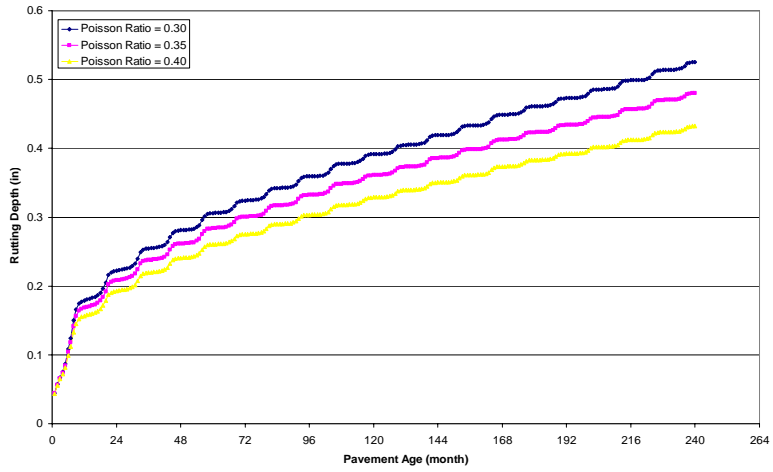


Figure 30B: Sensitivity of Poisson's ratio to IRI for Phase III (GMQ 70-22)

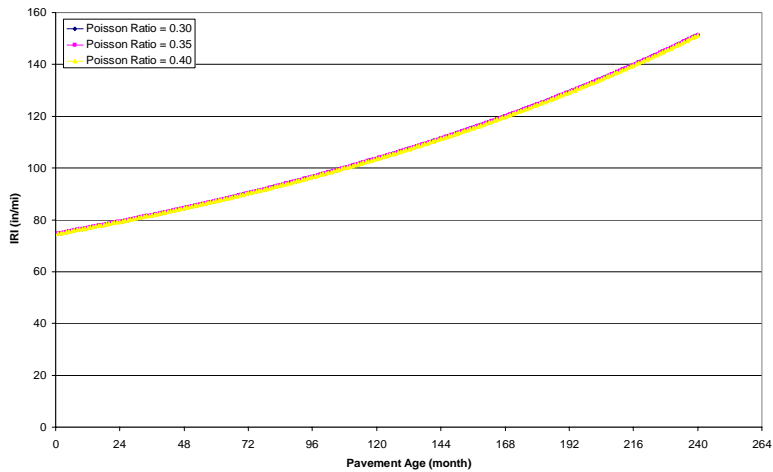


Figure 31B: Sensitivity of Poisson's ratio to SDC 1 for Phase III (JET 70-22)

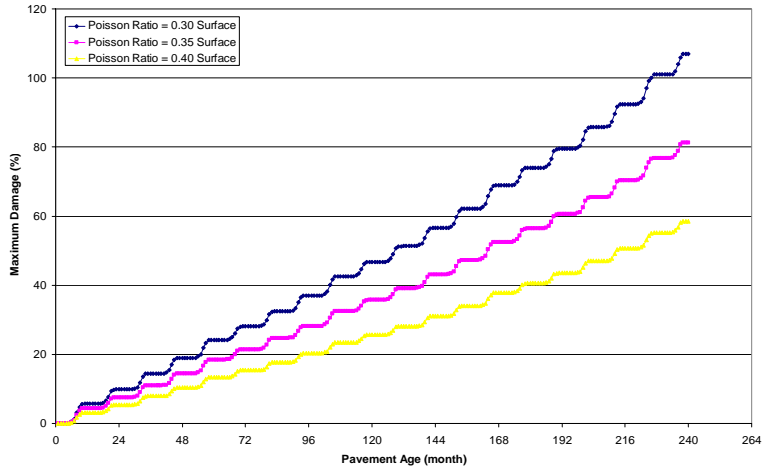


Figure 32B: Sensitivity of Poisson's ratio to SDC 2 for Phase III (JET 70-22)

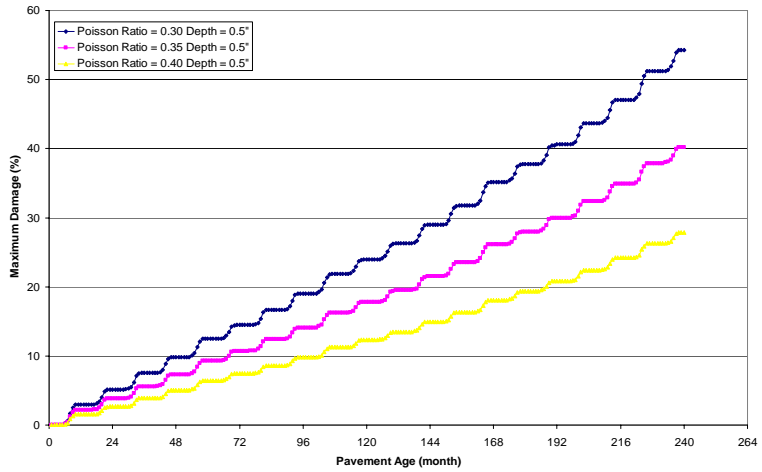


Figure 33B: Sensitivity of Poisson's ratio to BUD for Phase III (JET 70-22)

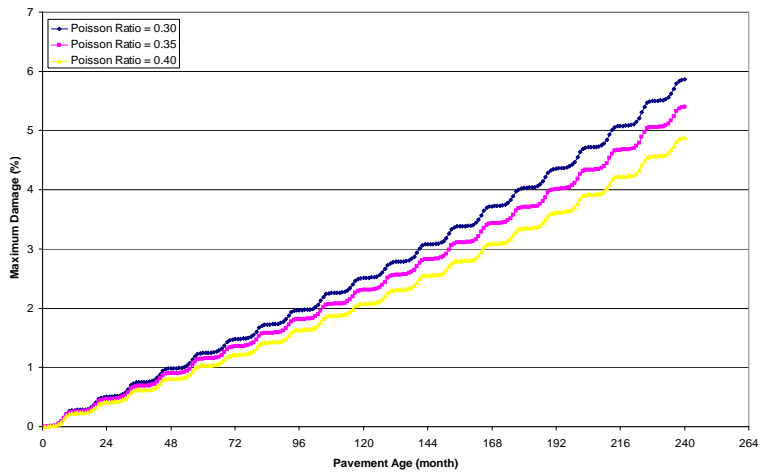


Figure 34B: Sensitivity of Poisson's ratio to Rutting for Phase III (JET 70-22)

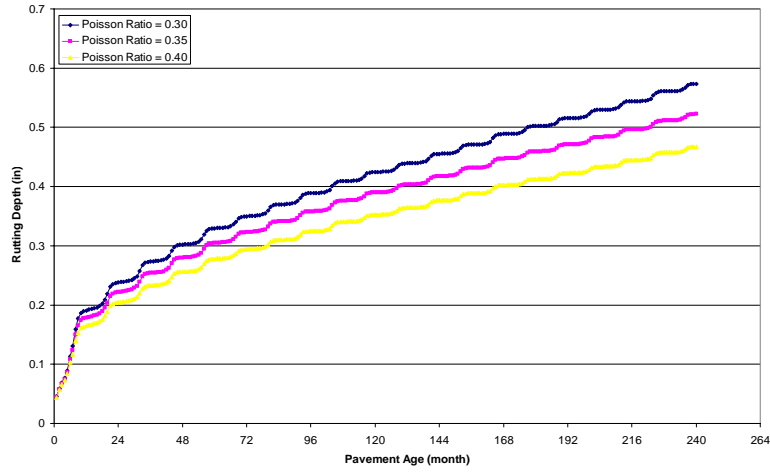


Figure 35B: Sensitivity of Poisson's ratio to IRI for Phase III (JET 70-22)

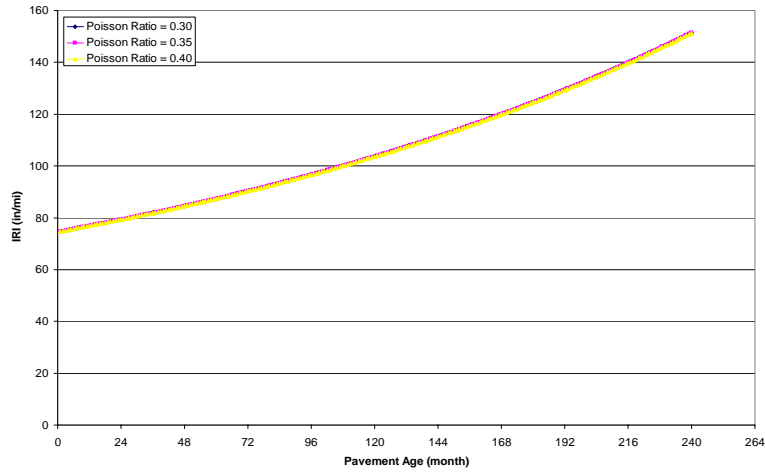


Figure 36B: Sensitivity of Poisson's ratio to SDC 1 for Phase III (MCA 70-22)

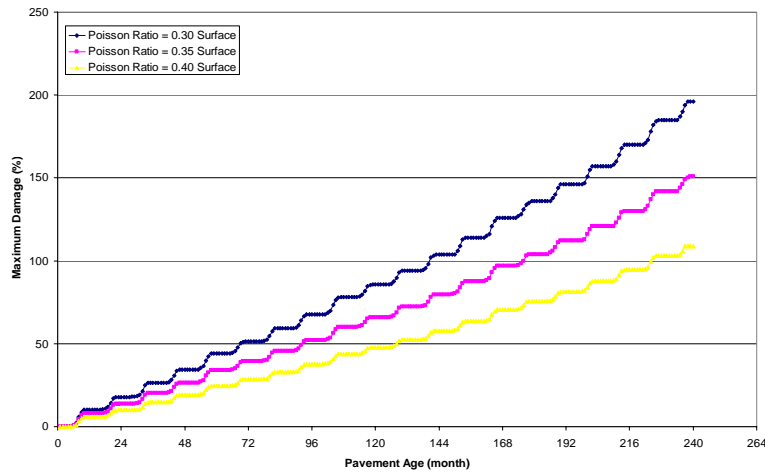


Figure 37B: Sensitivity of Poisson's ratio to SDC 2 for Phase III (MCA 70-22)

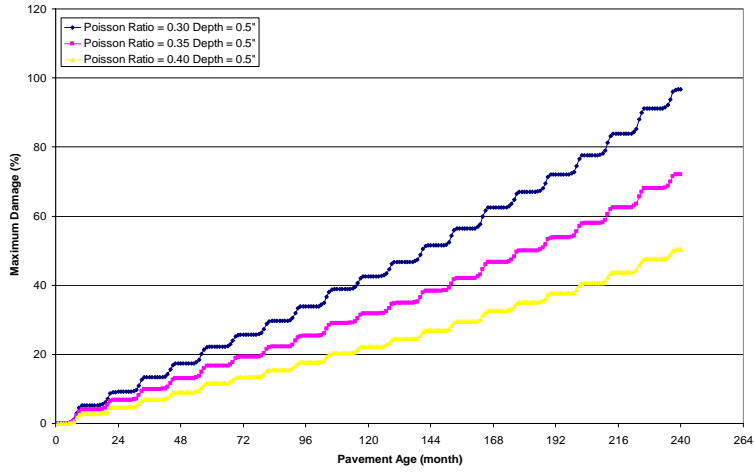


Figure 38B: Sensitivity of Poisson's ratio to BUD for Phase III (MCA 70-22)

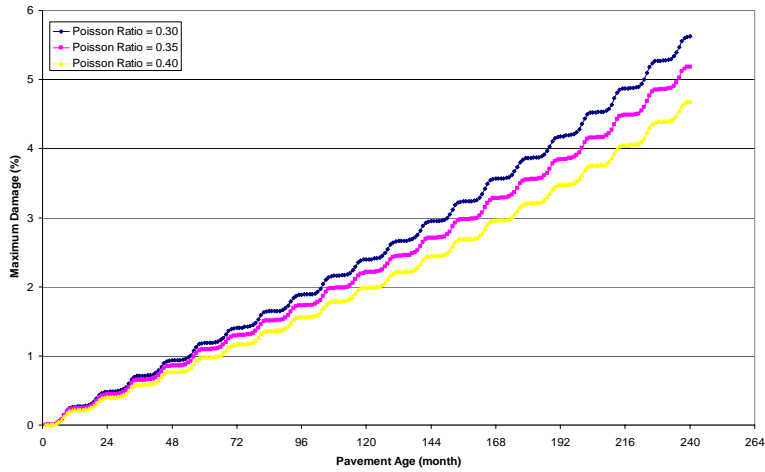


Figure 39B: Sensitivity of Poisson's ratio to Rutting for Phase III (MCA 70-22)

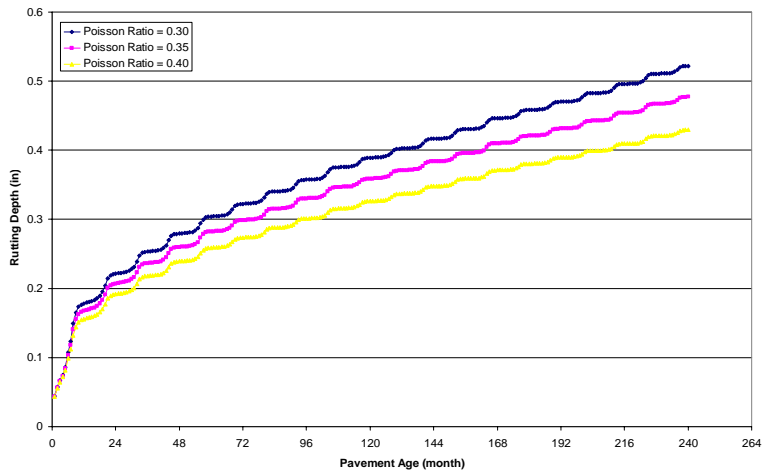


Figure 40B: Sensitivity of Poisson's ratio to IRI for Phase III (MCA 70-22)

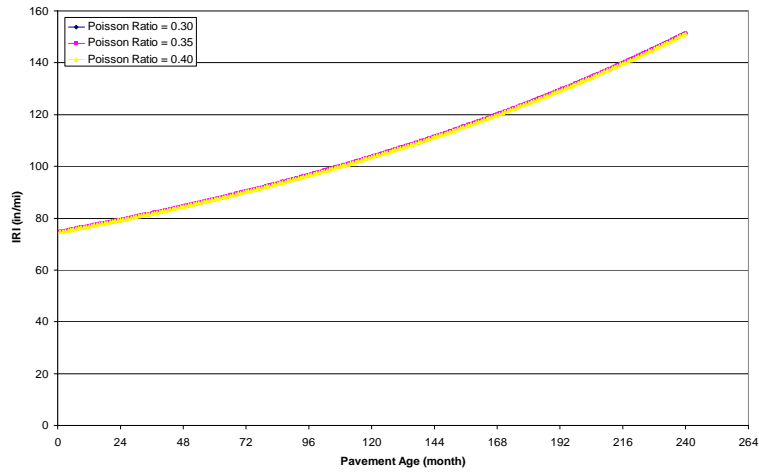


Figure 41B: Sensitivity of SSA to SDC 1 for Phase III (ARK 70-22)

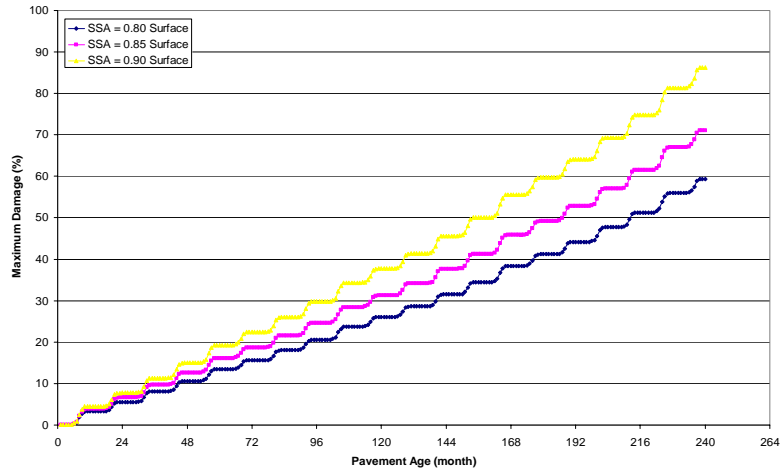


Figure 42B: Sensitivity of SSA to SDC 2 for Phase III (ARK 70-22)

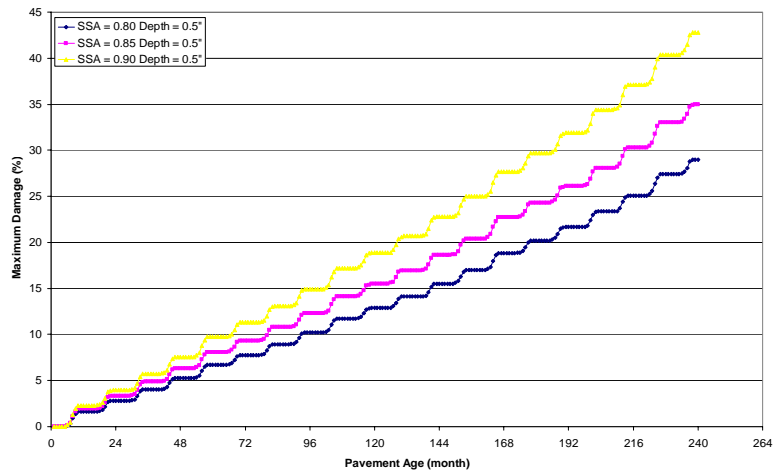


Figure 43B: Sensitivity of SSA to BUD for Phase III (ARK 70-22)

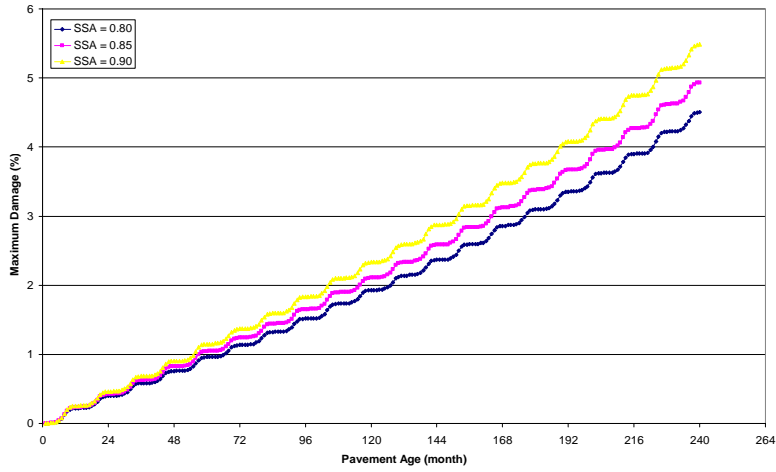


Figure 44B: Sensitivity of SSA to Rutting for Phase III (ARK 70-22)

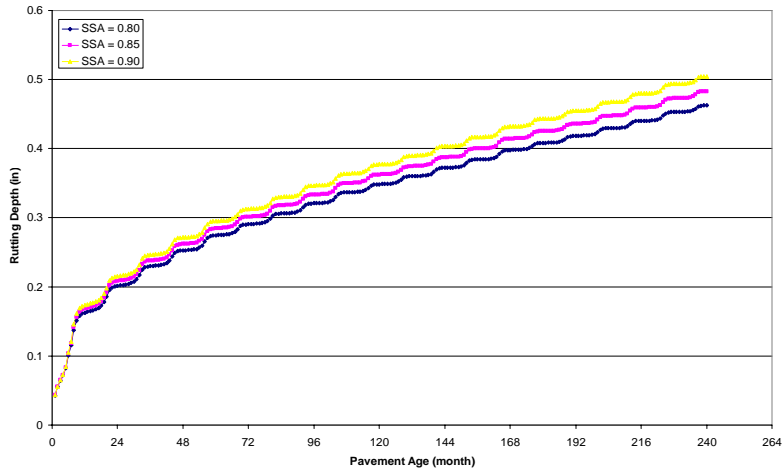


Figure 45B: Sensitivity of SSA to IRI for Phase III (ARK 70-22)

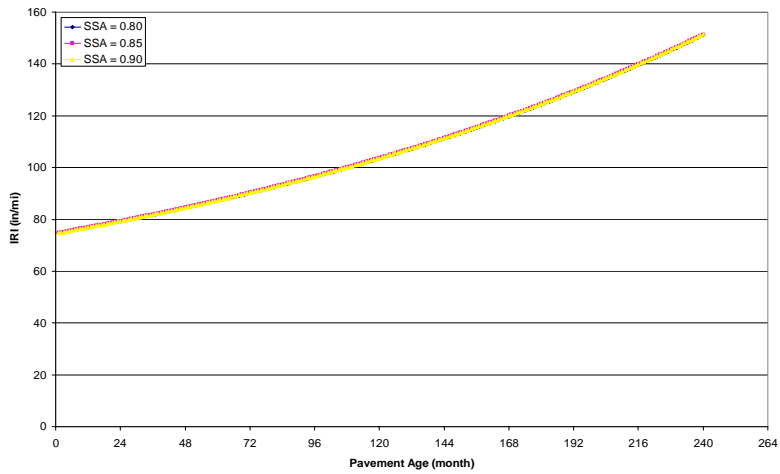


Figure 46B: Sensitivity of SSA to SDC 1 for Phase III (GMQ 70-22)

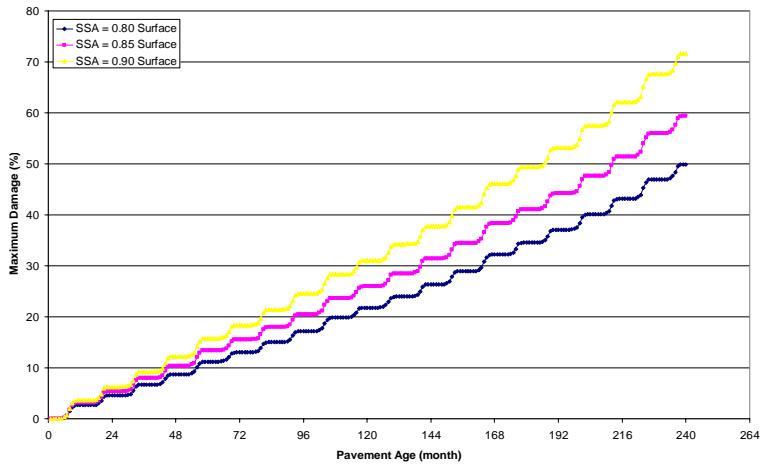


Figure 47B: Sensitivity of SSA to SDC 2 for Phase III (GMQ 70-22)

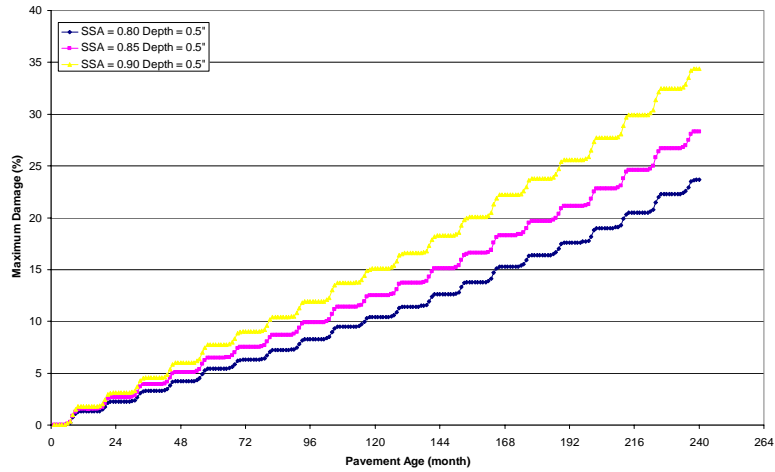


Figure 48B: Sensitivity of SSA to BUD for Phase III (GMQ 70-22)

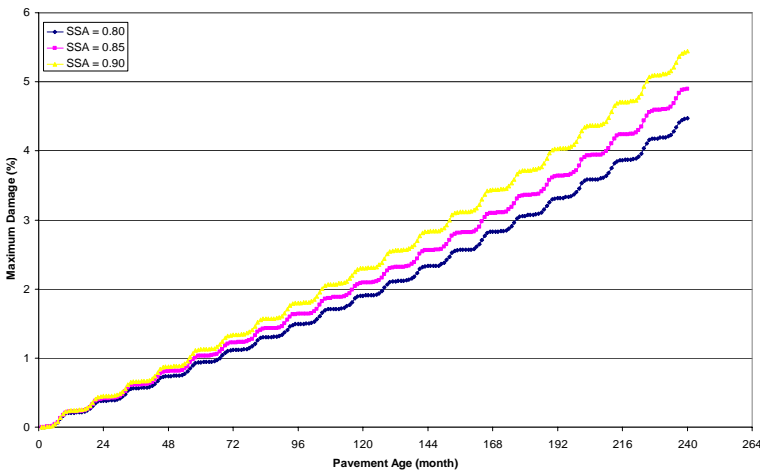


Figure 49B: Sensitivity of SSA to Rutting for Phase III (GMQ 70-22)

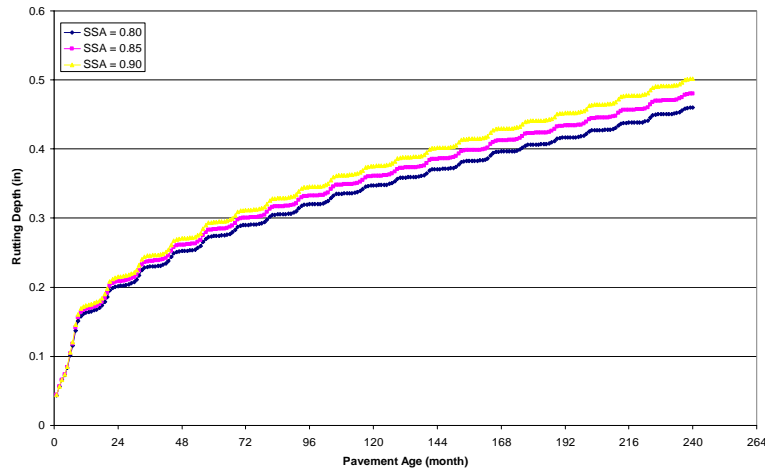


Figure 50B: Sensitivity of SSA to IRI for Phase III (GMQ 70-22)

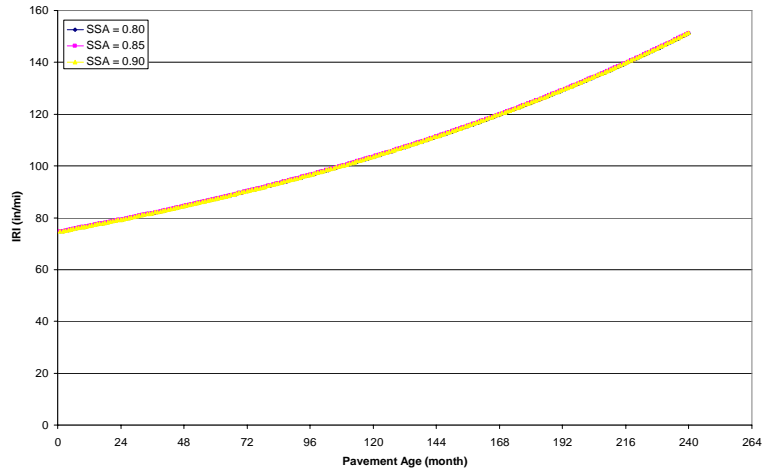


Figure 51B: Sensitivity of SSA to SDC 1 for Phase III (JET 70-22)

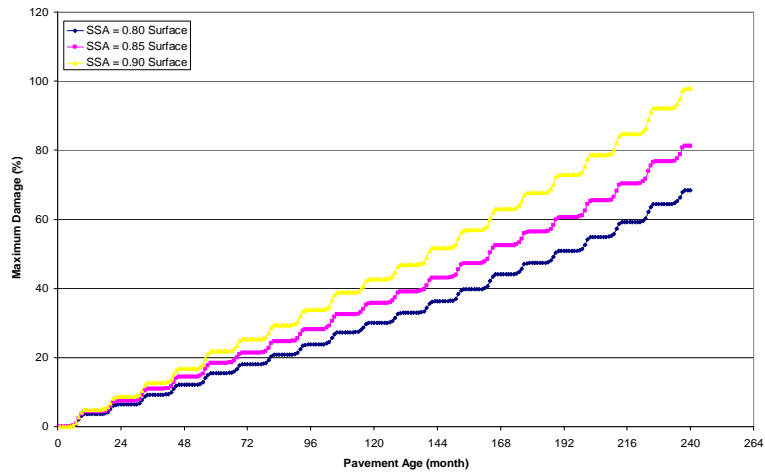


Figure 52B: Sensitivity of SSA to SDC 2 for Phase III (JET 70-22)

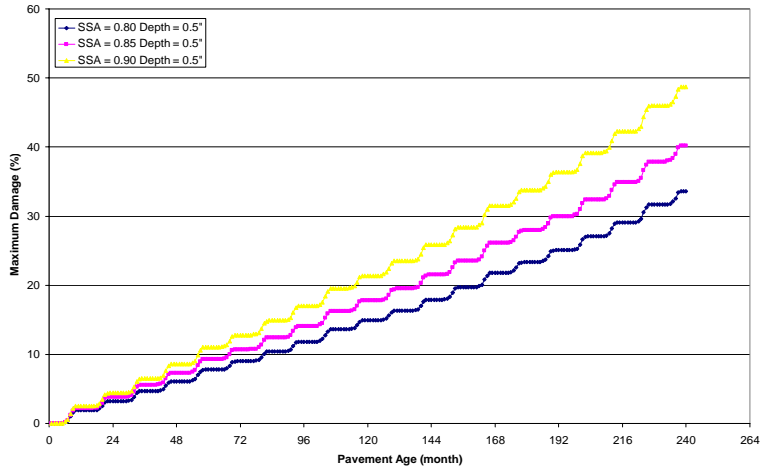


Figure 53B: Sensitivity of SSA to BUD for Phase III (JET 70-22)

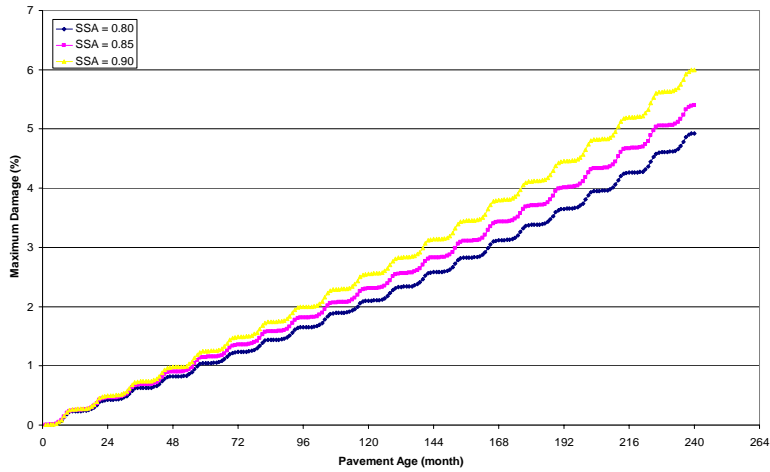


Figure 54B: Sensitivity of SSA to Rutting for Phase III (JET 70-22)

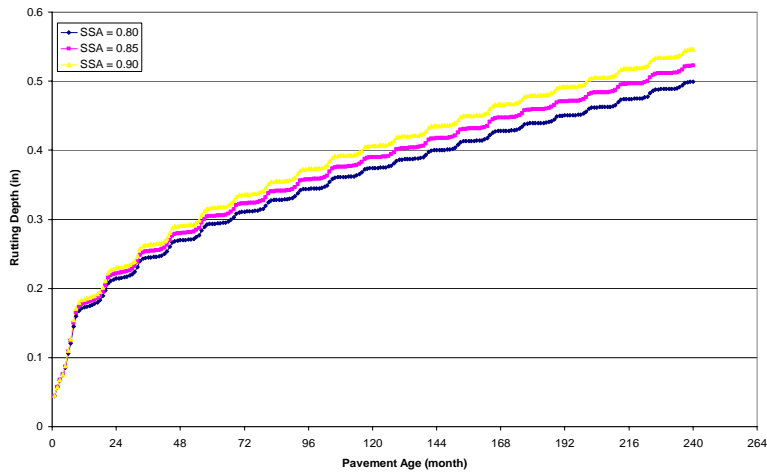


Figure 55B: Sensitivity of SSA to IRI for Phase III (JET 70-22)

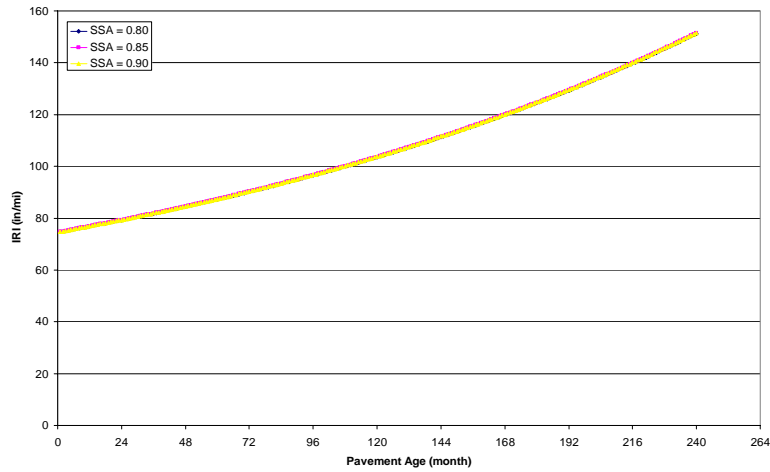


Figure 56B: Sensitivity of SSA to SDC 1 for Phase III (MCA 70-22)

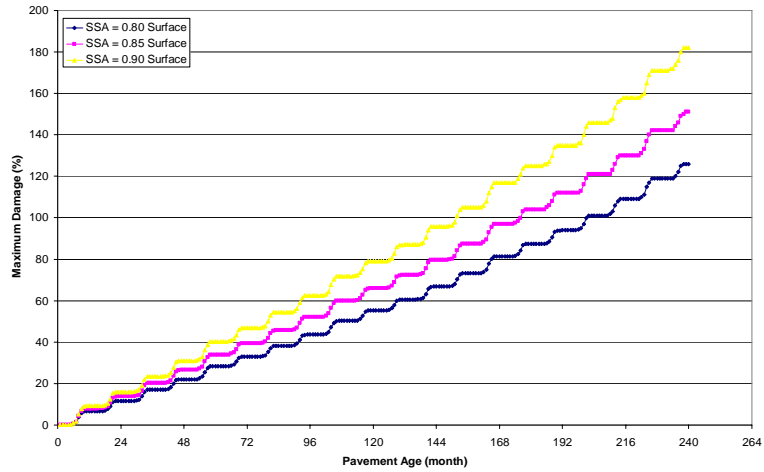


Figure 57B: Sensitivity of SSA to SDC 2 for Phase III (MCA 70-22)

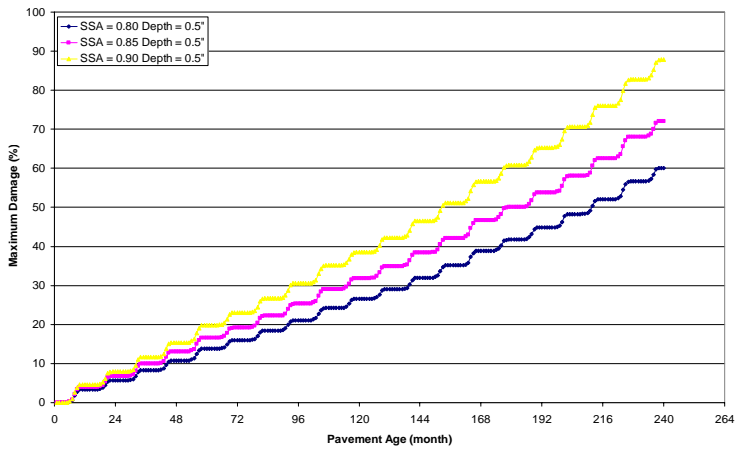


Figure 58B: Sensitivity of SSA to BUD for Phase III (MCA 70-22)

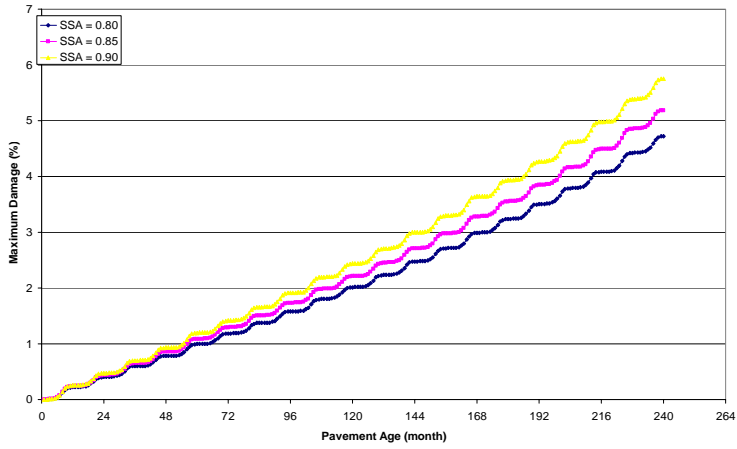


Figure 59B: Sensitivity of SSA to Rutting for Phase III (MCA 70-22)

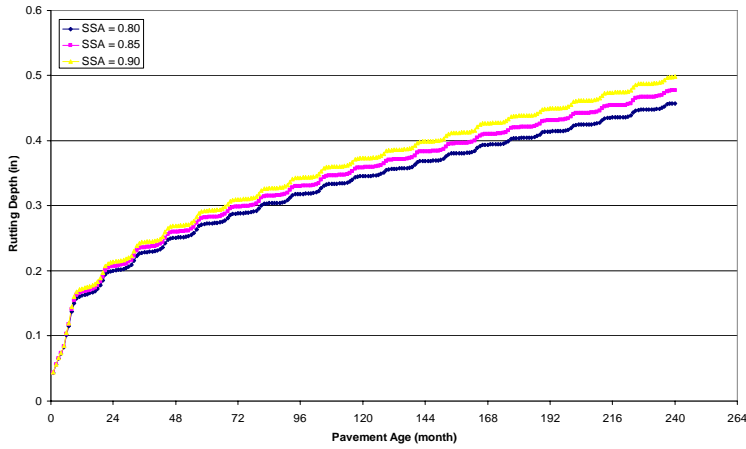


Figure 60B: Sensitivity of SSA to IRI for Phase III (MCA 70-22)

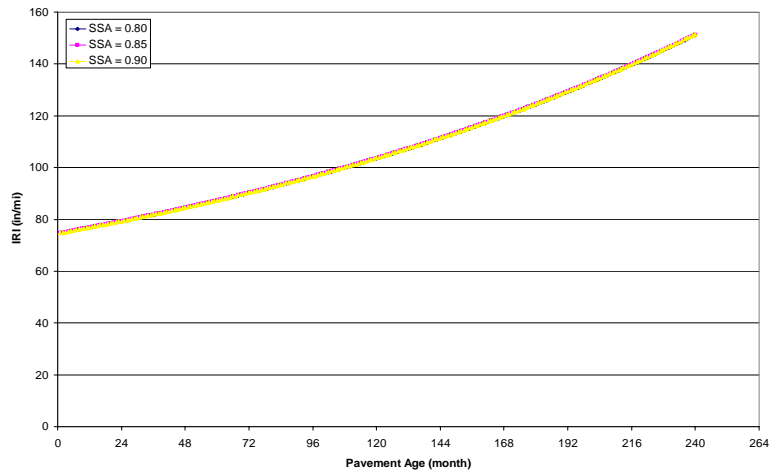


Figure 61B: Sensitivity of HC to SDC 1 for Phase III (ARK 70-22)

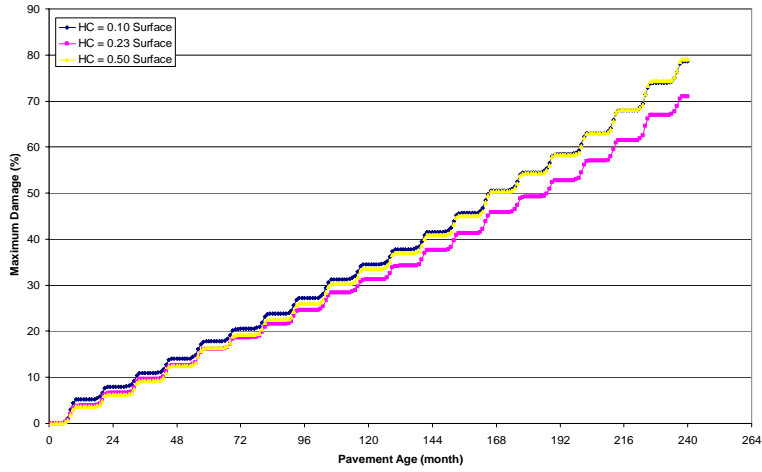


Figure 62B: Sensitivity of HC to SDC 2 for Phase III (ARK 70-22)

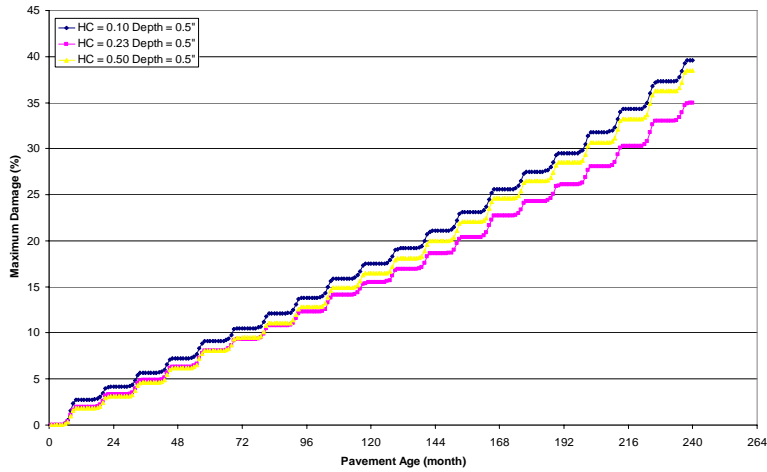


Figure 63B: Sensitivity of HC to BUD for Phase III (ARK 70-22)

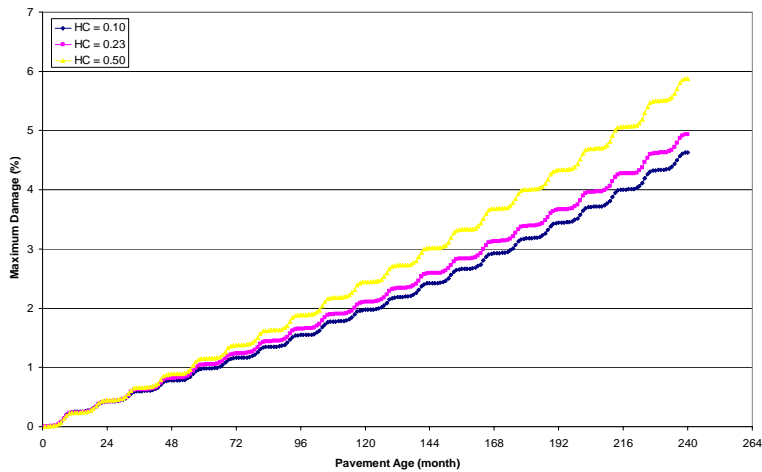


Figure 64B: Sensitivity of HC to Rutting for Phase III (ARK 70-22)

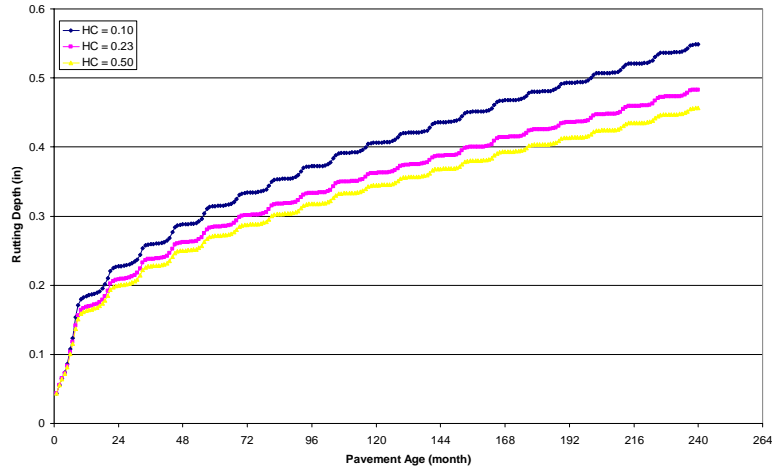


Figure 65B: Sensitivity of HC to IRI for Phase III (ARK 70-22)

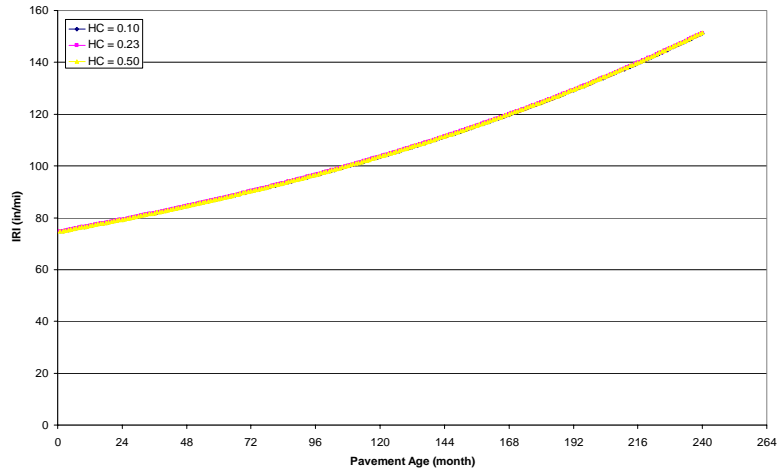


Figure 66B: Sensitivity of HC to SDC 1 for Phase III (GMQ 70-22)

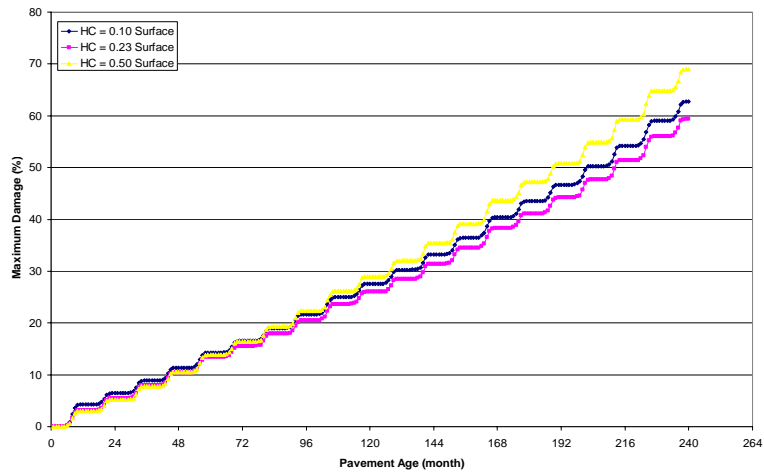


Figure 67B: Sensitivity of HC to SDC 2 for Phase III (GMQ 70-22)

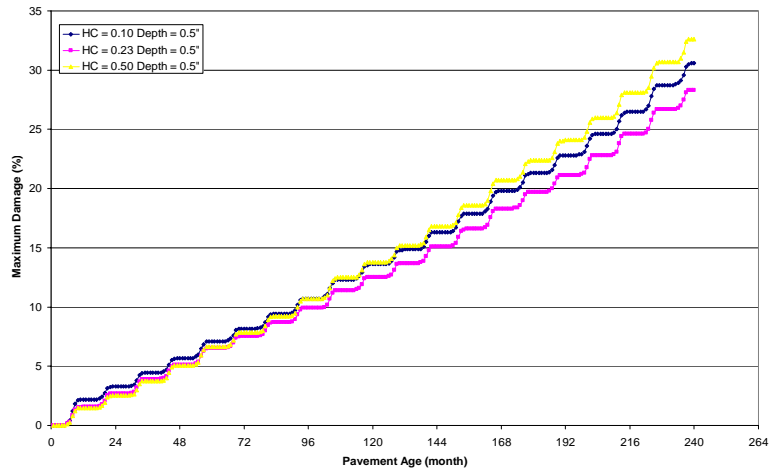


Figure 68B: Sensitivity of HC to BUD for Phase III (GMQ 70-22)

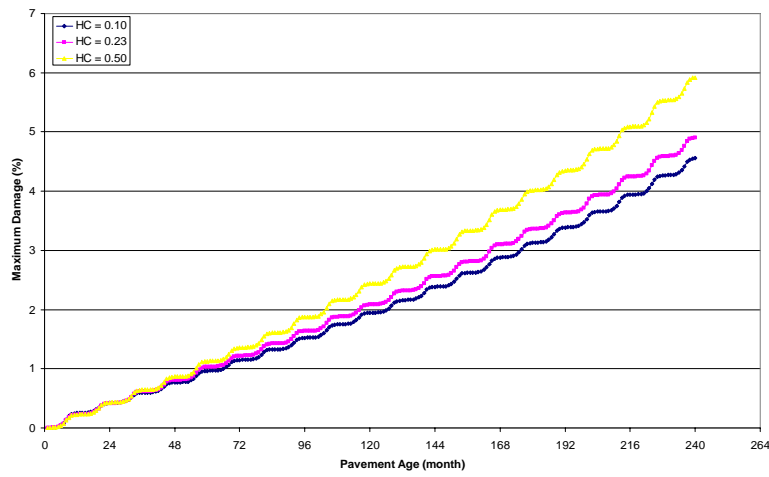


Figure 69B: Sensitivity of HC to Rutting for Phase III (GMQ 70-22)

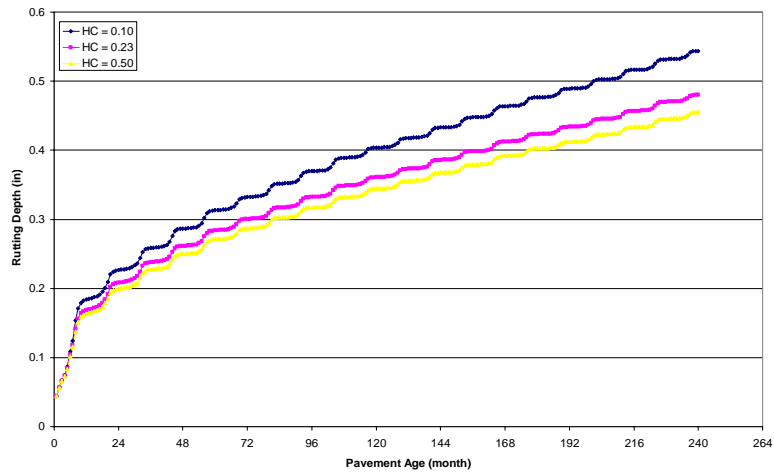


Figure 70B: Sensitivity of HC to IRI for Phase III (GMQ 70-22)

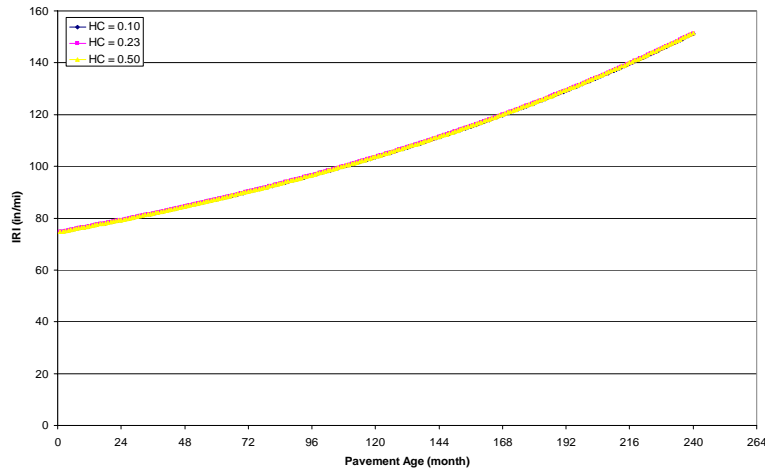


Figure 71B: Sensitivity of HC to SDC 1 for Phase III (JET 70-22)

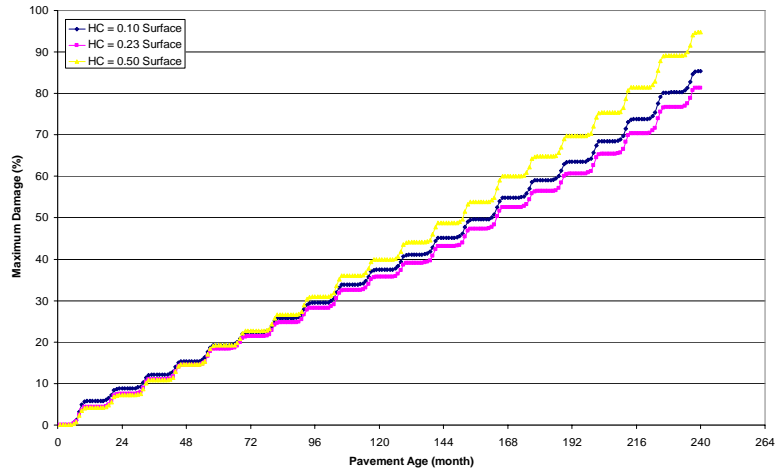


Figure 72B: Sensitivity of HC to SDC 2 for Phase III (JET 70-22)

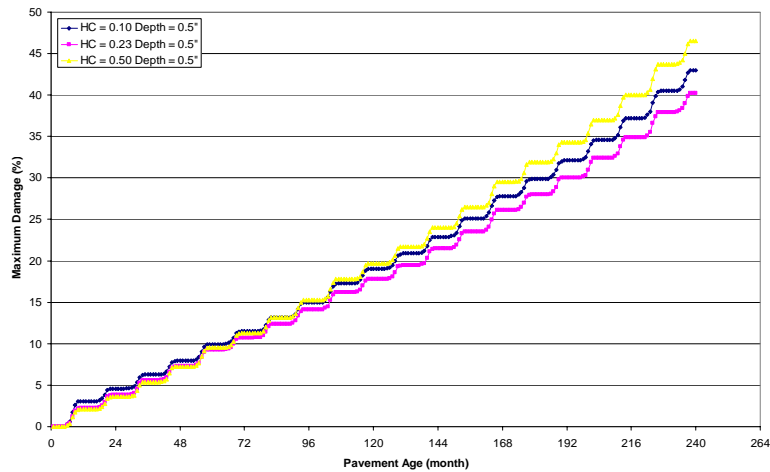


Figure 73B: Sensitivity of HC to BUD for Phase III (JET 70-22)

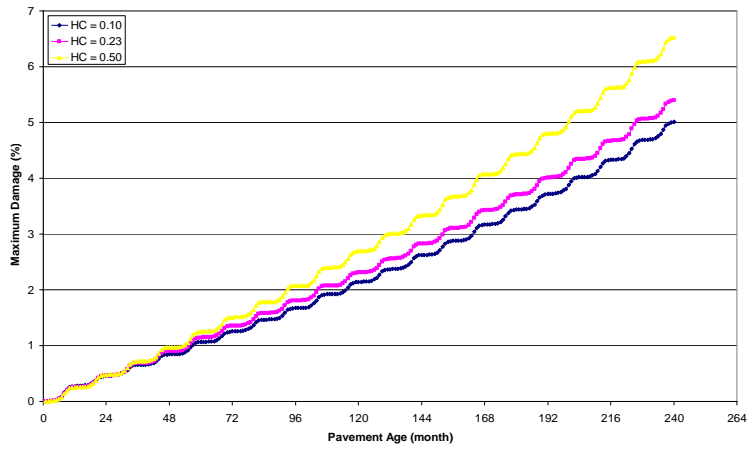


Figure 74B: Sensitivity of HC to Rutting for Phase III (JET 70-22)

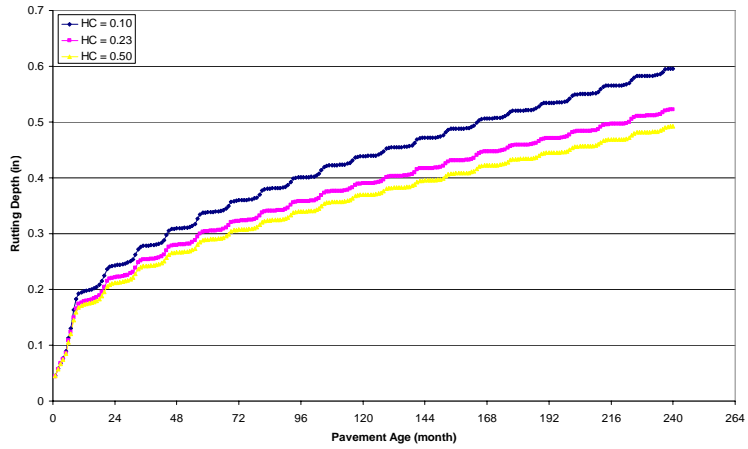


Figure 75B: Sensitivity of HC to IRI for Phase III (JET 70-22)

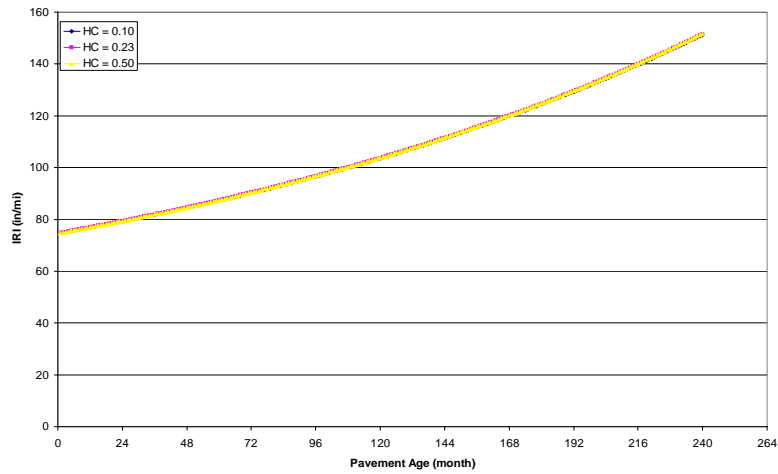


Figure 76B: Sensitivity of HC to SDC 1 for Phase III (MCA 70-22)

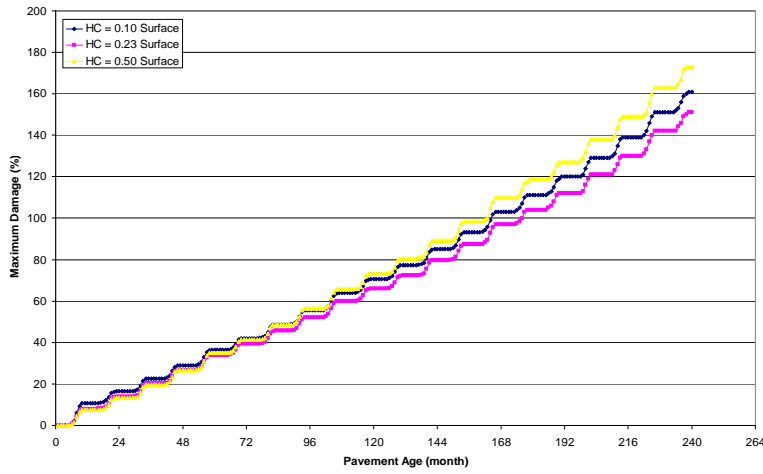


Figure 77B: Sensitivity of HC to SDC 2 for Phase III (MCA 70-22)

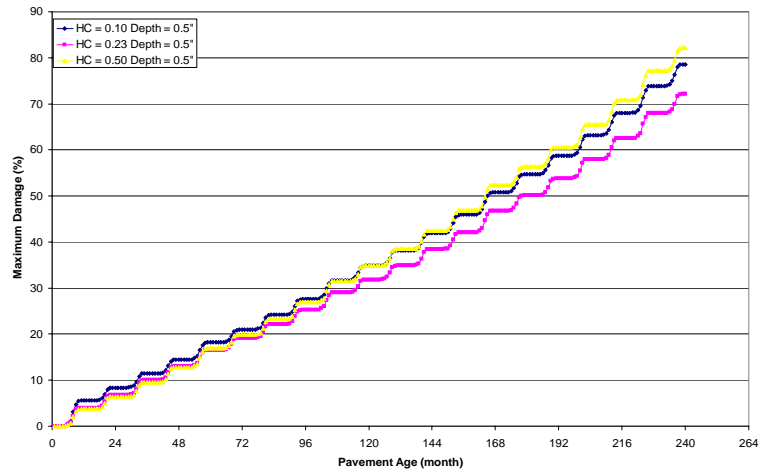


Figure 78B: Sensitivity of HC to BUD for Phase III (MCA 70-22)

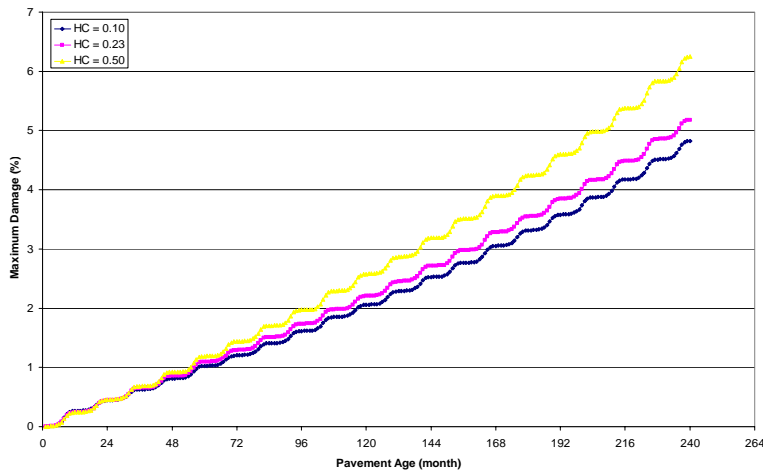


Figure 79B: Sensitivity of HC to Rutting for Phase II (MCA 70-22)

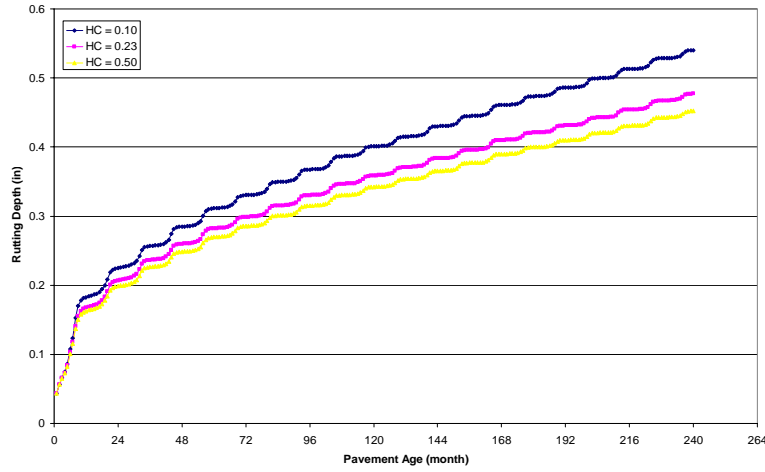


Figure 80B: Sensitivity of HC to IRI for Phase III (MCA 70-22)

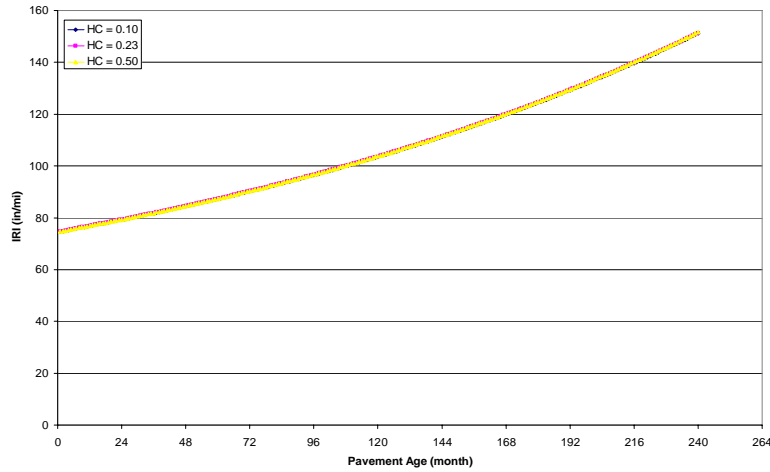


Figure 81B: Sensitivity of TC to SDC 1 for Phase III (ARK 70-22)

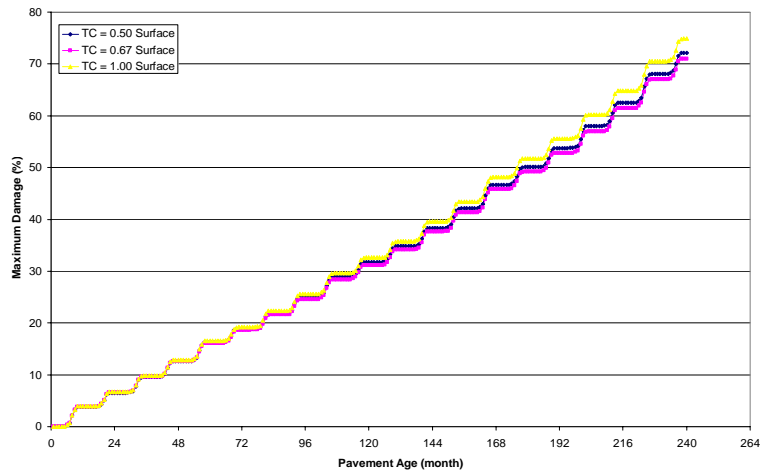


Figure 82B: Sensitivity of TC to SDC 2 for Phase III (ARK 70-22)

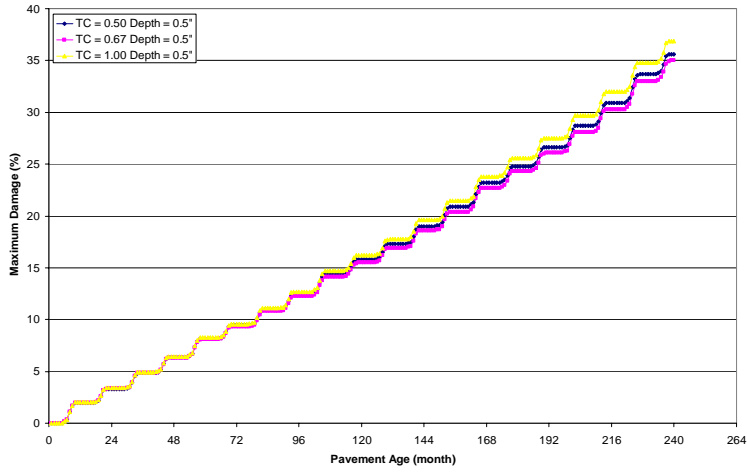


Figure 83B: Sensitivity of TC to BUD for Phase III (ARK 70-22)

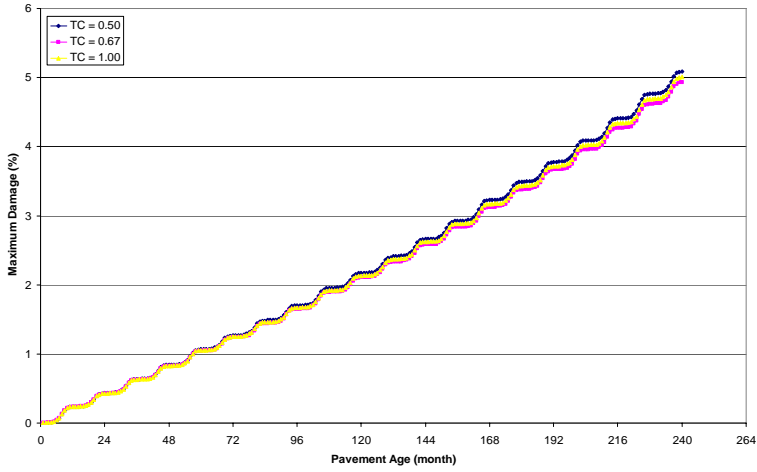


Figure 84B: Sensitivity of TC to Rutting for Phase III (ARK 70-22)

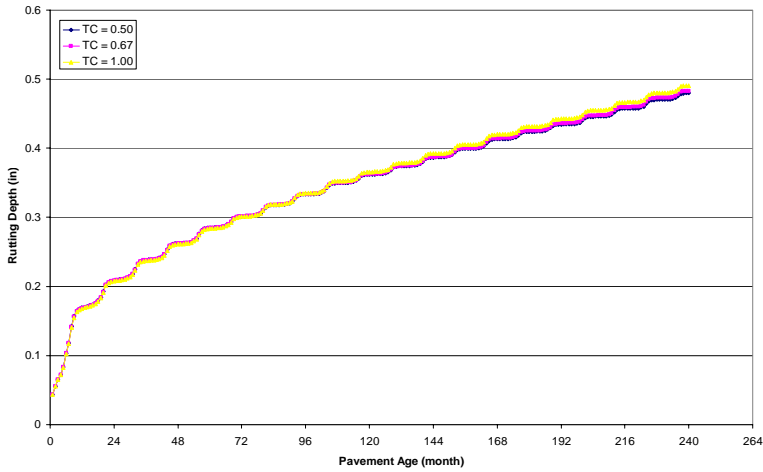


Figure 85B: Sensitivity of TC to IRI for Phase III (ARK 70-22)

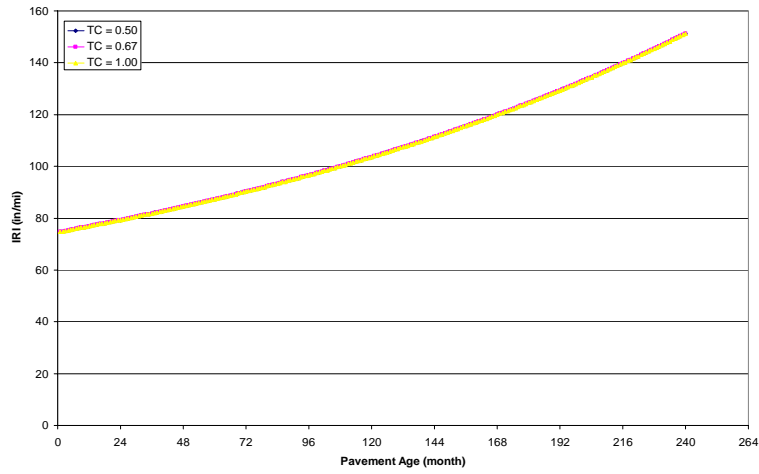


Figure 86B: Sensitivity of TC to SDC 1 for Phase III (GMQ 70-22)

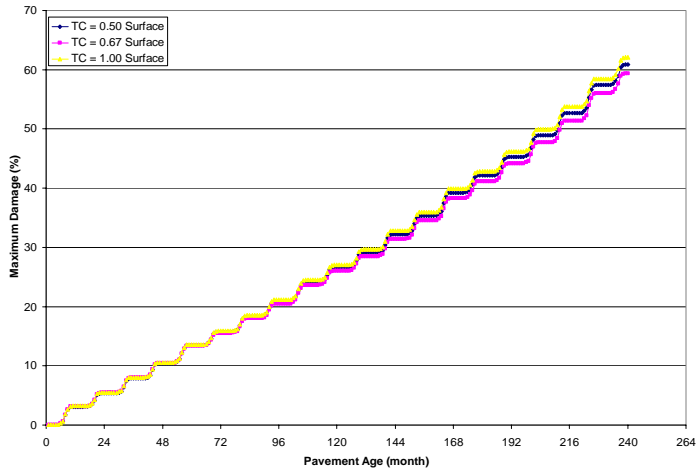


Figure 87B: Sensitivity of TC to SDC 2 for Phase III (GMQ 70-22)

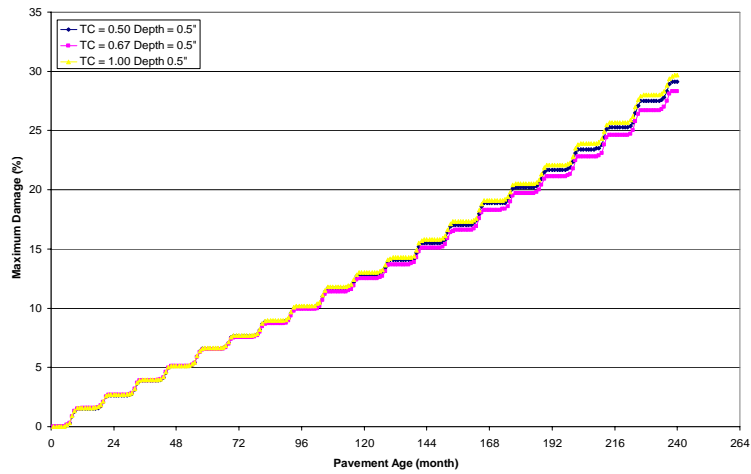


Figure 88B: Sensitivity of TC to BUD for Phase III (GMQ 70-22)

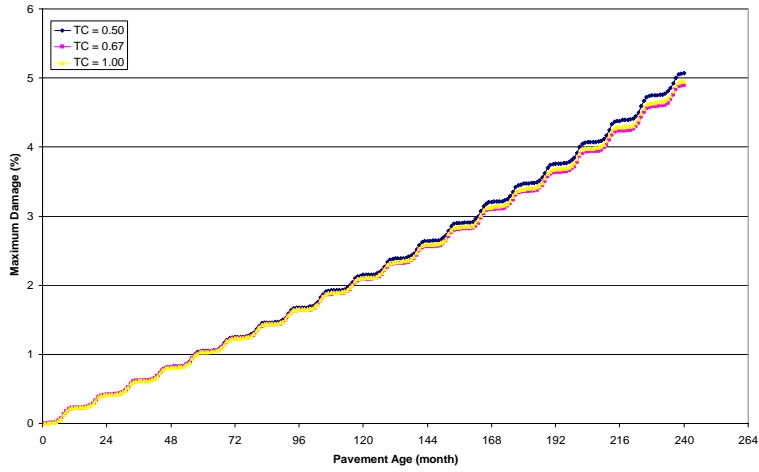


Figure 89B: Sensitivity of TC to Rutting for Phase III (GMQ 70-22)

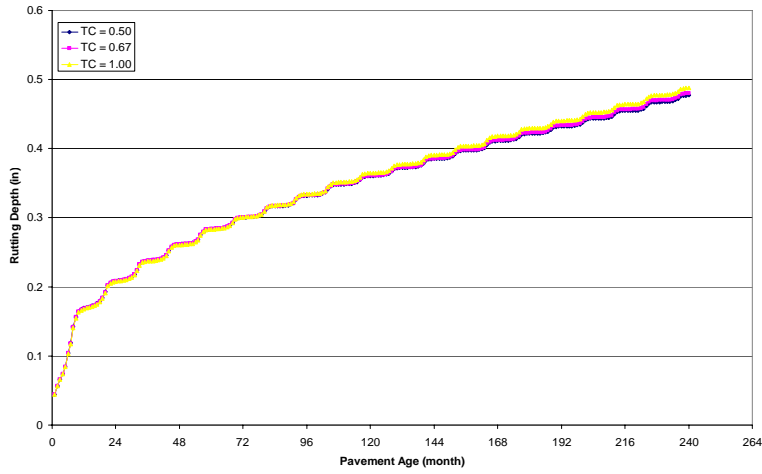


Figure 90B: Sensitivity of TC to IRI for Phase III (GMQ 70-22)

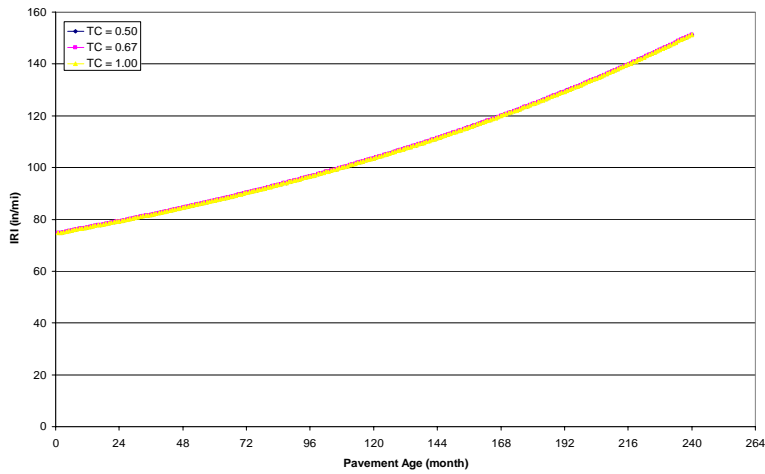


Figure 91B: Sensitivity of TC to SDC 1 for Phase III (JET 70-22)

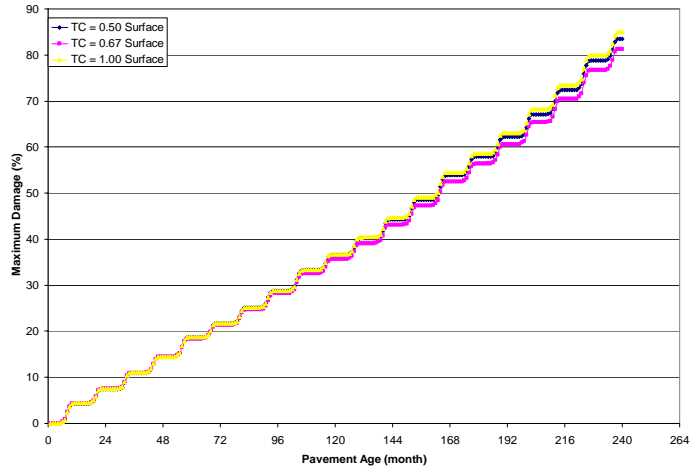


Figure 92B: Sensitivity of TC to SDC 2 for Phase III (JET 70-22)

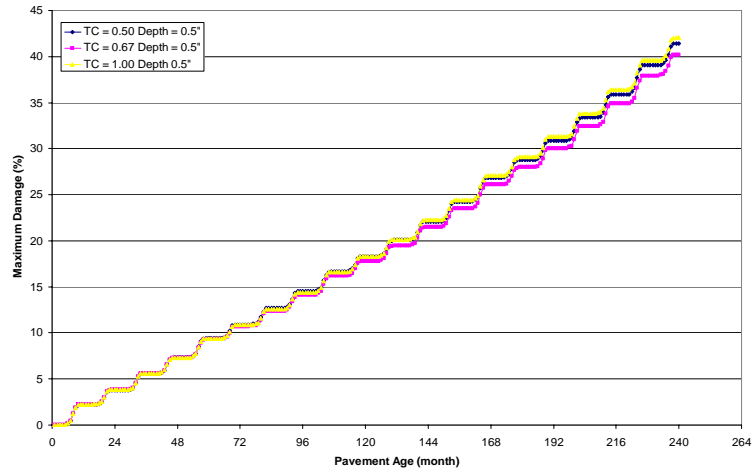


Figure 93B: Sensitivity of TC to BUD for Phase III (JET 70-22)

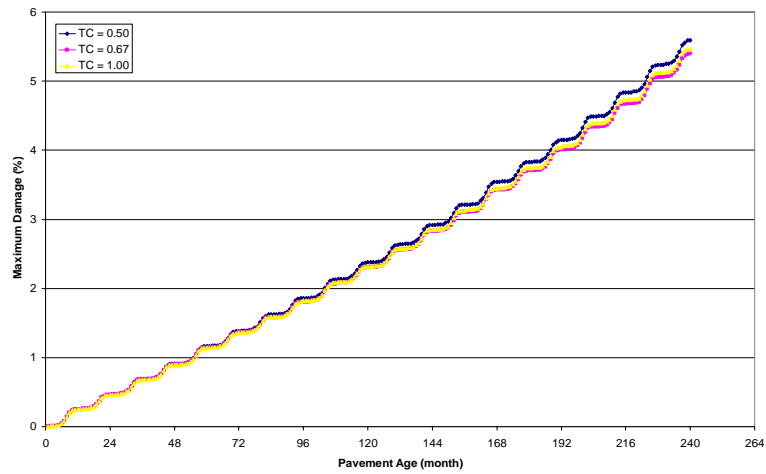


Figure 94B: Sensitivity of TC to Rutting for Phase III (JET 70-22)

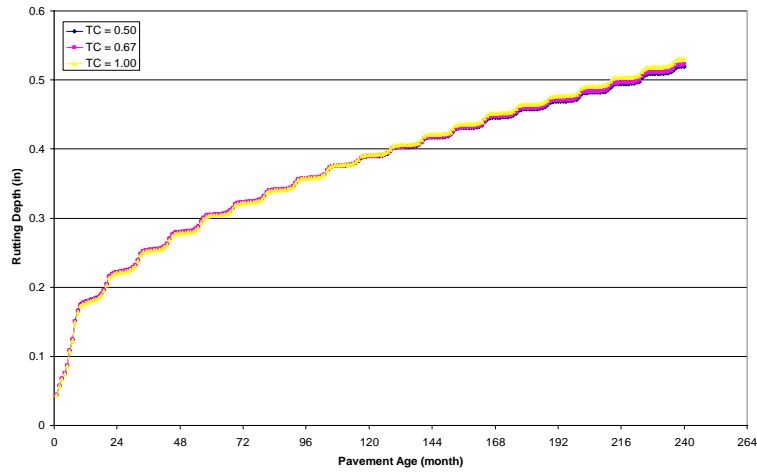


Figure 95B: Sensitivity of TC to IRI for Phase III (JET 70-22)

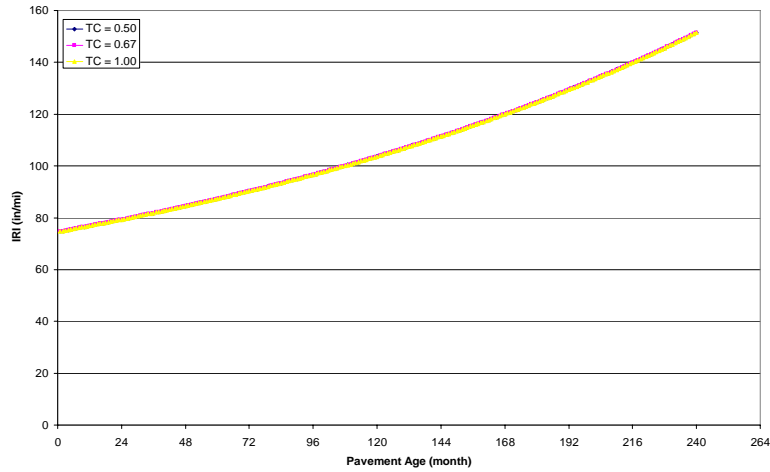


Figure 96B: Sensitivity of TC to SDC 1 for Phase III (MCA 70-22)

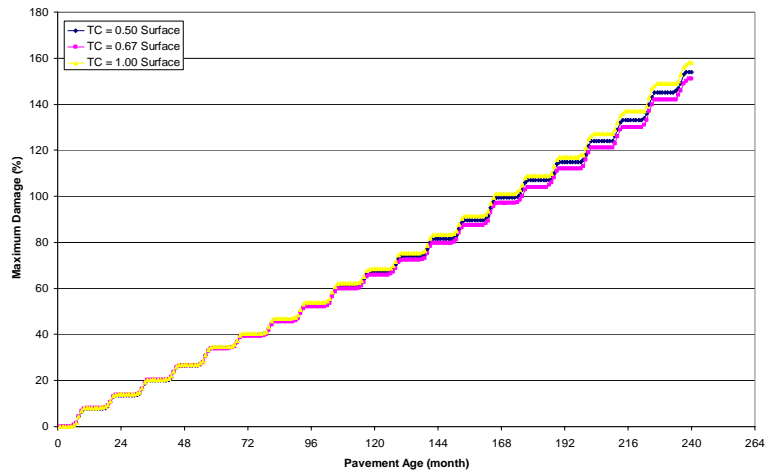


Figure 97B: Sensitivity of TC to SDC 2 for Phase III (MCA 70-22)

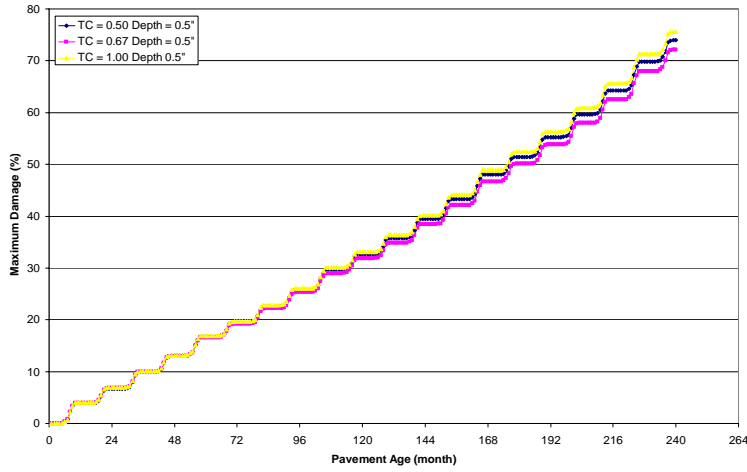


Figure 98B: Sensitivity of TC to BUD for Phase III (MCA 70-22)

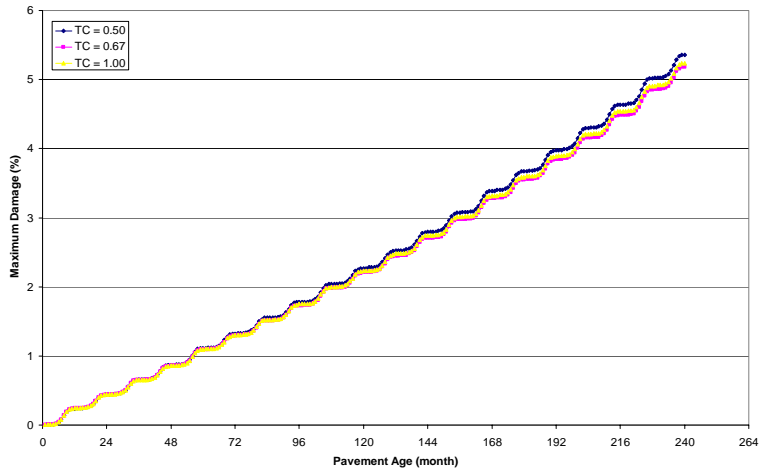


Figure 99B: Sensitivity of TC to Rutting for Phase III (MCA 70-22)

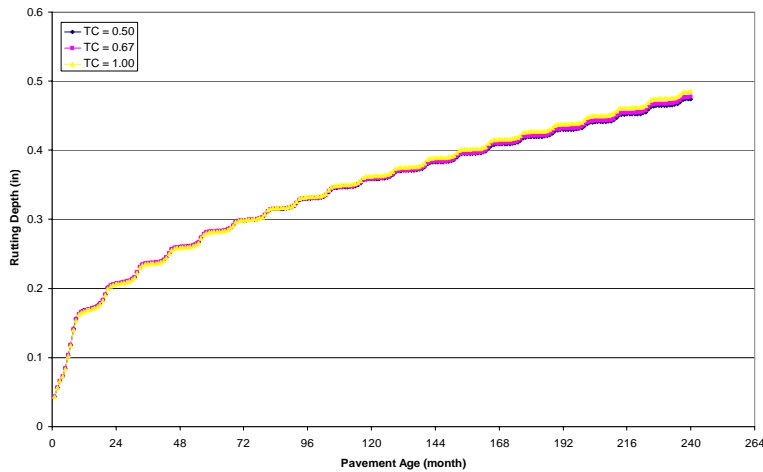


Figure 100B: Sensitivity of TC to IRI for Phase III (MCA 70-22)

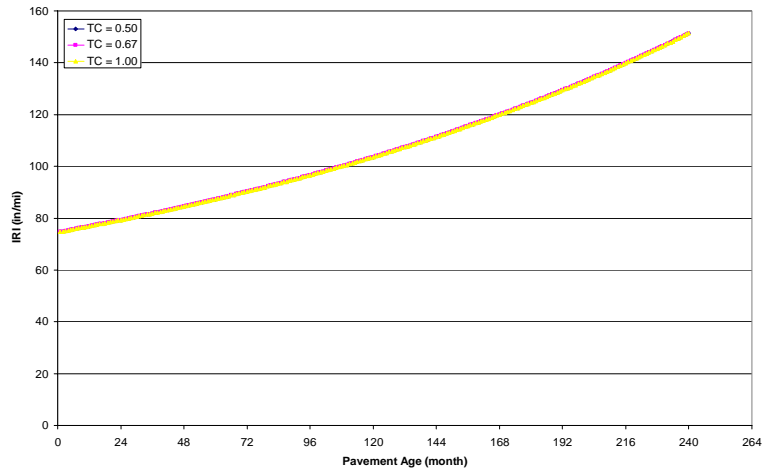


Figure 101B: Sensitivity of AV to SDC1 for Phase III (12.5mm ARK 64-22)

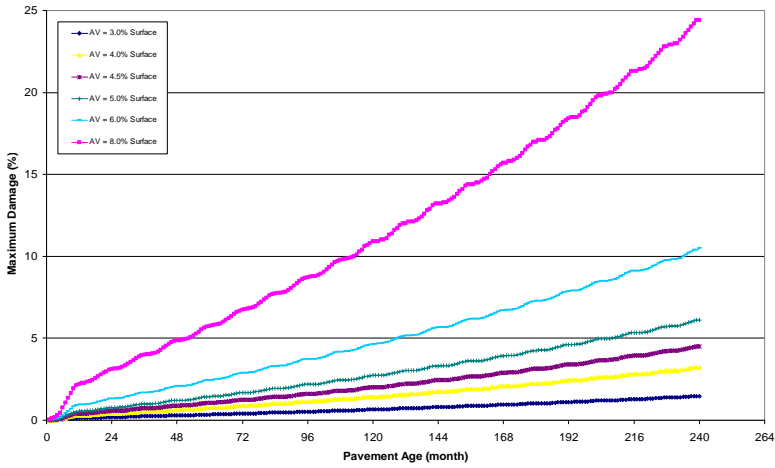


Figure 102B: Sensitivity of AV to SDC2 for Phase III (12.5mm ARK 64-22)

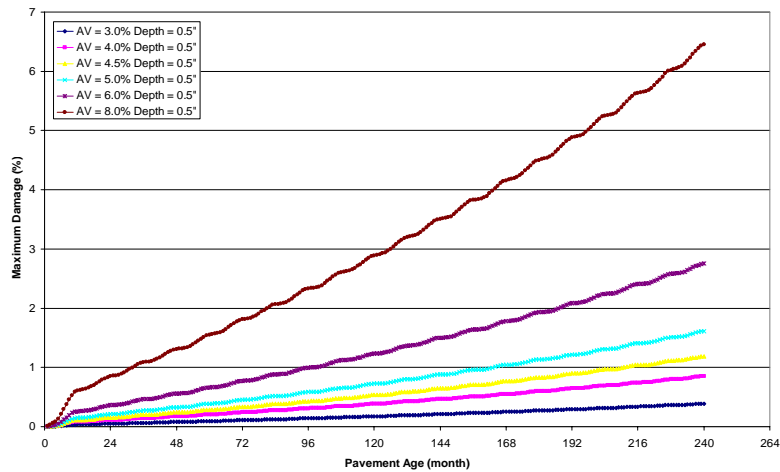


Figure 103B: Sensitivity of AV to BUD for Phase III (12.5mm ARK 64-22)

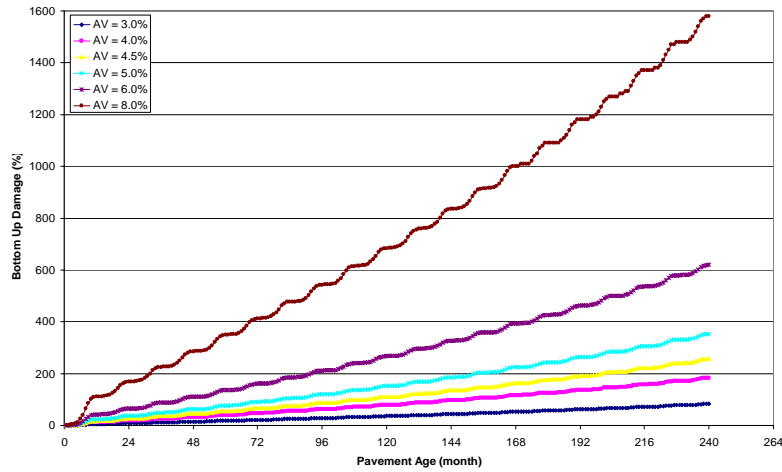


Figure 104B: Sensitivity of AV to Rutting for Phase III (12.5mm ARK 64-22)

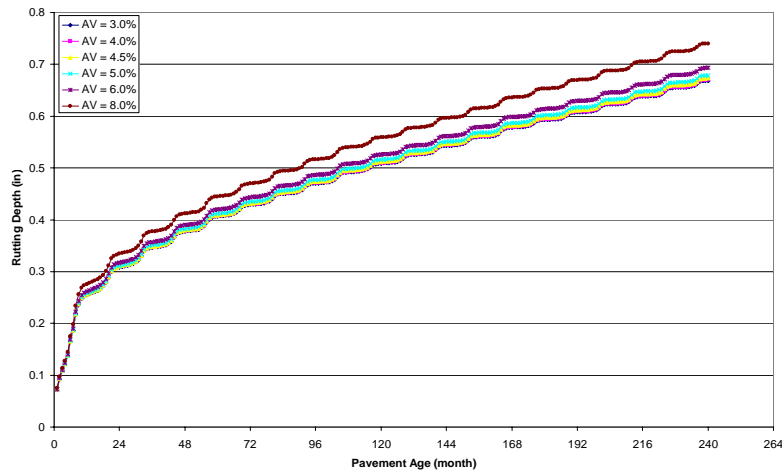


Figure 105B: Sensitivity of AV to IRI for Phase III (12.5mm ARK 64-22)

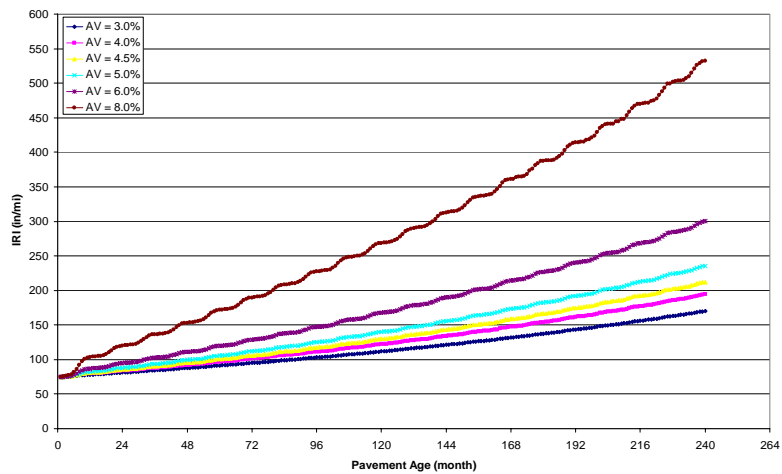


Figure 106B: Sensitivity of AV to SDC1 for Phase III (12.5mm ARK 70-22)

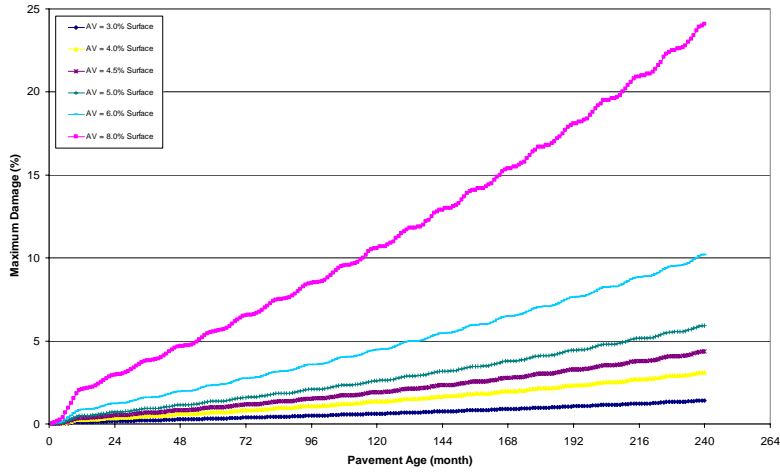


Figure 107B: Sensitivity of AV to SDC2 for Phase III (12.5mm ARK 70-22)

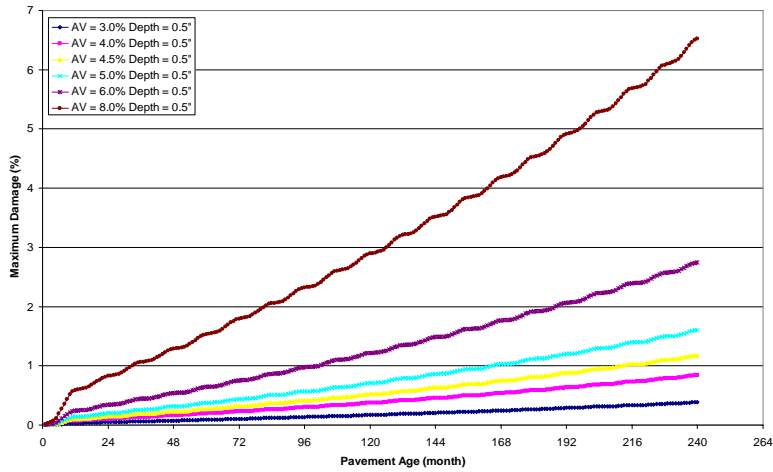


Figure 108B: Sensitivity of AV to BUD for Phase III (12.5mm ARK 70-22)

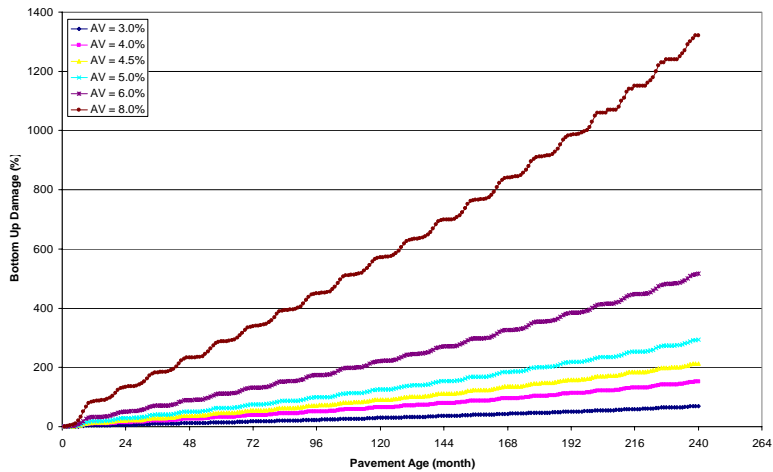


Figure 109B: Sensitivity of AV to Rutting for Phase III (12.5mm ARK 70-22)

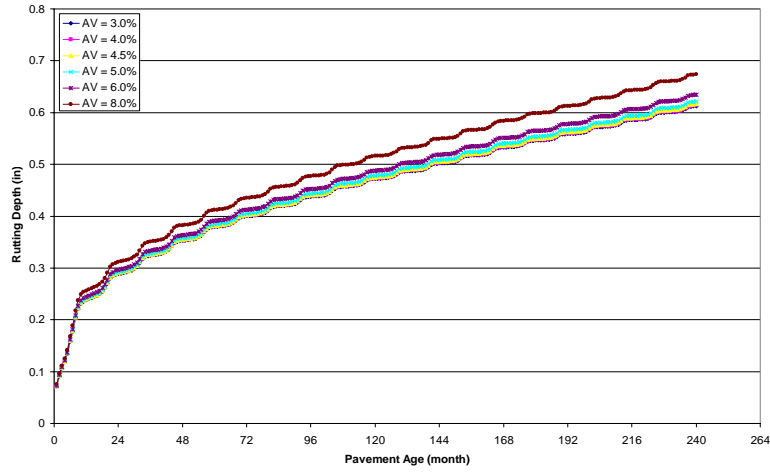


Figure 110B: Sensitivity of AV to IRI for Phase III (12.5mm ARK 70-22)

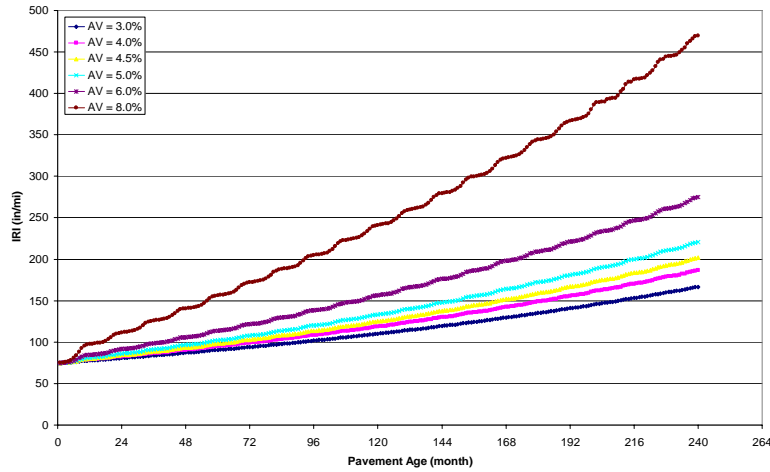


Figure 111B: Sensitivity of AV to SDC1 for Phase III (12.5mm ARK 76-22)

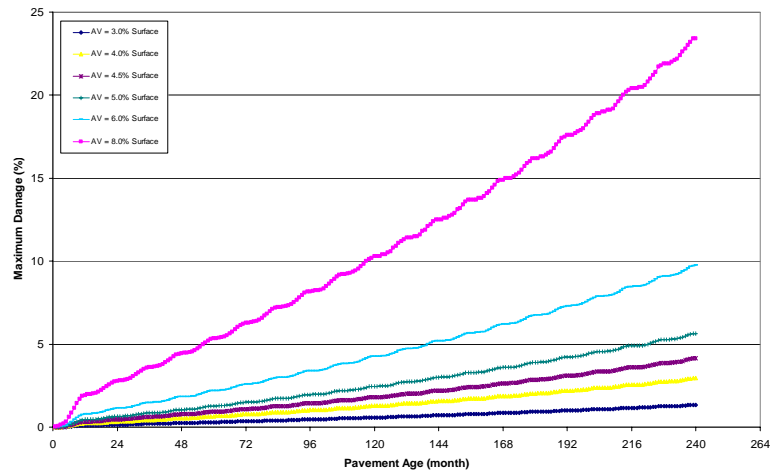


Figure 112B: Sensitivity of AV to SDC2 for Phase III (12.5mm ARK 76-22)

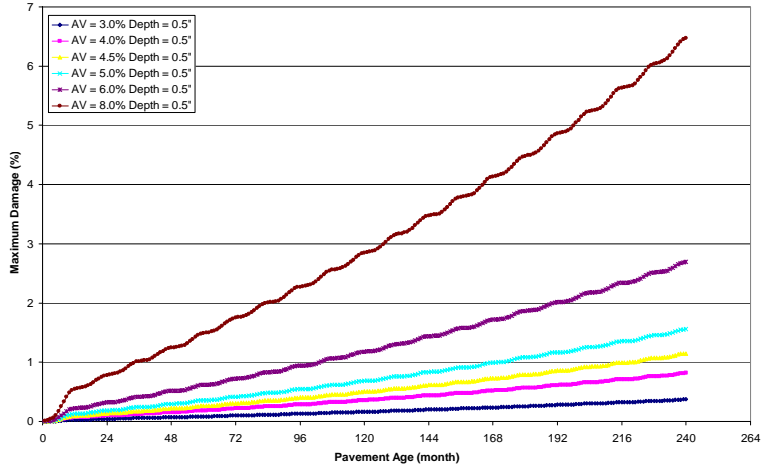


Figure 113B: Sensitivity of AV to BUD for Phase III (12.5mm ARK 76-22)

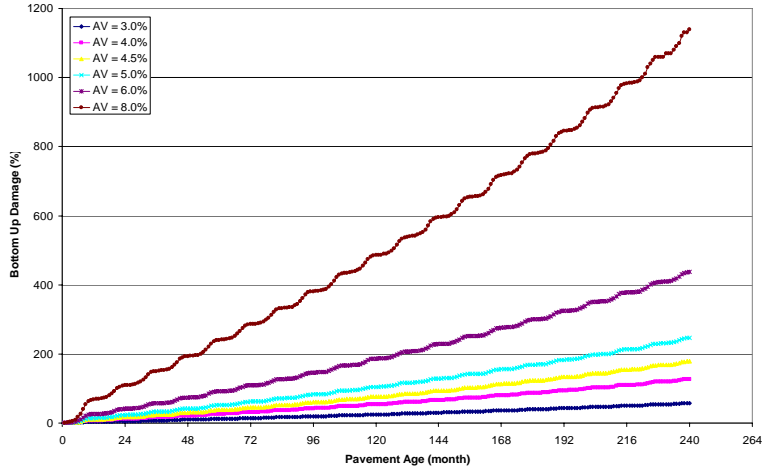


Figure 114B: Sensitivity of AV to Rutting for Phase III (12.5mm ARK 76-22)

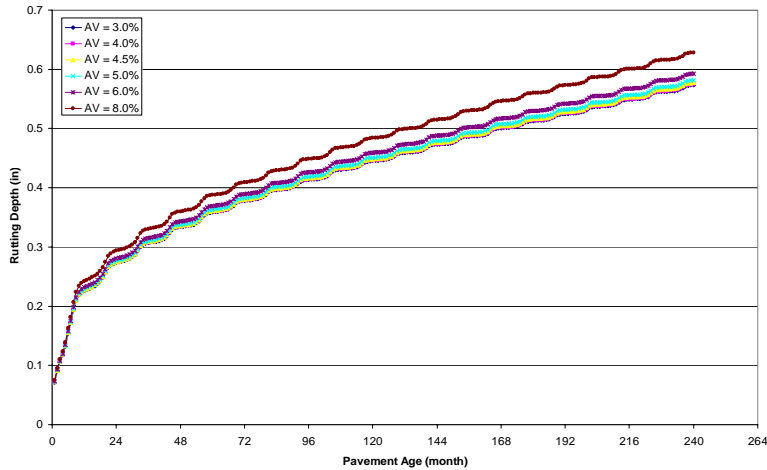


Figure 115B: Sensitivity of AV to IRI for Phase III (12.5mm ARK 76-22)

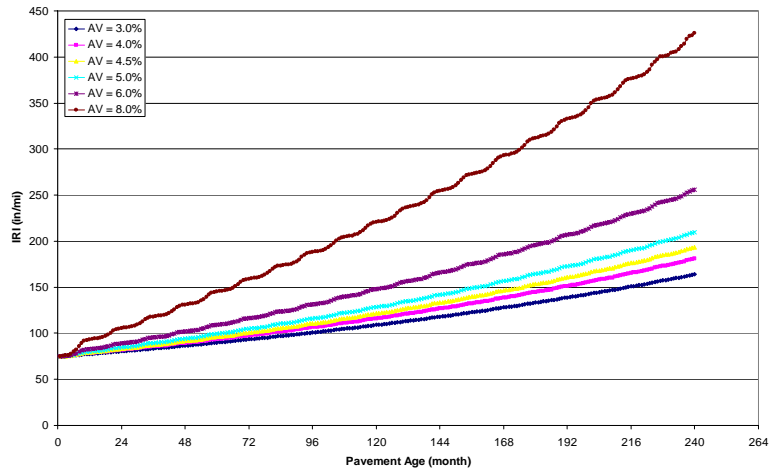


Figure 116B: Sensitivity of AV to SDC1 for Phase III (25.0mm ARK 64-22)

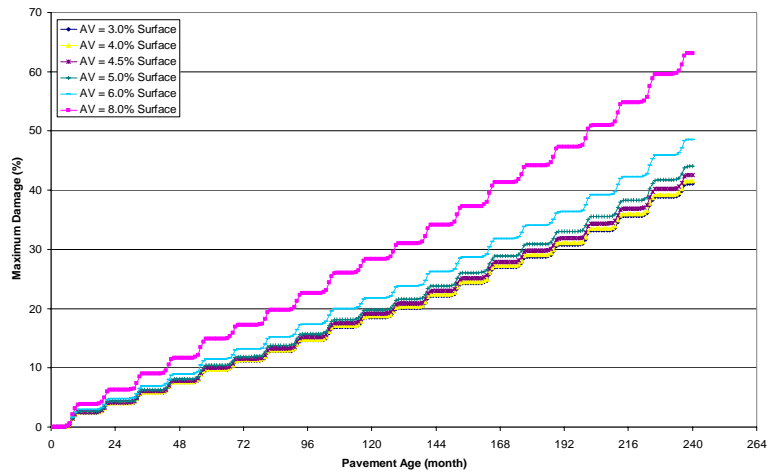


Figure 117B: Sensitivity of AV to SDC2 for Phase III (25.0mm ARK 64-22)

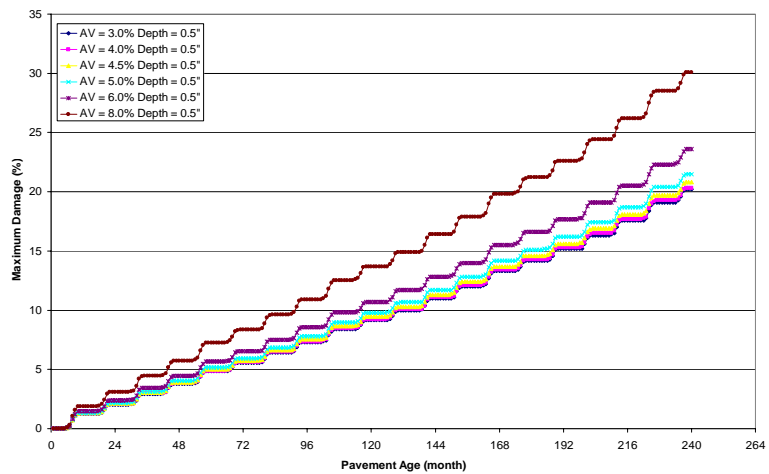


Figure 118B: Sensitivity of AV to BUD for Phase III (25.0mm ARK 64-22)

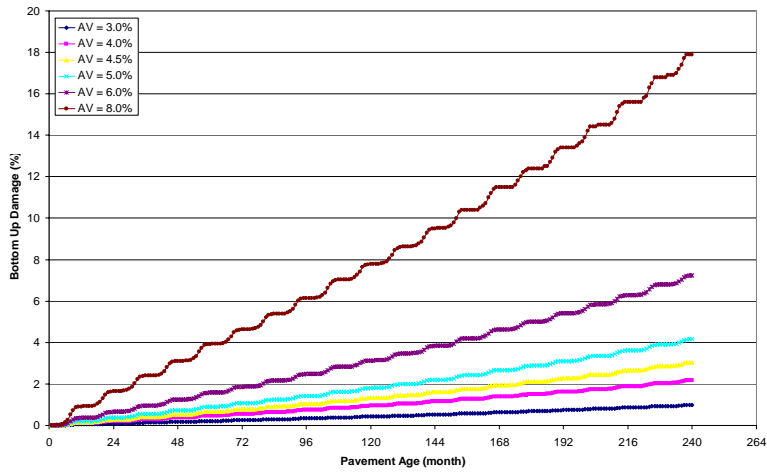


Figure 119B: Sensitivity of AV to Rutting for Phase III (25.0mm ARK 64-22)

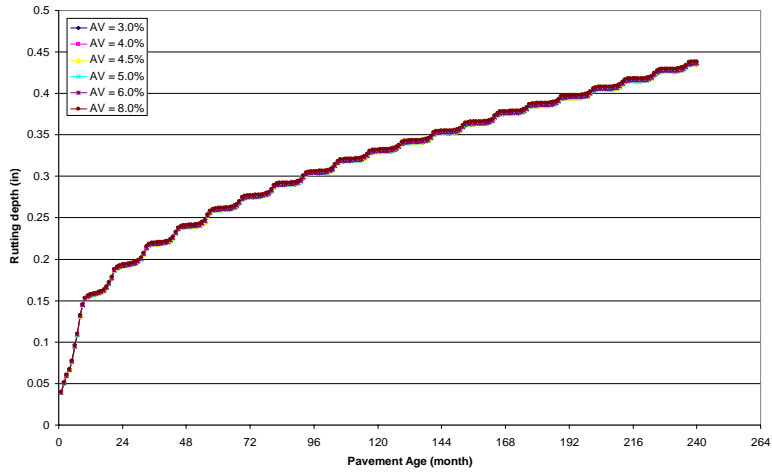


Figure 120B: Sensitivity of AV to IRI for Phase III (25.0mm ARK 64-22)

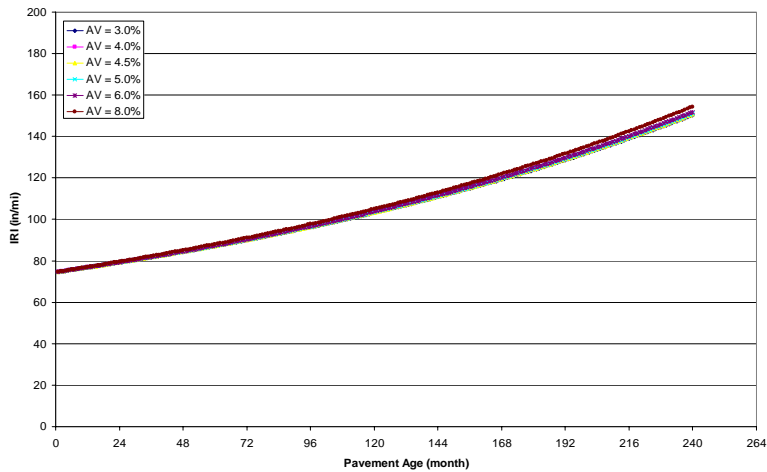


Figure 121B: Sensitivity of AV to SDC1 for Phase III (25.0mm ARK 70-22)

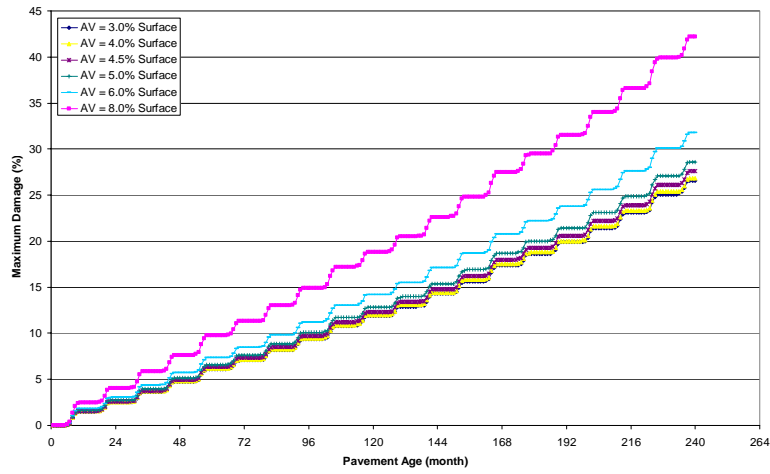


Figure 122B: Sensitivity of AV to SDC2 for Phase III (25.0mm ARK 70-22)

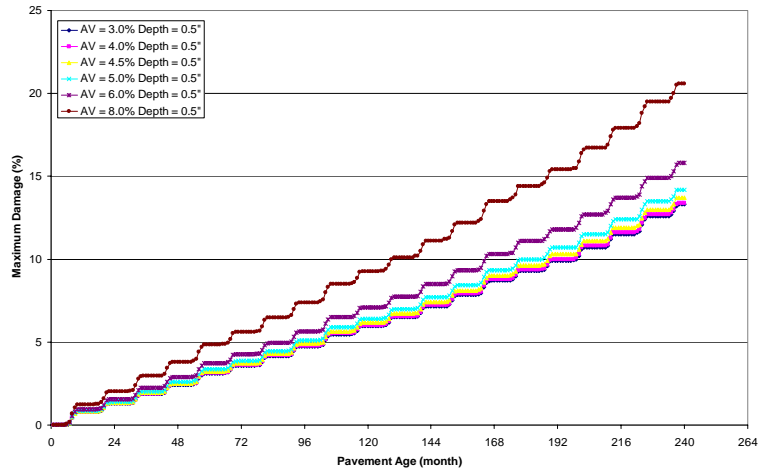


Figure 123B: Sensitivity of AV to BUD for Phase III (25.0mm ARK 70-22)

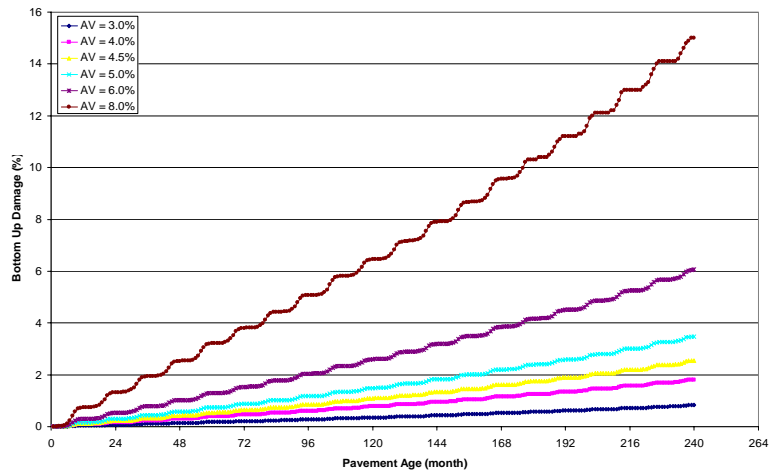


Figure 124B: Sensitivity of AV to Rutting for Phase III (25.0mm ARK 70-22)

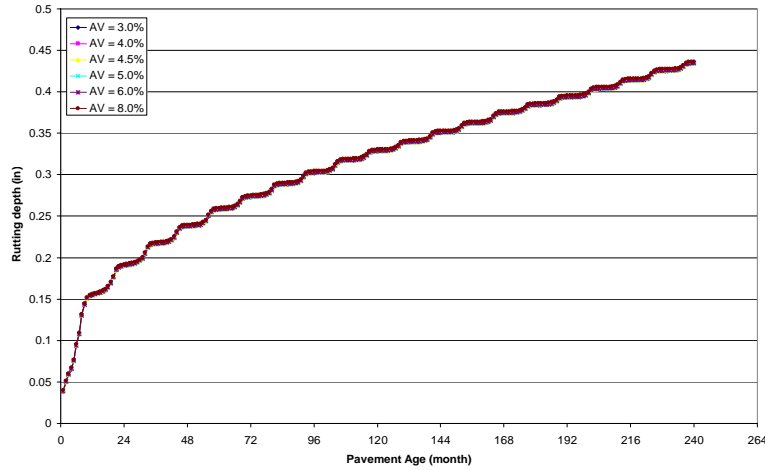


Figure 125B: Sensitivity of AV to IRI for Phase III (25.0mm ARK 70-22)

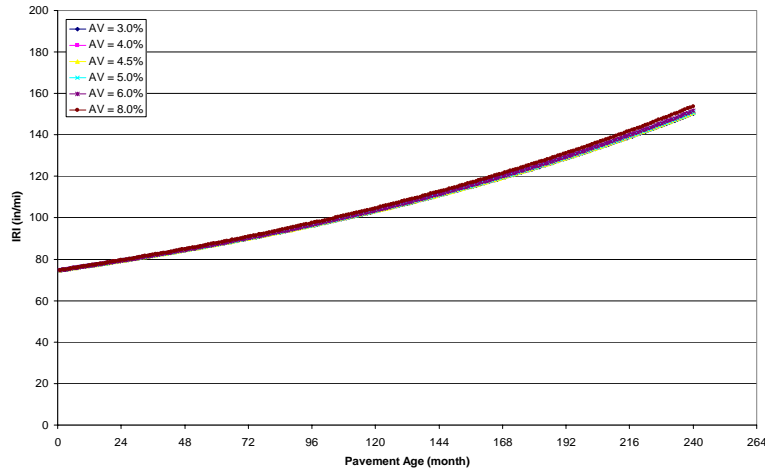


Figure 126B: Sensitivity of AV to SDC1 for Phase III (25.0mm ARK 76-22)

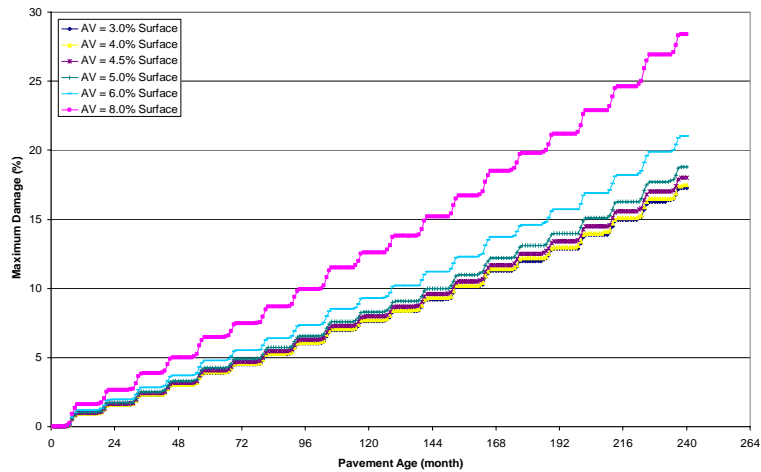


Figure 127B: Sensitivity of AV to SDC2 for Phase III (25.0mm ARK 76-22)

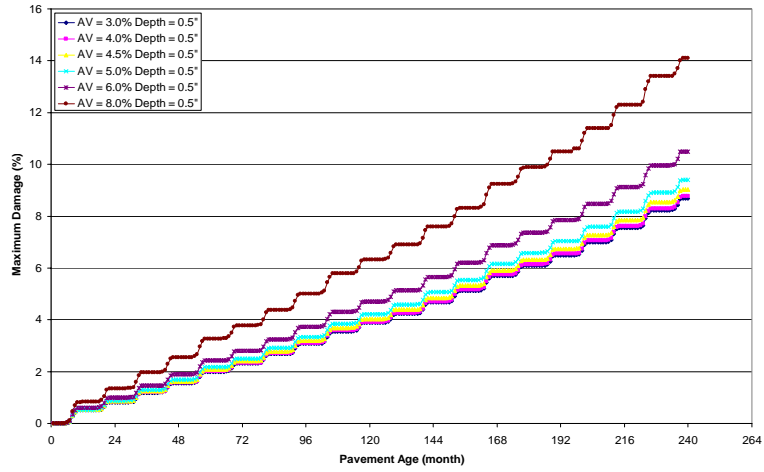


Figure 128B: Sensitivity of AV to BUD for Phase III (25.0mm ARK 76-22)

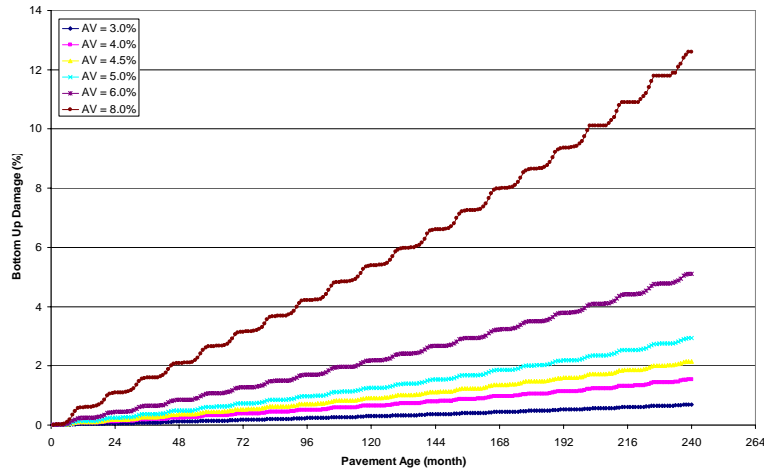


Figure 129B: Sensitivity of AV to Rutting for Phase III (25.0mm ARK 76-22)

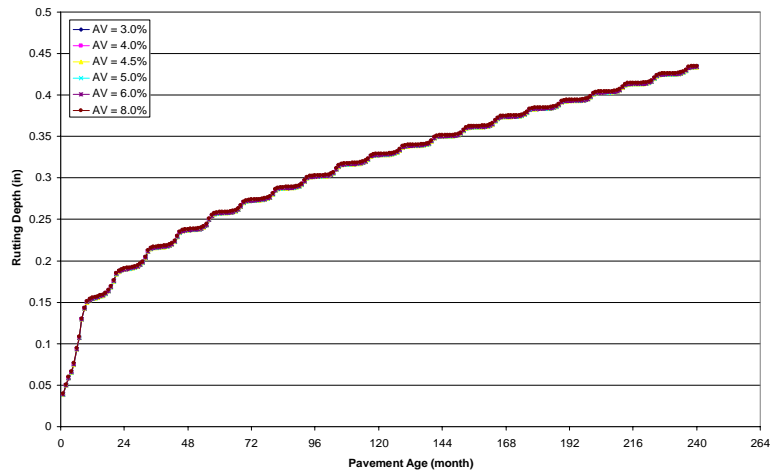


Figure 130B: Sensitivity of AV to IRI for Phase III (25.0mm ARK 76-22)

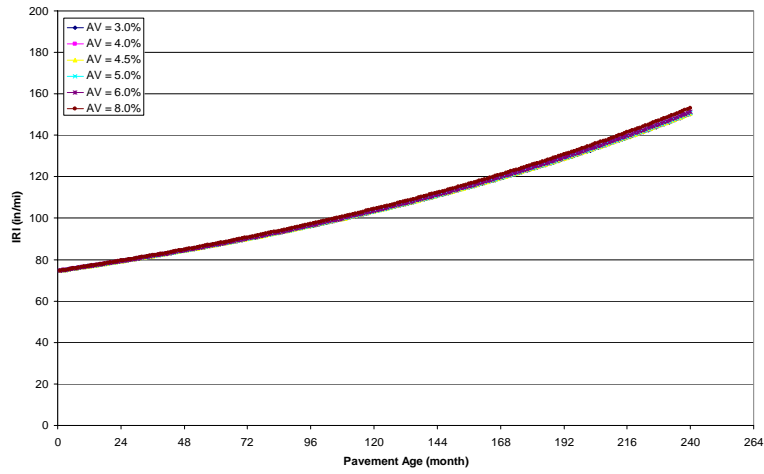


Figure 131B: Sensitivity of BG to SDC1 for Phase III (12.5mm ARK, AV = 6.0%)

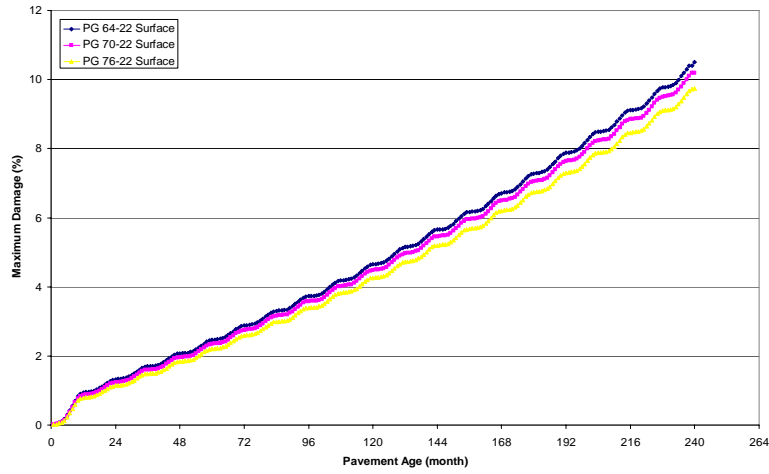


Figure 132B: Sensitivity of BG to SDC2 for Phase III (12.5mm ARK, AV = 6.0%)

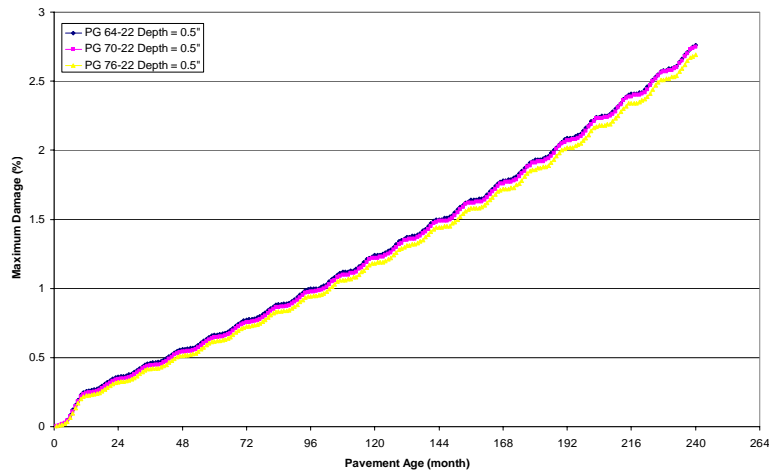


Figure 133B: Sensitivity of BG to BUD for Phase III (12.5mm ARK, AV = 6.0%)

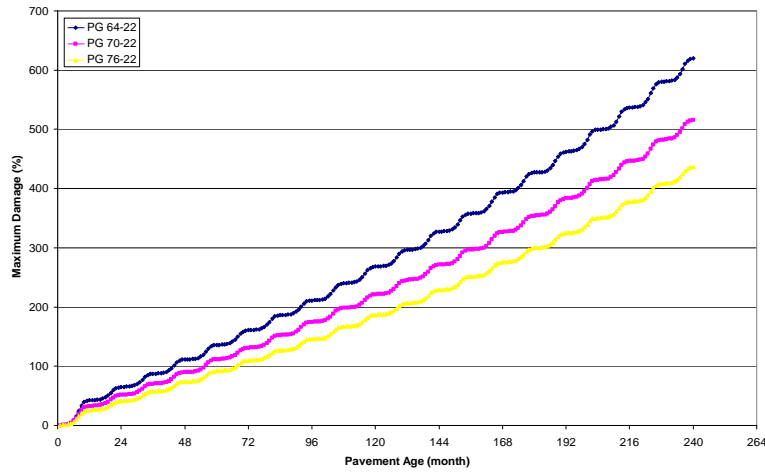


Figure 134B: Sensitivity of BG to Rutting for Phase III (12.5mm ARK, AV = 6.0%)

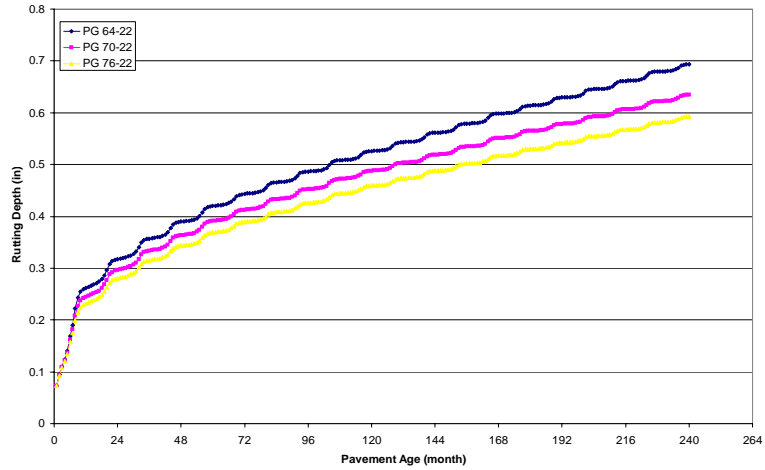


Figure 135B: Sensitivity of BG to IRI for Phase III (12.5mm ARK, AV = 6.0%)

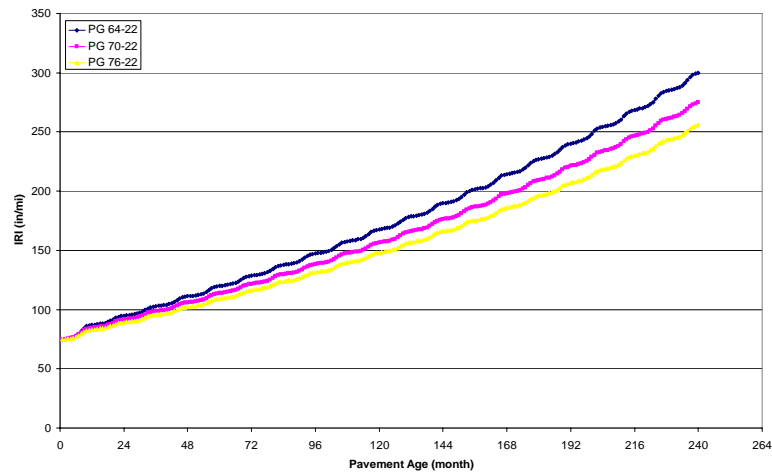


Figure 136B: Sensitivity of BG to SDC1 for Phase III (12.5mm ARK, AV = 8.0%)

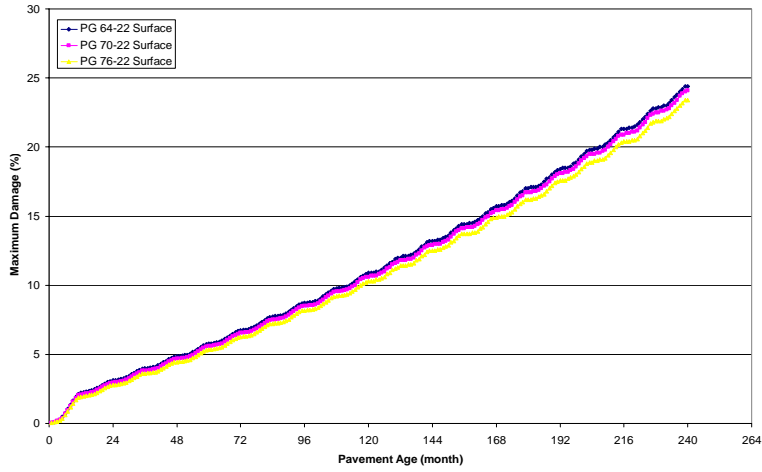


Figure 137B: Sensitivity of BG to SDC2 for Phase III (12.5mm ARK, AV = 8.0%)

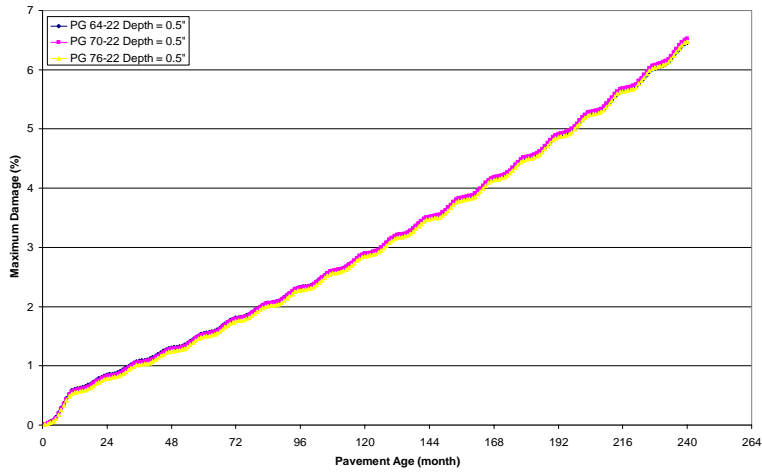


Figure 138B: Sensitivity of BG to BUD for Phase III (12.5mm ARK, AV = 8.0%)

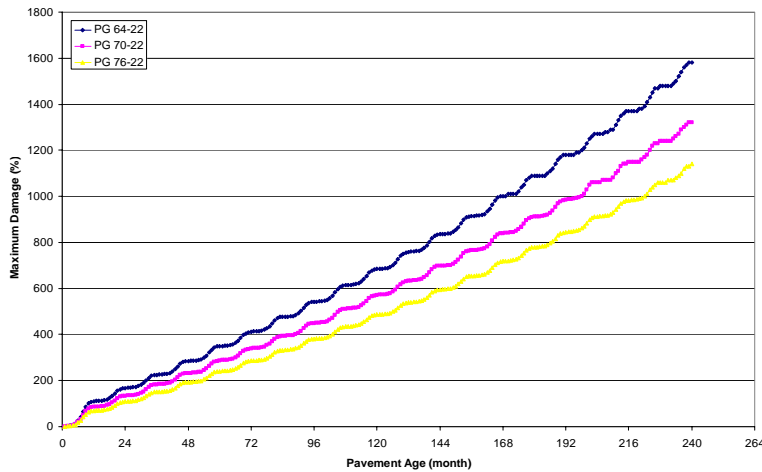


Figure 139B: Sensitivity of BG to Rutting for Phase III (12.5mm ARK, AV = 8.0%)

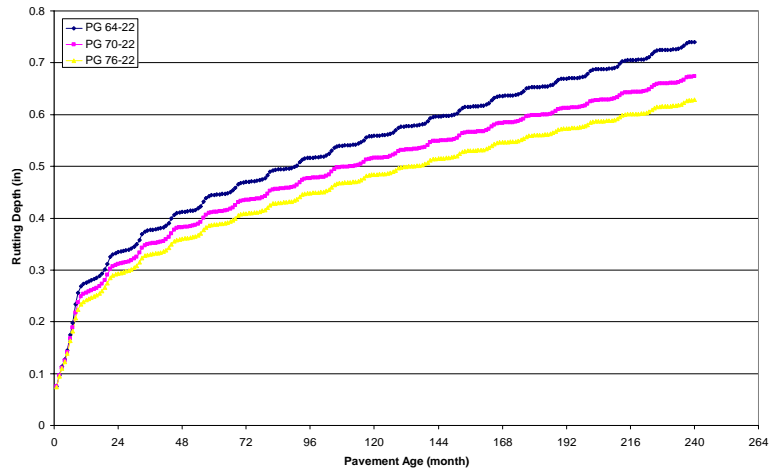


Figure 140B: Sensitivity of BG to IRI for Phase III (12.5mm ARK, AV = 8.0%)

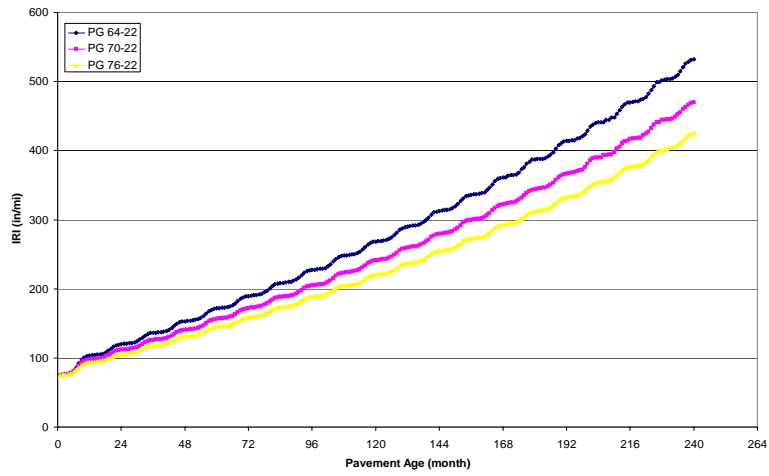


Figure 141B: Sensitivity of BG to SDC1 for Phase III (25.0mm ARK, AV = 6.0%)

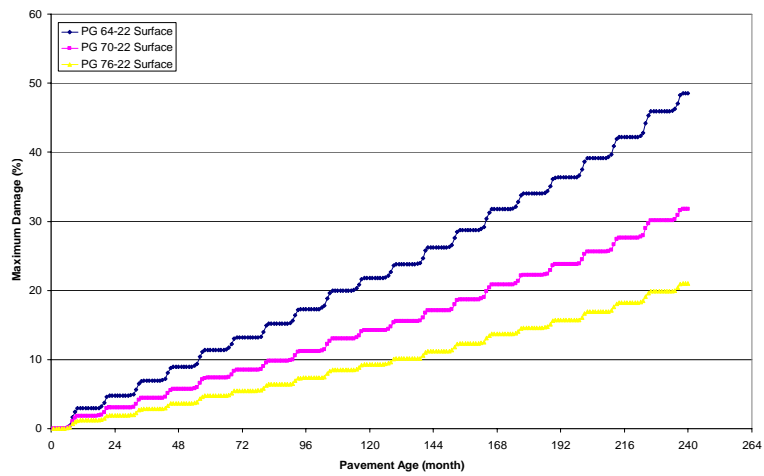


Figure 142B: Sensitivity of BG to SDC2 for Phase III (25.0mm ARK, AV = 6.0%)

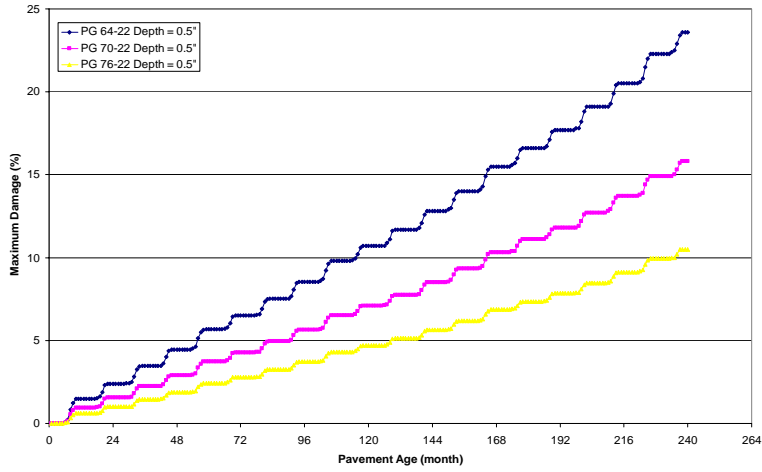


Figure 143B: Sensitivity of BG to BUD for Phase III (25.0mm ARK, AV = 6.0%)

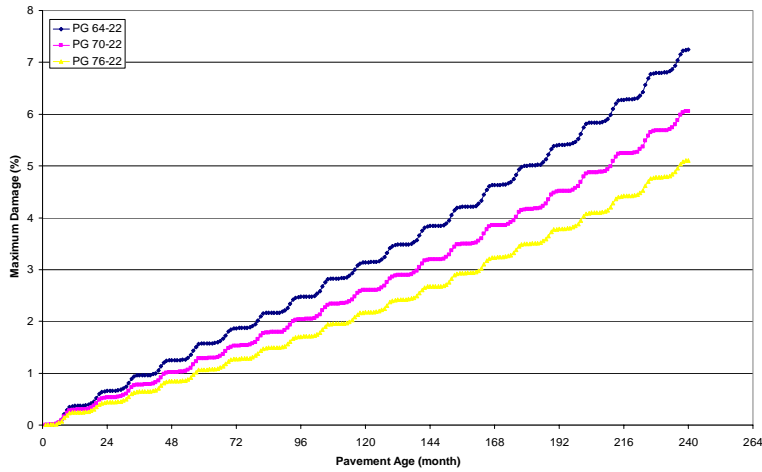


Figure 144B: Sensitivity of BG to Rutting for Phase III (25.0mm ARK, AV = 6.0%)

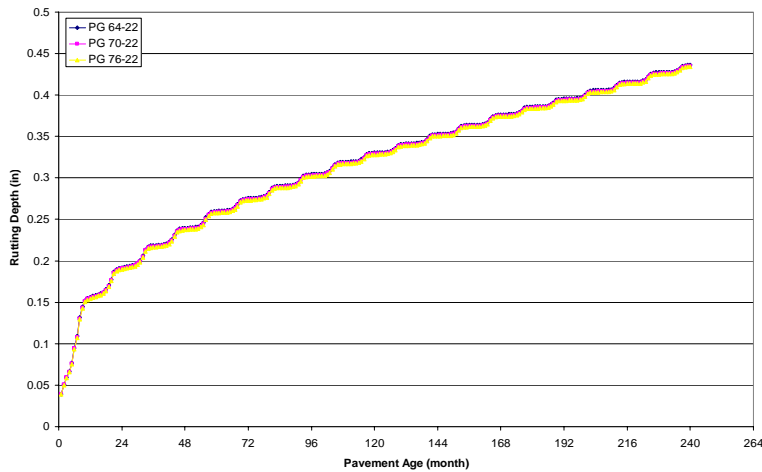


Figure 145B: Sensitivity of BG to IRI for Phase III (25.0mm ARK, AV = 6.0%)

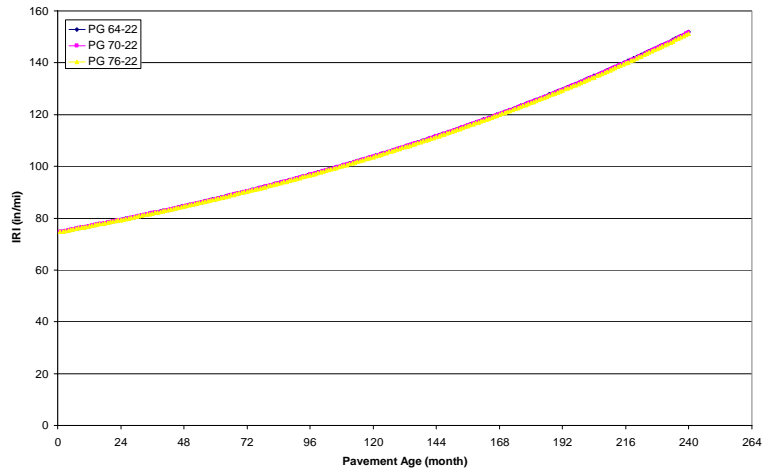


Figure 146B: Sensitivity of BG to SDC1 for Phase III (25.0mm ARK, AV = 8.0%)

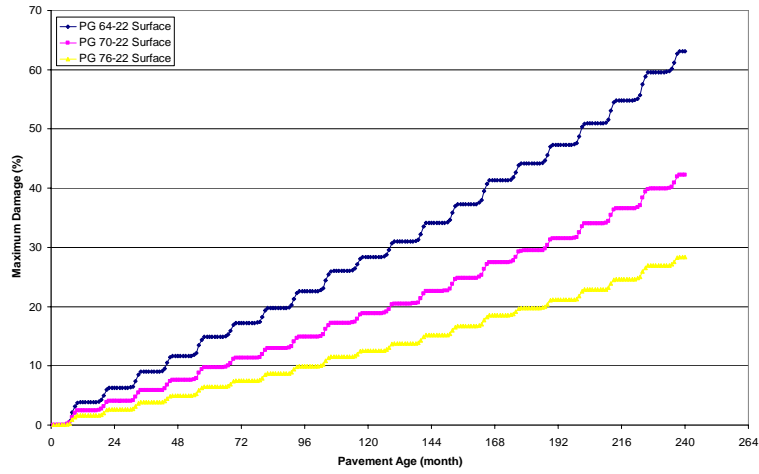


Figure 147B: Sensitivity of BG to SDC2 for Phase III (25.0mm ARK, AV = 8.0%)

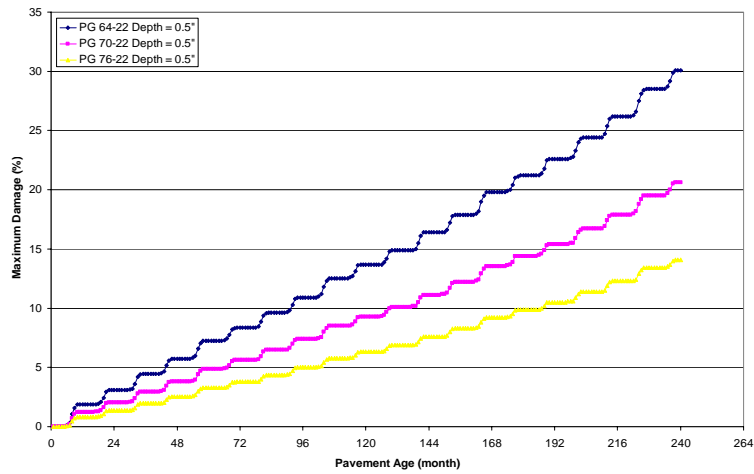


Figure 148B: Sensitivity of BG to BUD for Phase III (25.0mm ARK, AV = 8.0%)

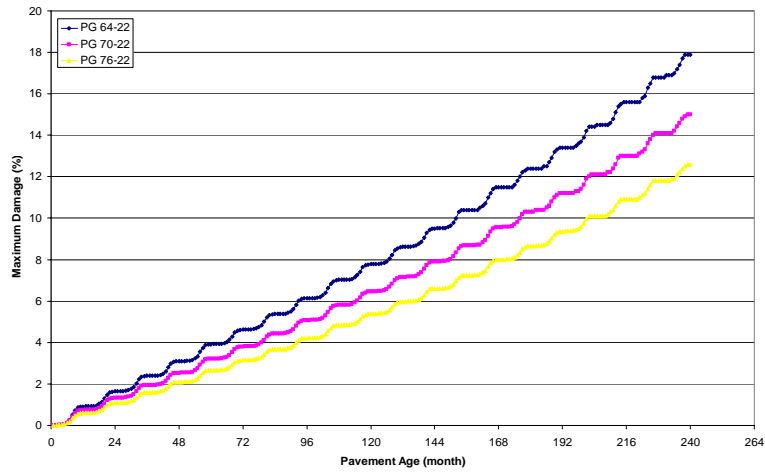


Figure 149B: Sensitivity of BG to Rutting for Phase III (25.0mm ARK, AV = 8.0%)

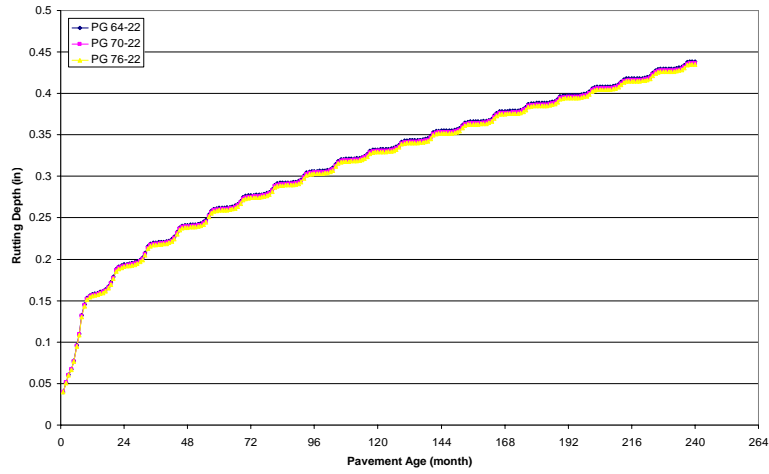


Figure 150B: Sensitivity of BG to SDC1 for Phase III (25.0mm ARK, AV = 8.0%)

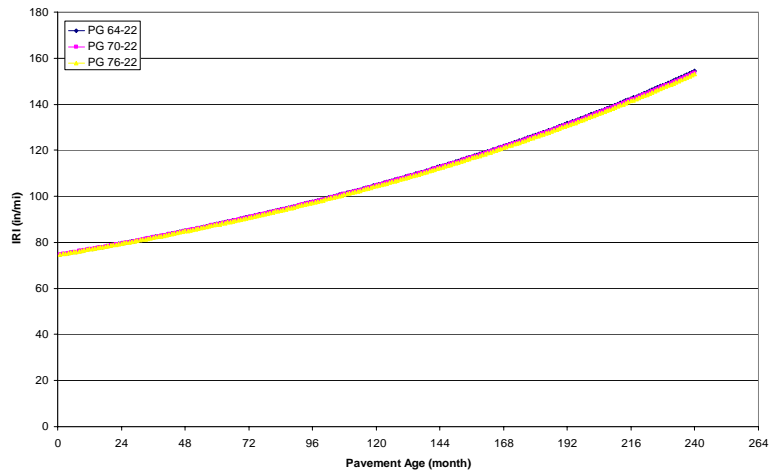


Figure 151B: Sensitivity of TUV to SDC1 for Phase III (12.5mm ARK 64-22)

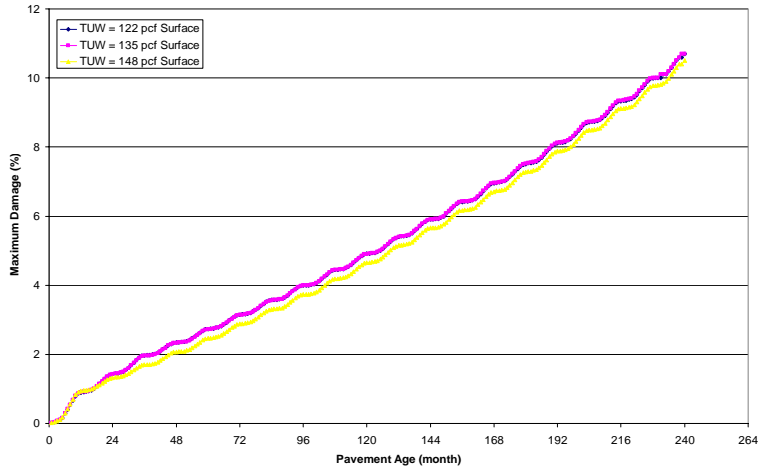


Figure 152B: Sensitivity of TUV to SDC2 for Phase III (12.5mm ARK 64-22)

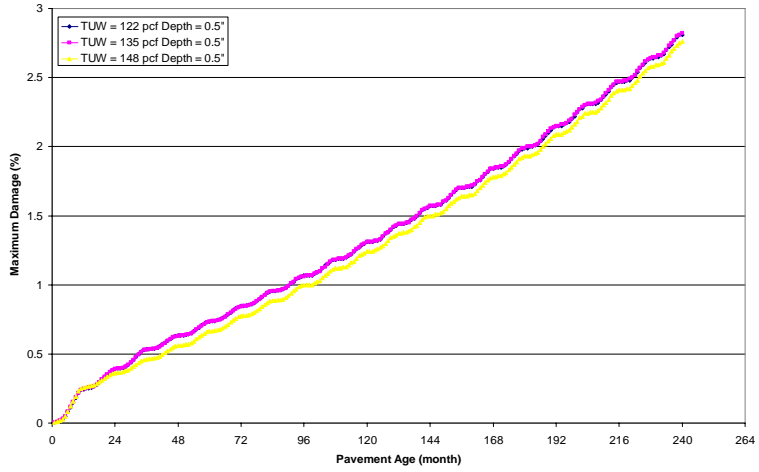


Figure 153B: Sensitivity of TUV to BUD for Phase III (12.5mm ARK 64-22)

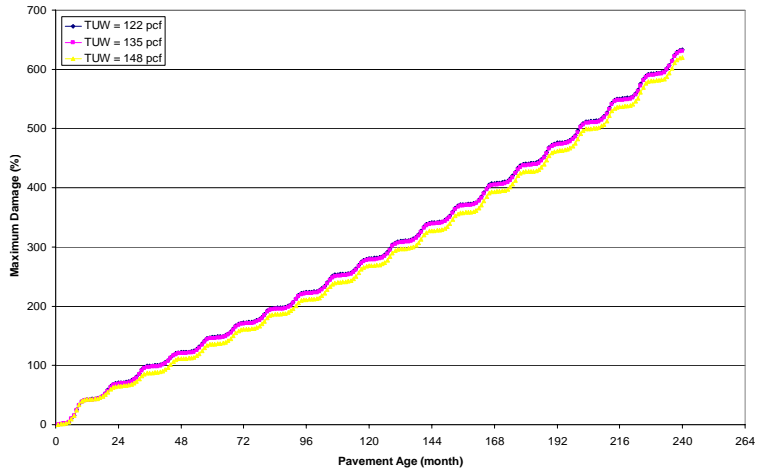


Figure 154B: Sensitivity of TUV to Rutting for Phase III (12.5mm ARK 64-22)

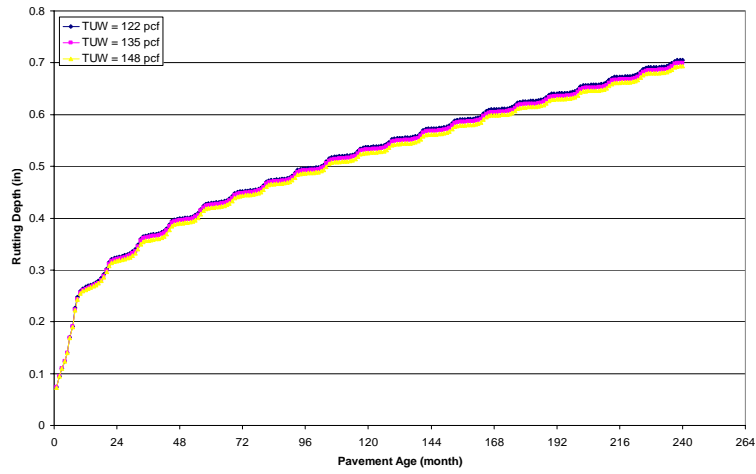


Figure 155B: Sensitivity of TUV to IRI for Phase III (12.5mm ARK 64-22)

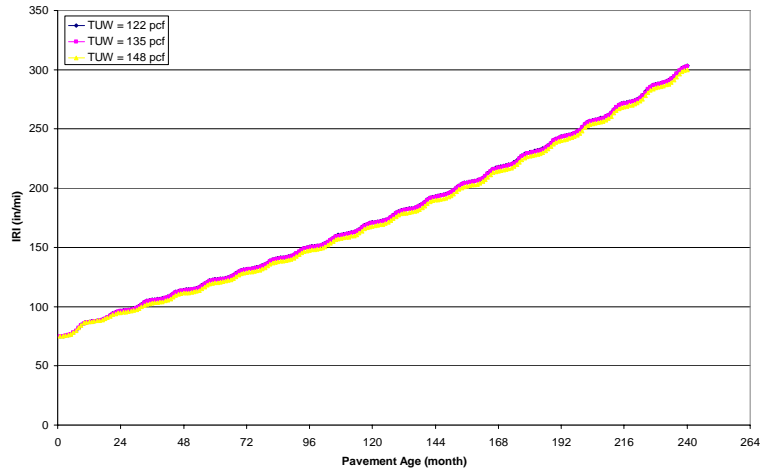


Figure 156B: Sensitivity of TUV to SDC1 for Phase III (12.5mm GMQ 64-22)

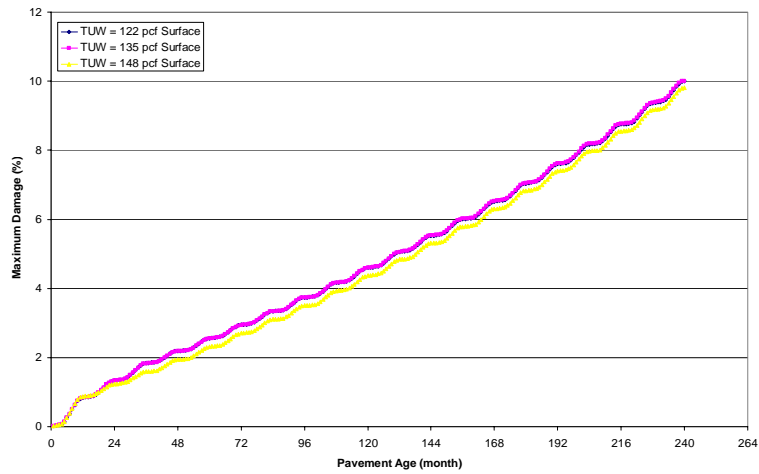


Figure 157B: Sensitivity of TUV to SDC2 for Phase III (12.5mm GMQ 64-22)

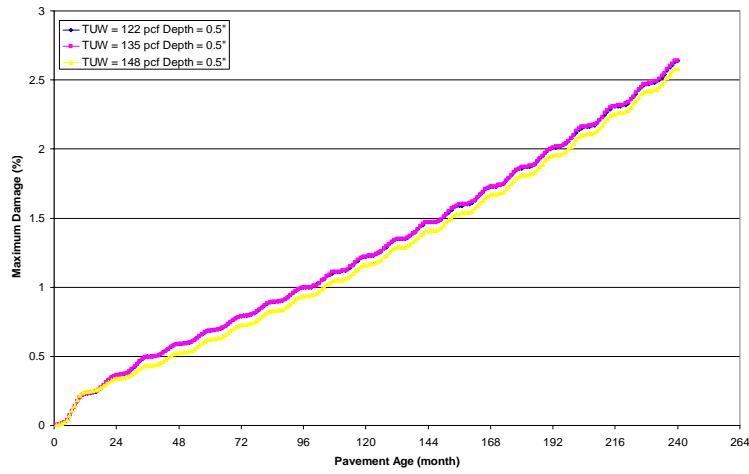


Figure 158B: Sensitivity of TUV to BUD for Phase III (12.5mm GMQ 64-22)

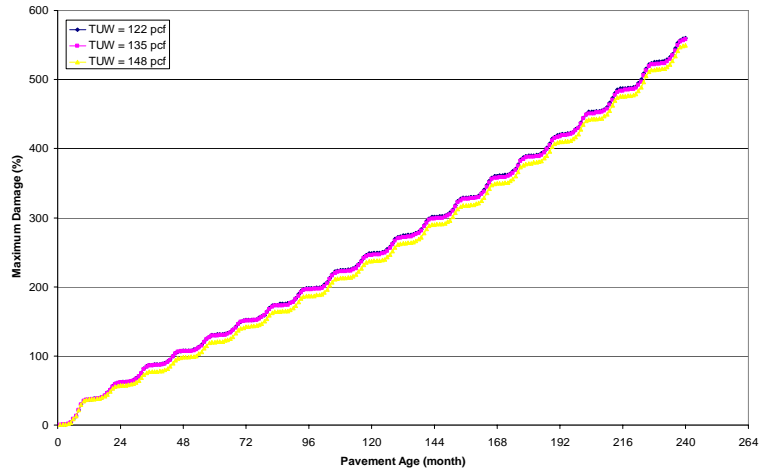


Figure 159B: Sensitivity of TUV to Rutting for Phase III (12.5mm GMQ 64-22)

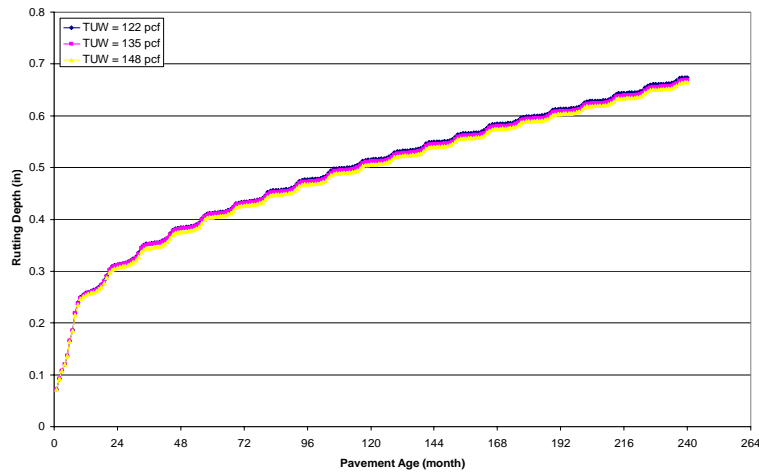


Figure 160B: Sensitivity of TUV to IRI for Phase III (12.5mm GMQ 64-22)

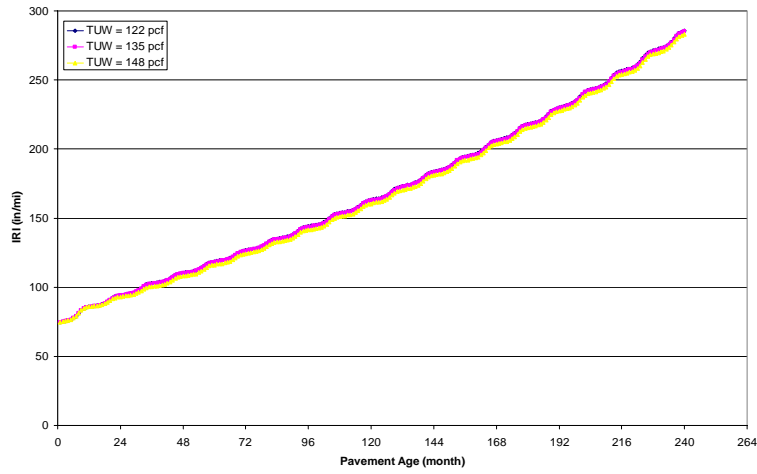


Figure 161B: Sensitivity of TUV to SDC1 for Phase III (25.0mm ARK 64-22)

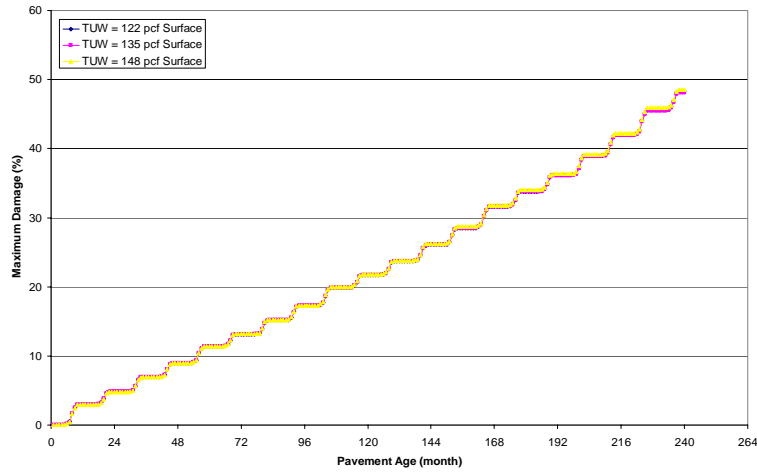


Figure 162B: Sensitivity of TUV to SDC2 for Phase III (25.0mm ARK 64-22)

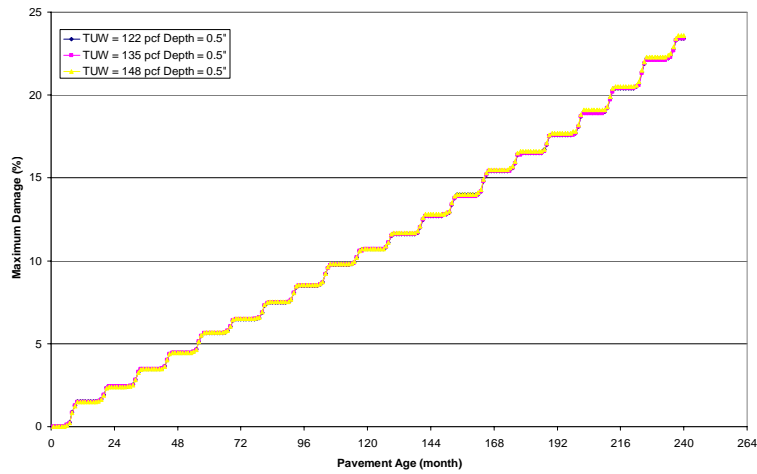


Figure 163B: Sensitivity of TUV to BUD for Phase III (25.0mm ARK 64-22)

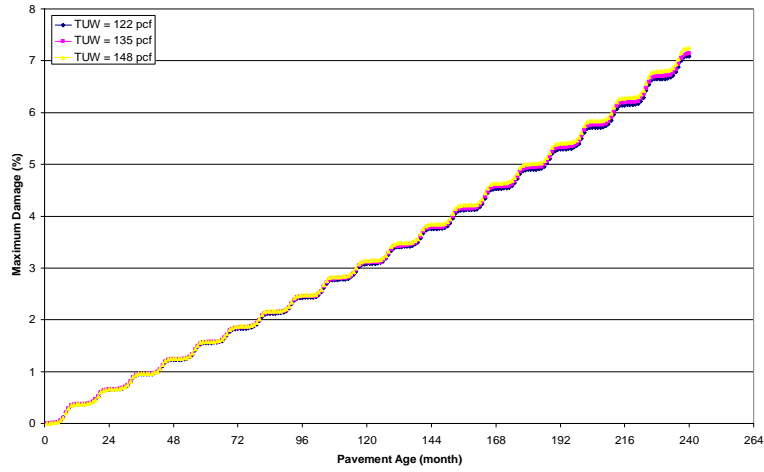


Figure 164B: Sensitivity of TUV to Rutting for Phase III (25.0mm ARK 64-22)

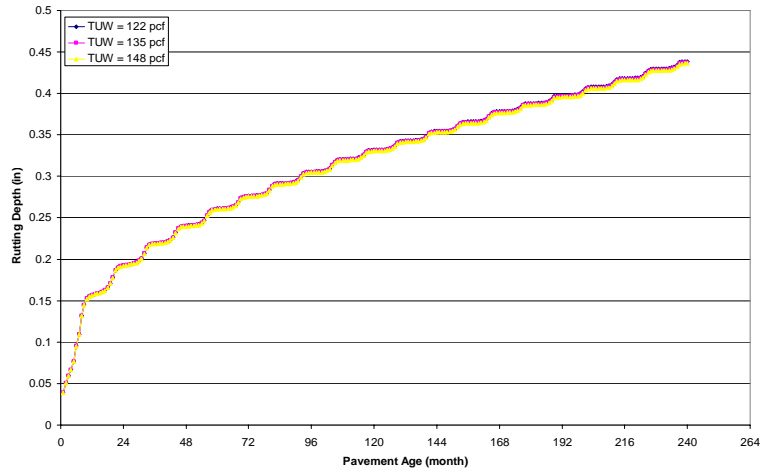


Figure 165B: Sensitivity of TUV to IRI for Phase III (25.0mm ARK 64-22)

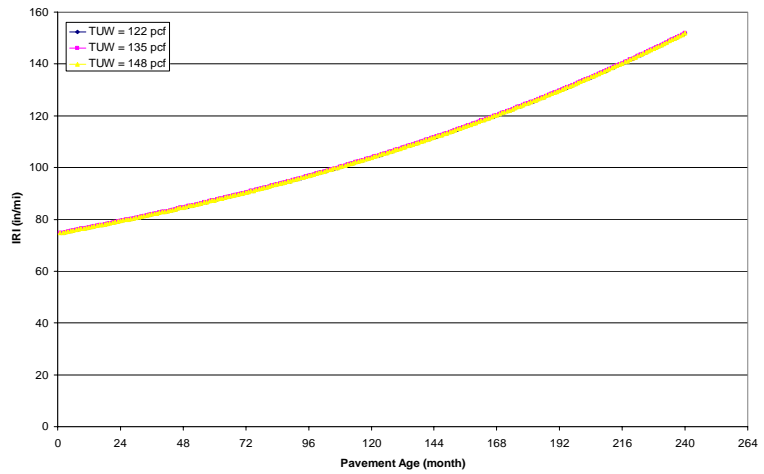


Figure 166B: Sensitivity of TUV to SDC1 for Phase III (25.0mm GMQ 64-22)

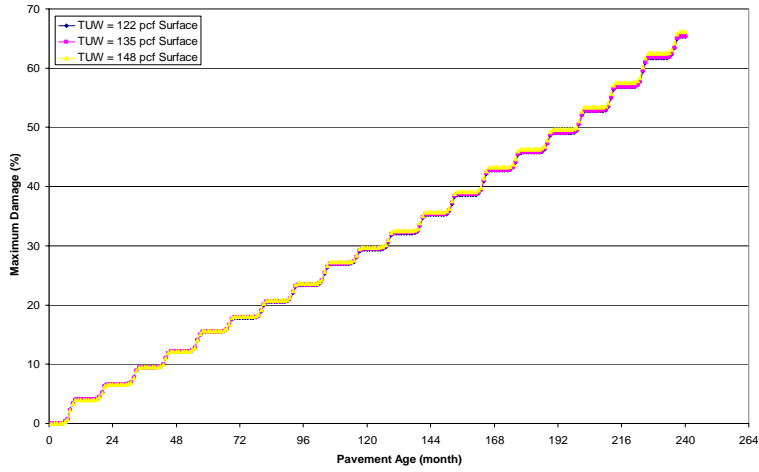


Figure 167B: Sensitivity of TUV to SDC2 for Phase III (25.0mm GMQ 64-22)

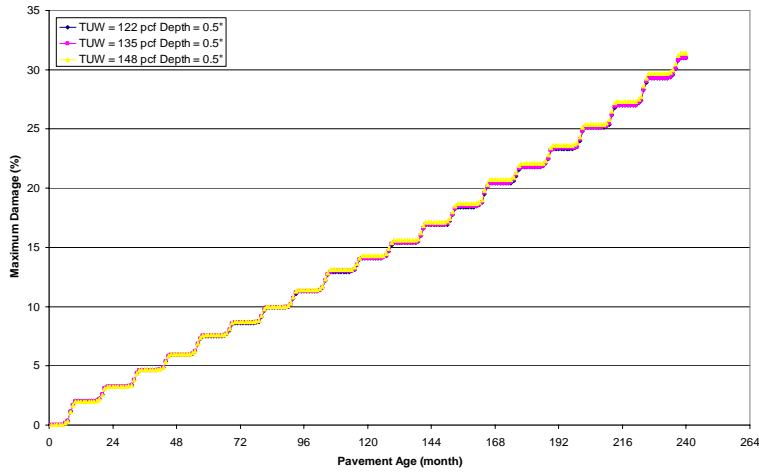


Figure 168B: Sensitivity of TUV to BUD for Phase III (25.0mm GMQ 64-22)

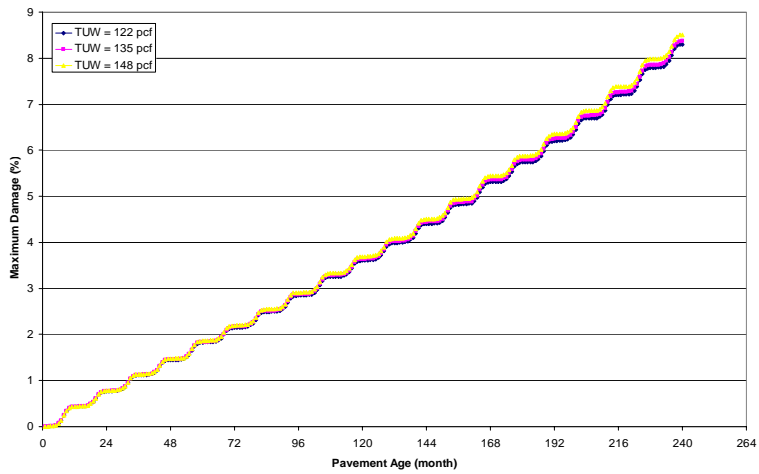


Figure 169B: Sensitivity of TUV to Rutting for Phase III (25.0mm GMQ 64-22)

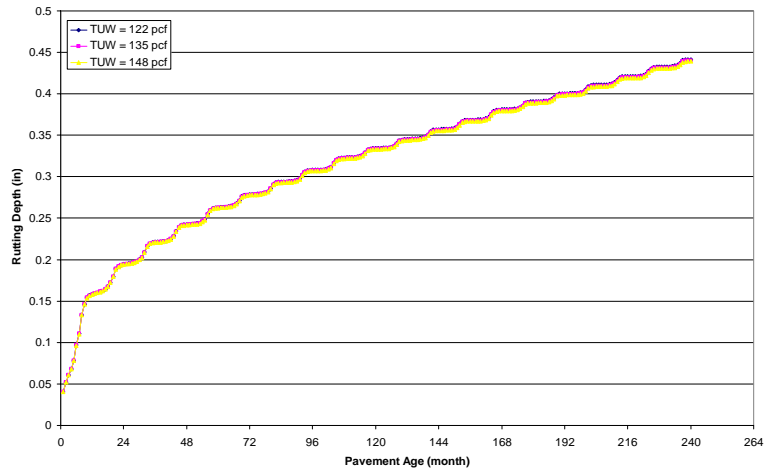


Figure 170B: Sensitivity of TUV to IRI for Phase III (25.0mm GMQ 64-22)

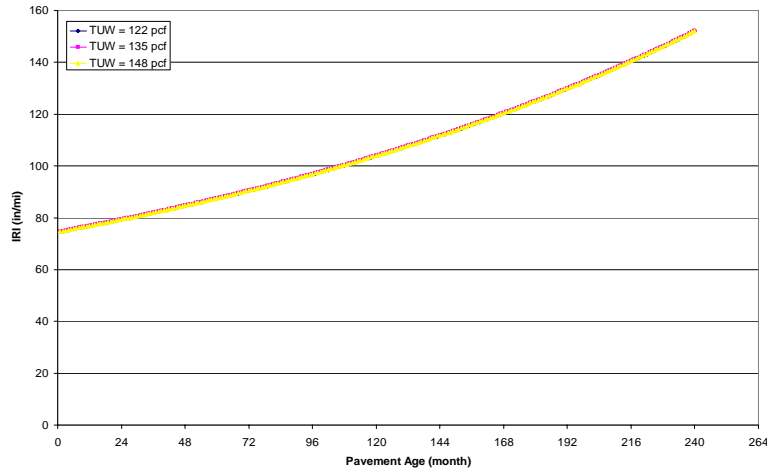


Figure 171B: Sensitivity of Pbe to SDC1 for Phase III (12.5mm ARK 70-22)

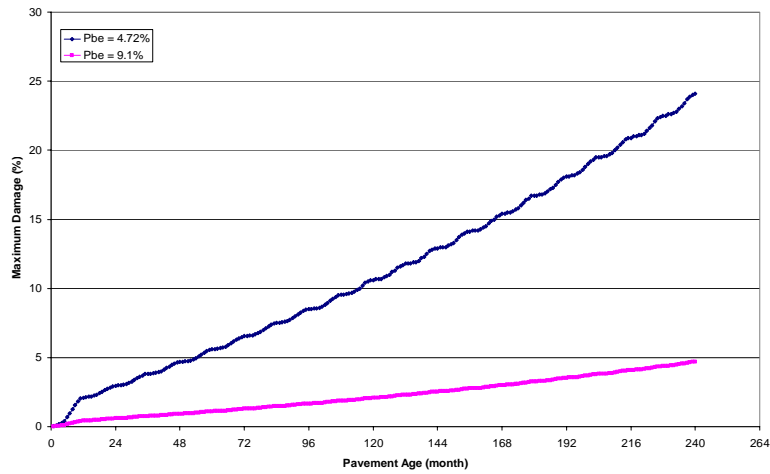


Figure 172B: Sensitivity of Pbe to SDC2 for Phase III (12.5mm ARK 70-22)

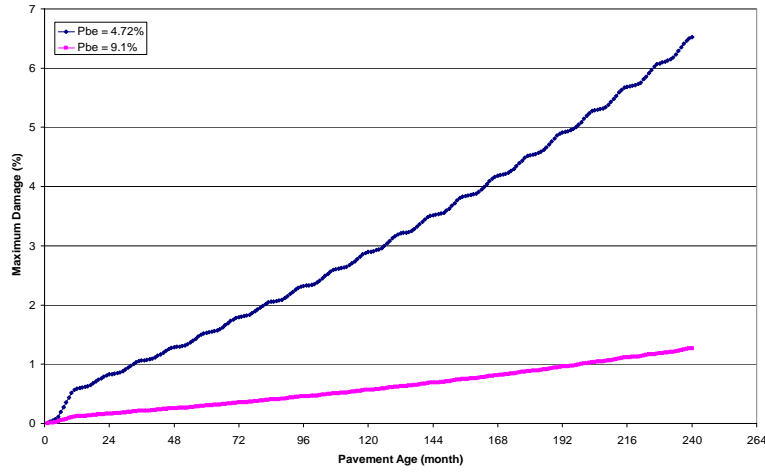


Figure 173B: Sensitivity of Pbe to BUD for Phase III (12.5mm ARK 70-22)

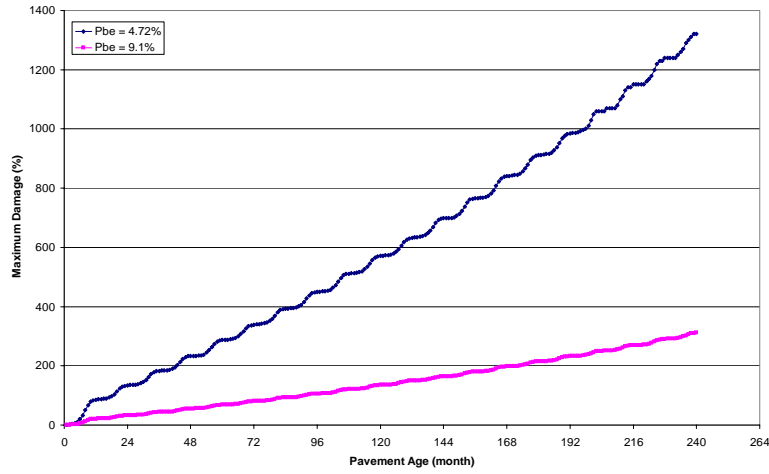


Figure 174B: Sensitivity of Pbe to Rutting for Phase III (12.5mm ARK 70-22)

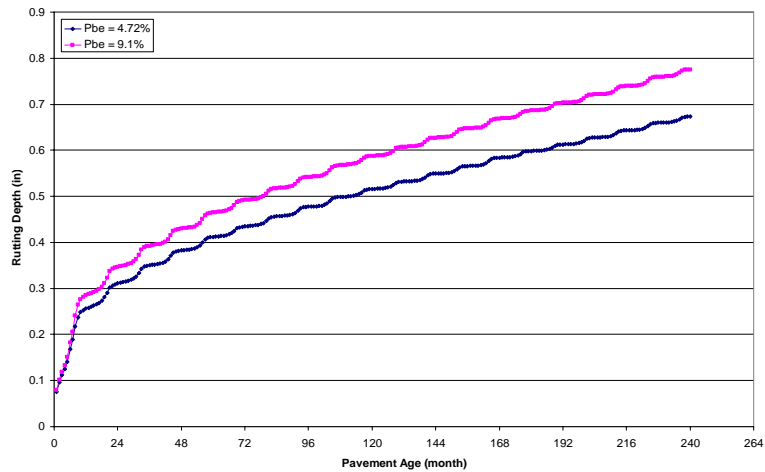


Figure 175B: Sensitivity of Pbe to IRI for Phase III (12.5mm ARK 70-22)

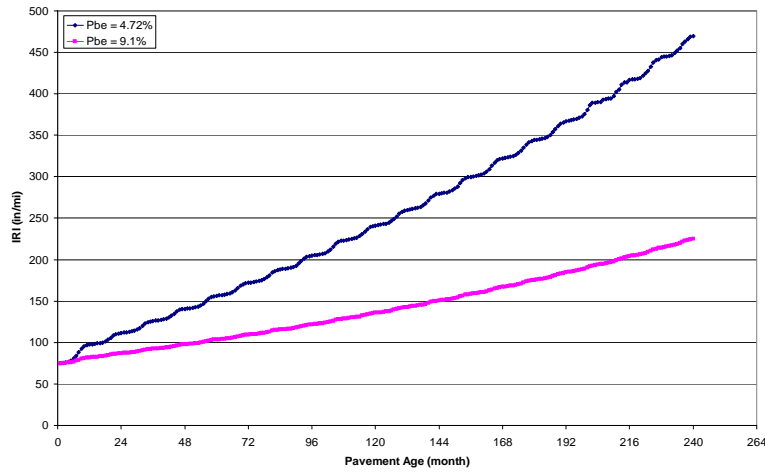


Figure 176B: Sensitivity of Pbe to SDC1 for Phase III (12.5mm GMQ 70-22)

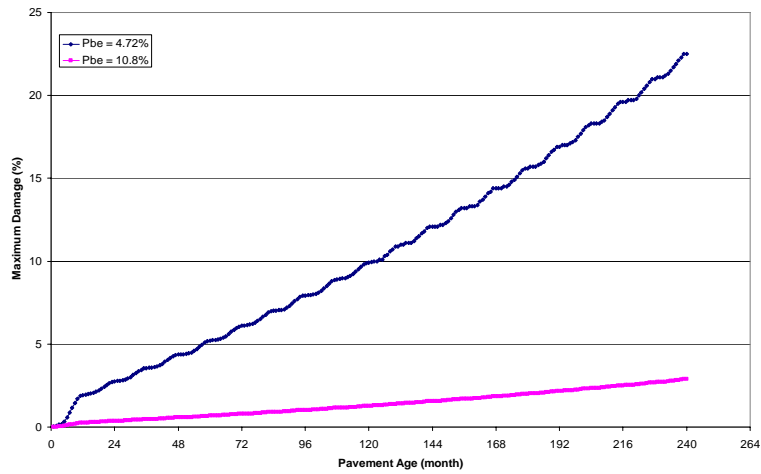


Figure 177B: Sensitivity of Pbe to SDC2 for Phase III (12.5mm GMQ 70-22)

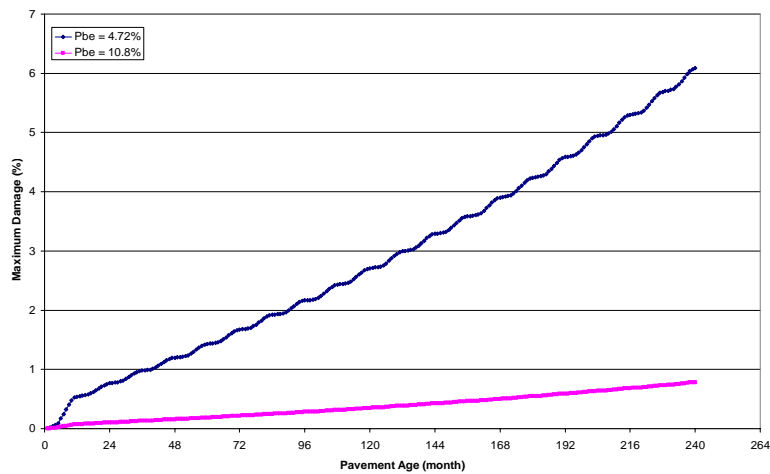


Figure 178B: Sensitivity of Pbe to BUD for Phase III (12.5mm GMQ 70-22)

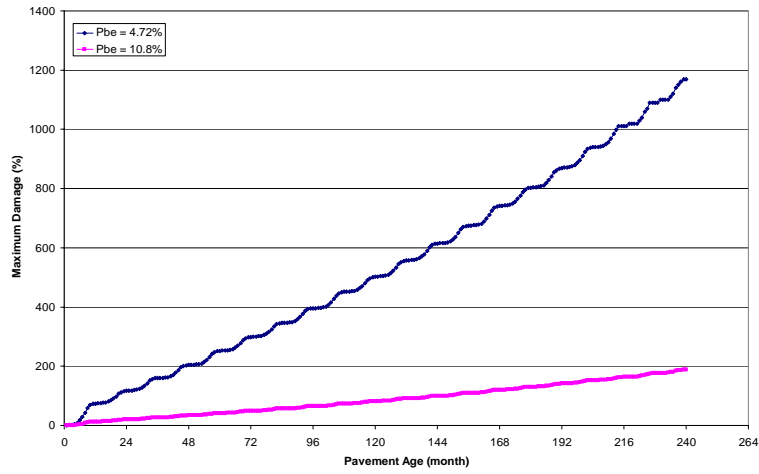


Figure 179B: Sensitivity of Pbe to Rutting for Phase III (12.5mm GMQ 70-22)

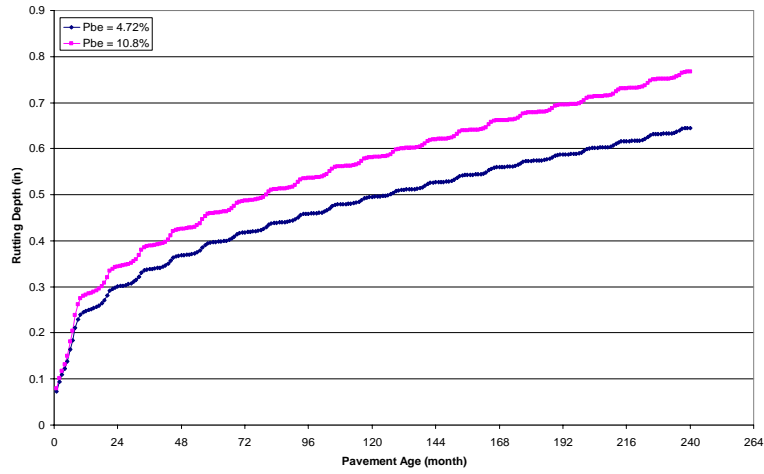


Figure 180B: Sensitivity of Pbe to IRI for Phase III (12.5mm GMQ 70-22)

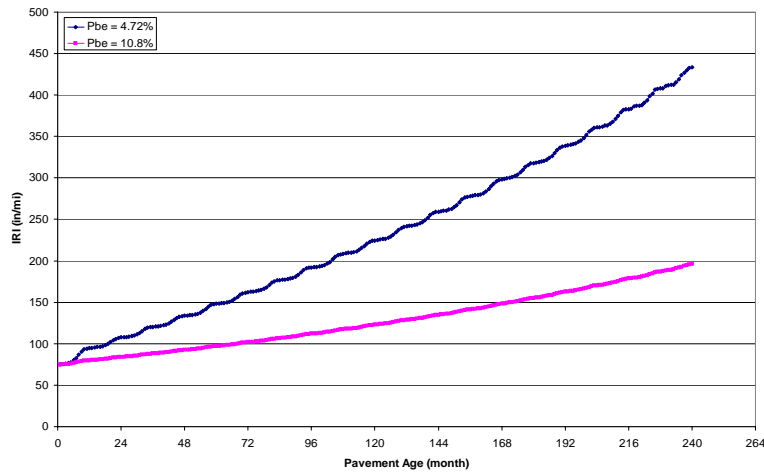


Figure 181B: Sensitivity of Pbe to SDC1 for Phase III (12.5mm JET 70-22)

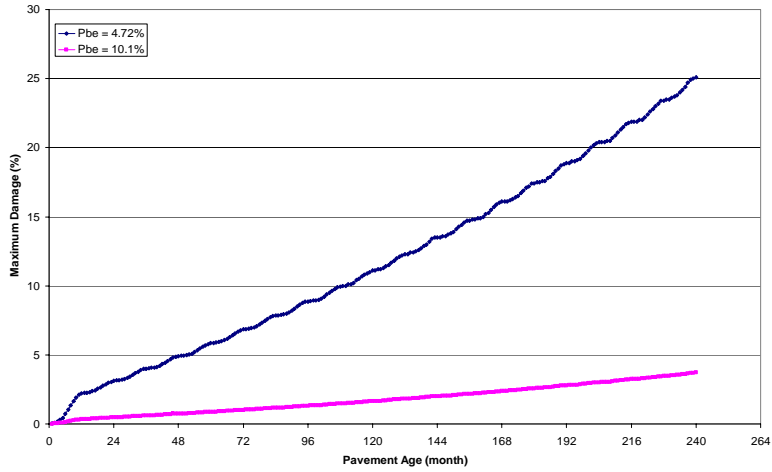


Figure 182B: Sensitivity of Pbe to SDC2 for Phase III (12.5mm JET 70-22)

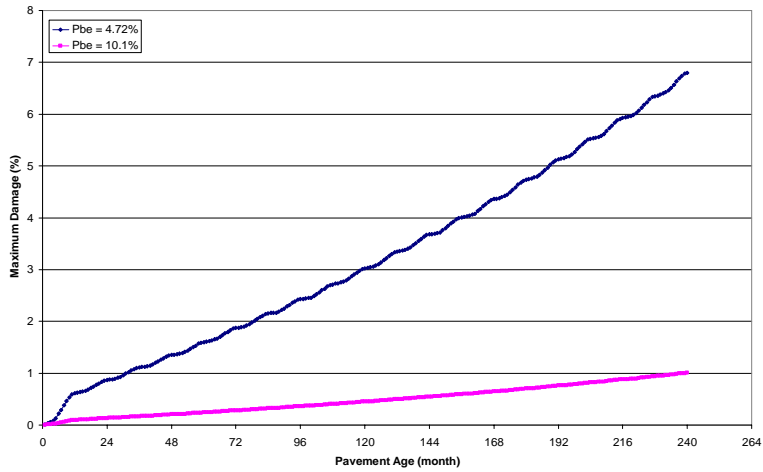


Figure 183B: Sensitivity of Pbe to BUD for Phase III (12.5mm JET 70-22)

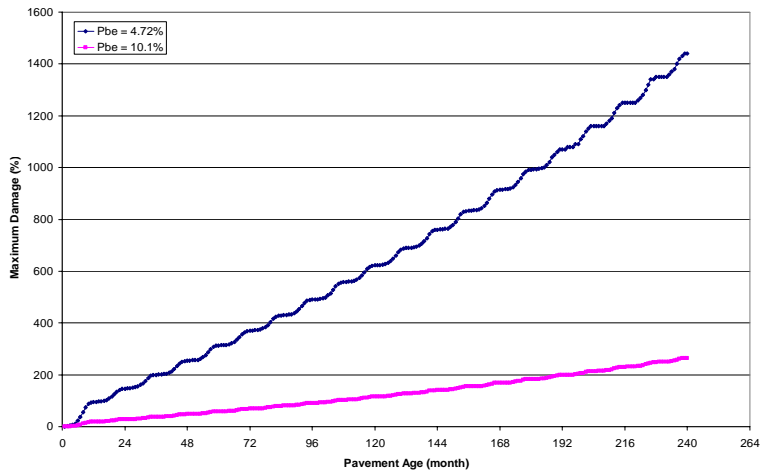


Figure 184B: Sensitivity of Pbe to Rutting for Phase III (12.5mm JET 70-22)

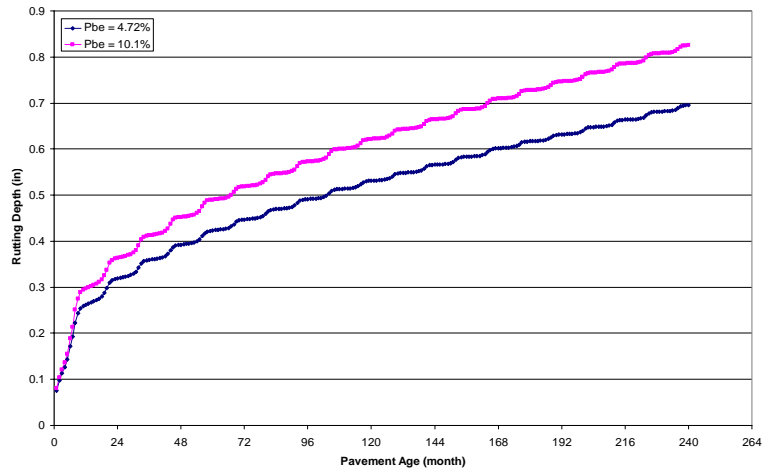


Figure 185B: Sensitivity of Pbe to IRI for Phase III (12.5mm JET 70-22)

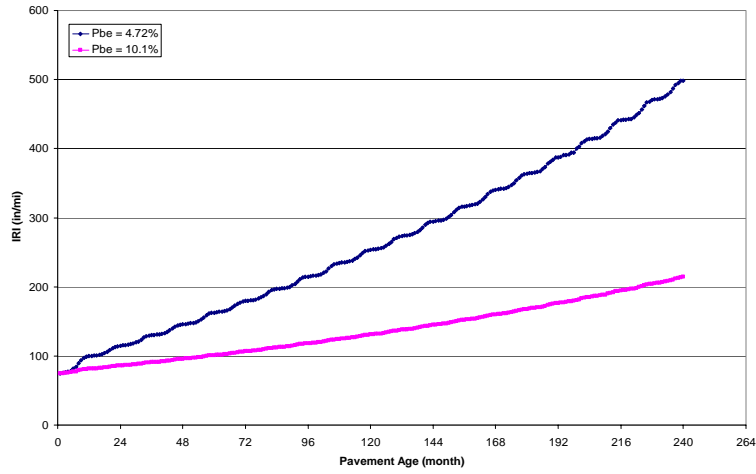


Figure 186B: Sensitivity of Pbe to SDC1 for Phase III (12.5mm MCA 70-22)

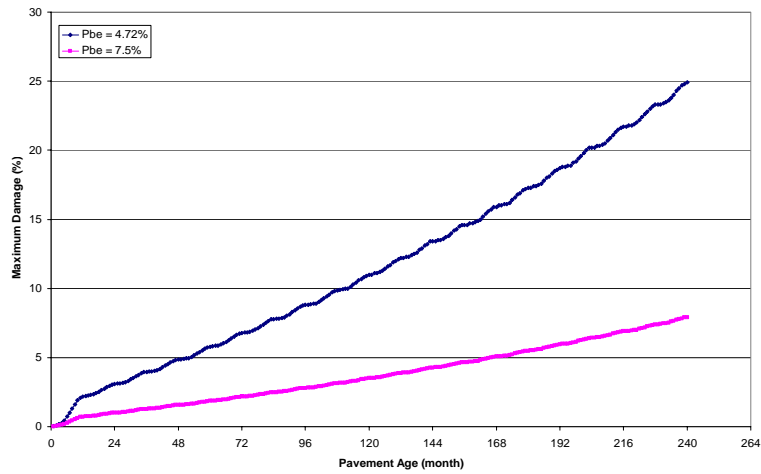


Figure 187B: Sensitivity of Pbe to SDC2 for Phase III (12.5mm MCA 70-22)

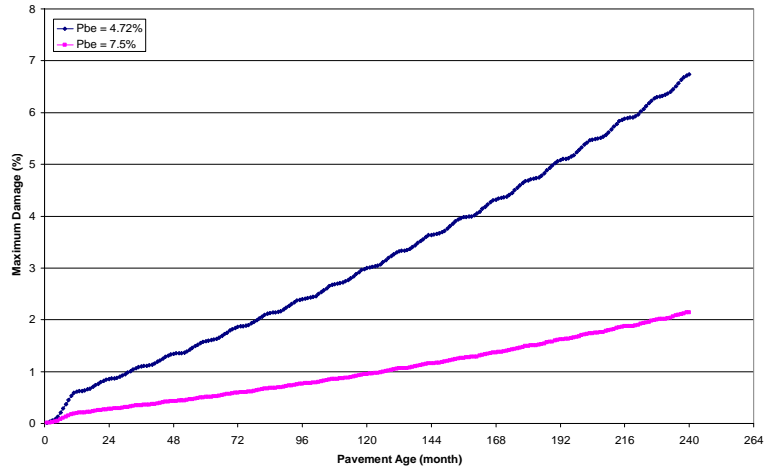


Figure 188B: Sensitivity of Pbe to BUD for Phase III (12.5mm MCA 70-22)

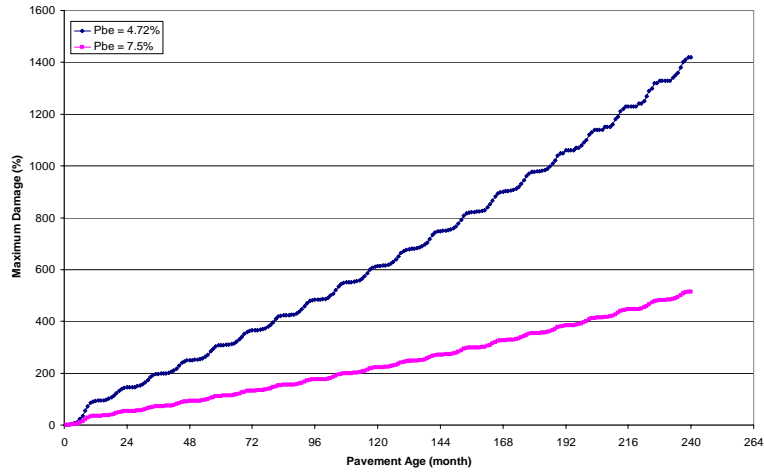


Figure 189B: Sensitivity of Pbe to Rutting for Phase III (12.5mm MCA 70-22)

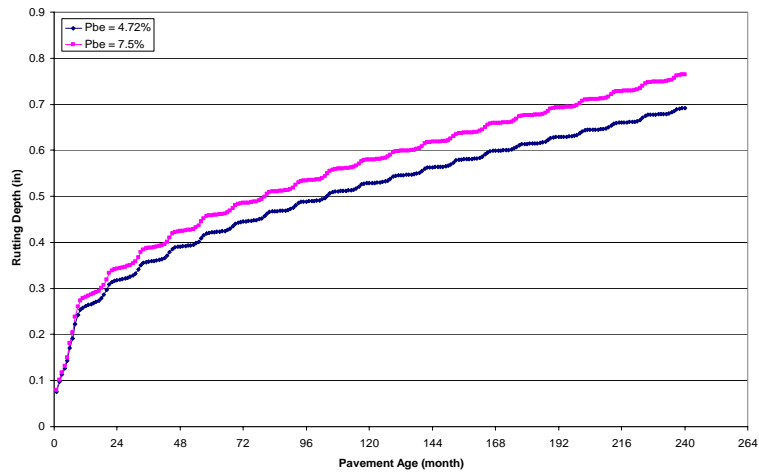


Figure 190B: Sensitivity of Pbe to IRI for Phase III (12.5mm MCA 70-22)

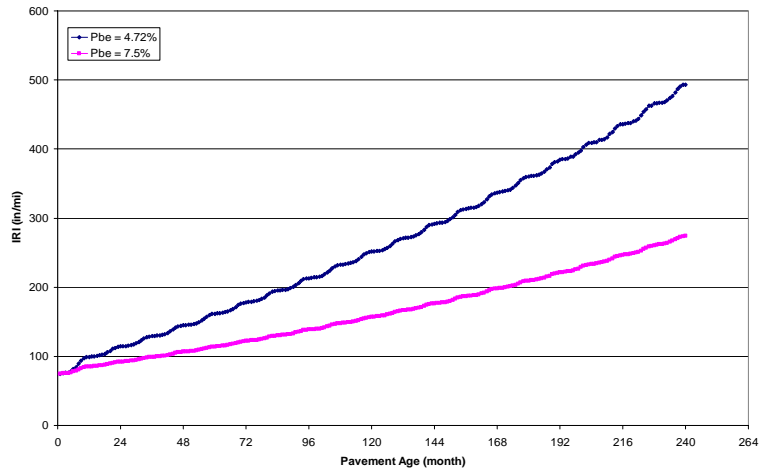


Figure 191B: Sensitivity of Pbe to SDC1 for Phase III (25.0mm ARK 70-22)

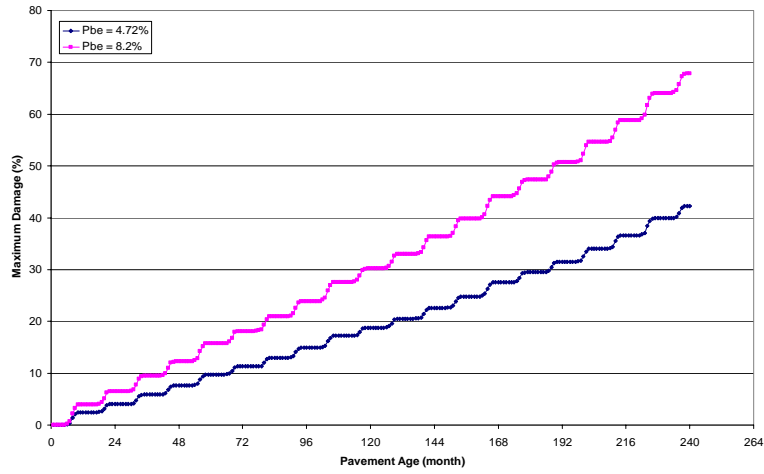


Figure 192B: Sensitivity of Pbe to SDC2 for Phase III (25.0mm ARK 70-22)

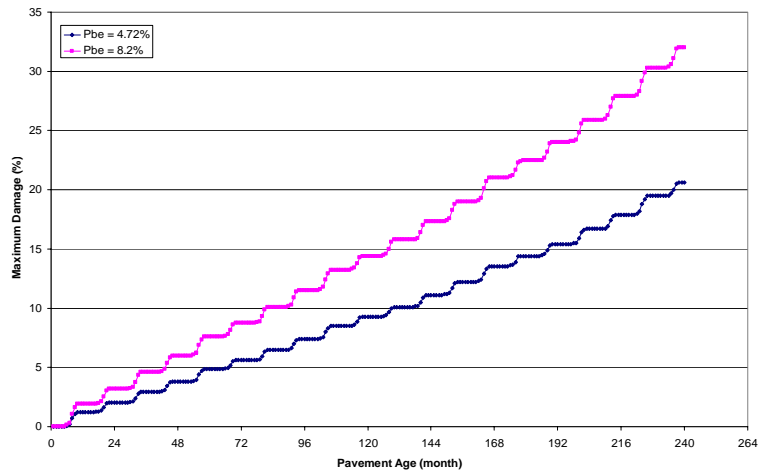


Figure 193B: Sensitivity of Pbe to BUD for Phase III (25.0mm ARK 70-22)

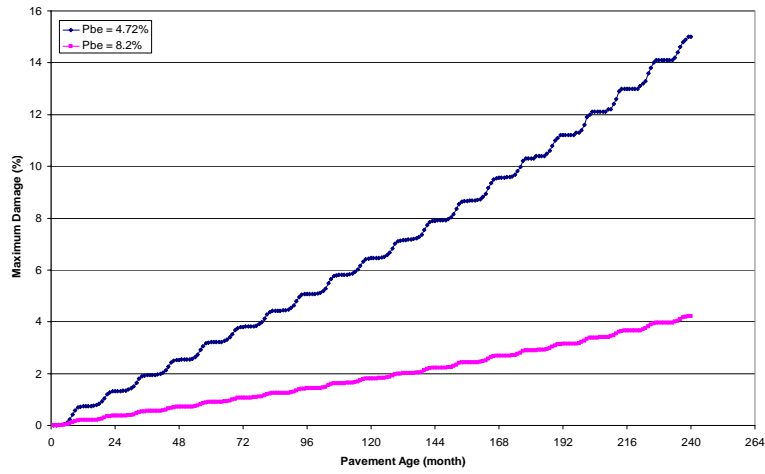


Figure 194B: Sensitivity of Pbe to Rutting for Phase III (25.0mm ARK 70-22)

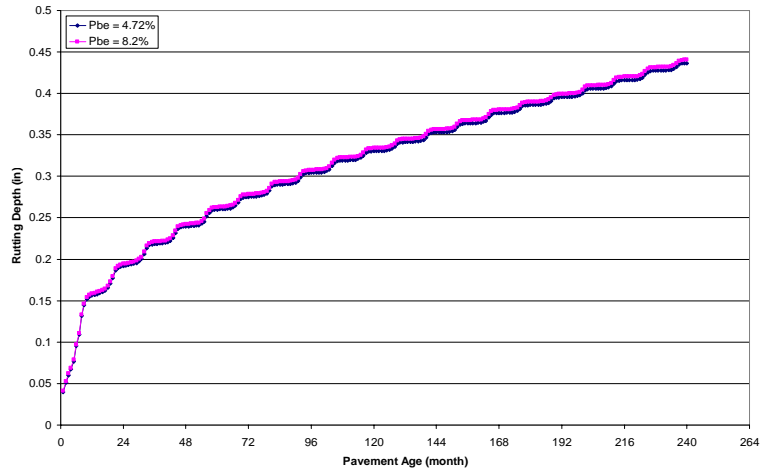


Figure 195B: Sensitivity of Pbe to IRI for Phase III (25.0mm ARK 70-22)

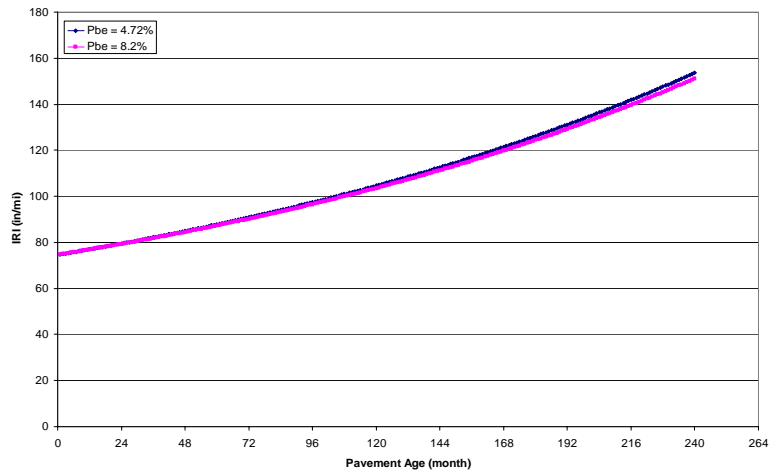


Figure 196B: Sensitivity of Pbe to SDC1 for Phase III (25.0mm GMQ 70-22)

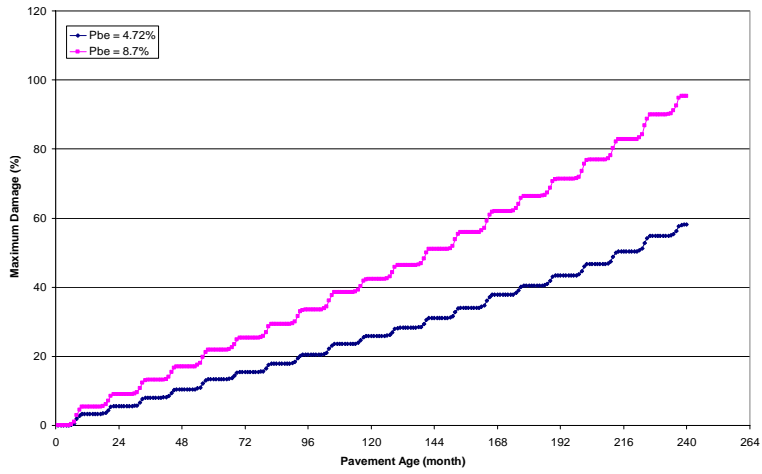


Figure 197B: Sensitivity of Pbe to SDC2 for Phase III (25.0mm GMQ 70-22)

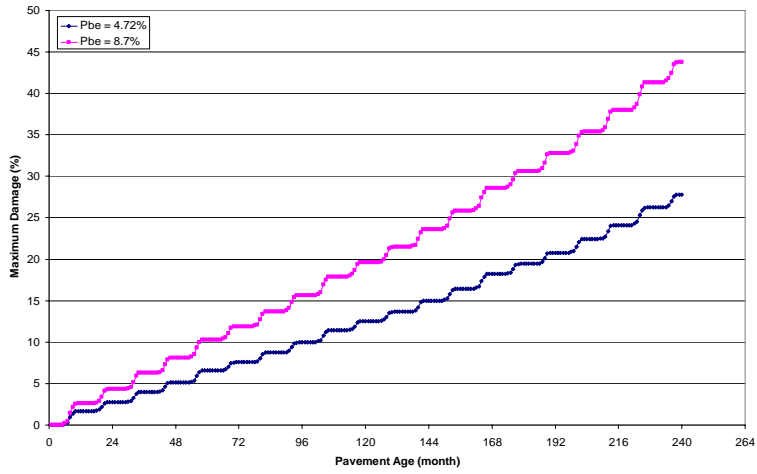


Figure 198B: Sensitivity of Pbe to BUD for Phase III (25.0mm GMQ 70-22)

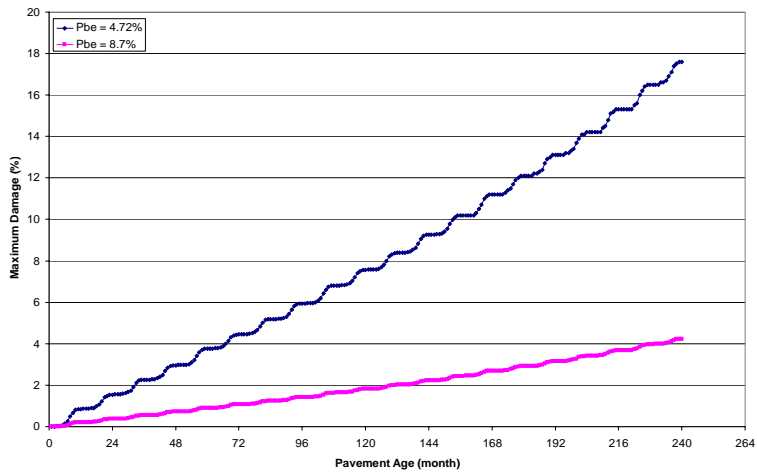


Figure 199B: Sensitivity of Pbe to Rutting for Phase III (25.0mm GMQ 70-22)

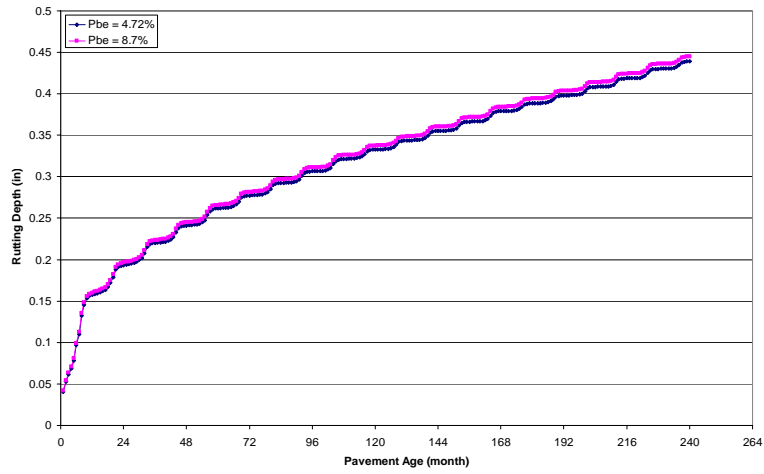


Figure 200B: Sensitivity of Pbe to IRI for Phase III (25.0mm GMQ 70-22)

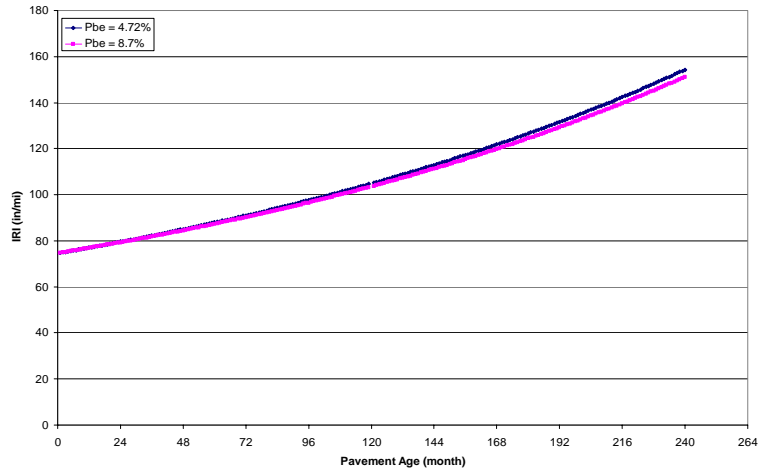


Figure 201B: Sensitivity of Pbe to SDC1 for Phase III (25.0mm JET 70-22)

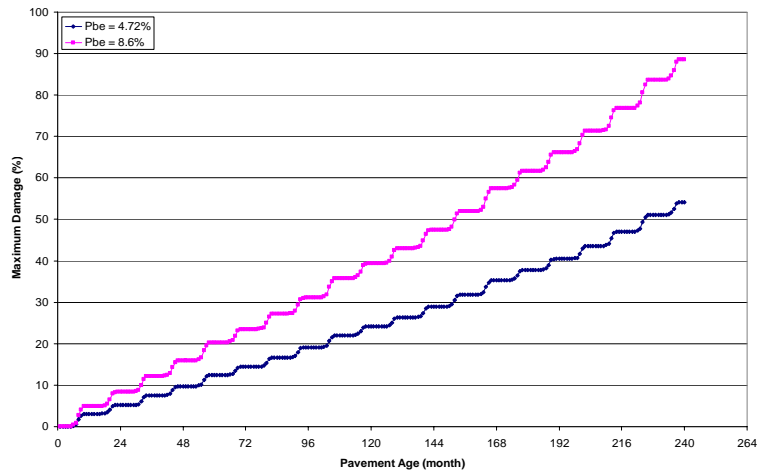


Figure 202B: Sensitivity of Pbe to SDC2 for Phase III (25.0mm JET 70-22)

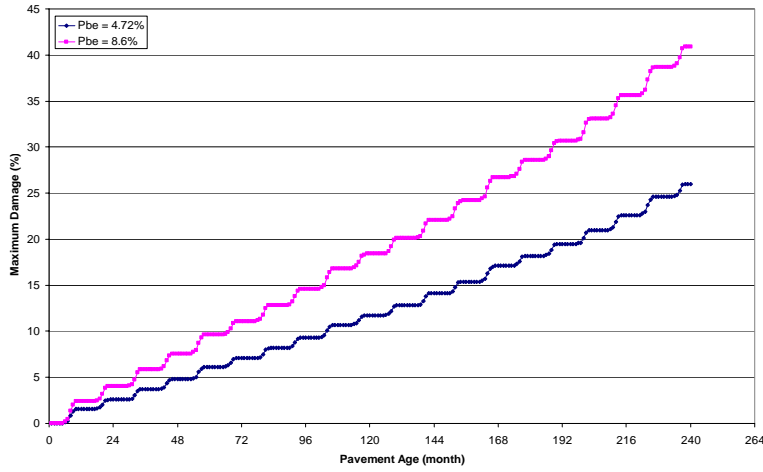


Figure 203B: Sensitivity of Pbe to BUD for Phase III (25.0mm JET 70-22)

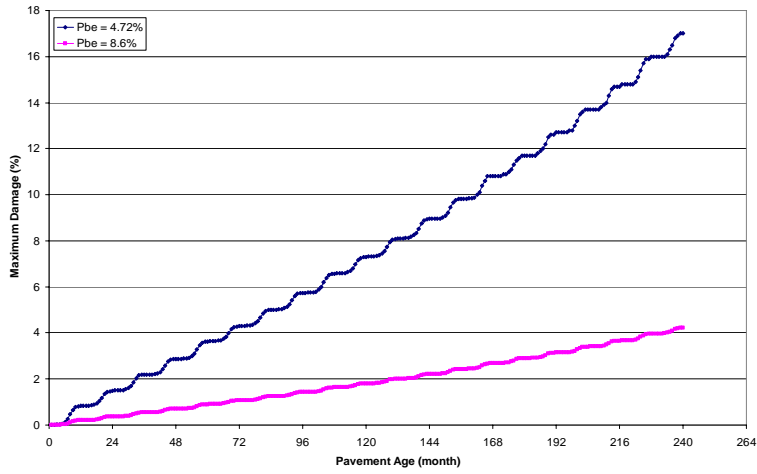


Figure 204B: Sensitivity of Pbe to Rutting for Phase III (25.0mm JET 70-22)

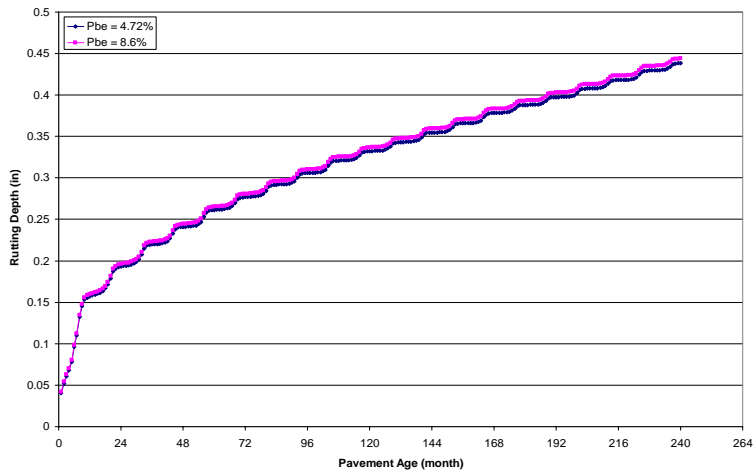


Figure 205B: Sensitivity of Pbe to IRI for Phase III (25.0mm JET 70-22)

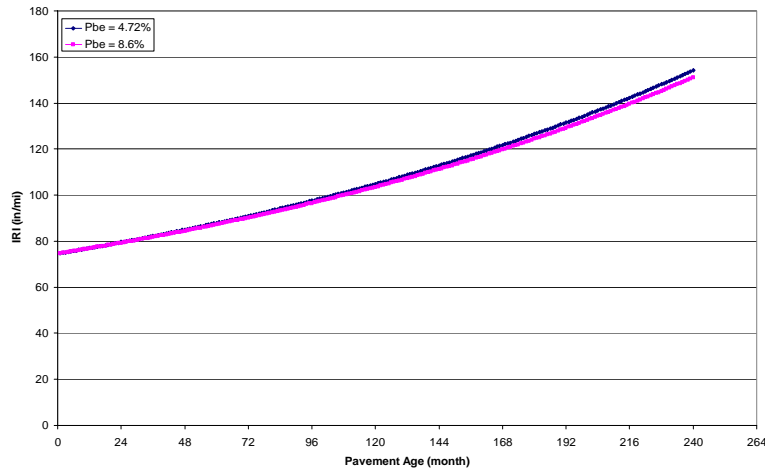


Figure 206B: Sensitivity of Pbe to SDC1 for Phase III (25.0mm MCA 70-22)

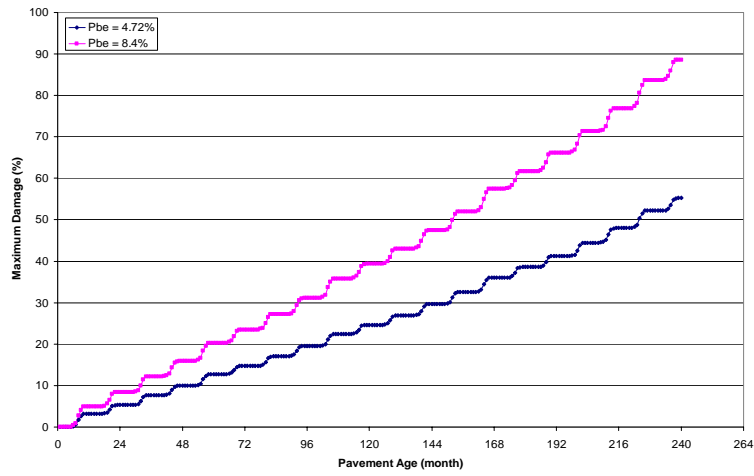


Figure 207B: Sensitivity of Pbe to SDC2 for Phase III (25.0mm MCA 70-22)

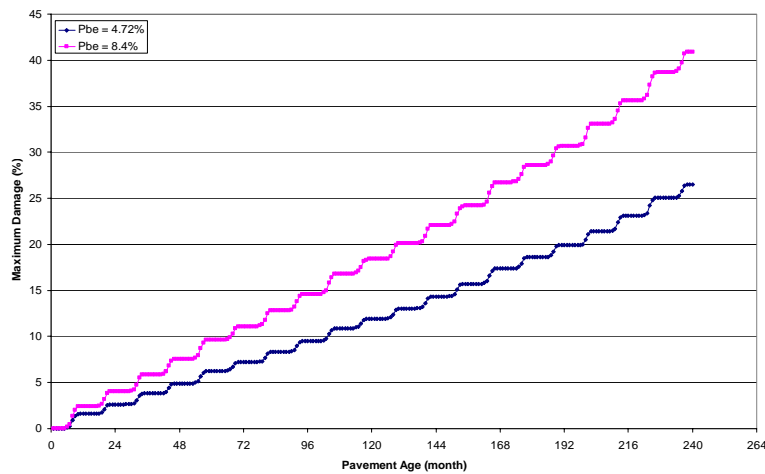


Figure 208B: Sensitivity of Pbe to BUD for Phase III (25.0mm MCA 70-22)

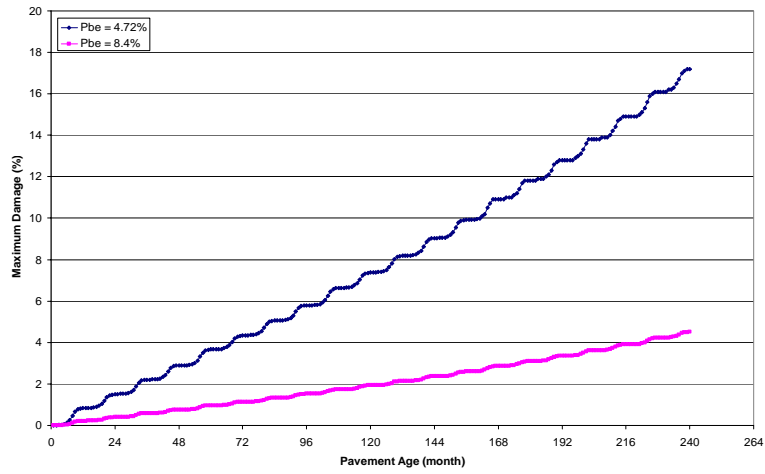


Figure 209B: Sensitivity of Pbe to Rutting for Phase III (25.0mm MCA 70-22)

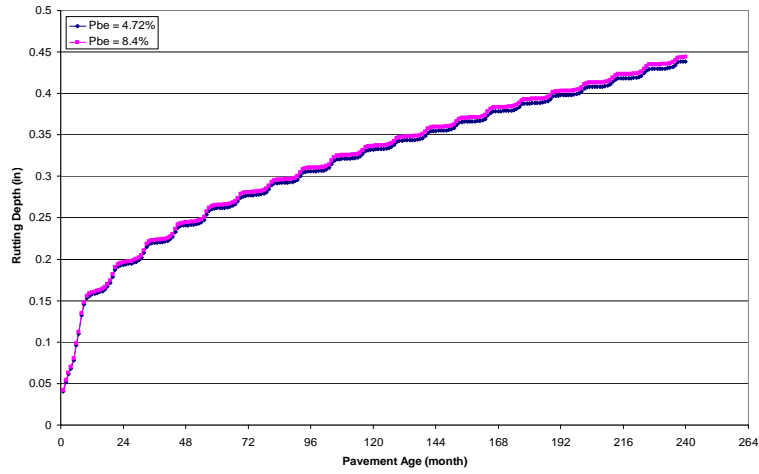
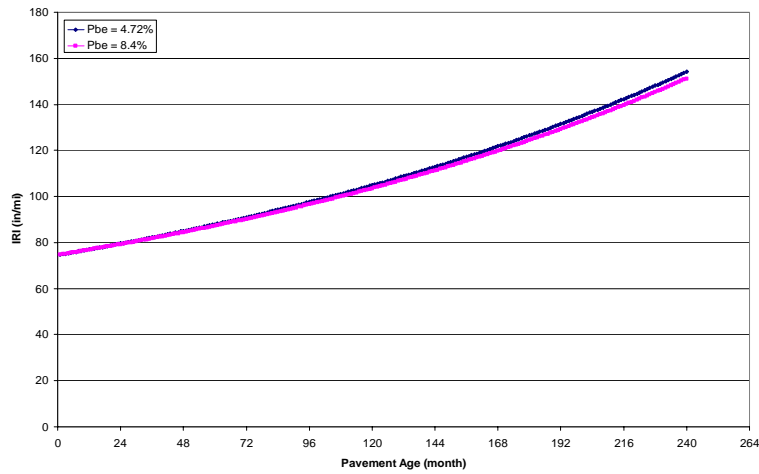


Figure 210B: Sensitivity of Pbe to IRI for Phase III (25.0mm MCA 70-22)



APPENDIX E
HOT-MIX ASPHALT MIXTURE DATA

Mix Type
Binder

ARK 12.5mm
70-22

Gradation Properties:

| Sieve Size (mm) | Blend |
|-----------------|-------|
| 50.00 | 100.0 |
| 37.50 | 100.0 |
| 25.00 | 0.0 |
| 19.00 | 100.0 |
| 12.50 | 92.9 |
| 9.50 | 85.1 |
| 4.75 | 55.3 |
| 2.36 | 29.2 |
| 1.18 | 20.2 |
| 0.60 | 17.3 |
| 0.30 | 13.7 |
| 0.150 | 9.7 |
| 0.075 | 5.7 |

| | Actual | Modified |
|--|--------|------------|
| % AC | 6.0 | 6.0 |
| % Air Voids | 4.6 | 8.0 |
| %VMA | 14.1 | 16.0 |
| %VFA | 67.2 | 50.0 |
| Dust/Asphalt Ratio | 1.3 | 1.5 |
| Max Specific Gravity, Gmm | 2.364 | 2.364 |
| Bulk Specific Gravity, Gmb | 2.254 | 2.175 |
| %Gmm @ Nini | 86.7 | |
| %Gmm @ Ndes | 95.4 | |
| Effective Specific Gravity of Blend, Gse | 2.576 | 2.576 |
| Specific Gravity of Binder, Gb | 1.031 | 1.031 |
| Specific Gravity of Aggregate, Gsb | 2.467 | 2.467 |
| %Binder effective by volume* | 9.4 | 9.1 |

*(calculated using HMA volumetric analysis spreadsheet)

Mix Type
Binder

GMQ 12.5mm
70-22

Gradation Properties:

| Sieve Size (mm) | Blend |
|-----------------|-------|
| 50.00 | 100.0 |
| 37.50 | 100.0 |
| 25.00 | 100.0 |
| 19.00 | 100.0 |
| 12.50 | 94.8 |
| 9.50 | 89.7 |
| 4.75 | 69.4 |
| 2.36 | 47.9 |
| 1.18 | 34.4 |
| 0.60 | 23.4 |
| 0.30 | 14.1 |
| 0.150 | 8.2 |
| 0.075 | 5.1 |

| | Actual | Modified |
|--|--------|-------------|
| % AC | 5.5 | 5.5 |
| % Air Voids | 5.0 | 8.0 |
| %VMA | 16.2 | 18.8 |
| %VFA | 68.9 | 57.4 |
| Dust/Asphalt Ratio | 1.0 | 1.0 |
| Max Specific Gravity, Gmm | 2.417 | 2.417 |
| Bulk Specific Gravity, Gmb* | 2.295 | 2.223 |
| %Gmm @ Nini | 88.4 | |
| %Gmm @ Ndes | 95.0 | |
| Effective Specific Gravity of Blend, Gse | 2.622 | 2.622 |
| Specific Gravity of Binder, Gb | 1.031 | 1.031 |
| Specific Gravity of Aggregate, Gsb | 2.587 | 2.587 |
| %Binder effective by volume** | 11.2 | 10.8 |

*(data was modified to maintain air voids at 8.0%)

** (calculated using HMA volumetric analysis spreadsheet)

Mix Type
Binder

Jet 12.5mm
70-22

Gradation Properties:

| Sieve Size (mm) | Blend |
|-----------------|-------|
| 50.00 | 100.0 |
| 37.50 | 100.0 |
| 25.00 | 100.0 |
| 19.00 | 100.0 |
| 12.50 | 93.6 |
| 9.50 | 86.4 |
| 4.75 | 55.6 |
| 2.36 | 34.2 |
| 1.18 | 23.2 |
| 0.60 | 16.8 |
| 0.30 | 10.3 |
| 0.150 | 5.7 |
| 0.075 | 3.5 |

| | Actual | Modified |
|--|--------|-------------|
| % AC | 5.5 | 5.5 |
| % Air Voids | 4.2 | 8.0 |
| %VMA | 14.7 | 18.1 |
| %VFA | 71.3 | 55.8 |
| Dust/Asphalt Ratio | 0.7 | 0.7 |
| Max Specific Gravity, Gmm | 2.407 | 2.407 |
| Bulk Specific Gravity, Gmb* | 2.306 | 2.214 |
| %Gmm @ Nini | 88.7 | |
| %Gmm @ Ndes | 95.8 | |
| Effective Specific Gravity of Blend, Gse | 2.610 | 2.610 |
| Specific Gravity of Binder, Gb | 1.031 | 1.031 |
| Specific Gravity of Aggregate, Gsb | 2.555 | 2.555 |
| %Binder effective by volume** | 10.5 | 10.1 |

*(data was modified to maintain air voids at 8.0%)

** (calculated using HMA volumetric analysis spreadsheet)

Mix Type
Binder

MCA 12.5mm
70-22

Gradation Properties:

| Sieve Size (mm) | Blend |
|-----------------|-------|
| 50.00 | 100.0 |
| 37.50 | 100.0 |
| 25.00 | 0.0 |
| 19.00 | 100.0 |
| 12.50 | 93.1 |
| 9.50 | 80.4 |
| 4.75 | 50.8 |
| 2.36 | 36.6 |
| 1.18 | 24.7 |
| 0.60 | 15.6 |
| 0.30 | 9.5 |
| 0.150 | 6.1 |
| 0.075 | 4.2 |

| | Actual | Modified |
|--|--------|------------|
| % AC | 5.0 | 5.0 |
| % Air Voids | 6.0 | 8.0 |
| %VMA | 13.7 | 15.5 |
| %VFA | 55.8 | 48.4 |
| Dust/Asphalt Ratio | 1.2 | 1.2 |
| Max Specific Gravity, Gmm | 2.417 | 2.417 |
| Bulk Specific Gravity, Gmb | 2.271 | 2.223 |
| %Gmm @ Nini | 86.0 | |
| %Gmm @ Ndes | 94.0 | |
| Effective Specific Gravity of Blend, Gse | 2.601 | 2.601 |
| Specific Gravity of Binder, Gb | 1.031 | 1.031 |
| Specific Gravity of Aggregate, Gsb | 2.499 | 2.499 |
| %Binder effective by volume* | 7.7 | 7.5 |

*(calculated using HMA volumetric analysis spreadsheet)

Mix Type
Binder

ARK 25.0mm
70-22

Gradation Properties:

| Sieve Size (mm) | Blend |
|-----------------|-------|
| 50.00 | 100.0 |
| 37.50 | 100.0 |
| 25.00 | 94.0 |
| 19.00 | 82.0 |
| 12.50 | 67.0 |
| 9.50 | 60.0 |
| 4.75 | 40.0 |
| 2.36 | 23.0 |
| 1.18 | 16.0 |
| 0.60 | 13.0 |
| 0.30 | 11.0 |
| 0.150 | 8.0 |
| 0.075 | 4.7 |

| | Actual | Modified |
|--|--------|------------|
| % AC | 5.3 | 5.3 |
| % Air Voids | 4.5 | 8.0 |
| %VMA | 13.1 | 16.2 |
| %VFA | | 50.6 |
| Dust/Asphalt Ratio | | 1.2 |
| Max Specific Gravity, Gmm | 2.398 | 2.398 |
| Bulk Specific Gravity, Gmb | 2.289 | 2.205 |
| %Gmm @ Nini | | |
| %Gmm @ Ndes | | |
| Effective Specific Gravity of Blend, Gse | 2.594 | 2.594 |
| Specific Gravity of Binder, Gb | 1.021 | 1.021 |
| Specific Gravity of Aggregate, Gsb | 2.492 | 2.492 |
| %Binder effective by volume* | 8.5 | 8.2 |

*(calculated using HMA volumetric analysis spreadsheet)

Mix Type
Binder

GMQ 25.0mm
70-22

Gradation Properties:

| Sieve Size (mm) | Blend |
|-----------------|-------|
| 50.00 | 100.0 |
| 37.50 | 100.0 |
| 25.00 | 98.0 |
| 19.00 | 86.0 |
| 12.50 | 64.0 |
| 9.50 | 51.0 |
| 4.75 | 29.0 |
| 2.36 | 21.0 |
| 1.18 | 16.0 |
| 0.60 | 13.0 |
| 0.30 | 9.0 |
| 0.150 | 6.0 |
| 0.075 | 3.1 |

| | Actual | Modified |
|--|--------|------------|
| % AC | 4.4 | 4.4 |
| % Air Voids | 4.0 | 8.0 |
| %VMA | 13.0 | 16.7 |
| %VFA | | 52.1 |
| Dust/Asphalt Ratio | | 0.8 |
| Max Specific Gravity, Gmm | 2.478 | 2.478 |
| Bulk Specific Gravity, Gmb | 2.380 | 2.279 |
| %Gmm @ Nini | | |
| %Gmm @ Ndes | | |
| Effective Specific Gravity of Blend, Gse | 2.650 | 2.650 |
| Specific Gravity of Binder, Gb | 1.028 | 1.028 |
| Specific Gravity of Aggregate, Gsb | 2.614 | 2.614 |
| %Binder effective by volume* | 9.0 | 8.7 |

*(calculated using HMA volumetric analysis spreadsheet)

Mix Type
Binder

Jet 25.0mm
70-22

Gradation Properties:

| Sieve Size (mm) | Blend |
|-----------------|-------|
| 50.00 | 100.0 |
| 37.50 | 100.0 |
| 25.00 | 97.0 |
| 19.00 | 90.0 |
| 12.50 | 66.0 |
| 9.50 | 54.0 |
| 4.75 | 37.0 |
| 2.36 | 24.0 |
| 1.18 | 17.0 |
| 0.60 | 13.0 |
| 0.30 | 8.0 |
| 0.150 | 5.0 |
| 0.075 | 3.2 |

| | Actual | Modified |
|--|--------|------------|
| % AC | 4.6 | 4.6 |
| % Air Voids | 4.5 | 8.0 |
| %VMA | 13.0 | 16.6 |
| %VFA | | 51.8 |
| Dust/Asphalt Ratio | | 0.8 |
| Max Specific Gravity, Gmm | 2.436 | 2.436 |
| Bulk Specific Gravity, Gmb | | 2.242 |
| %Gmm @ Nini | | |
| %Gmm @ Ndes | | |
| Effective Specific Gravity of Blend, Gse | 2.608 | 2.608 |
| Specific Gravity of Binder, Gb | 1.028 | 1.028 |
| Specific Gravity of Aggregate, Gsb | 2.565 | 2.565 |
| %Binder effective by volume* | 9.0 | 8.6 |

*(calculated using HMA volumetric analysis spreadsheet)

Mix Type
Binder

MCA 25.0mm
70-22

Gradation Properties:

| Sieve Size (mm) | Blend |
|-----------------|-------|
| 50.00 | 100.0 |
| 37.50 | 100.0 |
| 25.00 | 94.0 |
| 19.00 | 85.0 |
| 12.50 | 74.0 |
| 9.50 | 64.0 |
| 4.75 | 34.0 |
| 2.36 | 22.0 |
| 1.18 | 15.0 |
| 0.60 | 10.0 |
| 0.30 | 7.0 |
| 0.150 | 5.0 |
| 0.075 | 3.6 |

| | Actual | Modified |
|--|--------|------------|
| % AC | 5.0 | 5.0 |
| % Air Voids | 4.5 | 8.0 |
| %VMA | 13.3 | 16.4 |
| %VFA | | 51.2 |
| Dust/Asphalt Ratio | | 0.9 |
| Max Specific Gravity, Gmm | 2.430 | 2.430 |
| Bulk Specific Gravity, Gmb | 2.320 | 2.235 |
| %Gmm @ Nini | | |
| %Gmm @ Ndes | | |
| Effective Specific Gravity of Blend, Gse | 2.622 | 2.622 |
| Specific Gravity of Binder, Gb | 1.016 | 1.016 |
| Specific Gravity of Aggregate, Gsb | 2.540 | 2.540 |
| %Binder effective by volume* | 8.7 | 8.4 |

*(calculated using HMA volumetric analysis spreadsheet)